Study of Epithelial Cells on Polypyrrole based Conducting Polymers using Electrochemical Impedance Spectroscopy

Ateh, Davidson Day

Study of Epithelial Cells on Polypyrrole based Conducting Polymers using Electrochemical Impedance Spectroscopy

-

Davidson Day Ateh

Queen Mary
University of London

INTERDISCIPLINARY RESEARCH CENTRE IN BIOMEDICAL MATERIALS

Thesis submitted for the degree of Doctor of Philosophy

September 2005

Abstract

Polypyrrole (PPy) is a conjugated polymer that displays special electronic properties including conductivity. It may be electrogenerated with the incorporation of any anionic species including negatively charged biological molecules such as proteins and polysaccharides. For this thesis, variously loaded-PPy films were prepared on gold sputter-coated coverslips. The growth and characteristics of epithelial cells, namely keratinocytes, were studied on these films by microscopy, biochemical assay, immunocytochemistry and electrochemical impedance spectroscopy.

Keratinocyte viability was found to be PPy-load dependent. For chloride, polyvinyl sulphate, dermatan sulphate and collagen-loaded PPy films, polycarbonate and gold, keratinocyte viability, as assessed by the AlamarBlue™ assay, was respectively 47%, 60%, 88% and 23%, 75% and 61% of tissue culture polystyrene controls after 5 days. This was found to require a previously unreported polymer washing step prior to cell seeding due to the observed toxicity of untreated films. Keratinocytes stained positive for proliferation (PCNA), suprabasal differentiation (K10) and hyperproliferation (K16) markers although cell morphology was poor for organotypical cultures on dermatan-loaded PPy compared with de-epidermalised dermis. Cell-induced impedance changes were detected in a three-electrode format over PPy modified electrodes. Results obtained showed the effects of cell density, cell type and monitoring frequencies. In particular, it was seen that lower cell densities could be detected on PPy compared to unmodified gold electrodes. Keratinocyte confluence as determined by impedimetric analysis was reached more rapidly on PPy than bare gold in agreement with AlamarBlue™ measurements. Electrical equivalent circuit analysis using parameters whose contributions may be directly mapped to intracellular and intercellular spaces, and membrane components suggested that the technique can be extended to cell morphology discrimination.

This work shows that PPy biocomposites are attractive candidates for tissue engineering applications since they may incorporate biomolecules and are electrically addressable with the potential to both direct and report on cell activities.

'La science n' a donc pas de patrie, la science est internationale, elle est le bien commun de toute l'humanité. Cela revient á dire que la seule cité, c'est l'école.'

Ruben Um Nyobe

Eséka, 29 Septembre 1952

Acknowledgements

I am deeply indebted to my advisors, Professors Harry Navasaria and Pankaj Vadgama, for their help and guidance throughout my research and thesis writing. Over the past years, I have learned a great deal about the various aspects of scientific research from them and this has had a strong impact on my development as a professional researcher.

I would like to thank Drs Giosi Farace and Kemcho Ojeh for initial training in electrochemical and tissue culture techniques respectively as well as for their guidance and friendship. I would also like to thank Drs Muy-Teck Teh and Alan Waterworth for help with various practical aspects of my research. I very much appreciated the unwavering technical support from Mrs Mary Taylor, Mr Keith Pell and Mr Vincent Ford. I am also very grateful to Mrs Catherine Jones for administrative assistance. Finally, I would like to mention the students and staff of the IRC in Biomedical Materials and the Centre for Cutaneous Research for support and friendship over the course of my research at Queen Mary University of London.

I am truly thankful to my parents, Teresa and Davidson, for their encouragement and support all through my life. This inspired me to attempt such a gargantuan task as researching and writing a thesis for the degree of Doctor of Philosophy.

Last but not least, I would like to infinitely thank my wife and son, Cristelle and Tristan, for the happiness they have brought to my life. The sacrifices have been great and I hope so to will be the rewards.

Statement of Originality

I certify that this thesis, and the research to which it refers, are the product of my own work, and that any ideas or quotations from the work of other people, published or otherwise, are fully acknowledged in accordance with standard referencing practices.

During the course of this degree, parts of the research have been presented in poster or oral forms at various scientific meetings and conferences. Written articles have also been contributed for publication, including:

Ateh D. D., Navsaria H. and Vadgama P. Biocompatibility of Materials In: Nalwa H. S. ed. *Handbook of Nanostructured Biomaterials and their Applications in Nanobiotechnology*. American Scientific Publishers, Los Angeles (2005) Vol. 1, pp.411-434.

Ateh D. D., Vadgama P. and Navsaria H. Culture of Human Keratinocytes on Polypyrrole-based Conducting Polymers, *Tissue Engineering* – out in April 2006.

Ateh D. D., Waterworth A., Walker D., Brown B., Navsaria H. and Vadgama P. Impedimetric Sensing of Cells on Polypyrrole-based Conducting Polymers – To be submitted.

Ateh D. D., Navsaria H. and Vadgama P. Polypyrrole-based Conducting Polymers and their Interactions with Biological Tissues, *Journal of the Royal Society Interface* – To be submitted (as an invited review).

Contents

Figures

Tables

Abbreviations

θ - Phase Angle

ABC – Avidin-Biotin Complex

AC – Alternating Current

AES – Auger Electron Spectroscopy

AFM – Atomic Force Microscope

Al Bl – AlamarBlue™

ATR – Attenuated Total Reflection Spectroscopy

BM – Basement Membrane

BMZ – Basement Membrane Zone

BSA – Bovine Serum Albumin

C – Coulomb

C – Plasma Membrane Capacitance

Cl – Chloride

Col – Collagen

Ctrl - Control

CV – Cyclic Voltammetry

d – De-Ionised

DAB – Diaminobenzidine Tetrahydrochloride

DC – Direct Current

DED – De-Epidermalised Dermis

DMEM (E4) – Dubelcco's Modified Eagle's Medium

DMSO – Dimethyl Sulphoxide

DS – Dodecyl Sulphate

E – Electrical Potential

ECIS – Electric-Cell Substrate Impedance Sensing

ECM – Extracellular Matrix

EDS – Energy Dispersive X-Ray Spectroscopy

EDTA – Ethylenediaminotetraacetic Acid

EGF – Epidermal Growth Factor

EIS – Electrochemical Impedance Spectroscopy

EIT – Electrical Impedance Tomography

ESR – Electron Spin Resonance

ETCC – Electrochemical and Tissue Culture Cell

F12 – Ham's F12

Fbri – Fibrinogen

FBS – Foetal Bovine Serum

FN – Fibronectin

FTIR – Fourrier Transform Infrared Spectroscopy

GAG – Glycosaminoglycan

GOD – Glucose Oxidase

H&E – Haematoxylin and Eosin

HA – Hyaluronic Acid

Hep – Heparin

I or i – Electrical Current

IDE – Interdigitated Electrode

IGF – Insulin-Like Growth Factor

K – Keratin

LH – Leuteinising Hormone

M – Molar ($mol.dm^{-3}$)

MTT – 3-(-4,5-Dimethyl-2-Thiazyl)-2,5-Diphenyl-2H-Tetrazolium Bromide

NMR – Nuclear Magnetic Resonance

Ø – Diameter

P/R – Phenol Red

PBS – Phosphate Buffer Saline

PC – Polycarbonate

PCNA – Proliferating Cell Nuclear Antigen

PFA – Paraformaldehyde

PG – Proteoglycan

pI – Isoelectric Point

PPy – Polypyrrole

PrK – Primary Keratinocytes

PVS – Polyvinyl Sulphate

R – Intercellular Resistance

RM+ – Culture Media Mix for Keratinocyte Culture

RPM – Rotations Per Minute

S – Intracellular Resistance

SCC – Squamous Cell Carcinoma

SCF – Super Critical Fluid

SDS – Sodium Dodecyl Sulphate

SE – Standard Error

SEM – Scanning Electron Microscope

STM – Scanning Tunnelling Microscope

TBS – Tris Buffer Saline

TCPS – Tissue Culture Polystyrene

TEM – Transmission Electron Microscope

U – Unwashed

v/v – Volume for Volume

W – Washed

w/v – Weight for Volume

Z – Total Impedance

Z' – Real Impedance

Z'' – Imaginary Impedance

Chapter 1

-

Overview

1.1 Introduction

Loss of functional tissue and organ disorders are major healthcare problems that affect millions of individuals worldwide every year. In the United States alone, as reported by Langer and Vacanti (1993), at least 8 million surgical operations were carried out annually to tackle these problems, involving up to 90 million hospital days at a total cost of more than $400 billion per year. Medical advances, such as tissue and organ transplantation, drugs to replace metabolic products from lost or defective tissues and substitution of biological function by mechanical devices (artificial hip joints, prosthetic heart valves or dialysis machines) have all been directed at addressing these problems (Marler *et al.*, 1998). These issues remain of global concern in health provision. For their part, whole organ transplantations are chiefly constrained by the low number of available donors (Cheung and Luna, 1990).

Devices developed through biomaterial advances have saved and improved innumerable lives, but inherent flaws have restricted clinical progress made in this area. For example, a major cause of artificial hip joint revision surgery is component loosening, with the main problem being a divergence between the mechanical properties of the implant and its surrounding tissues (Li *et al.*, 2002). Other problems associated with synthetic substitutes include their inability to self-repair or remodel as occurs in biological tissue. They therefore have a limited lifetime and a high likelihood of patients suffering from secondary complications (*e.g.* inflammation, infection) with a requirement in some cases for lifelong drug therapy (*e.g.* anticoagulants) as an obligatory part of prosthesis use.

Tissue engineering is an emerging interdisciplinary field that combines the principles of engineering and the biological sciences in order to develop viable substitutes that can restore, maintain, or improve the function of human tissues or organs (Langer and Vacanti, 1993). The ultimate aim of tissue engineering would be to grow whole organs with all their intricate tissue blends *ex vivo*, thus providing a favourable solution to end-stage organ failure. Griffith and Naughton (2002) suggested that the field might have a broader impact if the technology was able to reduce the need for organ replacement by provision of engineered tissue and supplying platforms for the accelerated development of novel drugs.

In tissue engineering, there are three principal approaches to the creation of new tissue: (*i*) implantation of freshly isolated or cultured cells, (*ii*) *in situ* tissue regeneration and (*iii*) implantation of tissues assembled *in vitro* from cells and scaffolds. The cells employed may be autologous (from the patient), allogeneic (from a human donor), or xenogeneic (from another species). This third method probably presents the most challenges, as tissues are grown within artificial constructs outside the body. Tissues are designed and assembled in the laboratory from primary cells including stem cells and then seeded in appropriate scaffolds. These scaffolds can be made from natural or synthetic biocompatible materials. In both cases, they need to provide a suitable substrate and dimensional context within which the cells may develop to form tissues with appropriate mechanical and biological properties.

The majority of cell-supporting scaffolds currently studied are polymeric biomaterials (Seal *et al.*, 2001). They are generally porous, degradable structures fabricated from either natural materials, such as collagen or fibrin, or synthetic polymers such as polyglycolide or polylactide. These scaffolds (or substrates) and their associated bio-functionality are becoming increasingly important in tissue growth and guidance. For example both their topography (Curtis and Wilkinson, 1997) and their ability to allow controlled release of growth factors or other signal molecules (Saltzman and Olbricht, 2002) have been shown to influence cell behaviour significantly. Thus, developing biomaterials that can exert control over cell activity would be an essential facet of successful tissue engineering as well as a logical progression of the biomaterials field.

Hench and Polak (2002) examined the historical development of biomaterials from the first literature reports grouping them into three distinct generations. First generation biomaterials were those developed to mimic the physical properties of the replaced tissue with minimal toxic effects on the host. Second-generation biomaterials favoured bioactivity over bio-inertness where the biomaterial exerted a controlled action and reaction in the physiological environment. The third, and current, generation of biomaterials is being developed to stimulate specific cellular responses at the molecular level. This latest development of biomaterials is inspired by increasing understanding of the tissue-material interface through combined knowledge of molecular biology and material surface properties (Kasemo, 1998; Tiefenauer and Ros, 2002; Castner and Ratner, 2002).

Specific biomaterials properties could provide novel solutions for tissue engineered systems such as drug delivery (degradable polymers), controlled tissue release (thermoresponsive polymers) and integrated biosensing (electroactive polymers). In addition, such biomaterials provide a platform to study aspects of the fundamental science involved in cell-material interactions. It is in recognition of these expectations that researchers are engaging novel materials as substrates for the growth and manipulation of biological cells, as typified by the conducting polymer 'polypyrrole' studied in relation to skin cells during this project.

The present study was based on research into the use of polypyrrole as a substrate to grow and monitor cells, namely keratinocytes, the most abundant epidermal cell type. Skin was used as a model system for studying aspects of the value of polypyrrole tissue engineering as it was the first laboratory engineered organ and therefore well studied. In addition, research was carried out jointly within the IRC in Biomedical Materials and the Centre for Cutaneous Research at Queen Mary, both departments having relevant expertise for completion of the project.

In this first Chapter, skin biology topics are presented along with current methods in skin tissue engineering. Polypyrrole based conducting polymers are introduced and relevant research activities in this area are examined. Electrochemical impedance spectroscopy is also thoroughly elaborated as it was a core technique used in parts of this research, but relatively unapplied to the biological field. The Chapter ends with a summary of the concept for this research project, its objectives and an introduction to the work that is presented within the thesis.

1.2 Aspects of Skin Biology

1.2.1 Function and Structure of Skin

Function

Skin is the largest organ in terms of weight and surface area responsible for many important functions essential to homeostasis. Skin acts as a protective barrier preventing physical abrasion, bacterial invasion, dehydration and ultraviolet radiation from damaging underlying tissues. The regulation of sweat production and blood flow to the skin allows the body to maintain a constant temperature in relation to its environment and excrete waste products. Skin is also abundant with nerve receptors that detect sensations such as temperature or touch, immune cells that combat foreign aggressors and blood vessels that carry between 8 to 10% of the blood flow in a resting individual. It is also the organ responsible for vitamin D synthesis.

Structure

Anatomically, skin consists of two main parts: (i) the superficial outside portion called the epidermis and (ii) the inner thicker portion called the dermis (Fig 1.1). The relative sizes and structures of these skin parts vary according to the site of the body where they are located (*e.g.* eyelid skin is much thinner than palm skin). The epidermis is a multilayered epithelial tissue with keratinocytes the predominant cell type, accounting for over 80% of the cells present (Holbrook, 1994). The other epidermal cell types include the melanocytes (absorption of ultraviolet light), the langerhans cells (immunologic protection) and the Merkel cells (sensation). The dermis is composed of connective tissue containing collagen and elastin fibres. There are relatively few cells in this region of skin, mainly fibroblasts, macrophages and adipocytes. The dermis is where hair follicles are rooted and where blood vessels, sensory nerves, sweat glands and other appendages are located. The epidermal and dermal areas are separated by the basement membrane zone (BMZ).

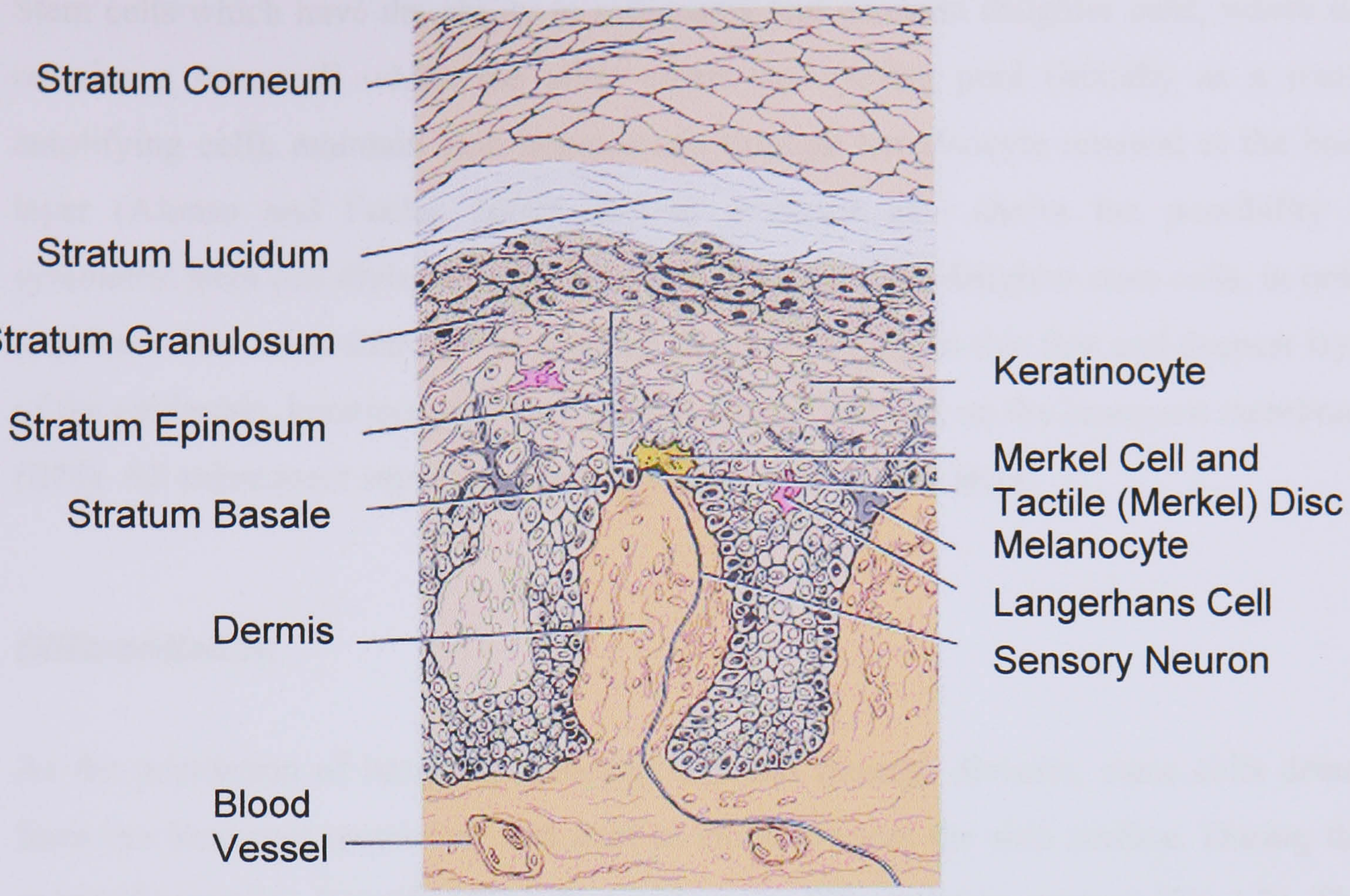

Figure 1.1: Sectional View of Thick Skin (Adapted from Tortora and Grabowski, 1996).

The basement membrane is a very fine layer at the intersection between the keratinocyte rich epidermis (light region) and dermis (darker region).

1.2.2 Keratinocytes

Function and Proliferation

As stated earlier, keratinocytes are the most abundant cell type of the epidermis. In addition, they are found as nonkeratinized varieties in other stratified squamous epithelia such as the lining of the mouth and are also present as basal cells in mixed glands such as breast. In the outer layers of skin, keratinocytes are exposed to a dry and harsh gaseous atmosphere. At the opposite interface, they are in contact with the hydrated environment of the body. The main function of keratinocytes is thus protection. For this reason, cell structure, composition and function changes according to its position within the epidermis.

Stem cells which have the ability to self-renew and generate daughter cells, where one remains a stem cell whilst the other enters the cycling pool (initially as a transit amplifying cell), maintain skin homeostasis through keratinocyte renewal at the basal layer (Alonso and Fuchs, 2003). Recent evidence also shows the possibility of symmetric stem cell division, where one cell generates two daughter stem cells, in order to preserve the adult stem cell population (Sherley, 2002). In this first and deepest layer of the epidermis, keratinocytes are cuboidal shaped and rest on the basement membrane (BM). All subsequent suprabasal cells are evolved from this layer.

Differentiation

As the population of basal keratinocytes expands through division, some cells detach from the basement membrane and start to move towards the skin surface. During this outward migration (stratification) they undergo a differentiation process (Fig 1.2). This developmental process includes morphological and biochemical changes, notably the accumulation of keratin (a tough, insoluble protein found in over 20 distinct types) alongside the disappearance of the organelles. Keratins are specific markers of epithelial cell differentiation. By the time the cells reach the outermost layer, the stratum corneum, they are flat, dead and completely filled with keratin. The entire process from cell formation at the basal layer to shedding at the superficial layer takes between 2 to 4 weeks. However, keratinocyte turnover may be accelerated in some skin conditions such as psoriasis, an inflammatory disease of the skin (Buxton, 2003); this is known as hyperproliferation.

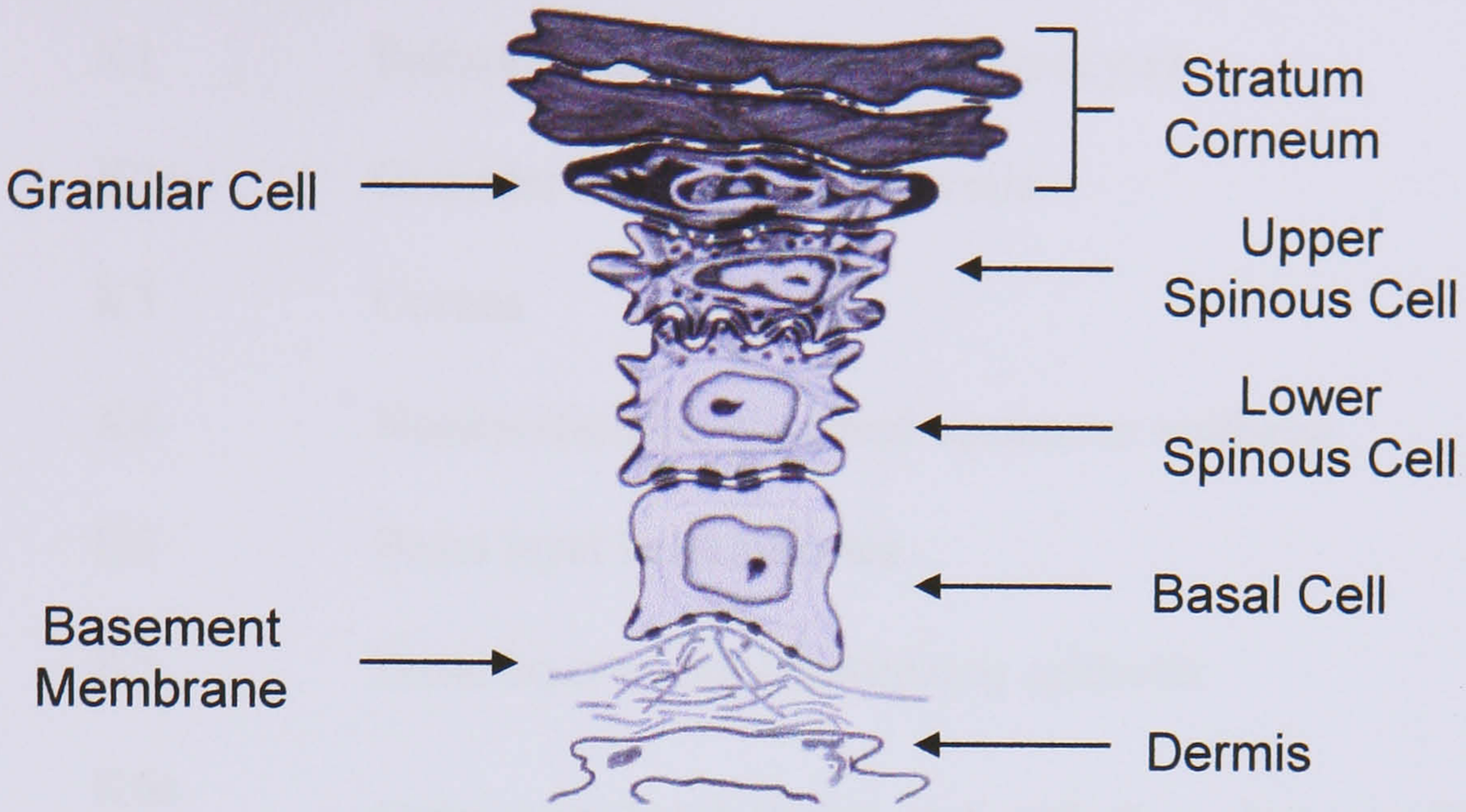

Figure 1.2: Morphological Changes during Keratinocyte Terminal Differentiation (Adapted from Bowden *et al.*, 1984). *The stratification of keratinocytes is characterised by the expression and accumulation of specific keratins at each layer culminating in cornified cells at the outermost layer, the stratum corneum.*

Keratins

Keratinocyte differentiation is characterised by the expression of specific keratin types depending on cell location within the epidermis (Table 1.1). Keratins are alpha-helical molecules belonging to two multigene families of protein: (i) type I (acidic) and (*ii*) type II (basic). They form 10 nm intermediate filaments from type I-type II heterodimers. Together with tubulin (microtubules) and actin (microfilaments), keratins form the cell cytoskeleton. Through interactions between keratin filaments and desmosomes (cell-cell junctions) a continuous cytoskeletal network is formed with adjacent cells providing mechanical integrity to skin. Similar interactions occur with hemidesmosomes (cell-BM junctions). The main purpose of keratin is thus the provision of structural integrity to the tissue. However, the full list of functions is still unclear and it is probable that they have important roles in chemical toxicity and osmotic stress protection for example (Owens and Lane, 2003). Certainly, genetic mutations in keratin genes are responsible for numerous disorders in skin tissue including epidermolysis bullosa simplex, palmoplantar keratoderma and pachyonychia congenita (McLean *et al.*, 2003).

Type I	Type II	Major Sites of Expression
K10	K1	Suprabasal epidermal keratinocytes
K9	K1	Palmoplantar suprabasal keratinocytes
K10	K2e	Granular layer of the epidermis
K12	K3	Cornea
K13	K4	Nonkeratinizing stratified squamous epithelia
K14	K5	Basal layer keratinocytes
K15	K5	Basal layer of nonkeratinizing epithelia
K16	K6a	Outer root sheath (hair), oral epithelium, hyperproliferative keratinocytes
K17	K6b	Nail bed, Myoepithelium, inflammatory conditions
	K7	Various partners in transformed cells
K18	K8	Simple epithelia
K19		Bulge cells (hair follicle), Simple epithelia
K20		Gastrointestinal epithelium

Table 1.1: Types of Keratins and their Major Sites of Expression. *Keratins appear in pairs with type I been acidic and type II basic and are used in immunohistochemistry to identify cell differentiation and stratification.*

Regulation

Cell communication, migration, adhesion and their interplay coordinate proliferation and are essential in sustaining tissue. Keratinocyte proliferation, crucial to healthy skin, is regulated by three main factors: (*i*) differentiation state (Gandarillas, 2000), (*ii*) adhesion to the extracellular matrix (Assoian, 1997) and (*iii*) regulation of growth factors and inhibitors (Gniadecki, 1998). In order to maintain skin tissue, keratinocytes form cell-cell (*e.g.* desmosomes, adherens) and cell-matrix (*e.g.* hemidesmosomes) junctions. At the molecular scale, transmembrane glycoproteins, namely integrins

(Hynes, 1992; Hemler and Mihich, 1993) and the calcium dependent cadherins (Furukawa *et al.*, 1997) mediate keratinocyte-keratinocyte and keratinocyte-matrix adhesion. Integral membrane proteoglycans such as syndecan (Saunders, 1989) can also facilitate keratinocyte adhesion to the matrix *via* their attached heperan sulphate and chondroitin sulphate chains. Keratinocytes also secrete and respond to growth factors and cytokines, especially important during pathological conditions and wound healing (Pittelkow *et al.*, 1991; Mckay and Leigh, 1991). These diffusible molecules can mediate communication between them or other cell types (*e.g.* fibroblasts, langerhans cells) and interact with the matrix. The signalling molecules could be proteins, small peptides, amino acids, nucleotides, steroids, even gas molecules such as nitric oxide. Mostly, they bind to cell surface receptors such as transmembrane proteins, but in the case of sufficiently small and hydrophobic molecules that can diffuse through the membrane, their receptors are intracellular.

1.2.3 Dermis

Dermal Fibroblasts

Fibroblasts are slender, spindle shaped cells with elongated nuclei and the most common resident cells in ordinary connective tissue (Fig 1.3). There, they are responsible for secreting extracellular matrix components in response to tissue needs (*i.e.* environmental conditions, injuries and diseases). Fibroblast function and phenotype varies slightly depending on their connective tissue of origin and even location within the tissue. Fibroblasts are versatile cells and display an ability to differentiate into other connective tissue cells or at least take up some of their functions when required (Alberts *et al.*, 2002). Fibroblasts are also known as fibrocytes and those of dermal origin, as dermocytes.

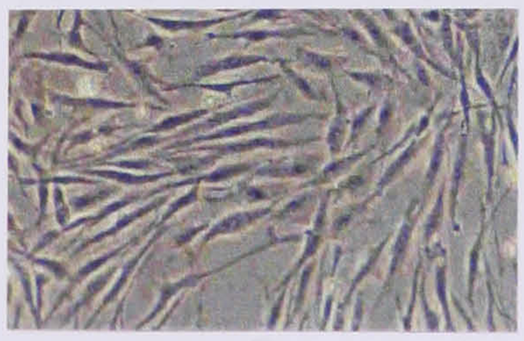

Figure 1.3: Human Dermal Fibroblasts in Culture

(Taken from Cell Applications Inc., 2004).

Dermal fibroblasts are mesenchymal cells located in the dermis of skin where they secrete and organise the extracellular matrix of the dermis but also play a vital role in regulating skin physiology through interactions with each other and other cell types. These matrix components include proteoglycans, collagen and elastic fibers that form the basis for dermal mechanical integrity as well as growth factors and other signalling molecules. There are further subpopulations of dermal fibroblast depending on their location; papillary and reticular dermal fibroblasts are the most tractable with a third group found in the hair follicle regions and a possibility that more subpopulations are in existence (Sorrell and Caplan, 2004). These different subpopulations have been shown to have specific effects on local matrix production, arrangement and function resulting in distinct phases within the dermis, notably the papillary and reticular regions.

Besides the production of matrix, growth factors, and other secretions, fibroblasts play a crucial role in skin pathologies and wound healing. For example, during wound healing, neighbouring fibroblasts proliferate and migrate to the site of injury after the initial clotting and immunological stages to deposit a fibrous infill and stimulate keratinocyte proliferation thus providing wound coverage (Mutsaers *et al.*, 1997; Eckes, 2000; Shakespeare, 2001). Environmental factors such as mechanical stress have also been shown to affect fibroblasts behaviour and subsequent matrix interactions through complex signalling pathways involving adhesion plaques and their tethered cytoskeletons (Grinnell, 2003).

Extracellular Matrix

Tissues are formed through cell growth and the production of intracellular substances that form a matrix. The native cells usually secrete this extracellular matrix (ECM) and its composition, mainly a mixture of proteins and polysaccharides is that of a structured framework in close association with the surface of surrounding cells. In the case of skin, dermal fibroblasts produce the dominant structural components of the ECM that forms the underlying support for the keratinocyte rich epidermis. These, in association with water, take the stress of movement, maintain shape and compartmentalise the skin appendages (*e.g.* hair roots, blood vessels, nerves and sweat glands). The ECM interacts with cells affecting their development, polarity, proliferation and differentiation while

the cells in turn actively remodel their surrounding matrix composition and function. The following are the principal macromolecules of the dermis:

Collagens: The collagens are a highly specialised family of glycoproteins constituting around 25% of the human body's mass with at least 20 distinct types identified at the present time (Alberts *et* al., 2002). Type I is by far the most common and it is a major component of skin ECM (90% of protein in dermis) where it forms sheet-like structures (Ayad *et al.*, 1994). Types III and IV are also quite common in skin with type VI and perhaps XII and XIII also present. The supramolecular structure of collagen varies slightly between the different types but generally, the collagen molecule consists of three peptide chains that wrap around each other to form a triple helix *via* hydrogen bonds, then microfibrils and fibrils (Wenstrup *et al.*, 1991). Collagens provide functional integrity to skin.

Elastin: This is the protein that provides many tissues with elasticity and resilience. In skin, elastin forms small, rope like fibres from molecular units that are stabilised by covalent crosslinks (Uitto *et al.*, 1991). Its elasticity is driven by the tendency of hydrophobic segments in the fibres to adopt a random coil configuration following extension. Elastin is often used as a late marker of dermal maturation.

Glycosaminoglycans and proteoglycans: Glycosaminoglycans (GAGs) are linear and highly negatively charged unbranched polysaccharides 70 to 200 sugar residues long. The main GAGs in skin are chondroitin sulphate, dermatan sulphate and hyaluronic acid, where they provide viscosity and hydration amongst other functions (Gawkrodger, 2002). Hyaluronic acid (HA), for instance, has been shown to play a major role in wound healing (Abatangelo *et al.*, 1983; Weigel *et al.*, 1986). Except for HA all other GAGs are found attached to proteins. Proteoglycan (PG) is the name given to molecules consisting of one or more GAG chains linked to a core protein. PGs are found tethered to cell membrane surfaces as well as in the ECM (Goetinck and Winterbottom, 1991). They have roles in cell-cell, cell-matrix interactions and act as high molecular weight polyelectrolytes in the control of molecular migration and ionic equilibrium within the ECM (Labat-Robert *et al.*, 1990). GAGs and PGs form the highly hydrated 'ground substance' in which fibrous proteins such as collagen and elastin are embedded.

Other proteins: Non-collagen structural glycoproteins such as fibronectin, laminin, entactin and others are found in the ECM of the dermis. They typically have multiple domains with specific binding sites for other ECM macromolecules and cell surface receptors. The fibronectin family has been the most studied example. They have been shown to interact with integrins on cell surfaces through a specific amino acid sequence, Arg-Gly-Asp or RGD, and mediate their adhesion and migration within the ECM (Labat-Robert *et al.*, 1990).

Basement Membrane Zone

The basement membrane of skin is formed of proteins, glycoproteins and proteoglycans that are critical in structuring and facilitating adhesion of epithelial cells to the dermis. In addition, the BMZ controls the transit of molecules (*e.g.* nutrients, cytokines) and cells (*e.g.* melanocytes, langerhans cells) between the dermis and the epidermis whilst preventing cell migration from the dermis. The BMZ components comprise type IV collagen with a limited amount of type V and VII, laminin, entactin (nidogen), fibronectin and antigens. Heparan sulfate and chondroitin 6-sulfate proteoglycans are also present in the basement membrane (Briggaman *et al.*, 1991; Fine, 1994). Figure 1.4 is a representation of the main layers recognisable within the BMZ.

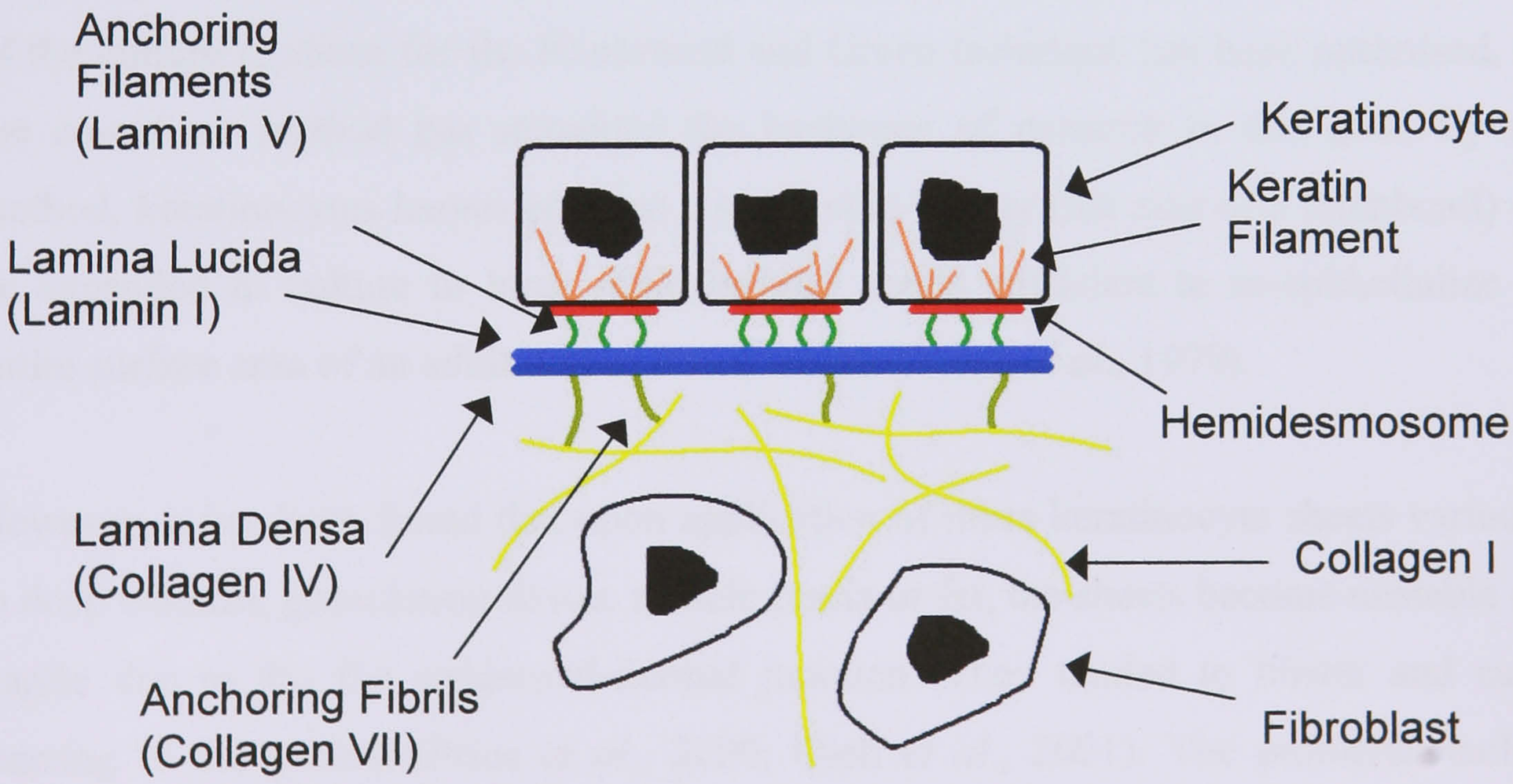

Figure 1.4: Basement Membrane Zone. *The basement membrane separates the keratinocyte rich epidermis from the dermis which contains dermal fibroblasts.*

Hemidesmosomes are specialised junctions studded along the ventral membrane of basal keratinocytes. They mediate the anchoring of the basal keratinocyte layer to the underlying BMZ *via* cytokeratins and transmembrane adhesion molecules. The lamina lucida is a continuous electron-lucent area consisting of laminin, bullous pemphigoid glycoproteins and collagen VII anchoring filaments. The lamina densa in contrast, is an electron-dense area consisting primarily of collagen type IV and heparan sulphate proteoglycan. The sub-lamina densa zone is rich in fibrous elements including anchoring filaments and type VII collagen that protrude into the reticular layer and complete the epidermal-dermal attachment (Briggaman *et al*., 1991).

1.2.4 Skin Tissue Engineering

Keratinocyte Culture

Extensive body surface burns or non-healing chronic ulcers are examples of skin tissue defects that are best treated by skin grafts. However, in severe cases of skin loss it is not always possible to use grafts. Therefore, researchers have turned their attention to tissue engineered skin equivalents for clinical use. Rheinwald and Green (1975) established a method for repeated sub-culture in the presence of an irradiated mouse fibroblast (3T3) feeder layer of single cell suspensions of keratinocytes. Over the years, the composition of the culture medium for the Rheinwald and Green technique has been optimised, but the co-culture method has remained the backbone of research in this area. By this method, keratinocytes harvested from a small skin biopsy (the size of a thumbnail) can be expanded in culture to large multi-layered sheets sufficient to re-epithelialize the entire surface area of an adult within 3 to 4 weeks (Green *et al*., 1979).

However, it has been found that upon application of these keratinocyte sheets variously to deep wounds, granulation tissue, muscle fascia or fat, the sheets become unstable and fragile due to the flat epidermal-dermal junction. They tended to blister and cause scarring in the patient (Price *et al*., 2000; Ojeh *et al*., 2001). The problems include handling difficulties of the grafts which result in poor success rates and it has become clear that the provision of an epidermal component alone is insufficient. This focused attention on the dermis of the skin. Two main avenues for the provision of an underlying dermis during cell expansion have since been investigated: (i) artificial

dermal equivalents and (ii) cadaveric de-epidermalised dermis (DED). The latter suffers from a lack of suficient supply of cadaver material (xenogeneic alternatives are in any case poor due to high immunogenicity) whilst with the former, it is difficult to replicate biological function seen in natural tissue.

Commercial Tissue Engineered Skin

The commercial substrates reviewed in Table 1.2 each have advantages and drawbacks, and researchers have carried out comparative studies. For example, Ojeh and co-workers (2001) compared Integra® Artificial Skin with cadaver de-epidermalized dermis (DED). They used the organotypic culture method (Leigh and Watt, 1994) where keratinocytes are seeded onto a dermal equivalent and grown at the air-liquid interface. This method allows a greater degree of morphological differentiation within multilayered cultures than the standard Rheinwald and Green technique. Their *in vitro* study through cell proliferation assays, showed histology and immunohistochemistry changes of a better cell morphology using DED. The findings supported the use of DED seeded with fibroblasts and keratinocytes as a single step rather than as a two-stage procedure for the best clinical outcome in an acute wound model. They also noted the fact that DED composites provided a better substrate for the organisation of keratinocytes in the epidermal layer due to the presence of basement membrane proteins. These proteins direct the attachment, subsequent proliferation and differentiation of keratinocytes and prevent dermal invasion by these cells. Such basement membrane components are lacking at initial stages in the Integra® Artificial Skin, and keratinocytes are able to grow into the material, promoted by the pore size and silicon composition of the scaffold.

Name	Composition	Uses/Limitations
Allogeneic whole skin	Fresh or preserved (cryo- or glycerol-) cadaver skin	Cuono technique, allogeneic cells cause rejection, possibility of infectious transmission with fresh material
Apligraft® (Graftskin®)	Bovine collagen I matrix with neonatal fibroblasts and keratinocytes	Living cellular product with good barrier function and developed dermis, potential for infectious transmission, cell longevity unknown
DED *e.g.* Alloderm®	Whole skin with cellular content removed by enzymatic digestion	Abnormal basement membrane profile, limited barrier function
Dermagraft®	Polyglactic matrix cultured with neonatal fibroblasts *in vitro* before been frozen to kill cells	Cellular, more complete dermal scaffold with limited potential for transmission of infection, no significant barrier function
Dermagraft-TC®	Nylon mesh with cultured fibroblasts	Biological dressing, not integrated as a dermis but provides cytokines etc… to wound bed
Integra® Artificial Skin	Bovine collagen I with chondroitin-6-sulfate, covered in silicone layer	Dermal matrix, full barrier function, good results in elective scar revision surgery
HYAFF® technologies *e.g.* Hyalograft-3D®	Hyaluronic acid (HA) derived matrices with variable esterification for chemical stability. Hyalograft-3D® has autologous fibroblasts	Dermal analogue, proven cellular responses to HA that enhance wound healing, autologous fibroblasts require time to culture
Laserskin®	Thin sheet of 100% esterified hyaluronic acid with pre-drilled micropores	Keratinocyte carrier system allowing primary seeding onto material, no dermal component
Permacol®	Porcine collagen matrix	Acellular scaffold with limited chemotactic properties, minimal barrier function

Table 1.2: Commercial Tissue Engineered Skin Equivalents Available

(Adapted from Price *et al.*, 2000).

1.3 Polypyrrole Based Conducting Polymers

1.3.1 Conducting Polymers

Brief History

Monkman (1989) studied the conducting polymer polyaniline, in the Queen Mary Physics Department and wrote in the introduction of his thesis: 'When considering the principal virtues of a polymer, one usually thinks of such properties as strength, elasticity, plasticity and toughness. Mention their electronic properties and most people would consider them to be insulators, period. However, over the last 20 years or so, this has been shown not to be the sole case.' Today, the same is probably true and conducting polymers, their characteristics and applications, remains a niche area of research for some chemists, physicists and engineers.

On an historical perspective, it was in 1862 that Letheby first reported the anodic oxidation of aniline in dilute sulphuric acid, yielding an insoluble blue-black shiny powdered deposit on a platinum electrode. Further experiments led Goppelsroeder in 1876 to establish that oligomers were formed by the oxidation of aniline (Heinze, 1989). Natta *et al.* (1958) synthesised polyacetylene and Dall'Olio *et al.* (1968) discovered yet another compound, polypyrrole, at the time called pyrrole black. They made their polymer by anodic oxidation at a platinum electrode and conductivity measurements carried-out on the brittle film of pyrrole black gave a value of 8 S/cm. However, it was not until 1977 that Shirakawa and his co-workers wrote their seminal paper showing that halogen doping of polyacetylene dramatically increased its conductivity (to around 10^3 S/m in the case of I-doped *trans*-polyacetylene).

The major breakthrough with regard to the synthesis of conducting polymers was achieved by Diaz and co-workers (Diaz and Kanazawa, 1979; Kanazawa *et al.*, 1979, Diaz, 1981) when they reported the formation of a highly conductive, stable and manageable polypyrrole film under controlled electrochemical conditions. Since then conducting polymers, of which there are currently over twenty-five known systems, have been produced mainly by chemical and electrochemical reactions. However, other polymerisation methods involve photochemistry, metathesis, concentrated emulsion,

inclusion, solid-state, plasma, pyrolysis and soluble precursor polymer preparation (Kumar and Sharma, 1998). The resultant physicochemical properties of the materials are dependent on the processing parameters. These include the nature and concentration of the reagents employed, reaction time, solution pH and temperature.

For the specific case of electrochemical synthesis by deposition on to an electrode (Brett and Brett, 1993; Oldham and Myland, 1994; Crow, 1994), additional factors need to be considered. These include the electrode material, electrochemical potential and current density. Electrochemical synthesis has been the preferred method of preparation for conducting polymers. This is mainly due to the simplicity of the technique, control over material thickness, geometry and location, the facility for doping during synthesis, the wide choice of dopant ions available and the production of good quality films (Kumar and Sharma, 1998; Inzelt *et al.*, 2000).

Structure and Properties

Conducting polymers have a conjugated π-electron backbone that is formed by the overlap of carbon p_z orbitals and alternating carbon-carbon double bonds (Fig 1.5). These systems display unusual electronic properties, notably, low energy optical transitions, low ionisation potentials and high electron affinities. The most important aspect of conjugated polymers from an electrochemical view is their ability to act as electronic conductors. This property is further controlled by redox switching at specific potentials. This reduction or oxidation is accompanied by the movement of electron donors or acceptors (i.e. dopant ions) into or out of the material depending on polymer charge.

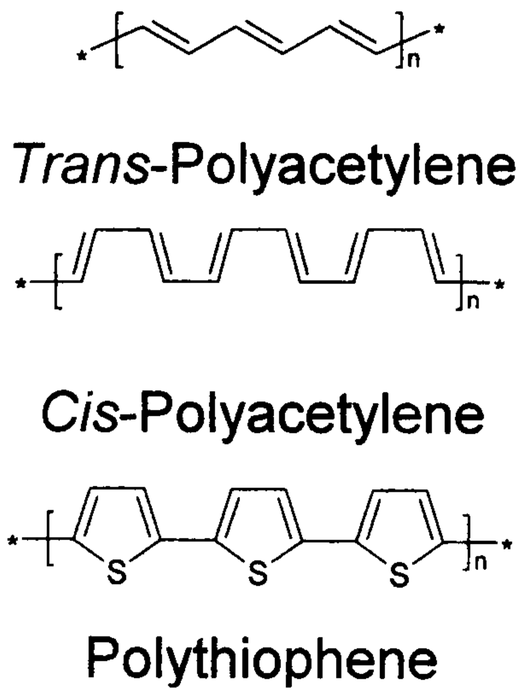

Figure 1.5: Examples of Conjugated Polymer Structures. *Conducting polymers share alternating single and double carbon bonds in their chemical structure.*

The morphology of conducting polymers has been investigated using techniques such as TEM, SEM, STM and AFM (Armes *et al.*, 1991; Wang *et al.*, 1995). The structure, *i.e.* chain homogeneity, regularity and length of conducting polymers has also been studied using EDS, AES, FTIR, ATR, NMR, ESR and X-ray diffraction amongst other techniques (Lee *et al.*, 1995; Malitesta *et al.*, 1995; Zhao and Nauer, 1996; Komolov *et al.*, 1999; Zhou *et al.*, 2002). It has been found through a combination of these techniques that the pyrrole and thiophene monomers, for example, are predominantly linked at the α-position of their heterocyclic rings, although α-β bonding also occurs. Despite the difficulty involved, as conventional techniques cannot be used owing to the extreme insolubility of these materials, researchers have also been able to estimate the chain lengths for various conducting polymers. There is however some disagreement amongst the data depending on the methods employed. In the case of polypyrrole, some researchers have quoted from spectroscopic findings that around 10 to 100 pyrrole units are involved whereas others have estimated chain lengths of between 100 and 1000 monomer units from radioactive labelling techniques (Heinze, 1989). The latter findings are further supported by the good mechanical properties often obtained with polypyrrole systems (Della Santa *et al.*, 1997; Ouyang and Li, 1997).

Chemically obtained conjugated polymers are initially insulators (*i.e.* in a neutral state). It is only through oxidation (p-doping) and less frequently reduction (n-doping) by chemical or electrochemical means, that the necessary mobile charge carriers for conductivity are formed. For most conducting polymers, their backbone is negatively

charged in the reduced state and positively charged in the oxidised state. Therefore, to maintain electroneutrality, the relevant counterions diffuse into the polymer during charging and out during neutralisation (Fig 1.6). The oxidation process may also be accompanied by significant changes in volume upon ingress of the anionic species, a characteristic exploited in actuator applications (*e.g.* artificial muscle as described by Otero and sausinema, 1995). Overoxidation of conducting polymers, notably polypyrrole, where the polymer is held at a high positive potential, leading to loss of conductivity and de-doping, has been investigated by researchers (Gao *et al.*, 1994; Farrington and Slater, 1997; Shiigi *et al.*, 2002). In this overoxidised state they found that polypyrrole acted as a selective ion-exchange film, favouring cation transport and exclusion of anions.

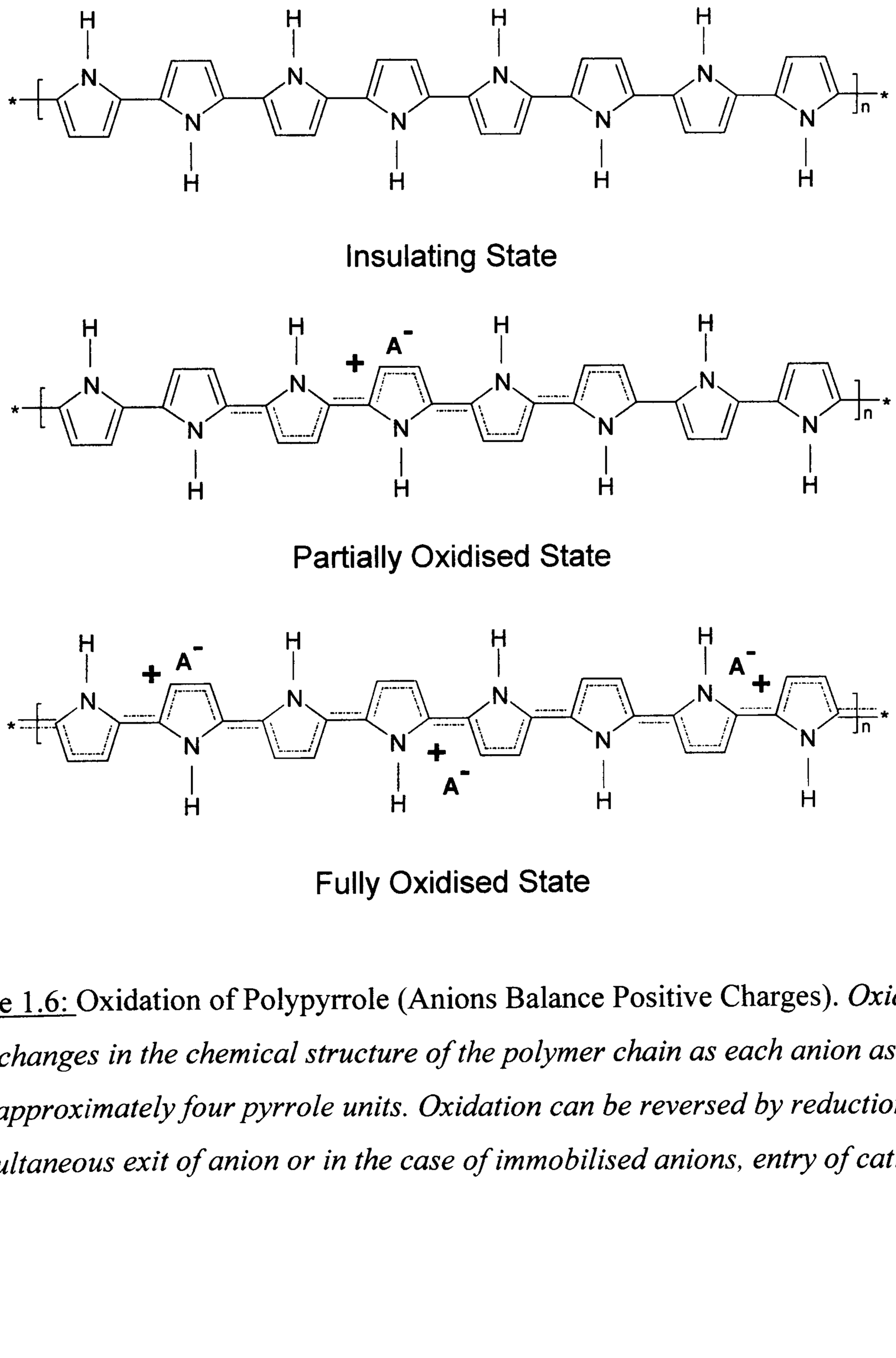

Figure 1.6: Oxidation of Polypyrrole (Anions Balance Positive Charges). *Oxidation causes changes in the chemical structure of the polymer chain as each anion associates with approximately four pyrrole units. Oxidation can be reversed by reduction with simultaneous exit of anion or in the case of immobilised anions, entry of cations.*

Conductivity

The conductivity of these polymers is due to electronic transfer along the conjugated π-molecular orbital backbone coupled with the motion of charge carriers in the material. In the example of polypyrrole, upon oxidation, an electron is removed from the π-system of the backbone producing a cation and a local distortion due to a change in geometry every four pyrrole units. This radical cation coupled to its local deformation forms a polaron. Upon further oxidation, at higher charging levels, pairs of polarons combine to form bipolarons as this is energetically more favourable.

Bipolarons can migrate along the conjugated polymer chain and this is the main charge transport mechanism within conducting polymers (Heinze, 1989; Inzelt *et al.*, 2000). However, other types of conjugated polymers, namely those with a degenerate ground state such has polyacetylene, have a slightly different charge transport mechanism involving the formation of 'solitons' (Chien *et al.*, 1988). Solitons are charged defects that are independent of one another; they freely separate along the polymer chain and can form domain walls that separate two phases of opposite orientation and identical energy.

Properties such as the conductivity of doped conjugated polymers depend on the charge transfer between the dopant and the polymer segment, charge carrier mobility within the conjugated segments of the same polymer chain and charge transfer (or 'hopping') between separate chains (Bhattacharya *et al.*, 1996). Essentially, it has therefore been postulated that it is the least efficient of any of these mechanisms in any given condition (*e.g.* temperature, pH) that limits the overall conductivity of the material on a macroscopic level. Research is still continuing with the aim of reaching a full and detailed understanding of the charge storage and transport mechanisms within these conjugated polymers.

Applications

There has been a large effort focussing on the development of conducting polymers for practical applications. One of the first was formulated when it was discovered that polyacetylene could function as an active electrode in a rechargeable battery. These materials have been investigated for other uses, including electrochromic displays,

information memory, anti-static materials, anti-corrosives, electrocatalysis, sensors, electromechanical devices, infra-red polarizers and radar (Stenger-Smith, 1998). However, in the context of this thesis, this Chapter will focus primarily on applications involving biological cells or their related molecules in the area of medical engineering.

Experiments have shown that small electrical currents can stimulate a tissue response such as bone re-growth and wound healing (Lindsey *et al.*, 1987; Kohavi *et al.*, 1992; Kloth and McCulloch, 1996; Reger *et al.*, 1999). These results were achieved using metallic electrodes inherently incompatible with biological tissues. The emergence of conducting polymers, a class of electroactive organic materials, brought the possibility of a more intimate relationship with biological systems. This provided the drive for their study as substrates in biological applications (Kane-Maguire and Wallace, 2001). Interest in conducting polymers such as polypyrrole, polythiophene and polyaniline was further increased because of the different surface and bulk properties that could be obtained by simply varying synthesis conditions.

Indeed, conducting polymers, easily prepared by either chemical or electrochemical oxidation with the incorporation of negatively charged counterions, allowed the inclusion of macromolecules such as proteins, enzymes or antibodies, and even whole living cells (Wallace *et al.*, 1999; Adeloju and Wallace, 1996). The prospect of electrical stimulation, while simultaneously monitoring cells during culture by electrochemical methods, further reinforced the idea that these compounds could have advantages as substrates in tissue engineering. Of this class of polymers, polypyrrole has become by far the most studied in tissue engineering applications due to its ease of preparation, relative stability, high conductivity and cytocompatibility.

1.3.2 Polypyrrole

Synthesis

Polypyrrole is generally synthesised by chemical or electrochemical means. Chemical synthesis is used when large quantities of material are required and involves mixing a strong oxidising agent (typically $FeCl_3$) with a monomer solution (Armes, 1987; Duchet *et al.*, 1998). For reasons outlined in the previous section, electrochemical synthesis is

much more commonly used in research. It involves the formation of an adherent deposit *i.e.* a solid film, from the polymerisation of monomer units dissolved in solution, onto a positively polarised working electrode. This process is known as electrodeposition and proceeds via a condensation reaction between the monomer units of the five-membered heterocycle pyrrole (Fig 1.7).

In the reaction, monomer units are adsorbed onto the surface of the working electrode resulting in one-electron oxidation to form a pyrrole cation radical. These cations will then couple with themselves, with other cations or with neutral monomers from solution. In each case, this leads to the formation of a dimer dication which undergoes a double deprotonation to give a neutral molecule. These more stable dimer radicals have a lower oxidation potential compared with the monomer units, and chain growth then occurs by preferential coupling between the dimers and monomers (Street, 1986). During electrochemical synthesis, negatively charged counterions must be present in the solution to maintain charge balance within the polymer. This process is referred to as doping and the choice of counterion affects formed polymer properties.

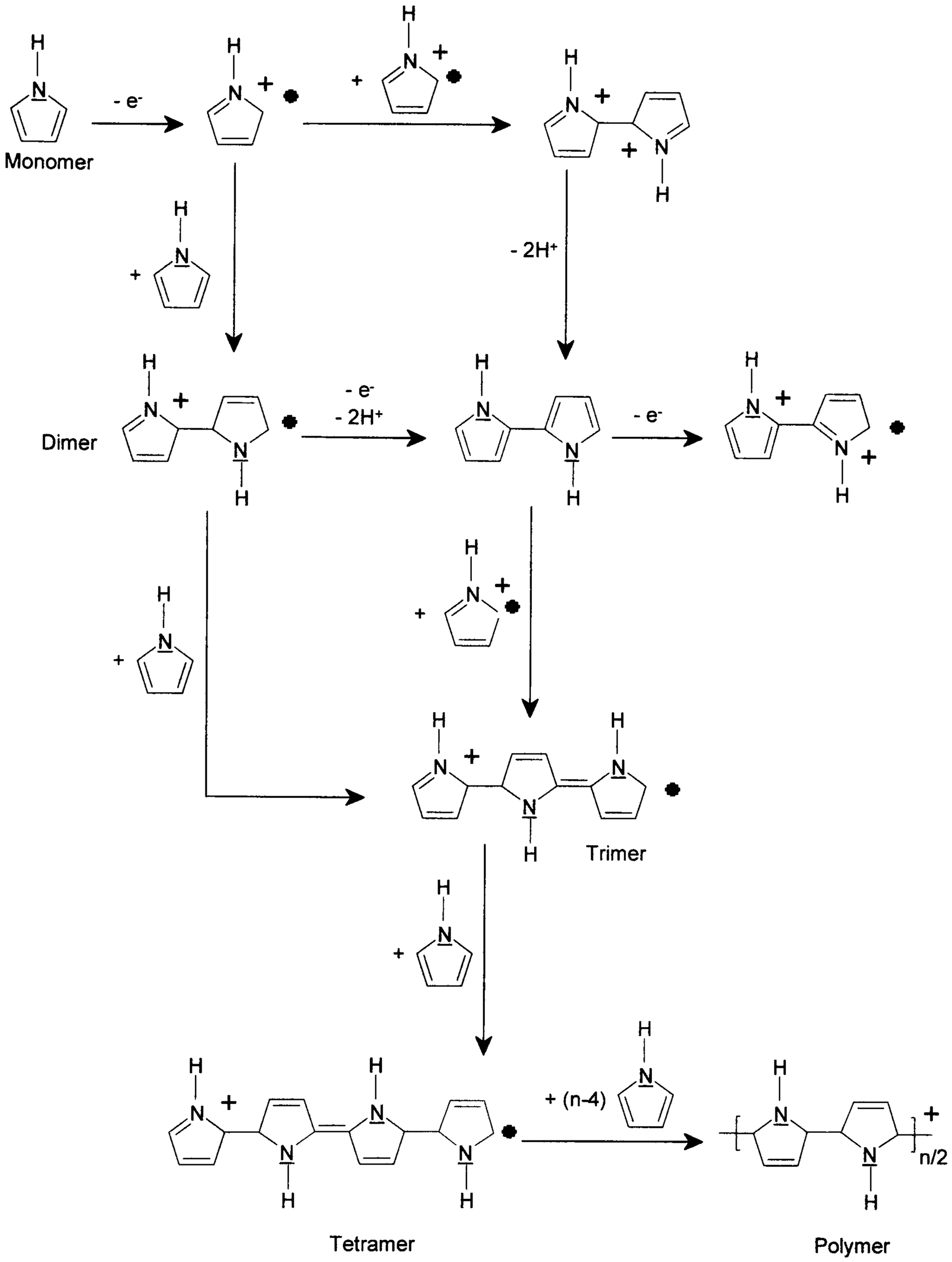

Figure 1.7: Electropolymerisaion Mechanism of Polypyrrole (Adapted from Lillie, 2001). *See text for more detailed explanation of reaction.*

The growth of polypyrrole depends on its electrical character. If it was non-conducting, its growth would be self-limiting, producing very thin films as in the case of polyphenol and its derivatives (Eddy *et al.*, 1995). In contrast, polypyrrole growth is virtually unlimited due to its conductivity. There are a large number of experimental recipes for the preparation of polypyrrole that significantly modify the phenomenological properties of the polymer. Generally, electrochemical polymerisation occurs at potentials above +600 mV versus the silver-silver chloride (Ag/AgCl) reference electrode. The morphology of the resultant film depends on the nature of the electrolyte, the crystallographic structure of the underlying electrode, the kinetics and potential of the deposition, the presence of anions and polyanions or surfactants and the concentration of the monomer. Temperature and pH can also have an effect on the ensuing film.

An example of electrochemical synthesis is given by the method developed by Diaz *et al.* (1981). They produced polypyrrole films through the oxidation of the pyrrole monomer under an inert atmosphere in a three electrode, undivided cell using a platinum working electrode, a gold counter electrode, and a sodium saturated calomel reference electrode (SSCE). Acetonitrile (solvent) and tetraethylammonium tetrafluorobate (electrolyte) were used, although Diaz (1981) later reported that other appropriate solvent/electrolyte combinations could be employed. The polypyrrole films were grown galvanostatically (*i.e.* at constant current) on the working electrode, with the films typically polymerised at +810 mV *vs.* SSCE.

There are other common polypyrrole electropolymerisation methods in use. These include the potentiostatic method where the working electrode is held at a constant potential and the potentiodynamic method (cyclic voltammetry) where a potential is cycled between two pre-determined voltages (Lillie *et al.*, 2001). The latter, potentiodynamic, method generates a cyclic voltammogram of the electropolymerisation and is often used as a method to switch conducting polymers between their reduced and oxidised states. Film thickness may be easily varied by controlling current density, potential, time and in the case of cyclic voltammetry by increasing or decreasing the number of cycles and scan rate.

Characterisation

The literature on characterisation studies of polypyrrole is quite abundant due to the different techniques employed and the endless combination of doping agents and electrolyte solutions with which these materials can be synthesised. However, due to their conductive nature, most researchers use electrochemical techniques to rapidly and inexpensively characterise their properties. Of these techniques, two are prevalent: (i) cyclic voltammetry (CV) and (ii) electrochemical impedance spectroscopy (EIS). EIS is thoroughly discussed in a dedicated section (1.4).

In a CV experiment, the applied voltage is made to oscillate between two switching potentials at a constant scan rate. Each electrochemical reaction has a specific potential at which oxidation or reduction occurs. Therefore, by scanning through a potential range these different electrochemical processes may be identified by characteristic current peaks developed on the cyclic voltammogram. Diaz *et al.* (1981) used this technique to study the effect of cycling their formed polypyrrole films in different electrolytes and at different scan rates. The traces they recorded using Bu_4N^+ salts (Fig 1.8) produced two discrete redox peaks, with Bu_4NBF_4 influencing the reduction reaction whereas Bu_4NClO_4 influenced the oxidation reaction. Their results demonstrated that both the scan rate (reaction kinetics) and the electrolyte salts affected the redox reaction of polypyrrole.

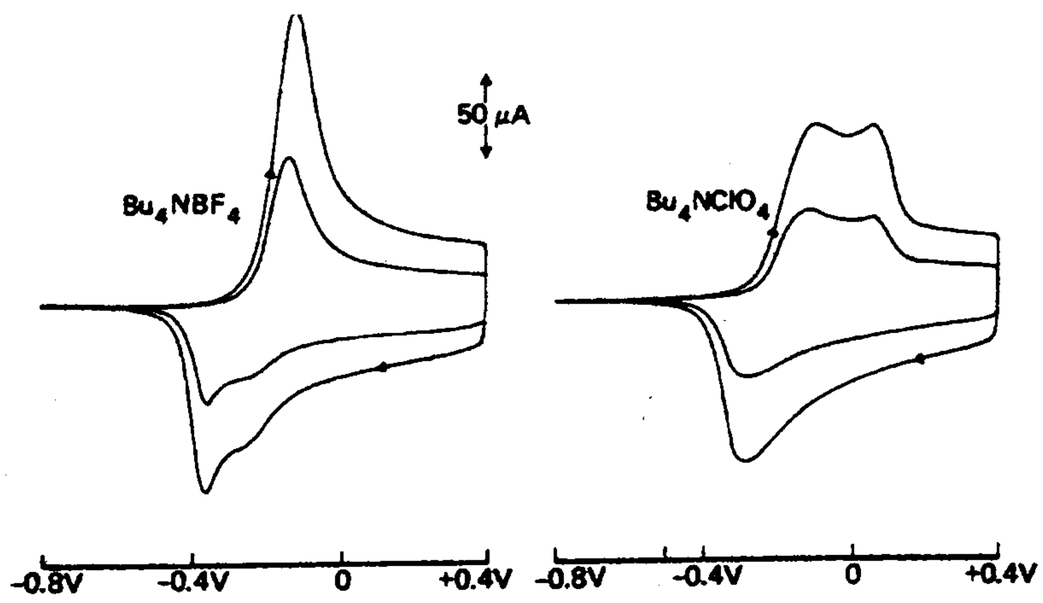

Figure 1.8: Cyclic Voltammograms of Polypyrrole in CH_3CN Containing Various Salts at Two Sweep Rates (50 and 100 mVs^{-1}) (Adapted from Diaz *et al.*, 1981). *CH_3CN is acetonitrile, Bu_4NBF_4 is tetrabutylammonium tetrafluorobate and Bu_4NClO_4 is tetrabutylammonium perchlorate.*

Levi and colleagues (1997) studied the influence of ionic size on the doping of polypyrrole films by cyclic voltammetry. They cycled de-doped polypyrrole films in a perchlorate (ClO_4^-) containing solution followed by one containing the larger sized tetraphenylborate (BPh_4^-) ion. Their studies revealed that the overall redox activity was decreased in the solutions of larger sized anions by approximately one order of magnitude, with the reaction shifted towards the cathodic side of the voltammogram. They suggested that the much bigger ionic radius of the BPh_4^- anions made them less mobile within the film, playing an important role in the observed reduction of redox activity. However, they recommended further studies to investigate other parameters that might have an effect such as a specific interaction of ionic species with the polymer matrix due to their hydrophilic, hydrophobic or amphiphilic nature.

The more recent work of Lillie *et al.* (2001) showed that in aqueous NaCl electrolyte, the CV for a chloride loaded film differed significantly from a dodecyl sulphate (DS) loaded film (Fig 1.9). This was attributed to the presence of different counterions in the films, the DS^- and Cl^- ions having dissimilar abilities to enter and exit the polypyrrole film during the redox cycle. The DS^- ion was essentially immobilised within the film whereas the smaller Cl^- ion was highly mobile. They attributed the cathodic process (in the region of negative currents) to the immobilised SDS^- ion and the anodic process (in the region of positive currents) to the mobile Cl^- ion.

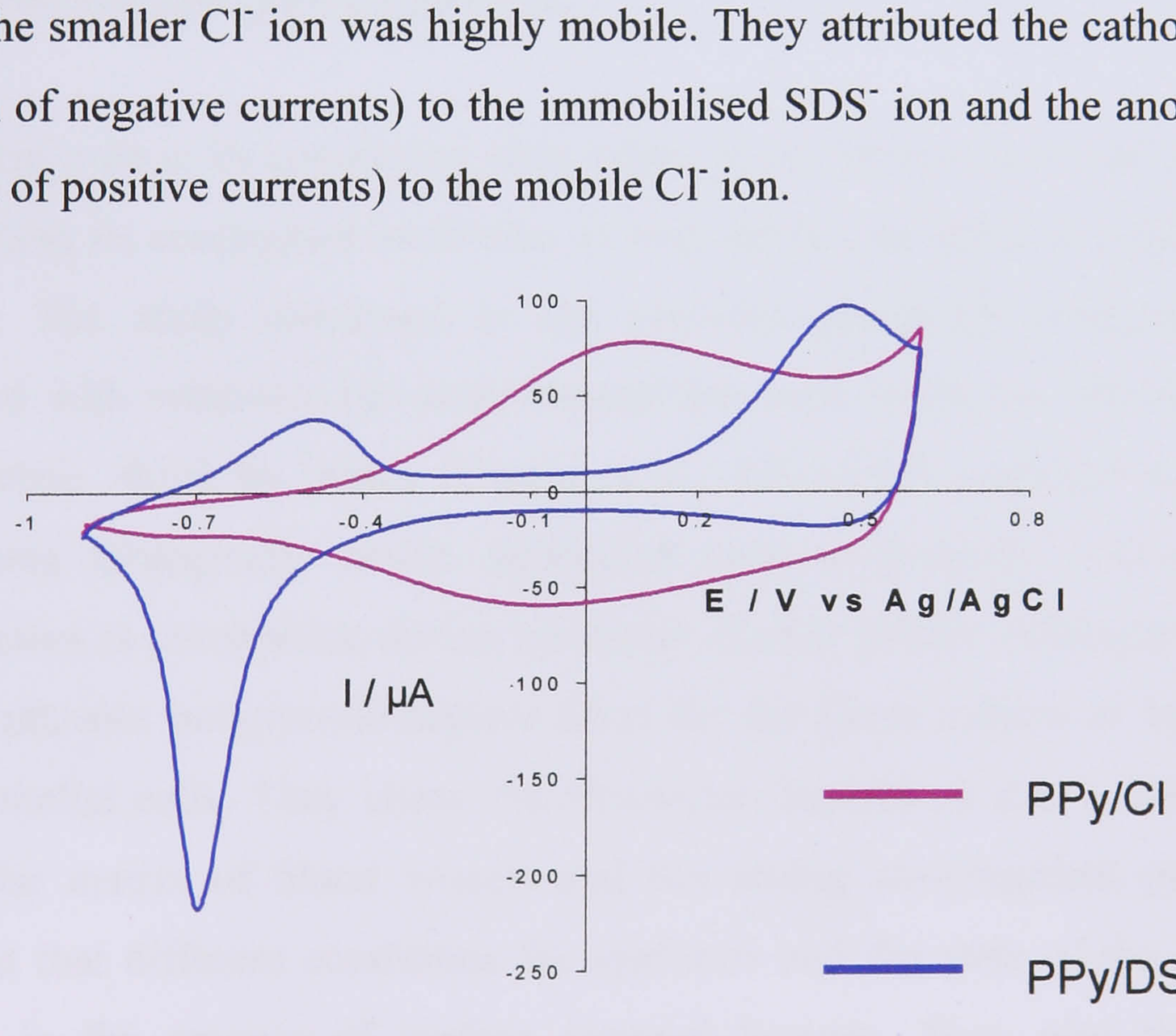

Figure 1.9: CVs for Polypyrrole Films Loaded with Chloride or SDS in 50mM NaCl

(Adapted from Lillie *et al.*, 2001)

1.3.3 Polypyrrole in Medical Engineering Applications

Cell Viability on Polypyrrole

Wong *et al.* (1994) studied the control and growth of mammalian cells on thin polypyrrole films. They cultured bovine aortic endothelial cells on polypyrrole substrates, in some cases pre-coated with fibronectin. In the case of non-coated films, cell attachment and spreading were found to be poor. However, on fibronectin coated films, good attachment and distribution was observed. Further experiments where the cell-seeded fibronectin coated films were switched from their oxidised state to their reduced state by applying a small negative electrical potential (-0.5 V *vs*. SCE) revealed cellular responses within an hour of the modification. The cellular reactions, involved cell rounding (where the cell tends to detach from the substrate), and appeared to be determined by the electrochemical state of the polypyrrole film. The authors suggested that this might be due to the local removal of fibronectin anchors or to mechanical changes in the reduced film. They also showed that these responses could be used to exert control over cell cycle progression.

Since polypyrrole in its conducting state exists as a polycation with delocalised positive charges along its conjugated backbone, as seen earlier, an anion is required for charge neutrality. The study discussed in the previous paragraph examined polypyrrole synthesised with relatively bio-inert counterions, onto which the relevant protein was later adsorbed. Work by others (Garner *et al.*, 1999a) has explored the feasibility of incorporating biologically active molecules such as proteins, polysaccharides and growth factors as counterions during synthesis. Garner and his colleagues (1999b) were able to synthesise polypyrrole-heparin films for the tissue culture of human umbilical vein endothelial cells. They chose the counterion heparin as it is a component of the extracellular matrix of blood vessels and has strong anticoagulant properties. They established that different conditions for synthesis and the state of the polymer led to variations in the amount of surface exposed heparin. They also showed that the polypyrrole-heparin substrate supported the growth of endothelial cells with a reduction in the normal amount of heparin required as a medium supplement.

The work of Collier *et al.* (2000) considered composites of polypyrrole and the ubiquitous GAG, hyaluronic acid (HA). They showed HA retention and biological

activity on the surface of the formed polymer through a binding assay using biotinylated HA binding protein. *In vitro* cell compatibility studies using PC-12 cells confirmed that the polypyrrole-HA composites supported cell attachment and viability. They went on to investigate the *in vivo* tissue response to the composites by implantation in rat subcutaneous pouches for 2 and 6 weeks. They found, from fixation and staining of the explanted polymers and surrounding tissues, that compared with a polypyrrole-polystyrene sulphate control implant, there was a statistically significant increase in vascularisation around the HA containing polymer. In tissue, HA is a known angiogenesis promoter during wound healing and other events; this study suggests it retains this ability whilst incorporated in polypyrrole films.

Campbell and co-workers (1999) demonstrated the viability of incorporating whole cells into a polypyrrole matrix. In their study, they were able to grow polypyrrole films galvanostatically from an aqueous electrolyte solution of 0.27 M sucrose, 0.1 M pyrrole, 1 g/L polyvinyl sulfonate (PVS) and erythrocytes (Fig 1.10). From unreported preliminary experiments, they found that the second counterion (PVS) was necessary to preserve erythrocyte integrity within the polymers. They were able to assess erythrocyte viability in the polymer matrix after fixation and staining with haematoxylin. They found that most of the erythrocytes incorporated were intact disks with strong red staining suggesting normal haemoglobin content. A few cells were pale with the presence of inclusion bodies and they attributed this to haemoglobin loss either as a result of electroporation or other oxidative damage during synthesis.

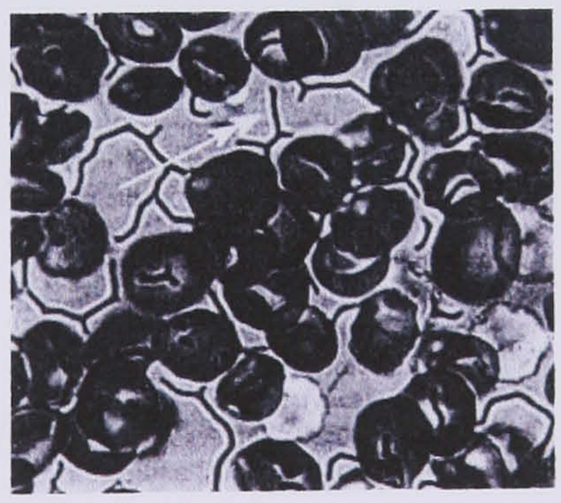

Figure 1.10: Erythrocytes (Dark Discs) Incorporation into Polypyrrole

(Taken from Campbell *et al*., 1999)

The biocompatibility of polypyrrole prepared from both chemical and electrochemical means was thoroughly evaluated by Wang *et al.* (2004). They carried out a series of systemic toxicity tests according to ISO 10993 and ASTM F1748-82 standards by applying a solution of extracts from polypyrrole powder to cell cultures and animal models. They found that the extract solution did not have adverse effects on cell cultures or on the animals tested. In the case of the animal models, this included no body temperature change, no haemolysis of red blood cells, no allergic responses or mutagenesis of cells. In addition, they showed good growth of Schawnn cells cultured on electrochemically polymerised polypyrrole compared to bare glass substrates. They also reported the novel electrochemical deposition of polypyrrole on the inner surface of a silicone tube. Further experiments, where polypyrrole-coated silicon tubes where used to bridge gaps created in the sciatic nerve of rats, showed slightly improved nerve regeneration compared to uncoated silicone tubes with only mild inflammation 6 months after implantation. The group envisage further work to exploit these polypyrrole-silicon conduits for nerve regeneration including the conductive properties of polypyrrole.

Mattioli-Belmonte *et al.* (2003) studied the tissue and cellular tolerance of non-resobable (polypyrrole, polyaniline and polyimide) and resorbable (poly(lactide-b- 1,5-dioxepan-2-one-b-L-lactide)) materials. They reported the absence of necrosis or degeneration around implants inserted subcutaneously in rats. The extent of fibrous encapsulation and number of surrounding inflammatory cells varied; PLLA-PDXO-PLLA < PANi < PPy < Polyimide for the former response and PANi < PPy < PLLA-PDXO-PLLA < Polyimide for the latter. They also studied the *in vitro* growth of a human keratinocyte cell line on polypyrrole films and found poor adhesion compared with other substrates including the resorbable triblock polymer based on PLLA.

Cell Stimulation on Polypyrrole

Recent evidence is uncovering important physiological roles for *in vivo* electric fields created by cell layers in providing wound healing and developmental cues for instance (Martindale, 2004). Certainly, it has been known for over two centuries that electrical stimulation induces modification of neural and nerve fibre activity (Velasco, 2000). Williams and Doherty (1994) investigated polypyrrole in contact with neurones, demonstrating film cytocompatibility and the potential for nerve guidance. The work of

Schmidt *et al.* (1997) built on these foundations by examining conducting polymer influence on neurite outgrowth during culture. They showed that positive electrical stimulation of polystyrene sulphonate-loaded polypyrrole films during the culture of rat PC-12 cells (neural cells) and primary chicken sciatic nerve explants enhanced attachment and neurite extension (Fig 1.11). In the case of PC-12 cells, no significant difference in neurite extension was recorded for cells grown on tissue culture polystyrene and unstimulated polypyrrole. For the electrically stimulated polypyrrole substrate, there was however, a 90% increase in neurite extension. They found that their data compared favourably with previous work on piezoelectric materials such as polyvinylidene fluoride where neurite length increases of only 20-40% had been reported (Valenti *et al.*, 1992).

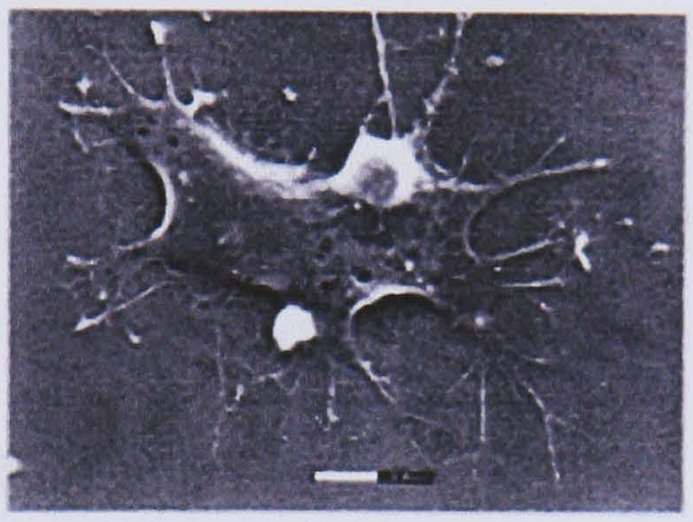

Figure 1.11: PC 12 Neurite Extension on Polypyrrole-Polystyrene Sulfonate

(Taken from Schmidt *et al.*, 1997)

Kotwal and Schmidt (2001) used PC-12 cells to investigate the effect of protein adsorption on polypyrrole and the subsequent outcome of this on neurite extension. Their study discovered that electrical stimulation increased the adsorption of fibronectin from solution onto the polypyrrole film prior to cell seeding. They postulated that this was due to fibronectin adopting a favourable conformation during electrical stimulation. Upon cell culture on the polypyrrole substrates after the protein adsorption regimen, they reported increased neurite extension for electrically driven fibronectin adsorption compared with the unstimulated material. Previously, Hodgson *et al.* (1996) had shown the possibility of including nerve growth factor amongst other bio-components within a polypyrrole-sulphated polysaccharide composite and achieving controlled release by electrical stimulation. Upon reduction of the polypyrrole backbone at a suitable

potential, they registered a release of nerve growth factor and subsequent differentiation of phaeochromocytoma (tumour) cells growing on the polymer surface.

Researchers at the Southeast University of China looked at the effect of polypyrrole electrical stimulation in relation to rat primary keratinocytes cultures (Pu *et al.*, 2001). They electropolymerised polypyrrole films on porous (120μm pore size) stainless steel filters and did not report on the nature of counterion used. Through a series of experiments, they optimised cell culture media composition and polypyrrole electrical stimulation potential. Their key finding was that under optimal conditions, including electrical stimulation for 2 hours at 100mV there was over a 20% increase in cell viability as measured by the MTT assay 3 days later compared to standard culture methods. However, their method was unusual as the keratinocytes were firstly seeded onto tissue culture plates and after 5-6 hours, the polypyrrole films on their stainless steel supports were placed on top of the adhered cells. Therefore, unlike other accounts, the cells were not directly grown on the conducting polymer.

Potential for Tissue Engineering

The above studies indicate a potential role for polypyrrole coatings in tissue engineering. This is further underlined by recent reports showing preparation routes for biodegradable conducting polypyrroles. Rivers *et al.* (2002) synthesised polypyrrole-polythiophene composites with degradable ester linkages whereas Zelikin *et al.* (2002) proposed erodible polypyrrole formed from β-substituted pyrrole monomers with ionisable/hydrolysable side groups. However, in both cases further work is needed to establish the suitability of such materials and their degraded components in physiological environments. Other research has been carried out to improve the mechanical stability of polypyrrole, for instance, Oh *et al.* (2001) synthesised 'stretchable polypyrrole films' made from dopants which act as plasticizers with draw ratio of 2.5 times the original length. These developments and others would improve the prospects of polypyrrole for routine tissue engineering use. In the next section, applications of polypyrrole in biosensors are explored. This is yet another advantage of the material as polypyrrole coated tissue engineering scaffolds could support tissue growth whilst simultaneously monitoring progress and requirements.

Biosensors

Turner and his co-authors (1987) defined biosensors as: 'Compact analytical devices incorporating a biological or biologically-derived sensing element either integrated within or intimately associated with a physiochemical transducer. The usual aim of a biosensor is to produce either discrete or continuous digital electronic signals which are proportional to a single analyte or a related group of analytes.' Biosensor devices have evolved from the necessity to provide a fast and accurate method for determining biochemical parameters, assisting clinicians, for example, in the rapid diagnosis and treatment of disease. A typical biosensor is composed of elements that provide selective recognition abilities often generating a detectable product, as with the case of an enzyme, if the transducer cannot directly detect the analyte employed.

The transducer element is typically a thermistor (heat), an optode (light), a piezoelectric (mass) or an electrically polarised conductor (electroactive substances). Clark (1962) pioneered the glucose biosensor in which glucose oxidase entrapped in a dialysis membrane facilitates the reaction between glucose and oxygen with one of the products, hydrogen peroxide, detected at an integrated platinum electrode. The current created by the release of 2 electrons per H_2O_2 molecule at the polarised electrode is proportional to the amount of glucose present in the sample (Fig 1.12). The ability to synthesise conducting polymers under mild conditions enables a range of biological components (*e.g.* enzymes, antibodies and whole living cells) to be incorporated into the polymer structure, retain their activity and assist in analyte detection (Hodgson *et al.*, 1996; Wallace *et al.*, 1999).

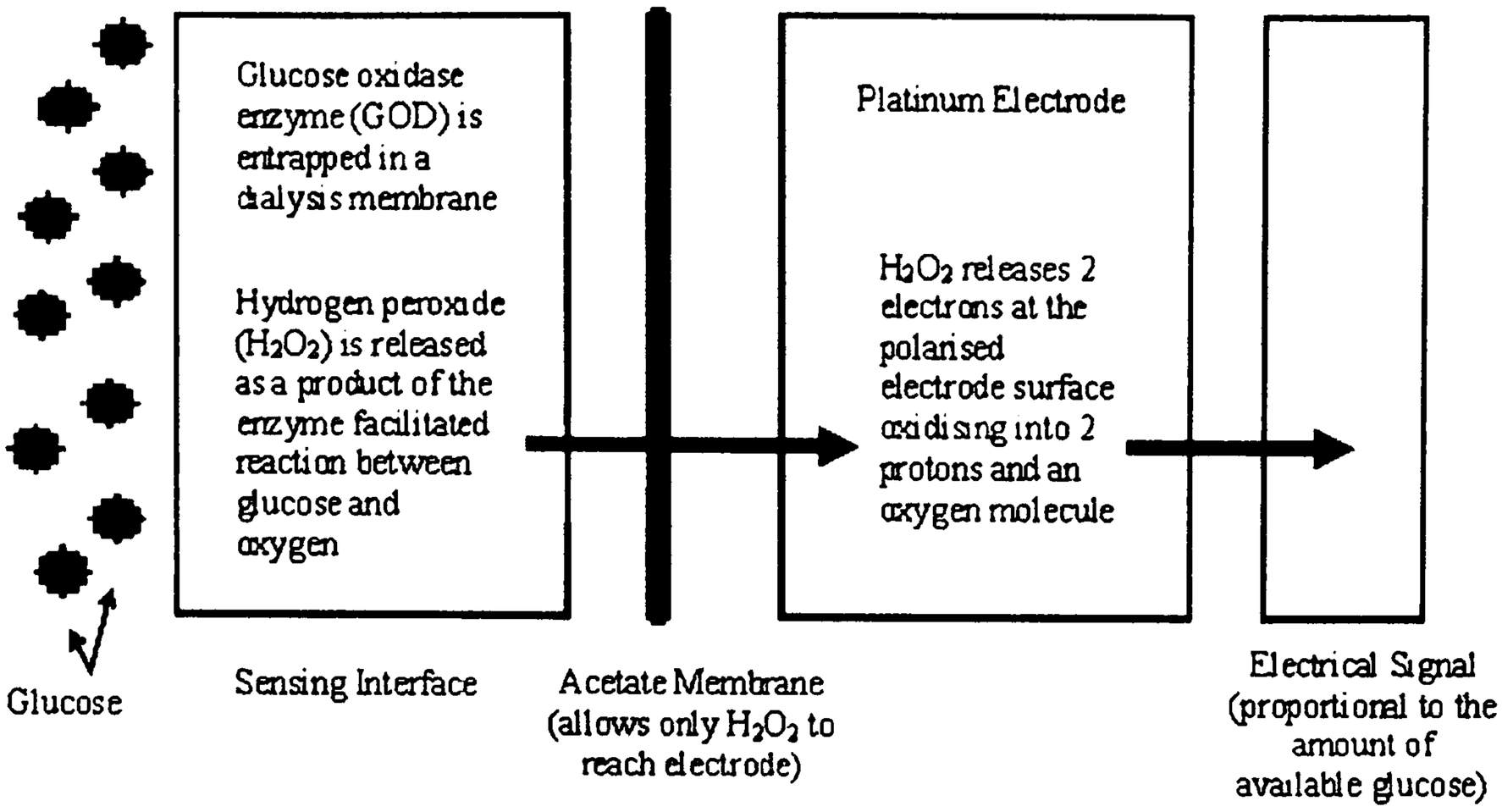

Figure 1.12: Glucose Biosensor

Polypyrrole-Enzyme Biosensors

Sun and Tachikawa (1992) studied the electrochemical behaviour of polypyrrole films incorporating glucose oxidase. They synthesised their films on glassy carbon working electrodes from a solution of the pyrrole monomer and the glucose oxidase enzyme. Varying synthesis time allowed them to consider films of different thickness. When they looked at the catalysis of glucose exposed to their films, by measuring the amperometric response current at the polarised modified electrode, they found a signal proportional to glucose concentration (Fig 1.13). They found that this response depended on film thickness. Their findings suggest that current responses are a function of hydrogen peroxide diffusion in the polypyrrole films, with thicker films being less permeable and the thinnest not carrying enough enzyme to generate a significant signal. These and other results helped to determine that optimal responses required pH 6-8 and *ca* 80 Å thick films. This means that direct measurements from blood samples would be possible.

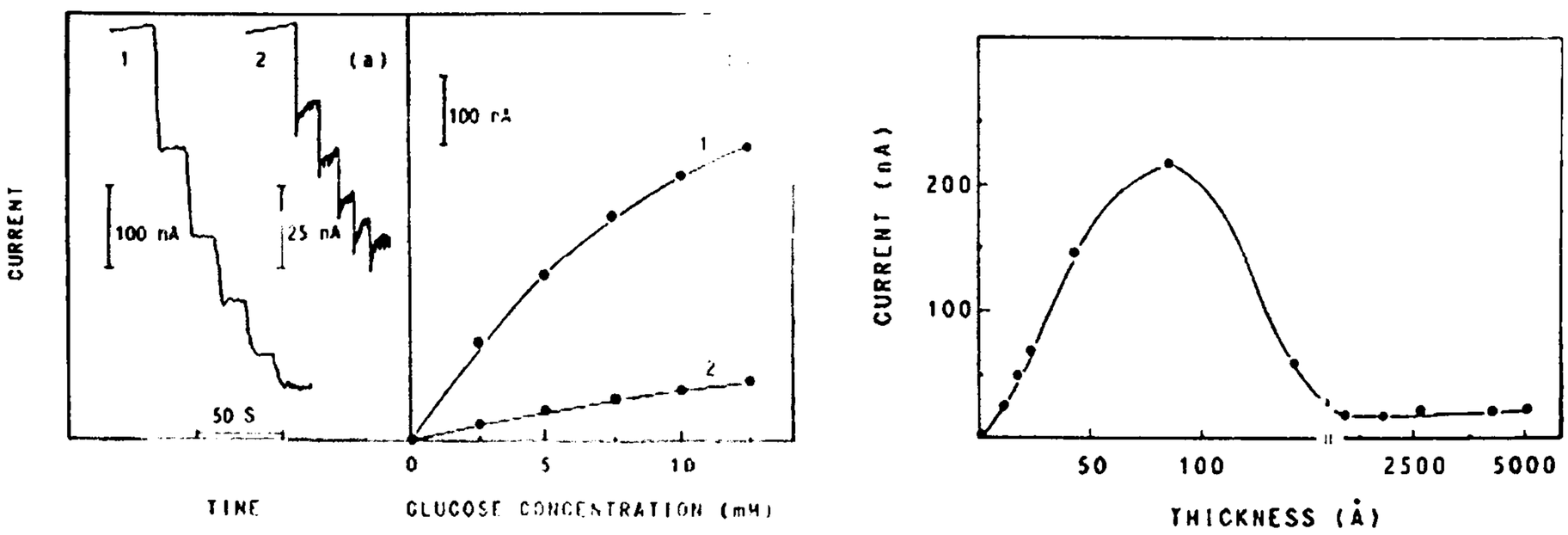

Figure 1.13: Catalytic Response of PPy-GOD to Glucose and Current *vs.* Thickness

(a) Successive Additions of 2.5 mM Glucose Solutions and (b) Calibration Curves in Phosphate Buffer (pH 7.4) solution (1) 80 Å Film and (2) 2000 Å Film

(Taken from Sun and Tachikawa, 1992)

Adejolu *et al.* (1996) incorporated urease with a conductive polypyrrole film producing a novel method to detect urea through flow injection. Their set-up consisted of an electrochemical flow-through cell where the working electrode was modified by the polypyrrole-urease film. When a solution carrying urea flowed through the cell at a specific rate, both catalysis and amperometric detection were performed at the electrode site. They studied the effects of flow rate, applied potential, buffer concentration, pH, polymerisation period, urease and urea concentrations and inorganic interference on the biosensor. They concluded that the biosensor allowed for the determination of urea between concentrations of 3 and 15 mg/L. However, they raised concerns about its use in complex samples such as blood or urine due to false signals recorded in the presence of other analytes such as ammonia and ammonium chloride.

Polypyrrole-Cell Biosensors

Whole cell biosensors are devices where the biological sensing component is a living cell and they have been considered by numerous researchers (Shear *et al.*, 1995; Bousse, 1996; Hodgson *et al.*, 1996). Also, the possibility of detecting or monitoring cell metabolites and behaviour has been vigorously pursued (Parce *et al.*, 1989; Ehret *et al.*, 1997; Cui *et al.*, 2001). In terms of conducting polymers, Campbell *et al.* (1999) have demonstrated the feasibility of incorporating erythrocytes into conducting polymers (discussed earlier) and suggested their use as biosensors. They showed that Rh (D)

antigens on erythrocytes remained intact after inclusion in polypyrrole and in the presence of antibody a resistometric signal indicated antigen/antibody binding. They concluded that erythrocyte-loaded polymers could be used as the basis of a novel blood group, antibody detection, immuno-biosensor.

Thus, polypyrrole based conducting polymers could offer unique ways of monitoring biological cells and through the incorporation of specific antibodies or enzymes, the possibility to detect cell metabolites. In the last example, resistometry was used to 'read' the antigen-antibody binding events. Electrochemical impedance spectroscopy is a similar but more powerful technique with the same advantage of reagentless sensing. The next section provides an overview of the technique and examples of its use.

1.4 Electrochemical Impedance Spectroscopy

1.4.1 Definition

Impedance may be defined as the total opposition a system or circuit offers to the flow of an alternating current (AC) at a given frequency. In direct current (DC) circuits, the resistance (R) is given by Ohm's law, R = V/I. The same law applies to AC circuits as well, but the resistance is termed impedance (Z), where $Z = \Delta V/\Delta I$. Electrical impedance is thus analogous to resistance, but is a more wide-ranging concept as it considers phase differences in the response of the target system. For convenience, it is represented as a complex quantity that can be shown on a vector plane. An impedance vector consists of a real part (resistance, Z') and an imaginary part (reactance, Z'') as shown in Figure 1.14. The reactance can be capacitive, inductive or a combination of both depending on the nature of the test system. The total impedance of a system can be expressed using either the rectangular co-ordinate form, $Z = Z' + iZ''$, or the polar form as a magnitude and phase angle, $Z = |Z| \angle \theta$.

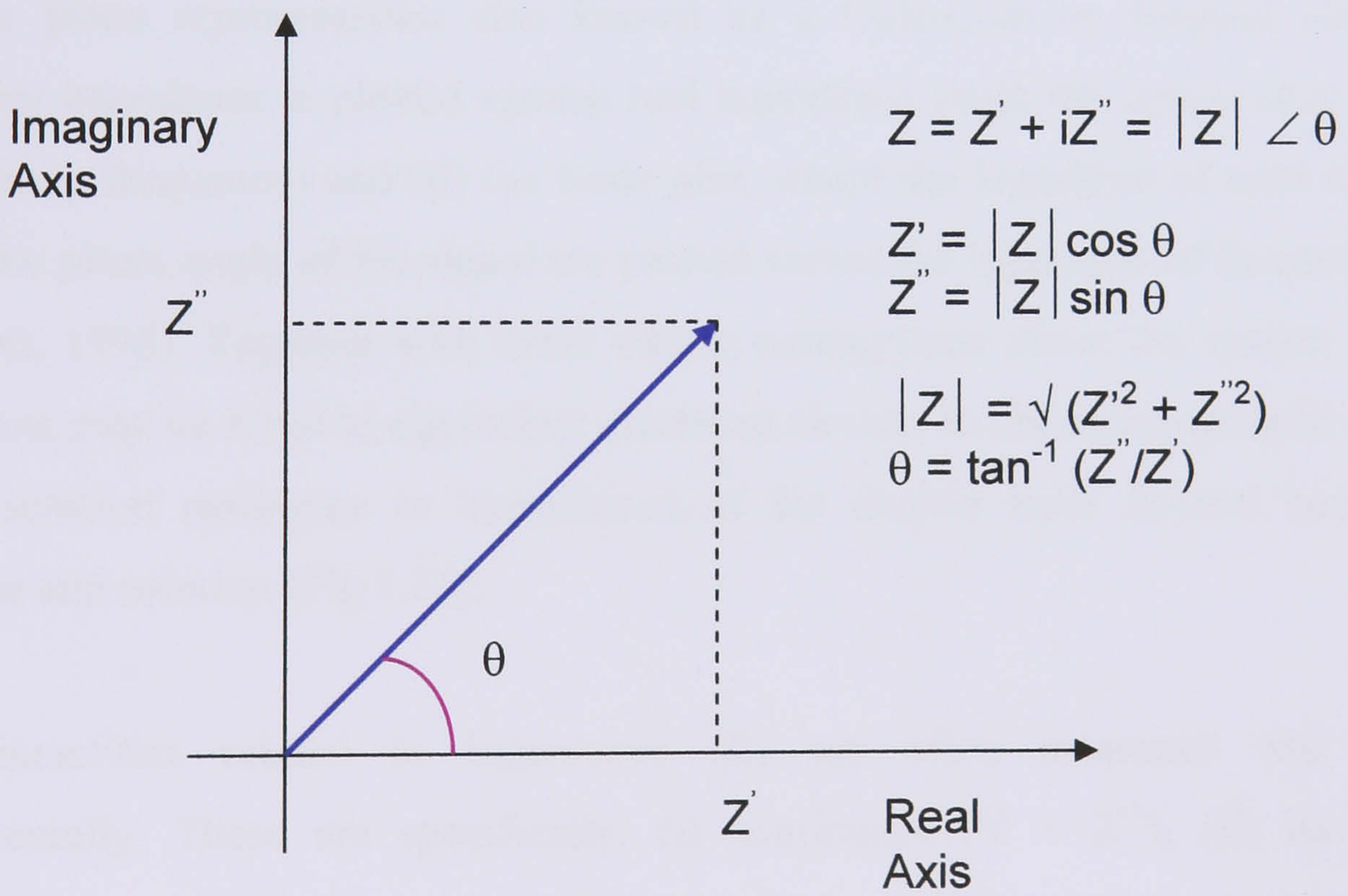

Figure 1.14: Vector Plane Representation of Impedance and Mathematical Relationships between the Terms (Adapted from Honda, 1989)

Electrochemical impedance spectroscopy (EIS) is a technique that measures Z as a function of frequency. In practice, an impedance analyser connected to a computer is used nowadays, and the whole process is automated over a wide frequency range. It is a powerful analytical tool for characterising many of the electrical properties of materials and their interfaces with electronic electrodes and/or ionic solutions. It may indeed be used to investigate the dynamics of bound or mobile charge in the bulk or interfacial regions of any kind of solid or liquid material: ionic, semiconducting, mixed electronic-ionic, and even insulator (Macdonald, 1987).

In electrochemical systems, current is composed of Faradaic and capacitive parts that may be respectively expressed in terms of a resistance and capacitance. Therefore, these systems are often considered as electrical elements in specific configurations, namely resistors and capacitors, with additional elements existing for more complex behaviour. During potentiostatic EIS, when a sinusoidal potential (AC potential) is applied at a specific frequency to the electrochemical system, the ensuing sinusoidal current (AC current) signal has a specific phase shift and amplitude in relation to the AC potential (Fig 1.15). The data from multiple frequency tests are then collated and expressed on an impedance spectrum plot. Two types of representations are commonly used: (i) the complex plane representation also known as a Cole-Cole or Nyquist plot, where imaginary impedance is plotted against real impedance (with the option of a third axis representing frequency) and (ii) the Bode plot, where the logarithm of total impedance and/or the phase angle of the signal are plotted versus the logarithm of frequency (Brett and Brett, 1998). Together with some simple assumptions about the system make-up, these plots may be fitted to equivalent electrical circuits to obtain meaningful data such as the solution resistance or capacitance at the double layer formed between the electrode and solution (Fig 1.16).

Other quantities related to impedance (Z) are often measured and analysed experimentally. These are specifically: (i) admittance ($Y = Z^{-1}$), (ii) the modulus function ($M = i\omega C_c Z$ where C_c is the capacitance of the empty cell and ω is the frequency) and (iii) the complex dielectric permittivity ($\varepsilon = M^{-1}$). These quantities are generically called immittances and all four are important in EIS especially due to their different dependence on and weighting with frequency (Macdonald, 1987).

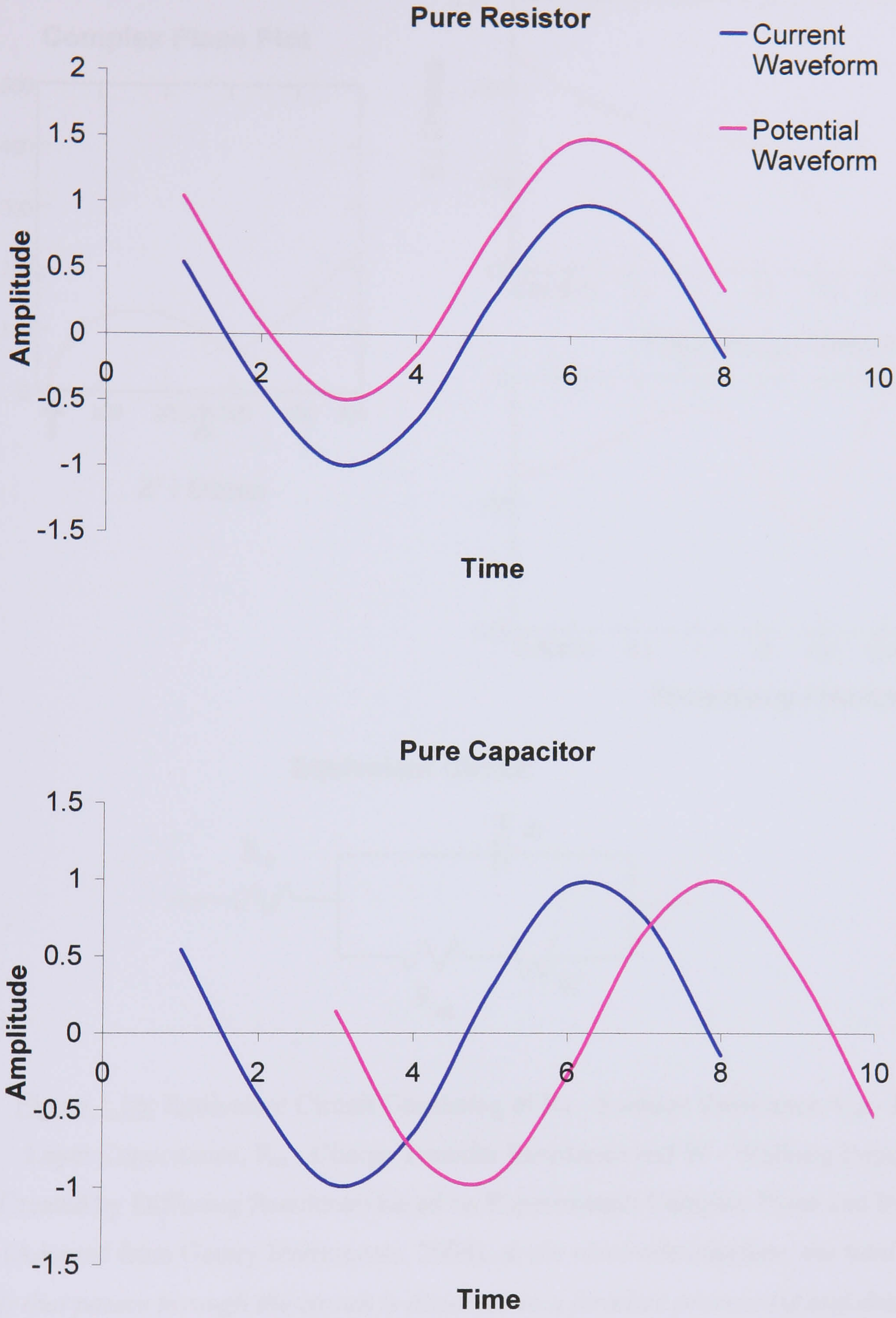

Figure 1.15: AC Potential and Resulting AC Current

For a pure resistor, $\theta = 0°$ (in-phase) and for a pure capacitor, $\theta = 90°$ (out-of-phase).

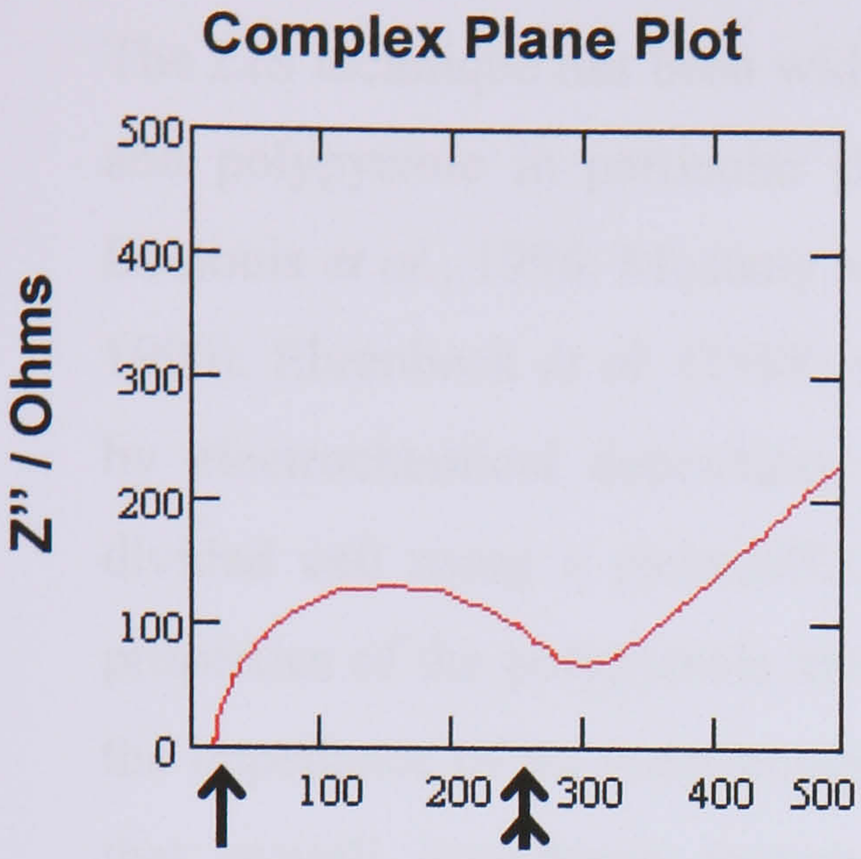

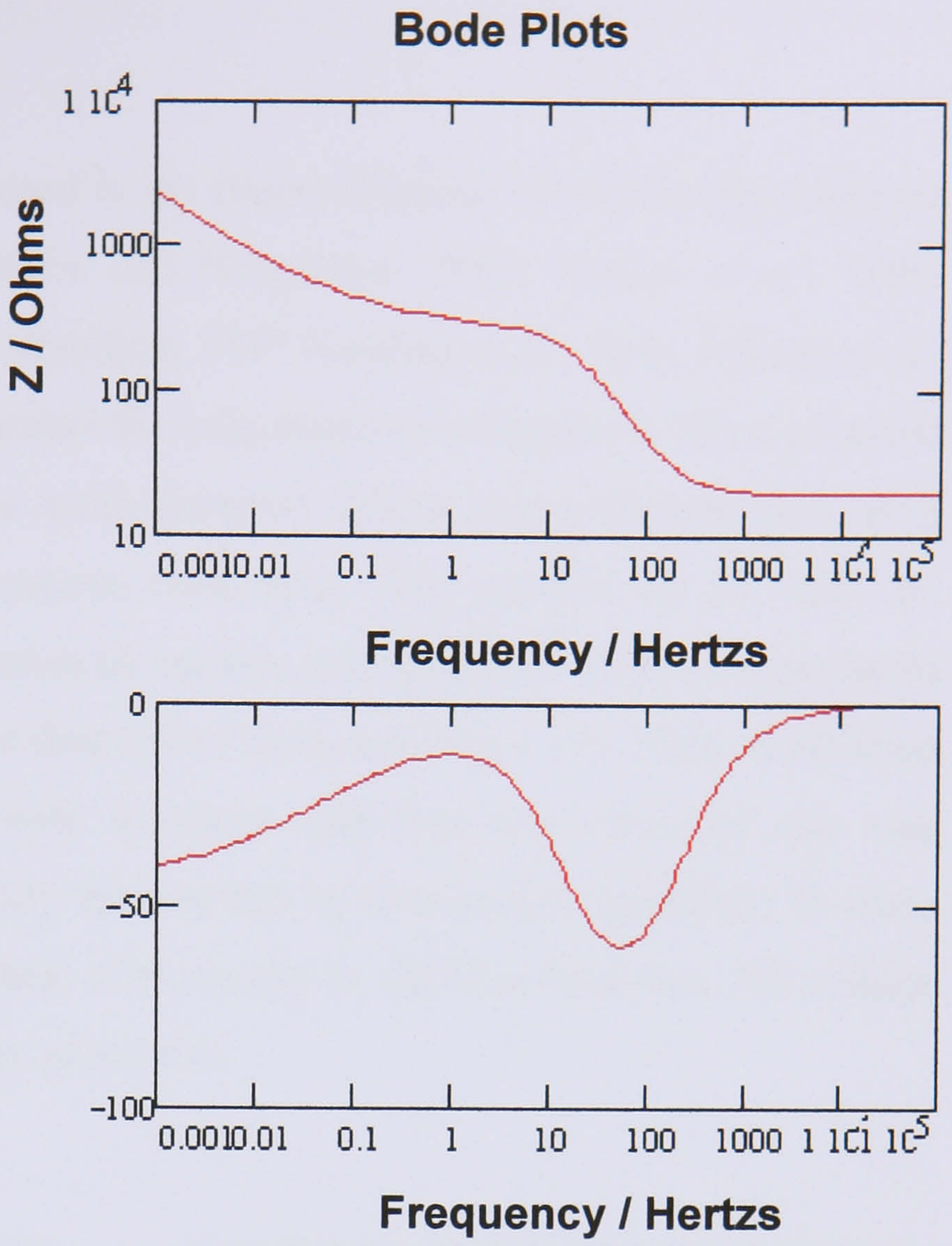

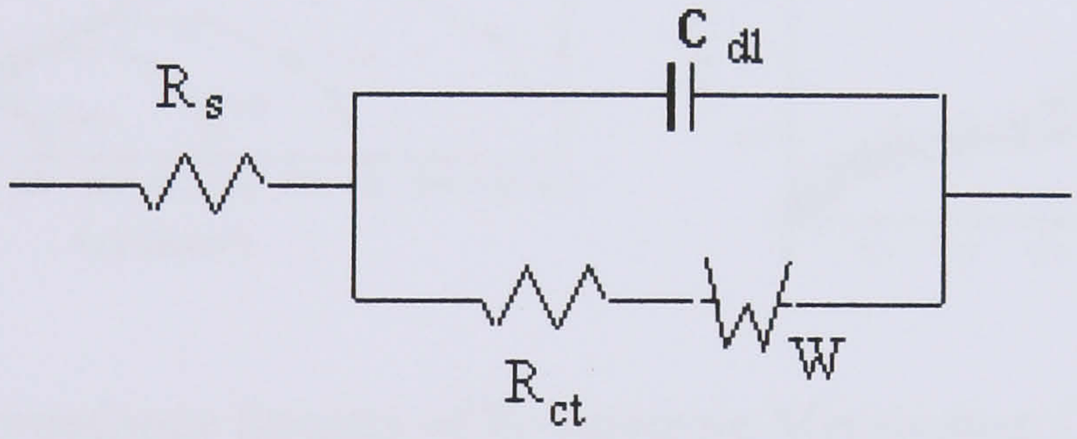

Figure 1.16: Equivalent Circuit Consisting of R_S - Solution Resistance, C_{dl} - Double Layer Capacitance, R_{ct} - Charge Transfer Resistance and W - Warburg Impedance (Created by Diffusing Reactants) based on Experimental Complex Plane and Bode Plots (Adapted from Gamry Instruments, 2004). *At the electrode interface, the total current (i) that passes through the circuit is divided into a faradaic process (i_f) and double layer charging (i_c) which are respectively represented as R_{ct} and W in parallel with C_{dl}. The current must then pass through the solution represented by R_s. On the complex plane plot, R_s is deduced from the intersection with the real impedance axis at low frequencies (single arrow) and R_{ct} from the intersection of the semi-circle projection at higher frequencies (double arrow).*

1.4.2 Applications

The EIS technique has been widely used in the characterisation of conducting polymers and polypyrrole in particular (Popkirov and Barsoukov, 1995; Ferloni *et al.*, 1995; Deslouis *et al.*, 1996; Mostany and Scharifker, 1997 Komura *et al.*, 1998; Refaey *et al.*, 1999). Ehrenbeck *et al.* (1998) measured the impedance of polypyrrole films prepared by electrochemical deposition on a gold-sputtered porous polycarbonate film in a divided cell using a pyrrole/KCl aqueous electrolyte. They studied the DC and AC properties of the polypyrrole membranes by various arrangements. They also measured the impedance of the membranes as a function of thickness (Fig 1.17). They established that overall impedance increased with thickness and that this observed rise was proportional to the film thickness. They showed this by obtaining a significant fit when plotting the normalised impedance data, with respect to the film thickness, for a range of film thickness on the same complex plane plot.

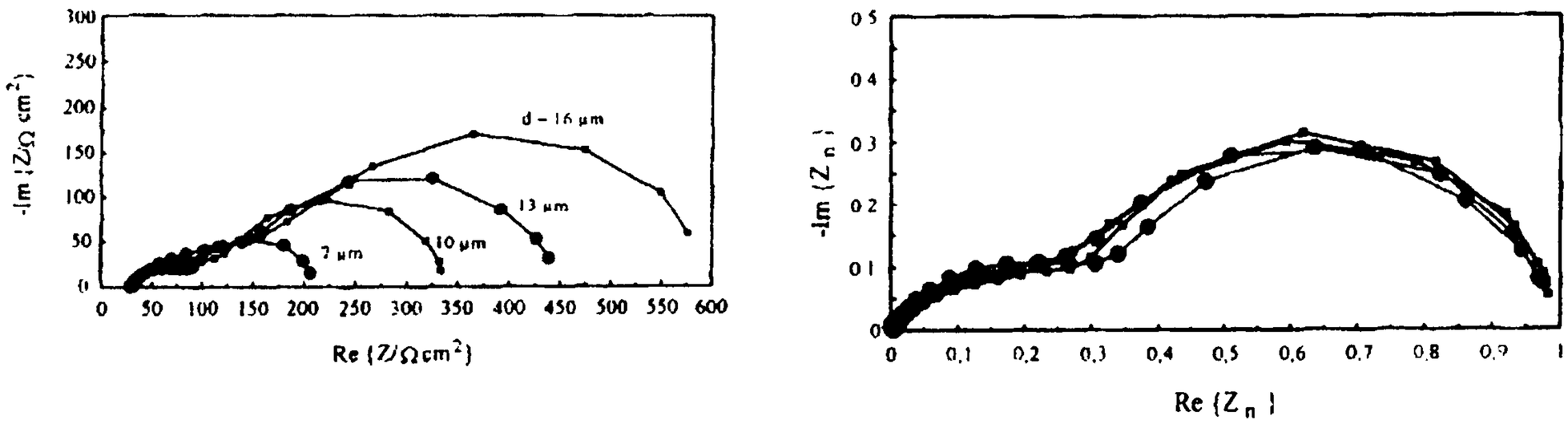

Figure 1.17: Impedance Spectra of Polypyrrole Membranes Obtained at Different Film Thickness (Left) and after Normalisation (Right)

Im: Imaginary Impedance and Re: Real Impedance

(Taken from Ehrenbeck *et al.*, 1998)

EIS can be used as a characterisation tool for materials such as polypyrrole, but also as a way of qualifying and/or quantifying analytes as in the case of biosensors. For instance, Lillie *et al.* (2001) exploited the possibility of loading polypyrrole films with antibodies and the EIS technique to develop a reagentless biosensor. They polymerised polypyrrole films incorporating avidin or antibody to leuteinising hormone (LH) on gold interdigitated electrodes and employed impedance spectroscopy to detect the responses of the loaded films to their relevant binding partners. When they exposed their films to

biotin in the case of avidin loaded films and LH in antibody loaded films respectively, they found significant responses in terms of impedance parameters. However, this response was only achieved following redox cycling. They suggested that this might be due to the realignment of the polymer chains around the bound complex following cycling. Their results suggest the possibility of determining non-degradative binding events without need for a label. Guan *et al.* (2004) have recently reviewed the use of enzyme, immuno-binding, nucleic acid and cell based impedimetric biosensors.

1.4.3 Bioimpedance

Impedance techniques have also been used to study the electrical properties of biological tissues, a discipline known as bioimpedance and bioelectricity (Grimmes and Martinsen, 2000). Electrical impedance tomography (EIT) is an example of a clinical application to emerge from these studies (Barber and Brown, 1984). Through direct application of electrode arrays onto patients, EIT is used to safely and non-invasively image cross-sections of living tissue by taking advantage of differences in their passive electrical properties. Electrochemical impedance spectroscopy using two, three or four electrode systems, less complicated in set-up and data interpretation than EIT has been used to investigate cells and tissues since the early 20th century. Importantly, these initial studies established the frequency dependant dielectric properties of biological materials.

Since their initial paper on the monitoring of fibroblast behaviour with an applied electric field (1984), Giaever and Keese have led research into the use of EIS to study the behaviour of anchorage dependant cells. Their set-up consisted of a modified polystyrene tissue culture well with red wax used to insulate electrodes and their connections from culture media (Fig 1.18). This left 4 small working electrodes (*ca* 3 × 10^{-4} cm^2) and one large counter electrode (*ca* 2 cm^2) exposed to cells in culture media which, during recordings, acted as an electrolyte. Measurements were carried out on one working electrode at a time connected to the counter electrode by a phase-sensitive lock-in amplifier with data collected on a chart recorder. The relative sizes of the electrodes meant that the measured impedance was dominated by the impedance at the interface between the tissue culture medium and the small working electrode. In that first study, they cultured mammalian fibroblasts directly on evaporated gold electrodes

subjected to a small potential (0.1 V) oscillating at 4000 Hz and reported cell induced changes in the resulting impedance. They explained the observed increases and fluctuations in impedance as the result of cell attachment and movement on the working electrodes causing variable obstruction to current flow.

In further published studies, they went on to show the sensitivity of their set-up in monitoring for instance the kinetics of cell attachment on various pre-adsorbed protein layers including fibronectin (1986). They demonstrated cell motility at the nanometer scale termed 'micromotion' and a mathematical model of this phenomenon that could be used to calculate the distances between the basal cell surface and the substratum (1989; 1991). They considered the effects of temperature, glucose starvation and the cytochalasin D drug on cell motion (Lo *et al*., 1993). They also looked at the effects of the prostaglandin E_2 drug (Smith *et al*., 1994), pulsed ac fields (Ghosh *et al*., 1994), and fluid flow (DePaola *et al*., 2001) on cell morphology as detected by impedance.

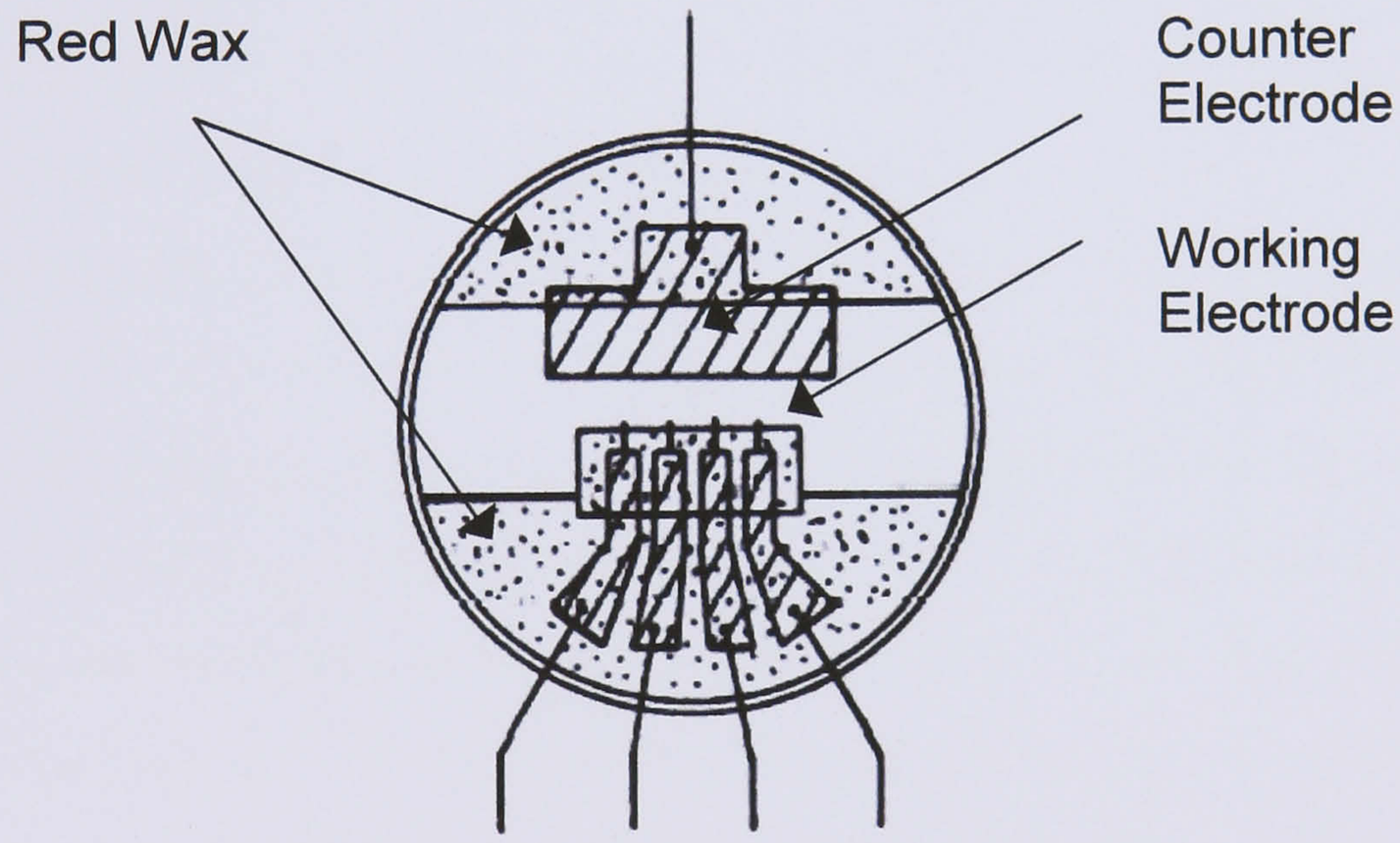

Figure 1.18: Modified Tissue Culture Dish for the Direct Measurement Impedance
(Adapted from Giaever and Keese, 1984)

Work by others has also confirmed the ability to monitor adherent cells through impedance. Wegener *et al*. (1996) used the technique to evaluate transepithelial and transendothelial resistance of cultured cell monolayers by subsequent equivalent circuit modelling. Another research group monitored the attachment, spreading and migration of cell populations and single cells on microelectrodes using impedance (Lind *et al*.,

1991) whilst Ehret *et al.* (1997) used interdigitated electrodes to measure cell growth under various conditions. Giaever and Keese's method, which they rebranded 'ECIS™' (Electrical-Cell Substrate Impedance Sensing), culminated in the establishment of a commercially available automated cell monitoring instrument of an improved design (Applied Biophysics Inc., New York, USA). The advantage of such a system is that it is non-invasive and does not require expensive reagents after initial purchase costs. Limitations would include the fact that the set-up only applies to fully adherent cells with the best results obtained for tight junction forming cells. Giaever and Keese's work and that of others shows that it is the physical obstruction and thus inhibition of current flow by cells during spreading and migration on the electrode surface that produces the impedance signals with variations depending on frequency and on whether it is resistive or capacitive effects that result (Wegener *et al.*, 2000). Numerous laboratories have gone on to use this ECIS™ system to study various aspects of cell biology. To date, no published data is available on the modification of these electrodes with conducting polymers for subsequent growth and impedance monitoring of cells.

1.5 Project Concept and Aims

The concept for this project stems from previous research which demonstrated reagentless bioaffinity sensing of proteins using polypyrrole-antibody composites in combination with EIS (Lillie, 2001; Lillie *et al.*, 2001). The question was asked whether this system could be adapted to biological cell sensing as previously achieved by other researchers with bare gold electrodes. The proposition was that polypyrrole modified electrodes could provide significant advantages or offer new opportunities over the standard gold electrodes of the past. In particular, it was hypothesized that the incorporation of relevant biological molecules such as dermatan sulphate, which is abundant in the extracellular matrix of skin, would lead to increased interactions between keratinocytes and polypyrrole thus improving the capability for impedimetric detection when compared to uncoated gold surfaces.

Project aims were therefore to develop and perform appropriate experiments to test this novel hypothesis. This included (*i*) the design of appropriate experimental rigs and methods, (*ii*) the synthesis of polypyrrole composites and (*iii*) their characterisation in terms of physical properties as well as on (*iv*) their ability to support cell growth. The final and principal objective was (*v*) the study of cells on polypyrrole based conducting polymers using EIS. The nature of the project was expected to be interdisciplinary and did indeed combine aspects of the life and physical sciences with contributions made in some areas of conducting polymer research (Fig 1.19). The experimental materials, instrumentation and methods employed are fully described in the next chapter. This is followed by result chapters on the synthesis and characterisation of polypyrrole films, growth of cells on these and their subsequent impedimetric sensing. The final chapter discusses the work presented in general and its implications along with future avenues to further the research initiated including the evaluation of some preliminary data.

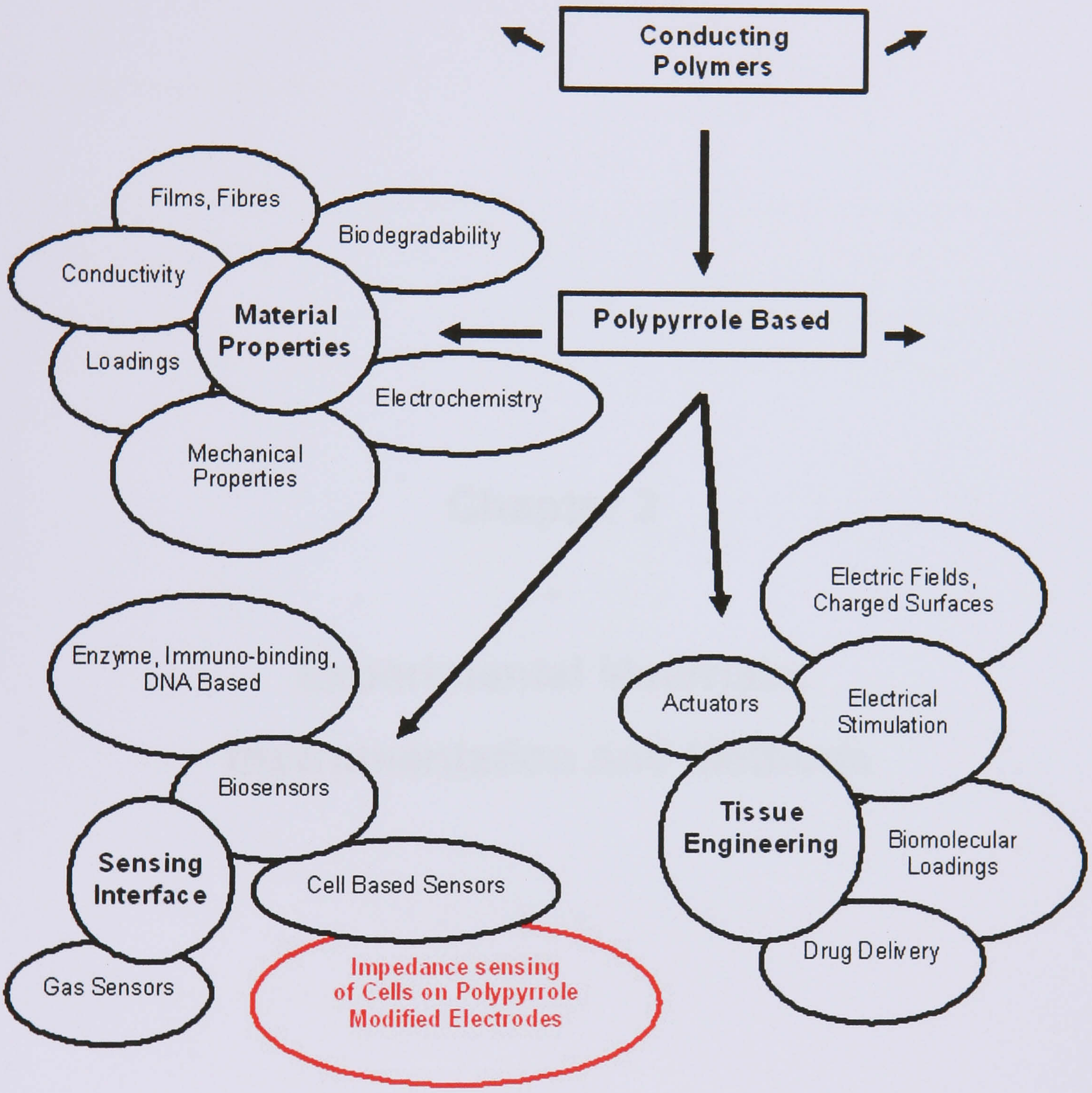

Figure 1.19: Examples of Polypyrrole Based Conducting Polymer Research Areas.

Chapter 2

Experimental Materials, Instrumentation and Methods

The full addresses for all source companies and organisations are listed at the end.

2.1 Materials

2.1.1 Electrodes and Substrates

Interdigitated Electrodes

Interdigitated electrodes (IDEs) were made on a silicon base, with a layer of silicon dioxide onto which the gold pattern was photo-etched (Fig 2.1). The spacing between each digit was 15 μm. The IDEs were manufactured by Dr Graham Ensell (Department of Electronics and Computer Science, University of Southampton, Southampton, SO17 1BJ, UK).

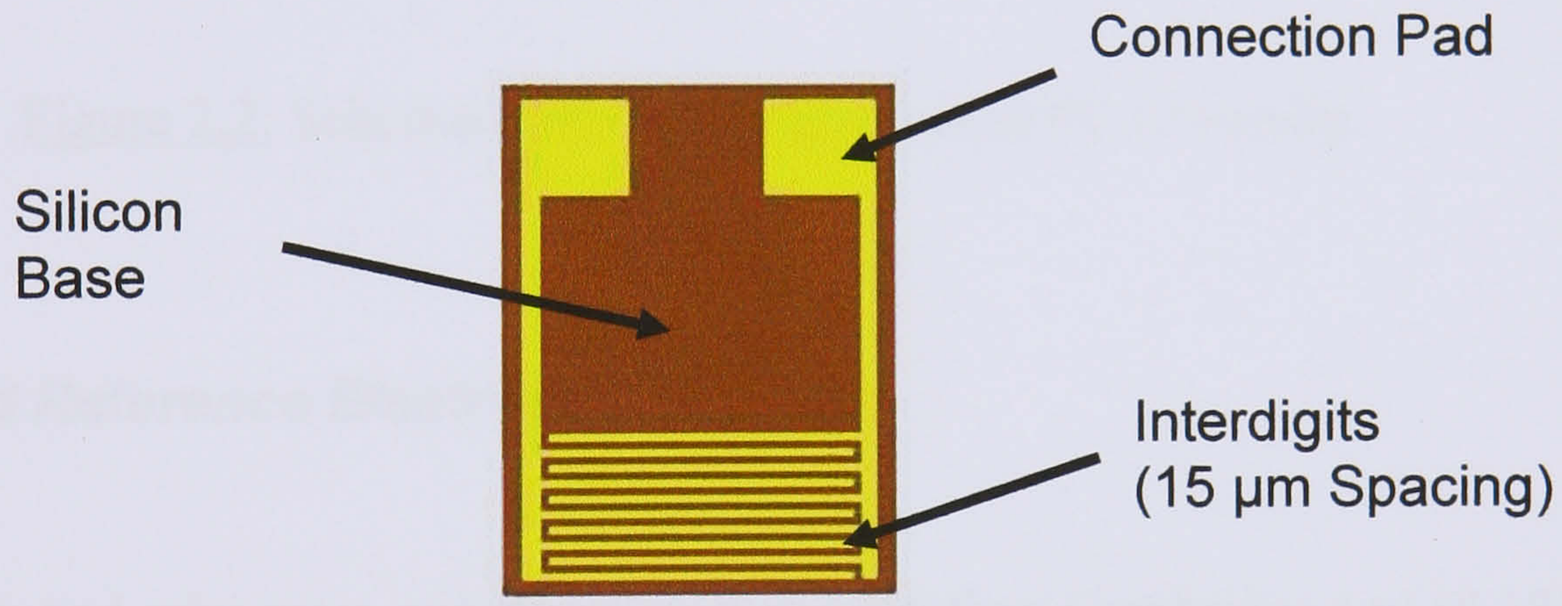

Figure 2.1: Schematic of the IDE.

Polycarbonate Substrates

Polycarbonate (PC) coverslips were purchased from Sigma-Aldrich Company Ltd in two different sizes (# Z36-590-4 for 22 × 22 × 0.25 mm and # Z36-591-2 for 40 × 22 × 0.25 mm).

PC Isopore™ membranes were purchased from Millipore S. A. S. – Molsheim (# GTTP 025 00). They were Ø 25 mm, 7-22 μm thick with Ø 0.22 μm pores and had a total porosity between 5-20%.

These substrates were then either used as received or gold-coated by sputtering for 180 s at the closest height to the gold target (Mr Keith Pell, EM unit, School of Biological Sciences, Queen Mary University of London, London, E1 4NS, UK). Some of the larger PC coverslips were masked before sputter-coating to obtain three individually addressable gold digits, each *ca* 2 mm wide (Fig 2.2). The sputter-coating technique used has been reported for gold (Ehrenbeck *et al*., 1998) and other elements such as carbon or platinum (Wallace *et al*., 1999). It produced an ultrathin, optically transparent gold layer that adhered well to the polycarbonate substrate. The layer was highly conductive as verified by very low electrical multimeter resistance readings.

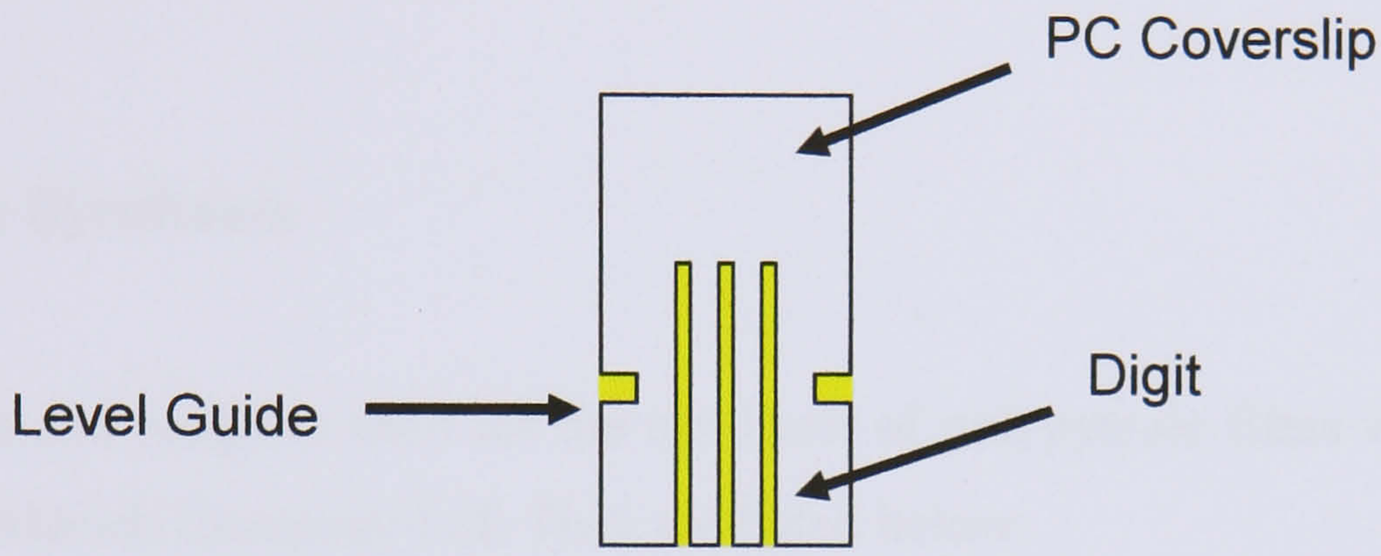

Figure 2.2: Schematic of Gold Digit-Coated PC Coverslip.

Counter and Reference Electrodes

Platinum mesh and wire were purchased from Goodfellow Cambridge Ltd (# 183-742-38 and # 620-377-72) to make counter electrodes. The mesh was cut into squares (*ca* 10 × 10 mm) leaving a total exposed area of *ca* 122 mm^2 that could be immersed in electrolyte.

Silver-silver chloride (Ag/AgCl) reference electrodes were used. These were either purchased pre-fabricated from Bioanalytical Systems Inc (# MF 2079) or self-made by chloridising a silver wire purchased from Goodfellow Cambridge Ltd (#017-233-06) in a dilute solution of hydrochloric acid (Janz, 1961).

Glassware and Disposable Plastics

These items were generally available sterile to the laboratory and included standard laboratory glass beakers, microscope slides, tissue culture polystyrene (TCPS) flasks, well plates, centrifuge tubes, pipette tips and other accessories for use in experiments and cell culture. Various suppliers were used (Costar®, Falcon™, Sterilin® and Corning®).

2.1.2 Chemicals and Reagents

Polypyrrole Synthesis

All chemicals and reagents used for the synthesis of polypyrrole films were purchased from Sigma-Aldrich Company Ltd. They are listed below:

- Pyrrole (C_4H_5N) – # P4892
- Sodium Chloride (NaCl) – # S7653
- Iron (III) Chloride ($FeCl_3$) – # F7134
- Sodium Hydroxide (NaOH) – # S8045
- Sodium Dodecyl Sulfate ($CH_2[CH_2]_{11}OSO_3Na$) – # L4509
- Polyvinyl Sulphate Potassium Salt (CH_2CHKO_3SO) (PVS) – # P6000
- Heparin Sodium Salt (Hep) – # H3400
- Dermatan Sulfate Sodium Salt (Chondroitin Sulfate B) (Derm) – # C3788
- Fibrinogen from Bovine Plasma (Fbri) – # F8630
- Fibronectin from Bovine Plasma (FN) – # F4759
- Collagen from Rat Tail (Col) – # C7661

Tissue Culture

Three main cell culture media compositions were obtained from Cancer Research UK:

E4: This was Dubelcco's modified Eagle's medium (DMEM) which includes inorganic salts, amino acids and vitamins.

E4, F12: This composition was made from 3 parts DMEM and 1 part Ham's F12. In addition, upon receipt from Cancer Research UK (CRUK), the following compounds obtained from Sigma-Aldrich Company Ltd were added:

- 0.4 μg/ml hydrocortisone - # H1009
- 10^{-10} M choleratoxin - # C9903
- 5 μg/ml transferrin - # T2252
- 2×10^{-11} M liothyronine - # T2877
  Initially dissolved in 1 part HCl and 2 parts ethanol
- 1.8×10^{-4} M adenine - # A9126
  Initially dissolved in NaOH at pH 9
- 5 μg/ml insulin - # I5500
  Initially dissolved in 0.05 M HCl
- 10 ng/ml EGF - # E1257

This mix was called RM+ medium.

Phenol red free E4, F12: This was the same composition as above except that media was obtained from CRUK without the phenol red (P/R) indicator. This mix was called RM+ -P/R medium.

The three compositions above were also further modified by addition of 10% foetal bovine serum (FBS) from Sigma-Aldrich Company Ltd (# F1051) and 1% L-glutamine from Invitrogen Ltd (# 13563) for tissue culture purposes.

For passaging cells, Ca^{2+} and Mg^{2+} free phosphate buffered saline (PBS), 0.05% trypsin and 0.02% ethylenediaminotetraacetic acid (EDTA or versene) solutions were obtained

from Cancer Research UK. In addition to FBS, dimethyl sulphoxyde (DMSO) purchased from VWR International Ltd (# 420931Q) was used for liquid nitrogen cryopreservation of cells. Industrial methylated spirits (IMS) obtained from the Royal London Hospital was used for sterilising equipment that could not be autoclaved.

For Experiments

Chemicals and reagents used are grouped below according to their source:

Agar Scientific Ltd:

- Osmium tetroxide - # R1022

BioGenex Laboratories Inc:

- 3, 3' – Diaminobenzidine chromogen solution (DAB) - # AD000-5M

Biosource UK

- AlamarBlue™ - # DAL1100

BOC Gases:

- Nitrogen gas cylinder - # L925

Cancer Research UK:

- 10% Formaline
- PBS

DakoCytomation Ltd:

- Mouse monoclonal proliferating cell nuclear antigen (PCNA) - # M0879

Gifts:

From Dr Muy-Teck Teh (Centre for Cutaneous Research, Queen Mary University of London, 4 Newark Street, London, E1 2AT, UK):

- Lysis buffer (0.05 M Tris Buffer, 1 mM $MgCl_2$, 0.2% IGEPAL)
- Protein lysis buffer (5 ml of 1 M Tris pH 8.5, 20 ml of 10% SDS, 200 µl of Na_2VO_4 and 75 ml of H_2O)

From Mr Keith Pell (EM unit, School of Biological Sciences, Queen Mary University of London, London, E1 4NS, UK):

- Uranyl acetate

Invitrogen Ltd:

- Fungizone - # 15290-026

Promega UK

- Cell-Titer Glo™ - # G7570

Royal London Hospital:

- Mouse monoclonal K10 antibody - # LHP2
- Mouse monoclonal K16 antibody - # LL025

Sigma- Aldrich Company Ltd:

- Bradford Reagent - # B6916
- Gentomycin - # G1397
- Glutaraldehyde - # G5882
- Hexamethyldisilazane (HMDS) - # H4875
- Mytomicin C - # M0503
- Paraformaldehyde - # P6148
- Penicillin-G - # PEN-NA
- Rhodamine B - # R6626
- Sodium cacodylate - # C0250
- Streptomycin Sulphate - # S0890
- Tannic acid - # T0125
- Trypan Blue - # T8154

Vector Laboratories Inc:

- Vectastain® Universal *Elite*® ABC Kit - # PK-6200

VWR International Ltd:

- Acetone - # 100033P
- DePex mounting medium - # 361252B
- Ehrlich's Haematoxylin - # 350175T

- Ethanol - # 283047K
- Methanol - # 101586B
- Xylene - # 102936H

2.1.3 Cells and Tissues

The human SVK14 keratinocyte cell line was obtained cryopreserved from the Centre for Cutaneous Research (Queen Mary University of London) and expanded. The Swiss mouse 3T3 fibroblast cell line (strain J2) was obtained in falcon tubes from Cancer Research UK and expanded. The human RTS3b squamous cell carcinoma (SCC) keratinocyte cell line was obtained cryopreserved from Dr Muy-Teck Teh and expanded.

Primary human keratinocytes and fibroblasts were obtained cryopreserved from Dr Nkemcho Ojeh (Centre for Cutaneous Research, Queen Mary University of London) who had previously isolated them from discarded infant foreskin after circumcision at the Royal London Hospital. This was under ethical committee approval (# T/01/034) and informed patient (or guardian) consent. The cells were expanded for use in experiments.

Cadaveric skin was kindly supplied (glycerol preserved) by Dr Nkemcho Ojeh ordered from the European Skin Bank in Holland.

2.2 Instrumentation

2.2.1 Electrochemical and Tissue Culture Cells

Electrochemical cells combining as tissue culture wells (ETCCs) were designed and fabricated in-house to enable reproducible deposition of polypyrrole films onto gold-coated PC coverslips, and then to facilitate their use as tissue culture substrates. These were manufactured by workshops in the Materials Department (Mr Vincent Ford, Materials Dept, Queen Mary University of London, London, E1 4NS, UK).

The ETCC and its components (Fig 2.3) consisted of two main detachable parts: A top plate made from transparent Perspex® (76 × 26 × 20 mm) with a cavity drilled out in its centre (15 × 18 × 20 mm) along with two screw holes on either side and a bottom plate made from polyvinyl chloride (76 × 26 × 2 mm) also with a cavity in its centre and screw holes. A gold-coated PC coverslip could thus be inserted between the two plates to form the lower surface of a well (edges sealed with PTFE tape from Homebase Ltd). This construct was held together with medical grade stainless steel (A4 316 S16) screws, washers and nuts (RS Components Ltd, # 130-656, # 527-381 and # 293-117) onto which the reference and counter electrodes could be mounted.

The assembled device was used in the synthesis and characterisation of polypyrrole films on gold-coated PC coverslips. It was further used as a tissue culture well for cell growth on gold or polypyrrole substrates when either impedance was monitored or electrical stimulation applied. The cavity in the lower plate of the device enabled optical monitoring of cells by inverted microscopy during culture.

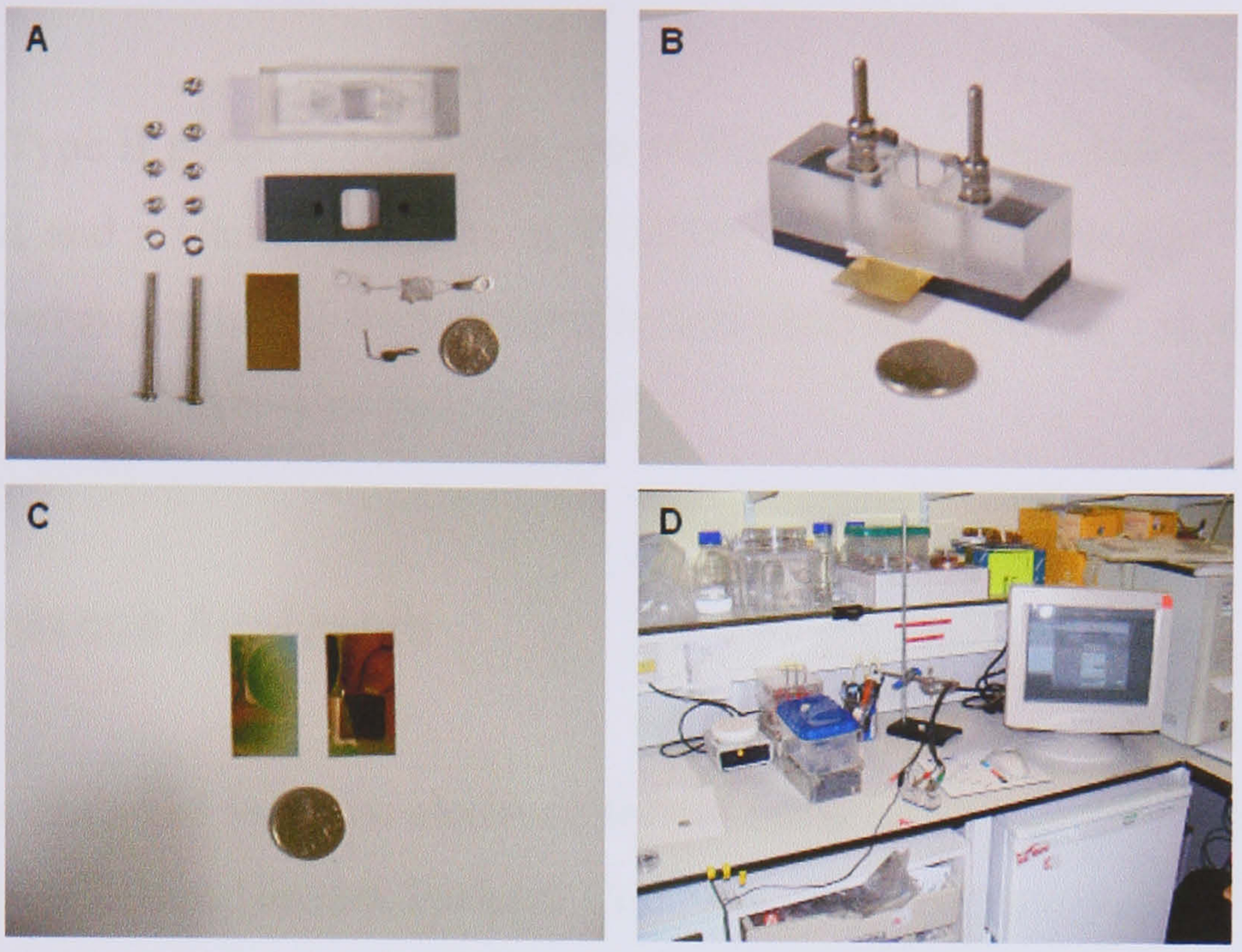

Figure 2.3: Electrochemical and Tissue Culture cell

(A) Components, (B) Assembled Cell, (C) Coverslips Before and After Polypyrrole Synthesis and (D) Polypyrrole Synthesis by Potentiostat.

2.2.2 ETCC Accessories

In order to maintain sterility during experiments involving cells, the ETCCs were placed in Perspex® boxes (Fig 2.4) that were modified by fitting screws, wires and connectors (RS Components Ltd, # 130-656, # 527-381, # 293-117, # 361-8733, # 483-837 and # 405-455 or -461). This allowed for the ETCCs to be linked to the potentiostat even whilst inside the incubators.

Figure 2.4: Example of Perspex® Box and Wiring.

2.2.3 Potentiostats

A μAutolab Type II potentiostat/galvanostat (GPES software) purchased from Windsor Scientific Ltd and a Gamry Instruments PC4/300 potentiostat (PHE200^{TM} and Echem Analyst software) purchased from Scientific and Medical Products Ltd were used for electrochemistry in a three-electrode format.

2.2.4 Impedance Analysers

EIS data was collected in a two-electrode format using an HP LF Impedance Analyser 4192A purchased from Hewlett Packard Company. The analyser included a two point test fixture for connection to the IDEs. Instrument control and data collection were performed with a previously written program (Section for Clinical Biochemistry, The University of Manchester, Hope Hospital, Clinical Sciences Building, Eccles old Road, Salford M6 8HD, UK) in LabVIEW software from National Instruments Corporation. The program performed logarithmic frequency sweeps between 5 Hz and 13 MHz recording a total of 130 data points over seven minutes. The data obtained could then be easily handled and presented within a spreadsheet package such as Microsoft® Excel.

EIS data was collected in a three-electrode format using the Gamry Instruments PC4/300 potentiostat (EIS300^{TM} and Echem Analyst software) from Scientific and Medical Products Ltd.

2.2.5 Microscopes

Light Microscopy

A Leica DM IRB inverted microscope, associated digital camera and software from Leica Microsystems (UK) Ltd were used to take digital pictures of substrates and cells.

A Nikon Eclipse E600 microscope, associated digital camera and software from Nikon UK Ltd were used to take high magnification pictures of stained slide sections.

Electron Microscopy

A Jeol JSM 6300 scanning electron microscope (SEM) from Jeol UK Ltd was used.

2.2.6 Other Instruments

Multilabel Reader

A Wallac 1420 Victor multilabel counter and associated software purchased from PerkinElmer Life Sciences Ltd was variously used in the measurement of absorbance, fluorescence and luminescence.

Modelling Software

MATLAB® form Math Works Ltd was used in conjunction with the 'Complex Non-Linear Least Squares Fitting of the Cole Equation to Measured or Simulated Impedance Data' program written and gifted by Dr Alan Waterworth (Dept. of Medical Physics, The Royal Hallamshire Hospital, Glossop Road, Sheffield, S10 2JF, UK).

Statistical Analysis Software

SigmaStat® from SPSS UK Ltd was used for statistical analysis.

2.3 Methods

2.3.1 Polypyrrole Synthesis

Cyclic Voltammetry

Cyclic voltammetry was run in the three-electrode format. The electrolyte was always made up in distilled water (used throughout project) from 1 M pyrrole (freshly distilled) and either 50 mM NaCl, 50 mM SDS, 0.2 mg/ml PVS, Hep, Derm, Fbri, FN, or Col. Prior to use, the electrolyte was degassed by passing nitrogen gas for 5 mins. Scans were then run between -0.9 V and +0.8 V *vs.* Ag/AgCl at a rate of 50 mV/s with the number of cycles varied as stated in the result figures. Scans were always started and terminated at -0.9 V *vs.* Ag/AgCl. In the case of films polymerised on IDEs, the electrodes were immersed in a 10 ml beaker containing the appropriate electrolyte. For those polymerised on gold-coated coverslips, the ETCCs were employed. The polymerisation data was digitally collected and transferred to Microsoft® Excel for further presentation and analysis.

Chronoamperometry

This method was used for the vast majority of polypyrrole films studied during this project. The electrolytes were at the same concentrations as for cyclic voltammetry. However, the fixed potential and time were varied depending on polymer loading. Again, data was digitally collected and easily transferred to Microsoft® Excel for further presentation and analysis. The conditions for each loading were:

- PPy/Cl: +0.7 V *vs.* Ag/AgCl for 30s (thin) or 2700/5400 s (thick)
- PPy/PVS: +0.8 V *vs.* Ag/AgCl for 90s (thin) or 2700/5400 s (thick)
- PPy/Hep: +0.7 V *vs.* Ag/AgCl for 30s (thin)
- PPy/Derm: +0.8 V *vs.* Ag/AgCl for 180s (thin) or 2700/5400 s (thick)
- PPy/Fbri: +0.8 V *vs.* Ag/AgCl for 90s (thin)
- PPy/FN: +0.8 V *vs.* Ag/AgCl for 60s (thin)

- PPy/Col: +0.9 V *vs.* Ag/AgCl for 300s (thin) or 2700/5400 s (thick). Electrolyte pH was raised to between 8-8.5 by dropwise addition of a dilute NaOH solution

Unless otherwise stated all films were then washed for 3 days in distilled water or dilute HCl solution at pH 2 prior to use in cell culture.

Chemical Polymerisation

Chemical Polymerisation of PPy was also carried out by mixing an equal volume of a 50 mM $FeCl_3$ solution and a 0.5 M PPy solution. This was done either in the form of droplets on coverslips or in 4 ml Petri dishes. The reactions were allowed to run to completion.

2.3.1 Polypyrrole Characterisation

Scanning Electron Microscopy

Polypyrrole films on IDEs and gold-coated PC coverslips were viewed under the electron microscope by fixing on aluminium stubs. The IDE samples were uncoated and a low filament voltage of 5 kV was therefore used. Those on the gold-coated PC coverslip were carbon coated to prevent charging of the polycarbonate coverslip under the electron beam and viewed at a filament voltage of 10 kV. To view cross-sections, some of the polypyrrole films on the gold-coated PC coverslip were freeze-fractured to obtain a clean break in the absence of plastic deformation by dipping into liquid nitrogen and snapping. They were then fixed upright on the stubs.

Cyclic Voltammetry

Polypyrrole films were characterised by cyclic voltammetry in the three electrode format. The films were removed from their polymerisation solution and triple washed with water. They were then immersed into a degassed (by N_2) monomer-free 50 mM NaCl electrolyte. For IDEs this was done in a 10 ml beaker whereas the gold-coated PC

coverslips were left in their original ETCCs. Scans were run between -0.8 V and +0.2 V *vs.* Ag/AgCl at a rate of 50 mV/s for a total of 10 cycles. Scans were started and terminated at -0.8 V *vs.* Ag/AgCl.

Electrochemical Impedance Spectroscopy

For polypyrrole film characterisation on IDEs, two-electrode impedance (current is passed between the digits in the plane of the polypyrrole film) analysis was carried out. The tests were performed whilst the previously formed and triple washed polymers were exposed to water or PBS (a specially designed container was used to retain solutions over the polypyrrole whilst preventing contact with the test fixture). The test fixture, a 'tweezer-like' device held in place by a clamp, connected one set of the IDE fingers to the low connector (or floating electrical ground) and the other set of fingers to the high connector (or frequency generator) of the analyser. The custom-made LabVIEW program was allowed to run with the oscillating potential set to 20 mV and data was collected between 5 Hz and 13 MHz then exported to Microsoft® Excel for presentation and analysis. For the characterisation of sterilised films, they were first exposed to 70% (v/v) ethanol in 1.8 ml Eppendorf tubes for 2 or 72 h.

2.3.2 Tissue Culture

General Culture

In preparation for experiments and to maintain stocks, cells were cultured from frozen in standard flasks (175 or 75 cm^2) containing the appropriate culture media at 37° C and 10% CO_2. RM+ (10% FBS) was used for human SVK14 keratinocytes, RTS3B SCC keratinocytes and primary keratinocytes. E4 (10% FBS) was used for mouse 3T3 fibroblasts and human primary fibroblasts. In all cases, the same subculture protocols were used except that culture in the presence of γ-irradiated 3T3 fibroblast (6000 Rads, Co^{60} for 32 mins), also called feeders, was required for primary keratinocytes. Cell culture media was changed every 2-3 days. At approximately 70% confluency in flasks, cells were passaged (*i.e.* a 1/10 or 1/20 reduction of cell numbers was made). To passage the cells, old media was aspirated from the flask, and the cell layer was washed

with 5 mL of PBS then 5 mL of EDTA. Cells were detached from the flask substrate by exposure to a 5 ml 0.05% trypsin/0.02% EDTA solution for up to 10 mins. An equal volume of culture media was then added to the flask to inhibit the protease activity of trypsin. Repetitive pipetting was used to achieve optimal mixing of the cells in solution. Either 1 or 0.5 ml of solution was then left in the flask depending on the desired passage ratio (1/10 or 1/20) and fresh culture media added. In the case of primary keratinocytes the feeder population was replenished at this stage by addition of 2×10^6 γ-irradiated 3T3 cells per 75 cm^2 flask.

The remaining cells were either transferred to a centrifuge tube for the experiments, to other flasks to expand the population, frozen down or discarded. For experiments, the cells were counted using a haemocytometer and Trypan Blue to highlight dead cells. They were then spun at 1000 RPM for 5 mins and resuspended in fresh media prior to experiments. The quantity in the re-suspension media was calculated so as to deliver the required number of cells in an adequate volume of solution. For cryopreservation, the spun down cells were resuspended so as to deliver 2×10^6 cells for every 1.8 ml cryovial in a 10% DMSO/90% FBS solution. The vials were labelled, wrapped in tissue and stored at -70° for 1 week before transfer to liquid nitrogen. Revival of cells was done by thawing the cryovials in a 37° bath and rapidly transferring them to a culture media containing centrifuge tube. The cells were mixed by repetitive pipetting, spun down (1000 RPM, 5 mins) to remove the supernatant and then mixed again with fresh culture media before transfer to a flask.

Organotypical Cultures

Organotypical culture of primary keratinocytes at the air/liquid interface was carried-out for experimental purposes. Polypyrrole-coated and uncoated PC coverslips and Isopore™ membranes were used. De-epidermalised dermis (DED) squares were used as the gold standard control substrate. DED was prepared from glycerol preserved skin by washing in PBS six times then incubating in PBS containing an antibiotic mix (600 units/ml penicillin-G, 600 μg/ml streptomycin sulphate, 250 μg/ml gentomycin and 2.5 μg/ml fungizone) at 37° C for 10 days. This facilitated the removal of the epidermis and cells from the dermis. The original sample was then cut into approximately 1.5 × 1.5 cm squares. These were put reticular side down into 6-well plates and sterile stainless steel

rings were placed on the papillary surface. The rings were filled with a 500 µl solution of RM+ media containing 4×10^5 primary keratinocytes between passage 1 – 4 and fresh RM+ added to the surrounding well keeping the DED moist. They were then incubated at 37° C for 24h after which the rings were removed and 4 ml of fresh media added so as to totally submerge the DED. The primary keratinocytes were then cultured until confluence (2-3 days), verified by control cells on TCPS. In parallel, 2×10^4 primary fibroblasts were grown in separate 6-well plates for up to 4 days in E4 media. This was the same procedure for cells seeded onto the other substrates. However, for some polypyrrole-coated PC coverslips, five holes were introduced through the confluent layer and substrate with a sterile needle to facilitate nutrient diffusion at the next stage.

Once the primary keratinocytes had reached confluence, the substrates were transferred to the primary fibroblast containing wells where they were placed on 2 × 2 cm square stainless steel elevated grids. In this arrangement, media could be added to the wells such that the primary keratinocytes were maintained at an air/liquid interface with the primary fibroblasts at the bottom of the well contributing the necessary factors for optimal keratinocyte growth (Fig 2.5). For some experiments involving PC substrates, the primary keratinocytes were slightly submerged to optimise nutrient delivery. The cells were maintained under these conditions for a further 8-10 in RM+ media refreshed every 2-3 days. After this time, the substrates were removed from culture, carefully cut in two halves and fixed in 4% (w/v) paraformaldehyde in PBS. The fixed samples were sent for wax embedding and H&E staining at Cancer Research UK for future analysis.

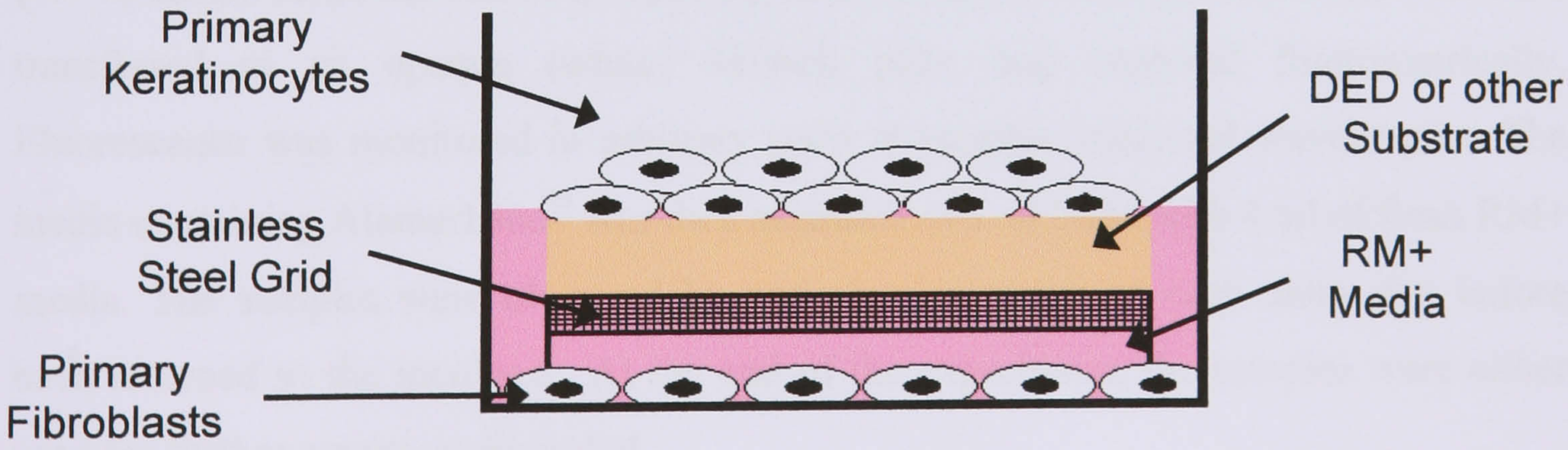

Figure 2.5: Organotypical Set-Up in Culture Well. *Keratinocytes at the top of DED or other preferably porous substrate (so as to enable nutrient delivery) are exposed to an air/liquid interface whilst fibroblasts at the bottom of the culture well produce factors that are necessary for optimal results.*

2.3.3 Assays

AlamarBlue™

On the first day (day 0) of each experiment, substrates were placed in 6-well plates and sterilised by immersion in 70% (v/v) ethanol or IMS for 20-30 mins. The sterilising solution was aspirated and the substrates allowed to air dry for at least 1 hr in a tissue culture hood. SVK14 keratinocytes were prepared as stated in the general tissue culture section above. They were then deposited on the centre of each substrate in 200 µl drops containing the appropriate number of cells (4×10^4 cells or 2×10^4 for 15 day long experiments) and incubated for 4 hours at 37°C/10% CO_2. At this stage, a droplet was used to localise the adhesion of cells on the actual substrate been studied. After this period, 4 ml of RM+ media was added to each well, micrographs were taken using the optical microscope (×100) and the cells incubated at 37°C/10% CO_2 for the experiment duration. Thereafter, RM+ media was refreshed every 2-3 days.

AlamarBlue™ (Fig 2.6), a safe non-toxic, aqueous dye was used to assess keratinocyte viability and proliferation (Fig 2.6). On day 1 (24h after initial incubation) and all other subsequent assay days (AlamarBlue™, days 2 and 5 for 5 day cultures; days 4, 8 and 15 for 15 day cultures), the media in each well was aspirated and replaced by 1.8 ml of fresh RM+ media with the addition of 0.18 ml (10% v/v) of AlamarBlue™ so as to completely submerge the cells. They were then incubated at 37°C/10% CO_2, for 4 hours (+/- 10 mins). After the end of that period, three samples of 200 µl from each well were transferred to an opaque (white) 96-well plate and analysed fluorometrically. Fluorescence was monitored in arbitrary units at supplier indicated wavelengths. The media containing AlamarBlue™ was then aspirated and replaced with 4 ml of fresh RM+ media. The samples were observed by optical microscopy on each assay day before been returned to the incubator. At the end of the experiment, the samples were either used for further assays or discarded.

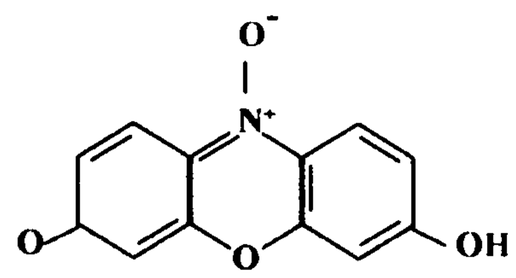

Resazurin

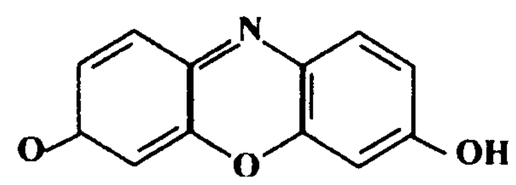

Resorufin

Figure 2.6: Resazurin and Resorufin Chemical Structures. Nonreduced AlamarBlue™ Corresponds to Resazurin and Reduced AlamarBlue™ to Resorufin (Taken form O'Brien *et al.*, 2000).

Total Protein

Bradford reagent was used to measure the total protein content of SVK14 keratinocytes after 5 days in culture. To obtain samples, 100 µl of lysis buffer was added to cells on their substrates in 6-well plates. Cells were detached from their substrates with a cell scraper and repetitive pipetting was used to obtain a homogeneous mix. The lysate from each well was transferred to an Eppendorf tube and frozen at -20°C. On the day of measurement, each lysate aliquot was defrosted, mixed in a vortex and spun down in a microcentrifuge for 15 s to avoid colloidal sediments (*e.g.* gold, polymer). After optimisation with test samples, it was decided to add 100 µl of Bradford reagent for every 2 µl of lysate. Three samples of 100 µl from the Bradford reagent containing lysate of each substrate were thus transferred to an opaque 96-well plate and left to stand for at least 2 mins before colorimetric measurement at 595 nm. The protein concentration was calculated from the colorimetric data by the following formula:

$$\text{Log[Protein]} = \frac{(\text{Absorbance} - 0.463)}{0.264}$$

This formula was obtained by Dr Muy-Teck Teh from linear regression analysis of curves generated from BSA standards. Protein concentration was obtained in µg per µl used *i.e.* µg/2 µl and represented graphically.

ATP

The Cell-Titer Glo™ assay was used to assess cell viability by quantifying the relative amounts of ATP present in cells after 5 days in culture. This was done on the same samples used in the total protein assay so as to express results in arbitrary luminescence units per μg of protein. Cell-Titer Glo™ reagent was previously prepared, aliquoted and frozen as per supplier instructions by Dr Muy-Teck Teh. After optimisation with test samples, it was decided to add 10 μl of Cell-Titer Glo™ reagent for every 10 μl of lysate. Samples were equilibrated for 10 mins and luminescence read from an opaque 96-well plate. The data was normalised with protein concentration and expressed graphically.

Rhodamine B Staining

Rhodamine B was used to stain SVK14 keratinocyte colonies at various stages in culture. Firstly, cells were removed from culture and fixed in their wells with a 10% formal saline solution overnight. The next day the fixative was removed, the cells were washed twice in PBS and a 1ml solution of 1% w/v rhodamine B was added to each well for 15 mins. To finish, the cell containing wells were washed under running tap water until all excess stain had been removed, air dried and stored for analysis.

SEM

SEM was used to take detailed images of SVK14 keratinocytes after 5 days of culture on various substrates. In order to prepare the samples for SEM, the following procedures were followed. Cells were removed from culture and triple washed in water. Then, they were placed at 4°C for 30 mins after which a chilled solution of 1.5% (w/v) glutaraldehyde buffered in 0.1 M sodium cacodylate (pH 7.2) was added to each cell containing well. They were then left in the fixative overnight at 4°C. On the next day, the fixative was removed and the cells were triple washed in water. The samples then underwent secondary fixation by the addition of 1% (w/v) osmium tetroxide buffered in 0.1 M sodium cacodylate for 60 mins at room temperature. This was followed by three 5 mins washes in 0.1 M sodium cacodylate buffer and 30 mins in 1% tannic acid

buffered in 0.05 M sodium cacodylate. The samples were then washed for four 5 mins periods in 0.1 M sodium cacodylate buffer and subjected twice for 5 mins to a graded series of methanol (30%, 50% and 70%). They were then left in 2% uranyl acetate dissolved in 70% methanol for 30 mins. Following this, they were subjected for three 5 mins periods to 90 % methanol and then for two 10 mins periods to 100% methanol. The fixed and dehydrated cells were then exposed to hexamethyldisilazane for 10 mins and finally air-dried overnight. The samples were then mounted on aluminium stubs, gold coated for 90 s and viewed under a 10 kV filament voltage.

PCNA and Keratin Staining

Immunocytochemistry was used to stain SVK14 and primary keratinocytes for the proliferation (PCNA) and differentiation (K10 and K16) markers. SVK14 and primary cells were fixed in 4% paraformaldehyde overnight. They were wax embedded in paraffin, sectioned and mounted so as to give two cross-sections per microscope slide. For each block, a section was stained with H&E. Embedding, some sectioning and H&E staining was carried out by CRUK's Histopathology Unit. All other work was done personally using the three layer staining method described below.

Slide mounted samples were de-waxed by successive washes in xylene (2 × 5 mins), descending ethanol grades (100%, 3 mins × 2; 90%, 3 mins; 70%, 3 mins) and tap water (3 mins). This was followed by 10 mins in 3% H_2O_2 diluted in methanol to block endogenous peroxidase activity, 3 mins in tap water and 5 mins in PBS. At this point, a hydrophobic marker was used to circle the two section containing areas on the slides and a humidifying tray was prepared. The samples were then blocked with 100 µl of horse serum for 15-20 mins at room temperature. Prior to sample application, primary antibodies were either used directly from supernatants or diluted in 0.2% (w/v) BSA and 5 mM tris buffer saline (TBS) at pH 7.6 as previously optimised by titration runs (Dr Nkemcho Ojeh) Each primary antibody (PCNA, K10 and K16) was added to one side of the slide, with the other used as a negative control by omission (PBS added instead) and incubated for 1h 30 mins at 37°C. After this, samples were washed three times for 5 mins in TBS buffer. The secondary and tertiary steps were done using the Vectastain® Universal *Elite*® ABC Kit components.

One drop of biotinylated horse secondary antibody was diluted in 2.35 ml TBS and 3 drops horse serum then 100 µl solutions were applied to each sample for 30 mins at room temperature. This was followed by three 5 mins washes in TBS and 20 mins in 100 µl per sample tertiary antibody. This had been made 30 mins prior to use according to supplier's instructions (2.5 ml TBS, 1 drop solution A and 1 drop solution B). Another three 5 mins washes in TBS were carried out and the sections were developed for 2-6 mins in DAB solution (2250 µl water, 250 µl substrate buffer, 2 drops liquid DAB and 1 drop H_2O_2 substrate). Upon appearance of the brown coloured stain at localised horseradish peroxidase activity, the slides were washed in TBS for 1 min and counterstained in haematoxylin for 30 sec. Finally, the samples were dehydrated through a series of ascending ethanol grades (70%, 2 mins; 90%, 2 mins; 100%, 2 mins × 2) and xylene (2 mins × 2) before top coverslips were mounted with DePex for future optical microscopy analysis.

2.3.4 EIS Monitoring of Cells

For EIS work, cells were seeded at different densities (4×10^4, 4×10^5 or 4×10^6 cells per well) on either gold or polypyrrole modified digit-coated working electrodes contained within ETCCs with reference and counter electrodes fitted. These were connected to the potentiostat *via* appropriate cabling. Impedance monitoring of cells was carried-out by three methods. The first was to consider the full impedance spectrum by measuring the impedance response at an oscillating potential of 20 mV *vs.* Ag/AgCl between 1 Hz and 100 kHz (with the biased potential set at 0 V *vs.* Ag/AgCl). The second method was to follow the impedance response at an oscillating potential of 20 mV *vs.* Ag/AgCl at a single frequency for a specified time length and time periods (with the biased potential set at 0 V *vs.* Ag/AgCl). The third was to analyse the data from portions of the full impedance spectra in terms of electrical equivalent circuit elements. All data were collected using the Gamry Instruments PC4/300 potentiostat (PHE200^{TM} and Echem Analyst software).

Impedance Spectroscopy

SVK14 keratinocytes were seeded at various densities on gold, PPy/Derm and PPy/Cl digit-coated electrodes. Impedance changes at the electrodes in each well were monitored in triplicates on day 0 (prior to cell seeding), 1, 2, 3, 4 and 7 against control wells with no cells. The same was done to compare washed and unwashed PPy/Derm and PPy/Cl films. SVK14s (4×10^5 per well) were seeded onto PPy/Derm digit-coated electrodes and cultured for 24 h. The impedance spectra of SVK14s on the PPy/Derm electrodes were then measured. After this, culture media was removed and replaced with either cell lysis buffer for 5 mins, 0.05% trypsin for 24mins or 4% paraformaldehyde for 10 mins. The various solutions were then replaced once more with culture media and the impedance spectrums measured after each treatment (in triplicates) for comparison. Similarly, SVK14s, SCCs, primary keratinocytes and primary fibroblasts were seeded (4×10^5 per well) on PPy/Derm coated electrodes and cultured for 24 h. Impedance spectra were measured in triplicate for comparison.

Single Frequency Impedance

Some data obtained from full impedance spectra was post-analysed in terms of single frequencies. However, for some experiments, measurements were made at a single frequency. This included the measurement of bare PPy/Derm and gold substrates as well as those supporting live or fixed cells. SVK14s were seeded (4×10^5 per well) on gold or PPy/Derm digit-coated electrodes and cultured for 24 h. They were then monitored in triplicate at 4, 40 or 400 Hz, 4 or 40 kHz every 0.1 mins for a total of 6 mins. They were then fixed in 4% paraformaldehyde for 10 mins and re-measured in the same way. The same measurements were also carried-out as controls for bare electrodes. The impedance of SVK14s seeded (4×10^5 per well) on PPy/Derm substrates and cultured for 24 h was monitored at 4 and 40 kHz during exposure to 0.05% trypsin diluted in E4 media (without FBS) every 0.1 mins for a total of 0.4 h. The impedance of SVK14s, SCCs, primary keratinocytes and primary fibroblast seeded (4×10^5 per well) on PPy/Derm coated electrodes was measured at 40 kHz every 5 mins for a total of 6 h immediately upon seeding and incubation at 37°C and 10% CO_2.

Equivalent Circuit Analysis

Some of the impedance spectra data collected was analysed further to obtain values for electrical elements of an equivalent electrical circuit. This was done in Matlab® using a complex non-linear least squares method written by Dr Alan Waterworth. For each spectrum, the data was chosen over the frequencies at which the semi-circle appeared. The fitting routine employed the Levenberg Marquardt technique with termination criteria specified so as to ensure the goodness of fit. The fitting routine is described in detail by Waterworth (2000) and is therefore not reprised further here.

2.3.5 Electrical Stimulation of cells

The effect of electrical stimulation on SVK14 keratinocytes was considered on either gold or PPy/Derm coated working electrodes in ETCCs with reference and counter electrodes fitted. These were connected to the Gamry Instruments PC4/300 potentiostat *via* appropriate cabling. SVK14s were seeded (4×10^4 per well) in phenol red free RM+ on the substrates, then stimulated immediately upon seeding and incubation at 37°C and 10% CO_2 by applying a potential of either +100, +50, -50 or -100 mV *vs.* Ag/AgCl for 1 h. The cells were then cultured for a further 19 h before assessment of viability was made by the AlamarBlue™ assay as described earlier (section 2.3.3). Controls were also assessed for cells in ETCCs without electrical stimulation as well as those on TCPS in 6-well plates. Further experiments considered the effect of electrical stimulation on established cell layers. For the latter, SVK14s were seeded (4×10^5 per well) in phenol red free RM+ on gold and PPy/Derm coated electrodes and cultured for 24 h. The established cell layers were then observed under the microscope. After stimulation at +100, +50, -50 or -100 mV *vs.* Ag/AgCl for 20 mins the cell layers were then observed once more under the microscope to verify the effect of stimulation on cell morphology. Additionally, stimulation over a range of potentials (-0.9, -0.6, -0.3, -0.1, +0.1, +0.3, +0.6, +0.9 and +1.5 V *vs.* Ag/AgCl) was done for bare gold and PPy/Derm over 5 mins to verify the effect on electrode structure.

2.4 Source Addresses

Agar Scientific Ltd

66A Cambridge Road, Stanstead, Essex, CM24 8DA, UK

Bioanalytical Systems Inc

BAS Riverside, Mountbatten Way, Congleton, Cheschire, CW12 1DY, UK

BioGenex Laboratories Inc

4600 Norris Canyon Road, San Ramon, CA 94583, USA

Biosource UK Ltd

8 Rue de l'Industrie, B-1400 Nivelles, Belgium

BOC Gases

10 Priestley Road, Surrey Research Park, Guildford, Surrey, GU2 7XY, UK

Cancer Research UK

Clare Hall Laboratories, Blanche Lane, South Mimms, Potters Bar, EN6 3LD, UK

DakoCytomation Ltd

Denmark House, Angel Drove, Ely, Cambridgeshire, CB7 4ET, UK

Goodfellow Cambridge Ltd

Ermine Business Park, Hutingdon, Cambridgeshire, PE29 6WR, UK

Hewlett-Packard Company

3000 Hanover Street, Palo Alto, CA 94304-1185, USA

Homebase Ltd

Beddington House, Railway Approach, Wallington, SM6 0HB, UK

Invitrogen Ltd

3 Fountain Drive, Ichinnan Business Park, Paisley, PA4 9RF, UK

Jeol UK Ltd

Jeol House, Silver Court, Welwyn Garden City, Herts, AL7lLT, UK

Leica Microsystems (UK) Ltd

Davy Avenue, Knowhill, Milton Keynes, MK5 8LB, UK

Math Works Ltd

Martin House, Cowley Park, Cambridge, CB4 0HH, UK

Millipore S. A. S. – Molsheim

BP 116, 67124 Molsheim Cedex, France

National Instruments Corporation

11500 North Mopac Expressway, Austin, TX 78759, USA

Nikon UK Ltd

Nikon House, 380 Richmond Road, Kingston upon Thames, Surrey, KT2 5PR, UK

PerkinElmer Life Sciences Ltd

204 Cambridge Science Park, Cambridge, CB4 0GZ, UK

Promega UK

Delta House, Chilworth Science Park, Southampton, SO16 7NS, UK

Royal London Hospital

Whitechapel Road, Whitechapel, London E1 1BB

RS Components Ltd

PO Box 99, Corby, Northamtonshire, NN17 9RS, UK

Scientific and Medical Products Ltd

Shirley House, 12 Gateley Road, Cheadle, Chesshire, SK8 1PY, UK

Sigma-Aldrich Company Ltd

Fancy Road, Poole, Dorset, BH12 4QH, UK

SPSS UK Ltd

St Andrew's House, West Street, Woking, Surrey, GU21 1EB, UK

Vector Laboratories Inc

30 Ingold Road, Burlingame, CA 94010, USA

VWR International Ltd

Merck House, Poole, Dorset, BH15 1 TD, UK

Windsor Scientific Ltd

264 Argyll Avenue, Slough Trading Estate, Slough, SL1 4HE, UK

Chapter 3

Synthesis and Characteristics of Polypyrrole Films

3.1 Introduction

The first project objective was to synthesise polypyrrole films and assess their properties in view of their subsequent use as substrates for epithelial cells. An important goal was to achieve viable films incorporating bioactive macromolecules such as proteins and polysaccharides as these were thought likely to provide cell compatible substrates. To accomplish the aims of this study, the prepared films would be required to maintain their mechanical integrity and electroactivity in prolonged culture use. In this Chapter, the synthesis methods for various polypyrrole compositions are presented. The characteristics of the obtained films are also investigated in terms of their physical and electrochemical properties. This serves as a basis for subsequent experiments.

3.2 Synthesis of Polypyrrole Films

3.2.1 Synthesis on Interdigitated Electrodes

At the initial stages of this project, polypyrrole films were electropolymerised onto gold IDEs with either chloride (Cl) or dodecyl sulphate (DS) as counterions. These were selected for their contrasting properties; Cl is a highly mobile anion, readily entering and exiting the film after synthesis, whereas DS is immobilised within the film once incorporated. For this reason, polypyrrole-dodecyl sulphate films were used as a model for protein loaded films, since proteins are also expected to be immobile within the film due to their high molecular weight. The films were polymerised on the gold IDEs by cyclic voltammetry, the conditions for which had been previously established (Lillie, 2001) and repeat cyclic voltammograms during film synthesis observed (Fig 3.1-3.2).

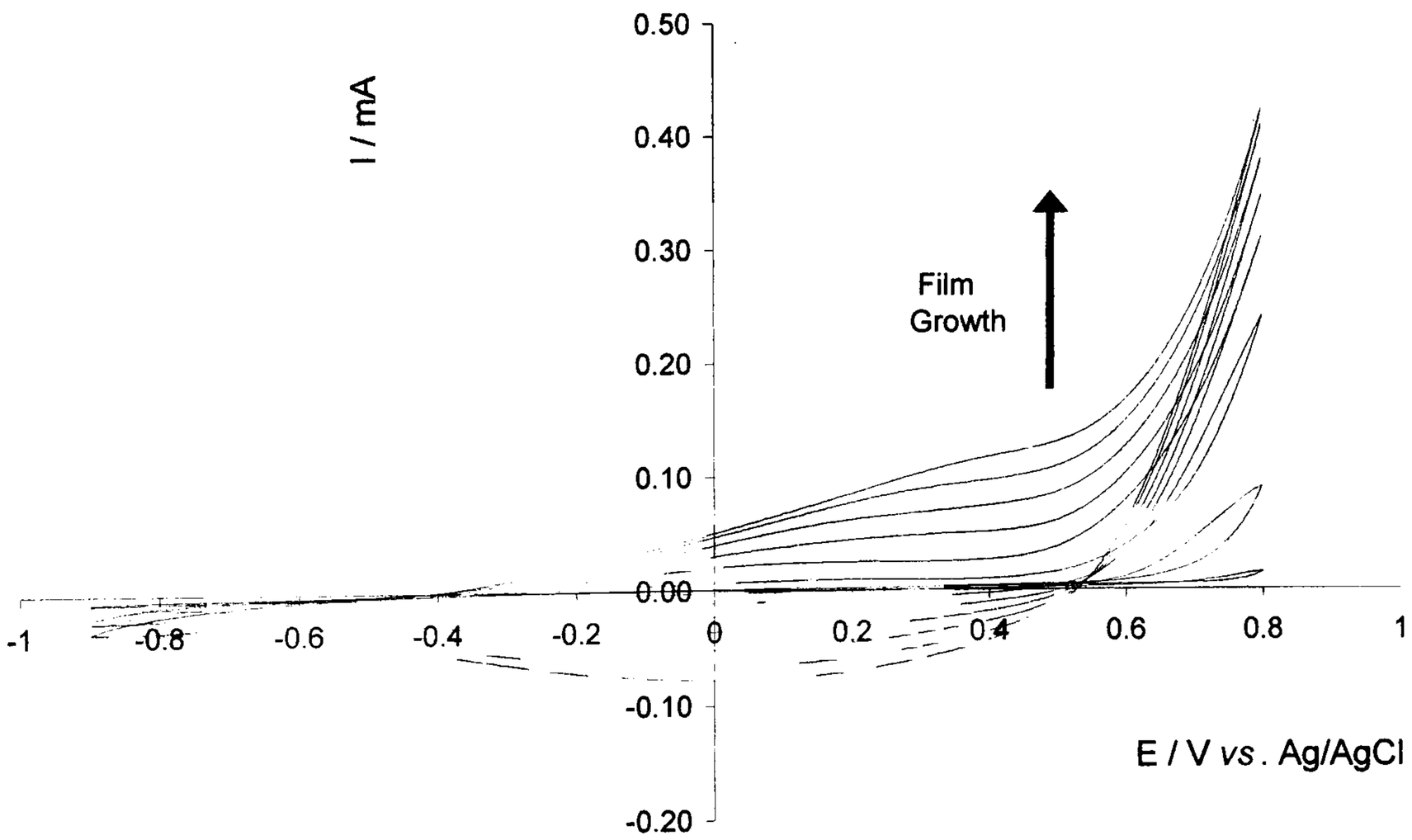

Figure 3.1: Cyclic Voltammogram of PPy Film Growth on 15 μm Gold IDE

(50 mV/s; 15 Scans; electrolyte: 1 M pyrrole and 50 mM NaCl).

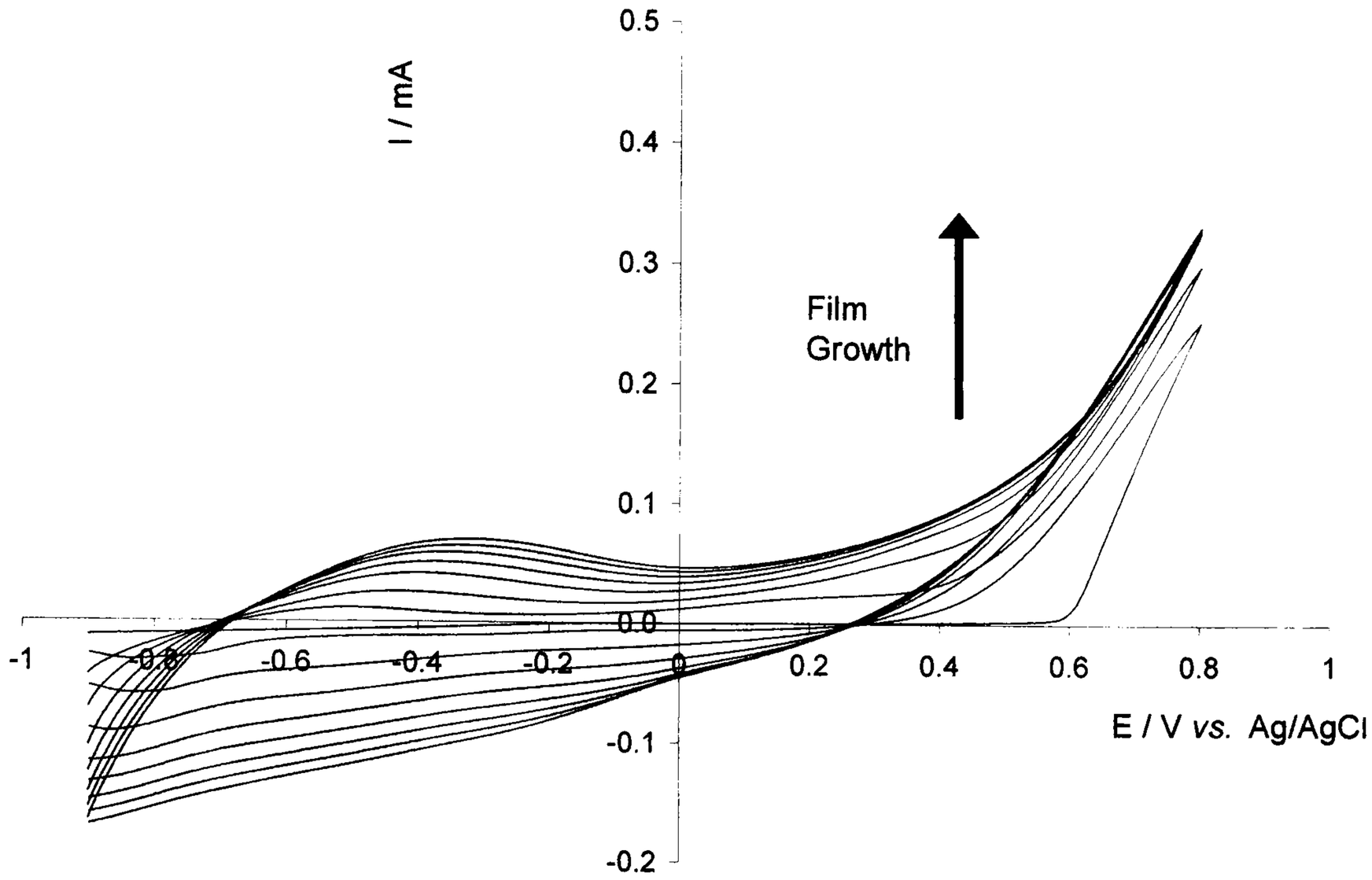

Figure 3.2: Cyclic Voltammogram of PPy Film Growth on 15 μm Gold IDE

(50 mV/s; 15 Scans; electrolyte: 1 M pyrrole and 50 mM SDS).

In both cases, the first sweeps are characterised by a sudden increase in current at around +0.6 V *vs.* Ag/AgCl, representing the monomer oxidation potential. Upon reversal of the potential sweep at +0.8 V *vs.* Ag/AgCl, the current remains above the forward scan, thus forming a loop, known as the nucleation loop. The nucleation loop is much more pronounced in the PPy/DS film compared with the PPy/Cl film. The more prominent nucleation loop is possibly due to the better adsorption rate of DS along with the pyrrole onto the working electrode due to its high molecular weight compared with Cl. Monomer oxidation currents initially increase rapidly with each successive sweep and stabilise towards final scans. This is due to the increase in surface area created by the successive deposition of the uneven polypyrrole film on the working electrode. Comparing the final scans to the initial scans for each case, it may be seen that positive currents are generated at much lower potentials (Fig 3.3). This suggests that the onset of film oxidation occurs before monomer oxidation in each case.

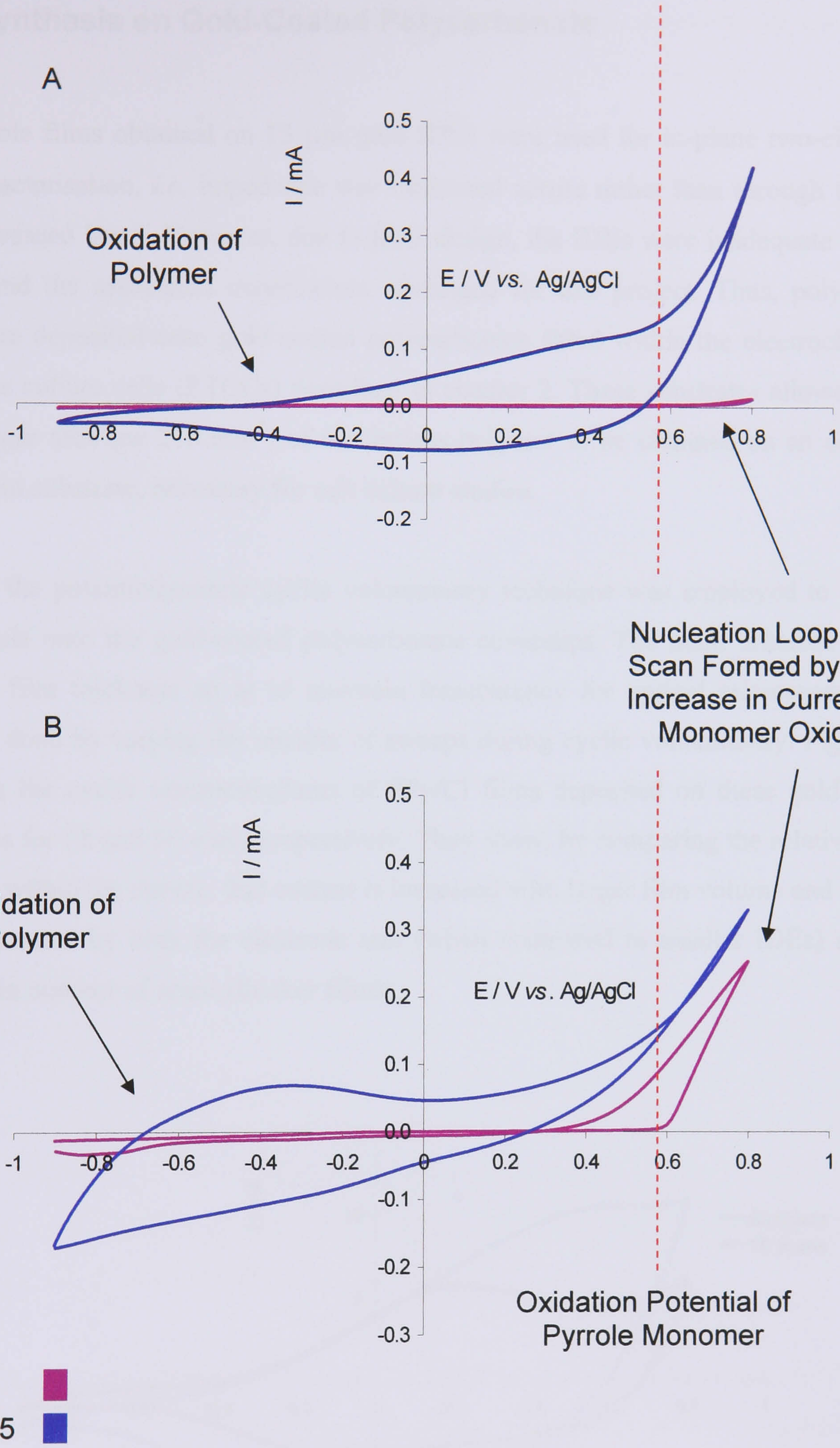

Figure 3.3: Cyclic Voltammogram for (A) PPy/Cl and (B) PPy/DS

(first and last scans from Fig 3.1 & 3.2).

3.2.2 Synthesis on Gold-Coated Polycarbonate

Polypyrrole films obtained on 15 μm gold IDEs were used for in-plane two-electrode EIS characterisation, *i.e.* impedance was measured across rather than through the PPy film (discussed later). However, due to their design, the IDEs were inadequate for cell culture and the associated experiments envisaged for this project. Thus, polypyrrole films were deposited onto gold-coated polycarbonate fitted within the electrochemical and tissue culture cells (ETCCs) described in chapter 2. These substrates allowed for a much larger area (*ca* 270 mm^2) of continuous polymer to be obtained on an optically transparent substrate, necessary for cell culture studies.

Initially, the potentiodynamic cyclic voltammetry technique was employed to deposit polypyrrole onto the gold-coated polycarbonate coverslips. The main criterion was to optimise film thickness so as to maintain transparency for optical microscopy. This could be done by varying the number of sweeps during cyclic voltammetry. Figure 3.4 compares the cyclic voltammograms of PPy/Cl films deposited on these gold-coated coverslips for 18 and 50 scans respectively. They show, by comparing the relative areas enclosed within the curves, that current is increased with larger film volume and surface area, generated by both the electrode size (when compared to smaller IDEs) and the increase in number of scans (thicker films).

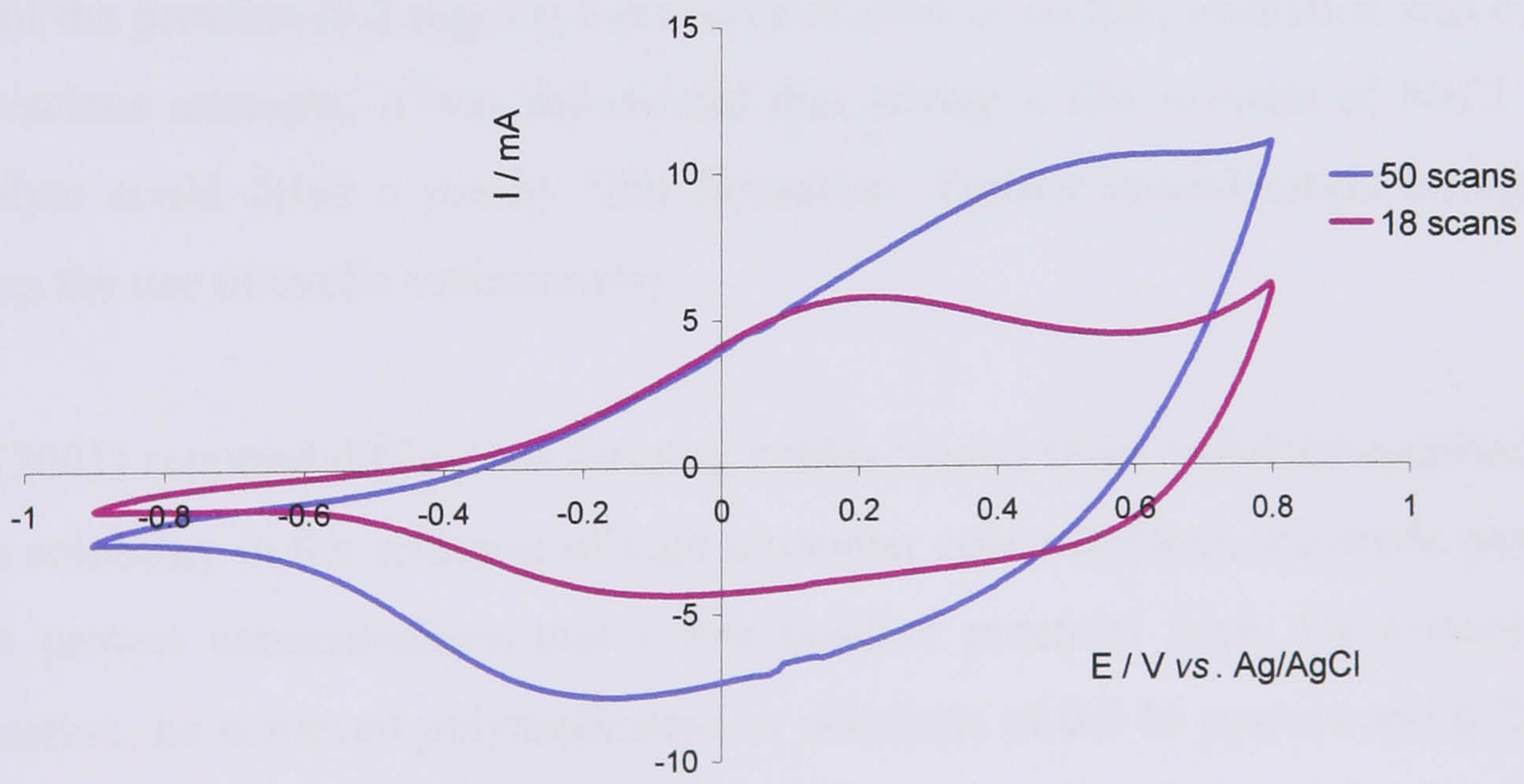

Figure 3.4: Cyclic Voltammograms for PPy/Cl after 18 and 50 scans

(50 mV/s; 10th scan; electrolyte: 50 mM NaCl).

The potentiodynamic method was successfully applied to produce polypyrrole films containing chloride or dodecyl sulphate anions. The synthesis of polypyrrole films with other counterions was then considered. These included the polyanion polyvinyl sulphate, the extracellular matrix GAGs heparin and dermatan sulphate and the proteins fibrinogen, fibronectin and collagen. In the case of polyvinyl sulphate, heparin and dermatan sulphate, polymer formation occurred with concentrations down to 0.2 mg/ml of counterion in electrolyte. The entrapment of these molecules was facilitated by the presence of negatively charged sulphate groups. With the exception of dermatan, also called chondroitin sulphate B, use of these counterions has been previously reported (Zhou *et al.*, 1999; Campbell *et al.*, 1999).

It was assumed that the proteins would be required to have an overall negative charge in order to facilitate inclusion. Proteins have an overall negative charge at pH values higher than their iso-electric point (pI) (Voet and Voet, 1995). In fact, this is the mechanism used for protein separation by isoelectric focusing in two-dimensional gel electrophoresis. Therefore, the strategy was to carry out the reaction in solutions with pH values above the pI of individual proteins (pI of fibrinogen is *ca* 5.1, fibronectin *ca* 5.5 and Collagen *ca* 6.3). Solutions containing 1 M pyrrole and 0.2 mg/ml fibrinogen or fibronectin were already at pH ~ 7.2 sufficiently above proteins pIs. In the case of 1 M pyrrole and 0.2 mg/ml collagen containing solutions, pH was increased to between 8-8.5 by dropwise addition of a dilute NaOH solution. However, attempts to polymerise films by cyclic voltammetry from an electrolyte containing pyrrole monomer (1 M) with either of the proteins (0.2 mg/ml) were unsuccessful as no film formation was observed. After various attempts, it was discovered that adding a few crystals of NaCl into the electrolyte could drive a patchy film formation. Further consideration brought in to question the use of cyclic voltammetry.

Lillie (2001) reported difficulties forming avidin-loaded films which he ascribed to poor protein solubility in the presence of high monomer concentrations, electrode passivation at high protein concentrations and a low positive potential limit. Nevertheless, after optimisation, he achieved polymerisation in solutions of 0.5 M pyrrole and 0.25 mg/ml avidin using an increased positive potential limit of +0.9 V *vs.* Ag/AgCl. In cyclic voltammetry synthesis the window for film formation extends above the formal oxidation potential of pyrrole, if considered as +0.6 V *vs.* Ag/AgCl (Lillie, 2001) at 50 mV/s scan rate, for *ca* 8 s every sweep. This may be insufficient time for the

incorporation of certain proteins such as collagen. Additionally, protein incorporation into polypyrrole and surface passivation may further compromise polymer formation. Instead of further optimisation attempts, potentiostatic polymerisation with a constant polarisation potential was used; this was also the predominantly reported method (see Chapter 1).

The potentiostatic technique allowed monomer exposure to a set oxidation potential for extended time periods above +0.6 V *vs.* Ag/AgCl which led to successful film growth. Conditions for each reaction (potential and duration) for a visually complete, transparent film were established for each counterion. Thus, PPy/Cl films formed rapidly at +0.7 V *vs.* Ag/AgCl for 30 s whereas for PPy/PVS, PPy/Derm and PPy/Col films, +0.8 V *vs.* Ag/AgCl for 90s, +0.8 V *vs.* Ag/AgCl for 180s and +0.9 V *vs.* Ag/AgCl for 180s were respectively used (Fig 3.5).

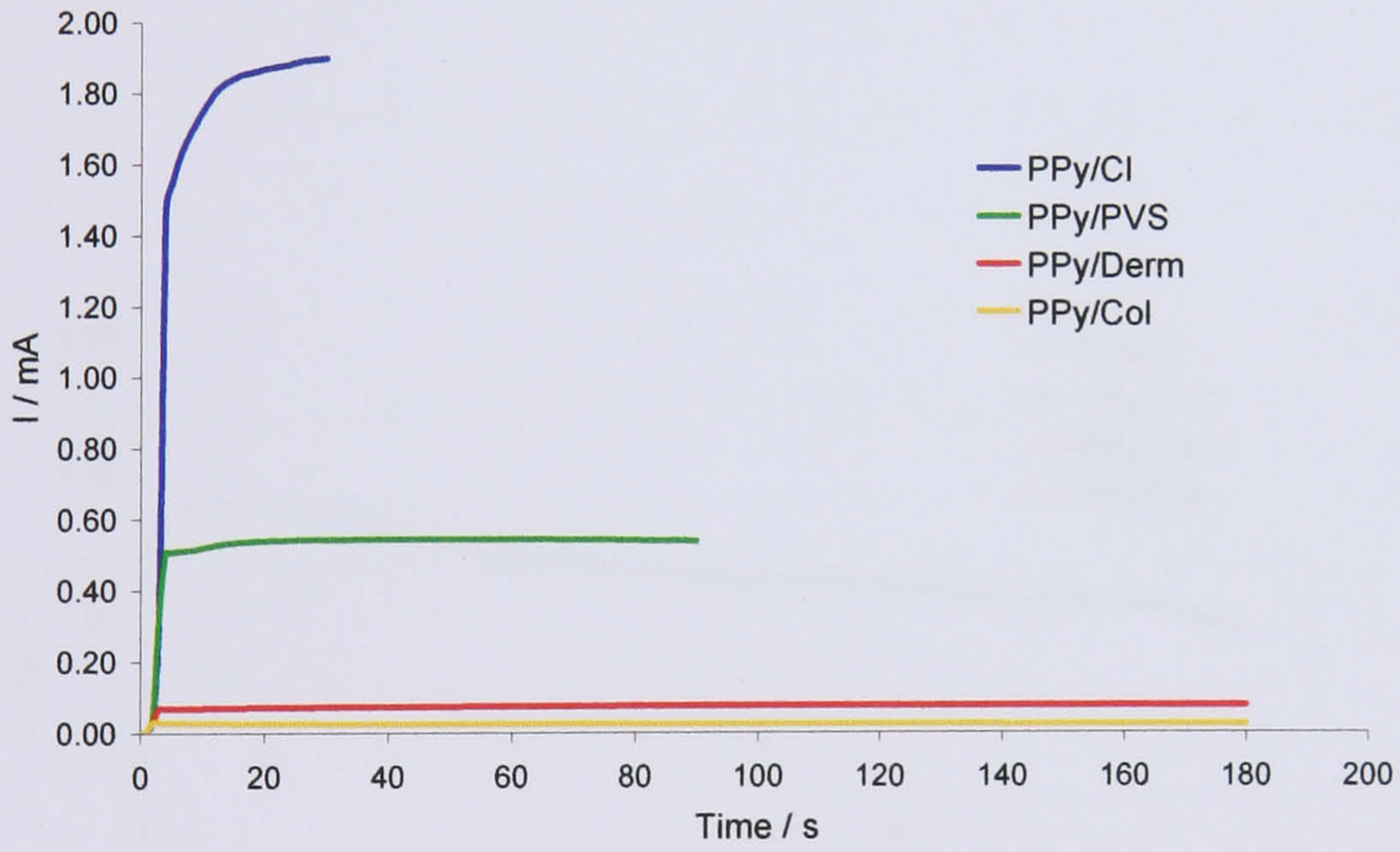

Figure 3.5: Chronoamperometry Plots of Polypyrrole Film Synthesis *(electrolyte: 1 M pyrrole and 50 mM NaCl or 0.2 mg/ml PVS, Derm or Col).*

Collagen required the highest voltage because of the low rate of formation for successful polymerisation. Fibrinogen and fibronectin containing films could be polymerised at +0.8 V *vs.* Ag/AgCl for 90 and 60 s respectively. Current recorded for PPy/Col films was especially low (Fig 3.5). Collagen's charge state, size and subsequent association with polypyrrole could have led to decreased film conductivity. However, direct protein incorporation did occur. Indirect evidence for protein

incorporation was that polymerisation did not occur in the absence of protein. For collagen, the reaction also required increased pH. However, if electrolyte solutions containing collagen at pH 8-8.5 were left standing for too long (*i.e.* over 30 mins), they failed to yield polypyrrole films. This was due to collagen which is preferentially soluble in acidic solutions precipitating out of the alkali solution over time (forming visible aggregates). Thus, immediate use of alkaline collagen solutions was necessary.

Extended polymerisation periods (45 and 90 mins) led to thicker films (Fig 3.6). Initial currents fell after a peak presumably due to loss of film conductivity; Valaski *et al.* (2002) showed that charge carrier mobility was lower in thicker polypyrrole films. This was considered to be due to less homogeneous deposition during film growth. This would put a limit on the thickness of electrogenerated films. Films were polymerised variously on fully gold-coated PC coverslips, patterned low surface area gold digit electrodes (Fig 2.2) and coated PC Isopore^{TM} membranes, where bridging of the Ø 0.22 µm pores was seen. Potentiostatic synthesis was used throughout.

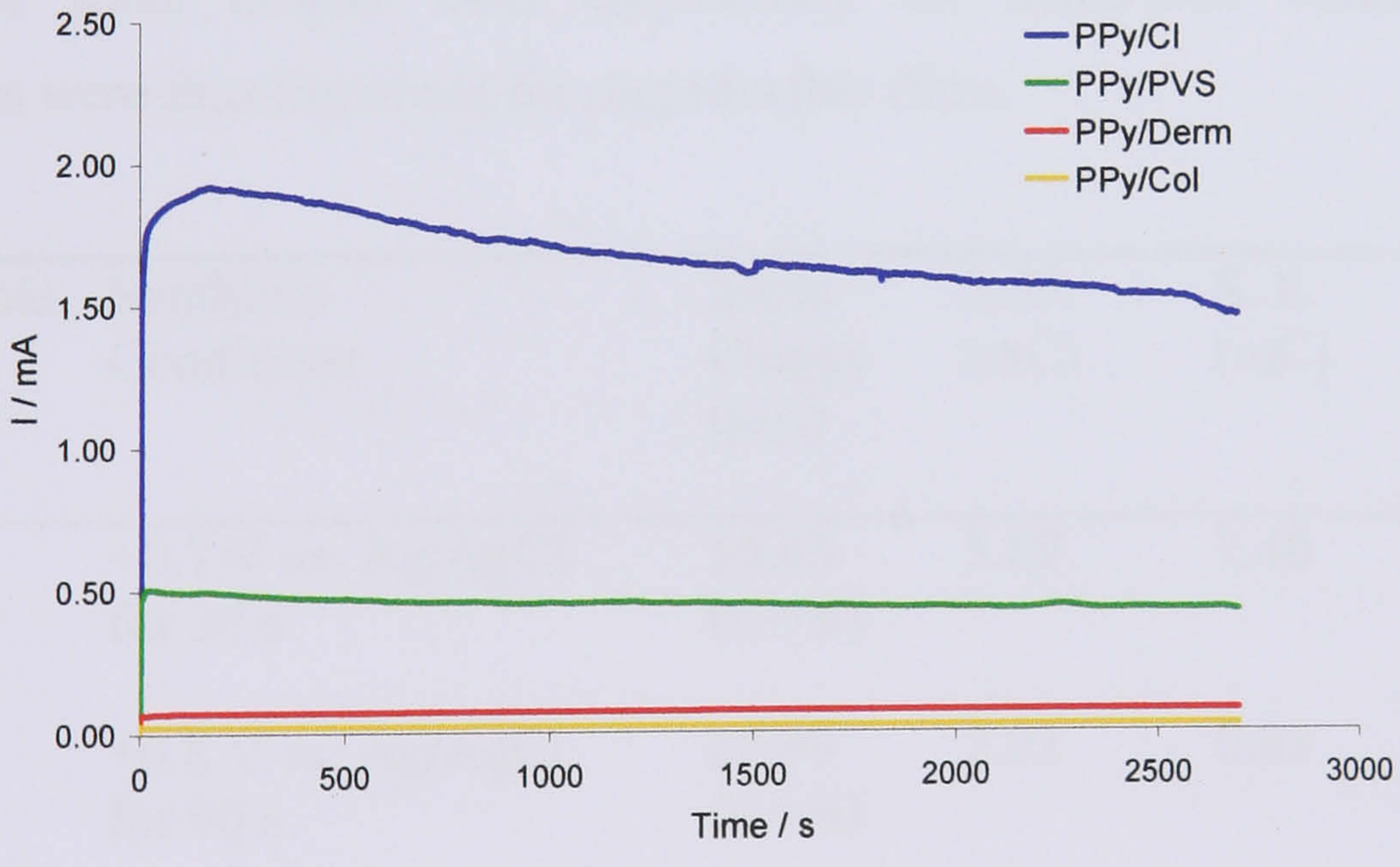

Figure 3.6: Chronoamperometry Plots of Thick Polypyrrole Film Synthesis *(electrolyte: 1 M pyrrole and 50 mM NaCl or 0.2 mg/ml PVS, Derm or Col).*

3.2.3 Chemical Synthesis

Polypyrrole films were also synthesised chemically on plastic coverslips and Petri dishes by mixing pyrrole solution with $FeCl_3$. Polymerisation proceeded immediately upon mixing and was characterised by solution darkening. However, films were powdery, brittle, of poor quality and were not further investigated.

3.2.4 Reproducibility of Polypyrrole Films

The project required new polypyrrole films to be used for each experiment, and with several hundred films produced, it was important to maintain reproducibility between batches. Chemicals from a fixed standard commercial source at constant concentration as well as synthesis in ETCCs of fixed volume and inter-electrode distances were therefore used. Total charge passed during synthesis (Table 3.1) were determined by integrating the area under chronoamperometry curves (current *vs.* time) using the Echem Analyst program from Gamry Instruments. Randomly selected samples showed low, acceptable variability between synthesis runs. This was even the case for thicker PPy/Derm films despite more opportunity for deposition variability. Synthesis conditions were thus important for reproducible films.

Polypyrrole Films	Synthesis Conditions	Mean Charge (mC)	S. D. (mC)	S. E. (mC)	95% Confidence Interval (mC)
Thin PPy/Cl	+0.7 V *vs.* Ag/AgCl for 30 s	55.65 (n = 6)	5.89	2.40	6.18
Thin PPy/PVS	+0.8 V *vs.* Ag/AgCl for 90 s	37.90 (n = 6)	2.02	0.83	2.12
Thin PPy/Derm	+0.8 V *vs.* Ag/AgCl for 180 s	13.61 (n = 6)	1.70	0.69	1.78
Thick PPy/Derm	+0.8 V *vs.* Ag/AgCl for 45 mins (triplicates)	808.32 (n = 9)	104.28	34.76	80.16

Table 3.1: Synthesis Charge and Descriptive Statistics for Selected Polypyrrole Films

3.2.5 Thickness of Polypyrrole Films

Charge passed can be used to determine film thickness. In their early report on polypyrrole film properties, Diaz *et al.* (1981) estimated thickness from electrode area, density measurement and the apparent number of pyrrole units per anion. They reported that *ca* 8 mC/cm^2 was passed during synthesis for every 20 nm of polypyrrole film. They verified their method by measuring thicker films using alternative means, finding for instance that a 20 μm film consumed *ca* 8 C/cm^2 as predicted. Others have gone on to use this relationship to estimate the thickness of their films from charge passed regardless of counterion employed. However, the film density and number of pyrrole units per anion are influential parameters in the relationship between charge and film thickness. Wernet and Wegner (1987) calculated polypyrrole film thickness with octanesulfonate, dodecylsulfate and polystyrenesulfonate counterions. They provided the following equation:

$$d = \frac{Q_s}{2F \cdot A \cdot \rho}(m_1 + m_2 / y)$$

Where d is thickness; Q_s is the charge used for synthesis; F is Faraday's constant; ρ is density; m_1 is the molecular weight of pyrrole unit; m_2 is the molecular weight of the anion incorporated in the film; and y is the number of pyrrole units per anion. This method could not be used here; density measurements were not carried-out, but importantly for macromolecule counterions (*e.g.* dermatan and collagen) there is no available model to provide y and m_2 values. SEM cross-sections of freeze-fractured polypyrrole films were tried but this proved very difficult, especially for thin films where it was impossible to distinguish between polypyrrole and the polycarbonate substrate. Energy dispersive X-ray elemental mapping of cross-sections (Ateh, 2003) to differentiate polypyrrole from polycarbonate were not successful; N, O, Na, K, Al, Si, Ca, Cl, Au, and S could be resolved, but were homogeneous over cross-sections. Measurements were made easier with thicker films due to delamination between the polypyrrole and polycarbonate.

PPy/PVS and PPy/Col electropolymerisation for 1.5 h at +0.8 V and +0.9V *vs.* Ag/AgCl respectively proved suitable; examples are given in figure 3.7. In many instances, measurements were hampered by poor images or film buckling. Cross-section thickness

was determined using the measure tool in the Adobe® Photoshop® (6.0) image analysis software calibrated using the scale bar on each micrograph. Measurements were taken at random locations along cross-sections; estimated means were 5.86 µm (± 0.12, n=12) for PPy/PVS and 19.91 µm (± 0.73, n=12) for PPy/Col.

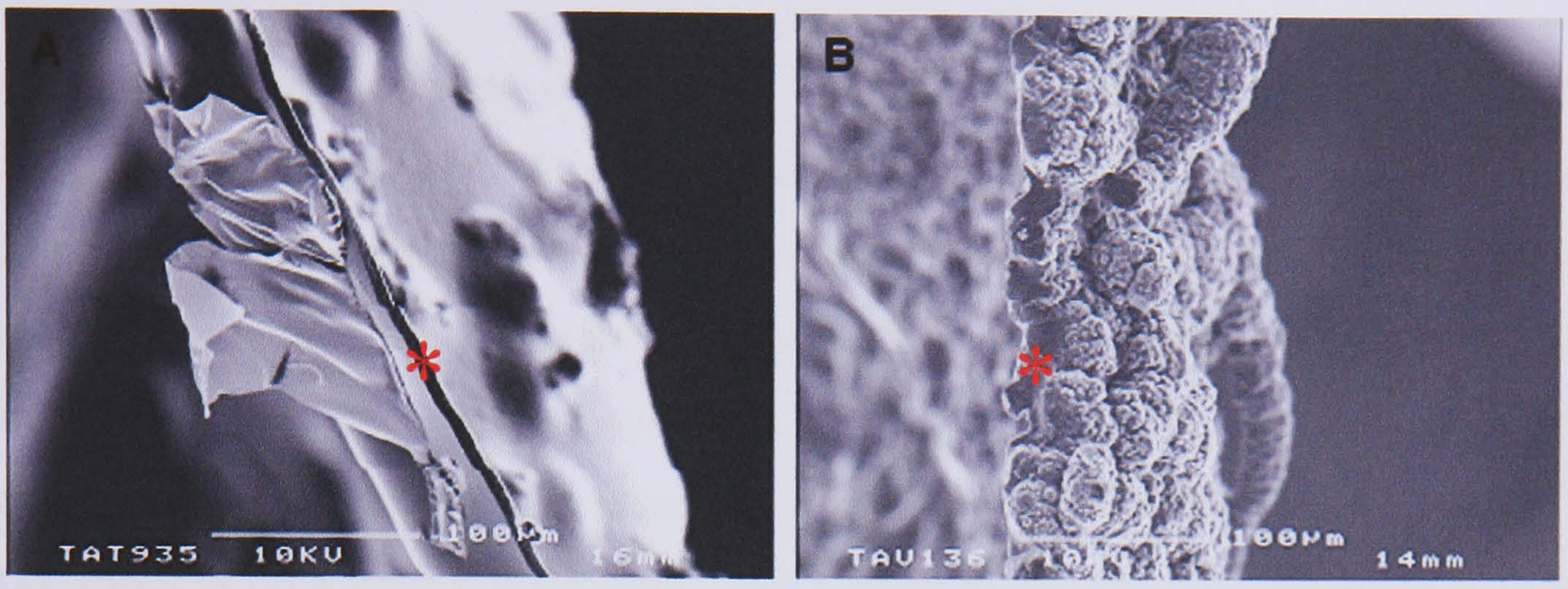

Figure 3.7: Cross-Section of (A) PPy/PVS and (B) PPy/Col. *Thick films delaminated from their support and it was possible to image and measure cross-sections (a red asterix marks the fractured cross-section surface for each film).*

Thicker PPy/Col films, despite less charge transfer (Fig 3.6), show that additional mechanisms could be relevant during polymerisation, *e.g.* protein adsorption without ionic association. The charge-thickness disparity precludes reliable thickness estimation from electropolymerisation data as advocated by Wernet and Wegner (1997).

3.3 Topography of Polypyrrole Films

3.3.1 Polypyrrole Films on Interdigitated Electrodes

Electron microscopy imaging of a PPy/Cl film on a gold IDE (Fig 3.8) shows strips where the polymer has been deposited along the gold digits as well as some areas of bridging. Despite synthesis over 20 voltammetry scans, bridging remained limited. Distinctive film topography may be observed on the PPy/Cl surface. Others have shown topography to vary according to synthesis conditions, including method (chemical or electrochemical), electrolyte and counter-ion amongst the other factors (Salmon *et al.*, 1982). PPy/DS on a gold IDEs (Lillie, 2001) show more complete coverage within 15 scans (Fig 3.9). SEMs of variously-loaded thick films, demonstrated the counterion effect on surface topography.

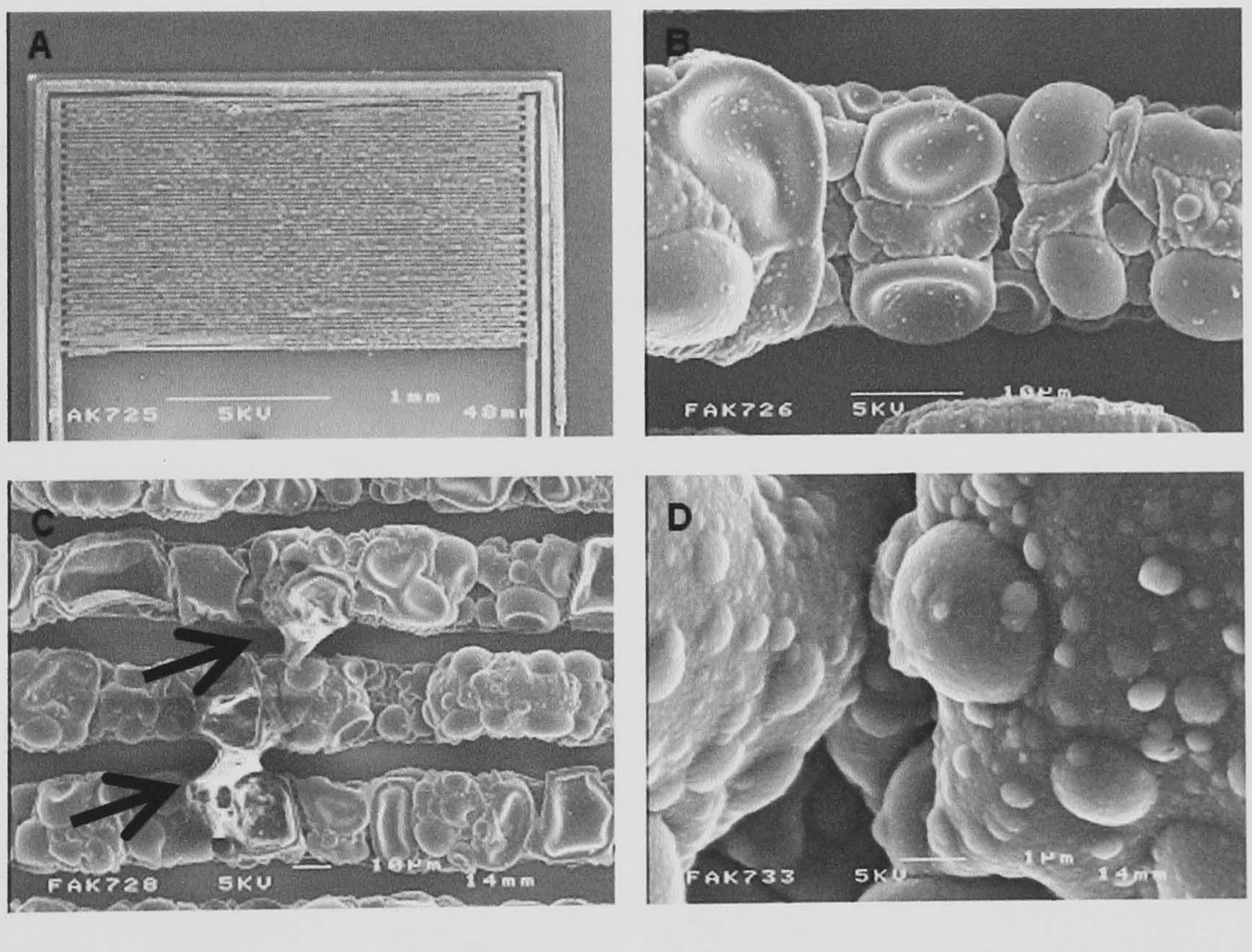

Figure 3.8: SEM of PPy/Cl on Gold IDE. (A) Whole IDE, (B) Single Digit, (C) Polymer Bridging between Digits (arrows) and (D) High Magnification Image of Surface.

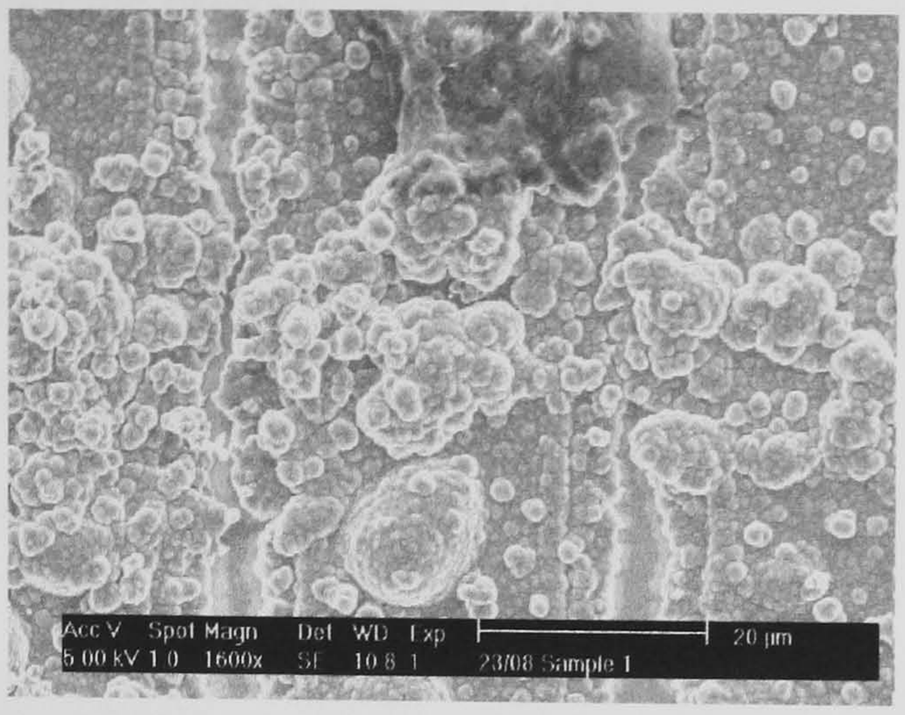

Figure 3.9: SEM of PPy/DS on Gold IDE (Taken from Lillie, 2001). *For PPy incorporating DS, the IDE surface is more extensively coveredafter synthesis and it is just about possible to make out the outline of individual digits.*

3.3.2 Polypyrrole Films on Gold-Coated Polycarbonate

The importance of a consistent method for film synthesis is highlighted in figure 3.10. Both PPy/Cl films were produced under the same conditions on a gold-coated polycarbonate coverslip except that A was immersed vertically in the electrolyte and B was held horizontally in the ETCC. Differences are observable on both surfaces including the formation of 'dendrite' type features for the vertical electrode absent from its horizontal counterpart. The ETCCs were subsequently used as conditions could thereby be kept more reproducible.

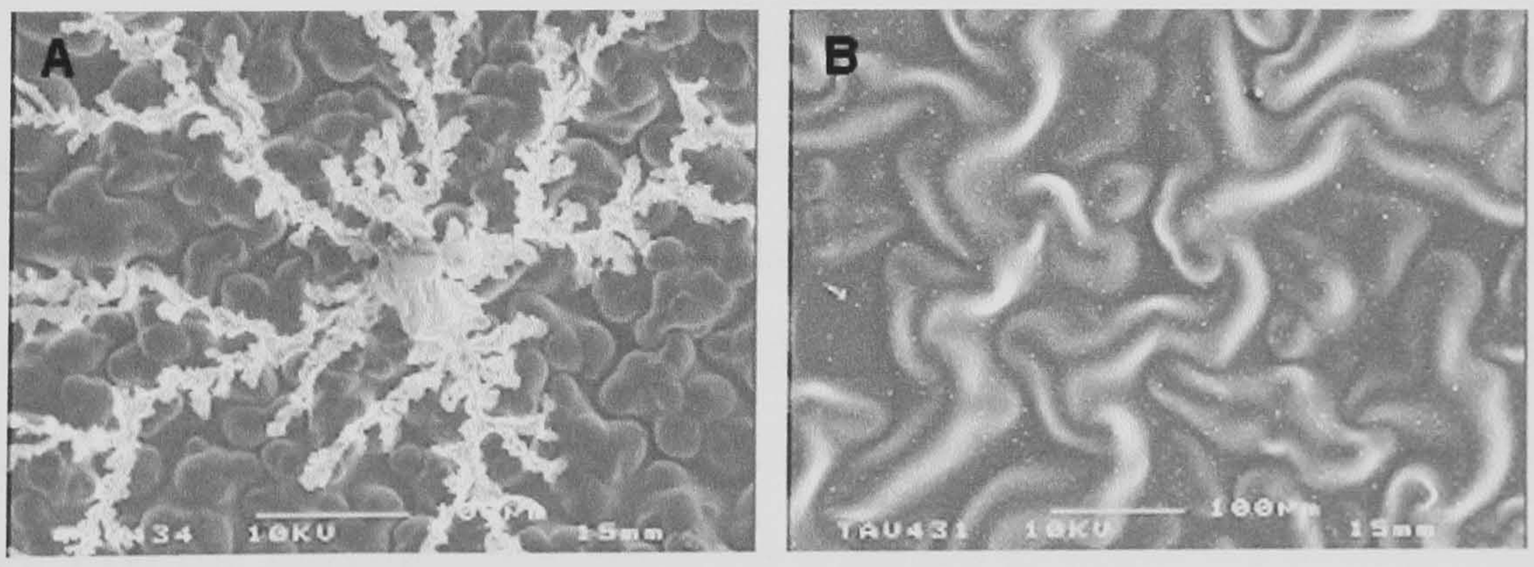

Figure 3.10: SEM of PPy/Cl on Gold-Coated PC (A) Immersed Vertically in Electrolyte and (B) Immersed Horizontally in Electrolyte. *A very different structure is seen for the same synthesis electrolyte when only the orientation of the electrode is changed. In the case of the vertically immersed electrode, a dendritic growth was observed.*

Figure 3.11 shows the patchy polymerisation for a fibrinogen-loaded film on a gold-coated PC coverslip. This was achieved when a few NaCl crystals where added to the electrolyte before cyclic voltammetry. Potentiostatic chronoamperometry was thus preferred as continuous films could be obtained. The higher magnification picture excess charging under the electron beam probably caused by the aggregation of non-conducting protein structures.

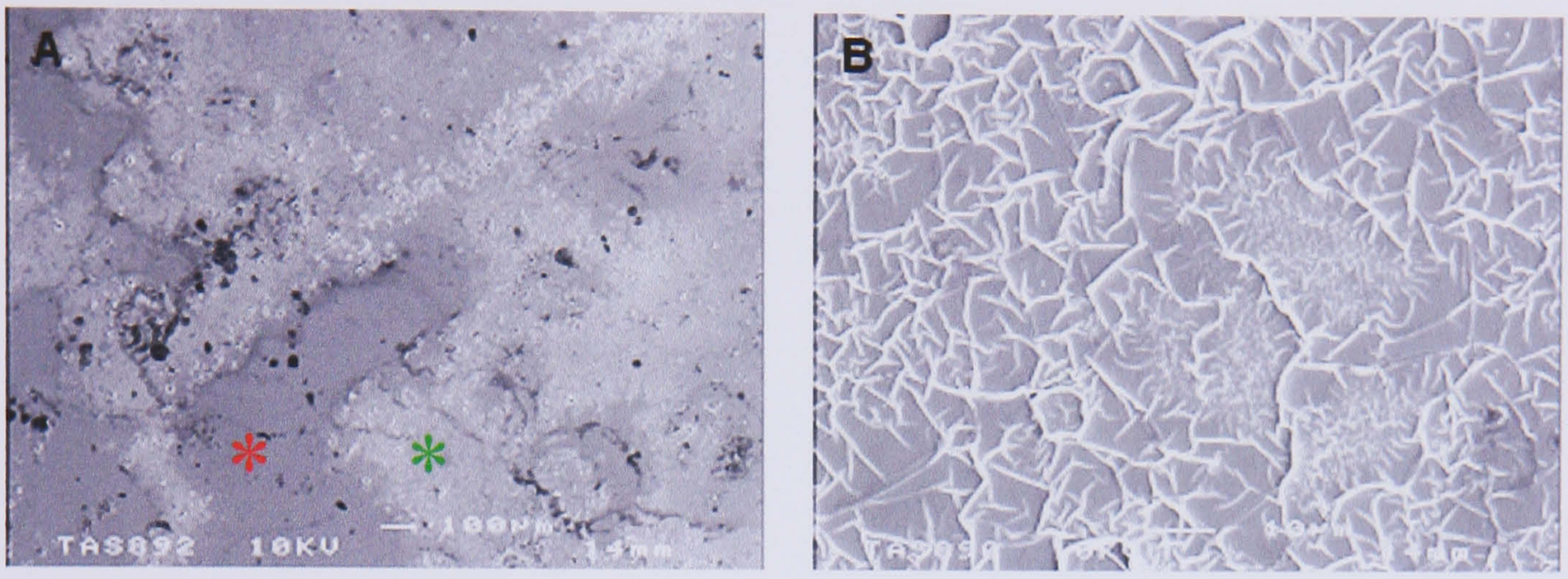

Figure 3.11: SEM of PPy/Fbri on Gold-Coated PC (A) Patchy Polymerisation at Low Magnification and (B) Distinctive Pattern at Higher Magnification. *The red asterix shows the gold electrode surface whilst the green asterix marks PPy.*

The subsequent SEMs (Fig 3.12) compare and contrast the topography of differently-loaded polypyrrole films. Thin films are characterised by featureless flat surfaces, except for collagen-loaded films where small nodules had started to emerge. For thick films, different topographies were generated for each counterion (polymerisation times up to 1½ h). For thick PPy/Cl films, nodules were observed at the surface. Thick PPy/PVS films exhibited undulations with nodules dotted on the surface. The undulations were accentuated for thick PPy/Derm films, presenting ridges and valleys. Thick PPy/Col films displayed the 'classical' cauliflower structure associated with other counterions such as dodecyl sulfate or avidin (Lillie, 2001). These pictures confirmed that varying the synthesis conditions for polypyrrole generates different surface characteristics on the polymer; and presents a means to tailor the surface topography of these materials. This is important in tissue engineering as cells are strongly influenced by micro- and nano-structure of substrates (Clark *et al.*, 1991; Curtis and Wilkinson, 1997; Desai, 2000).

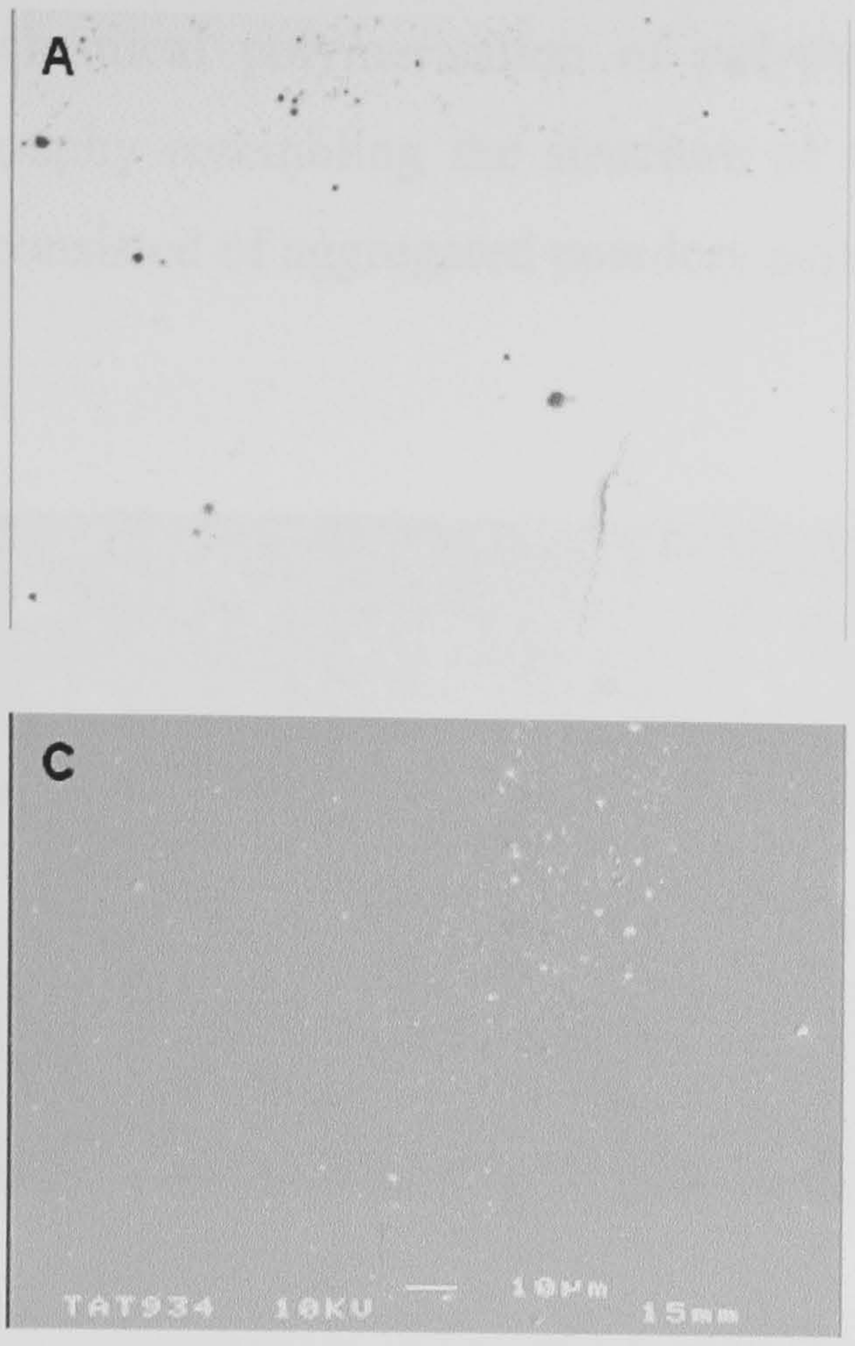

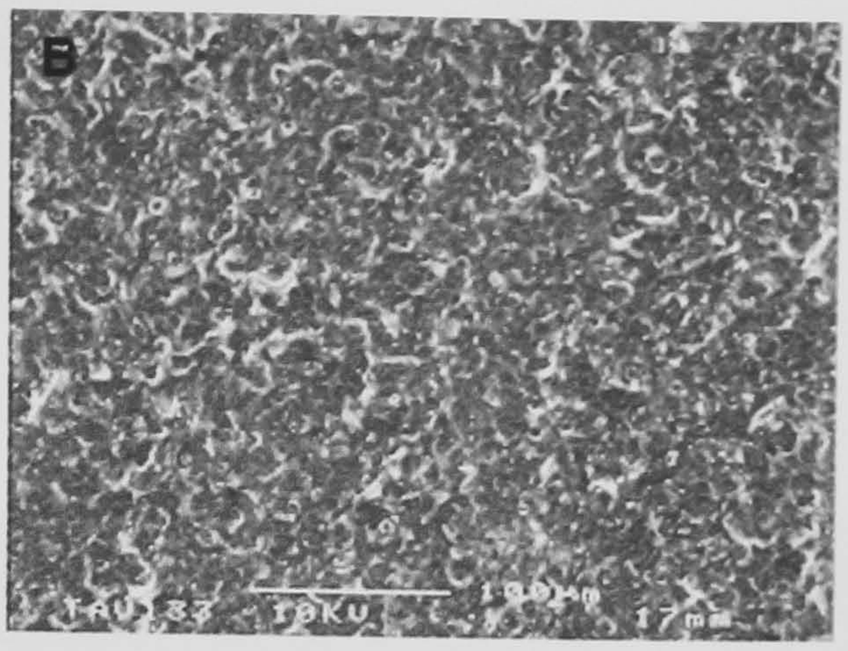

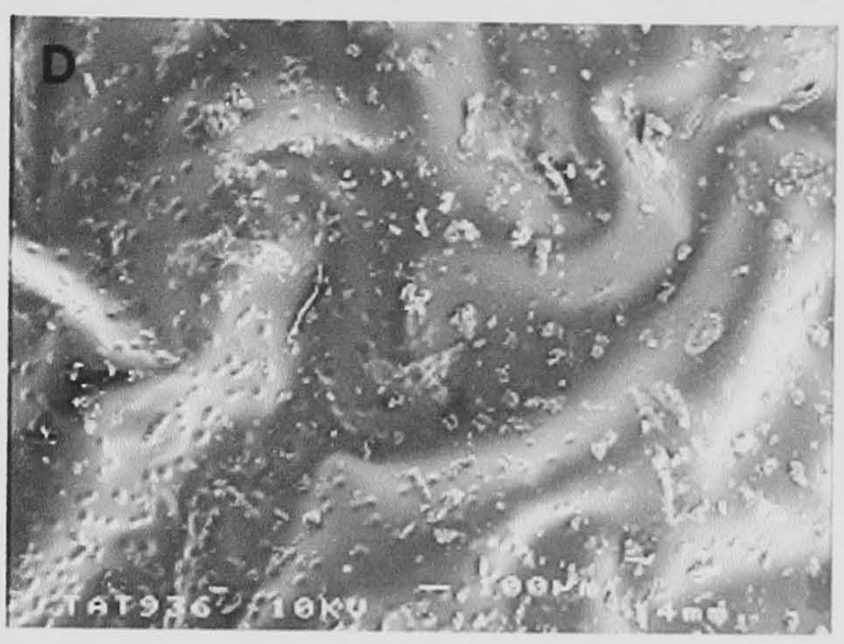

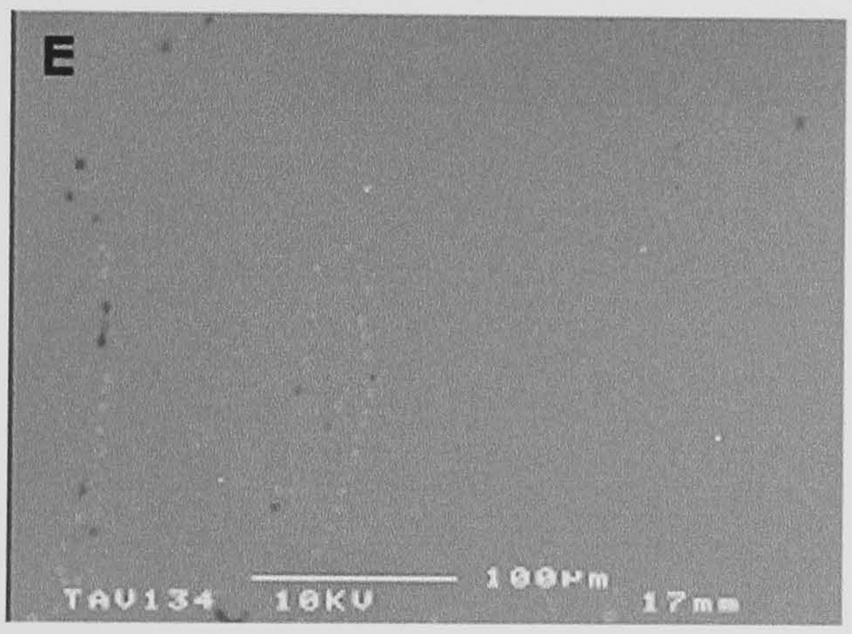

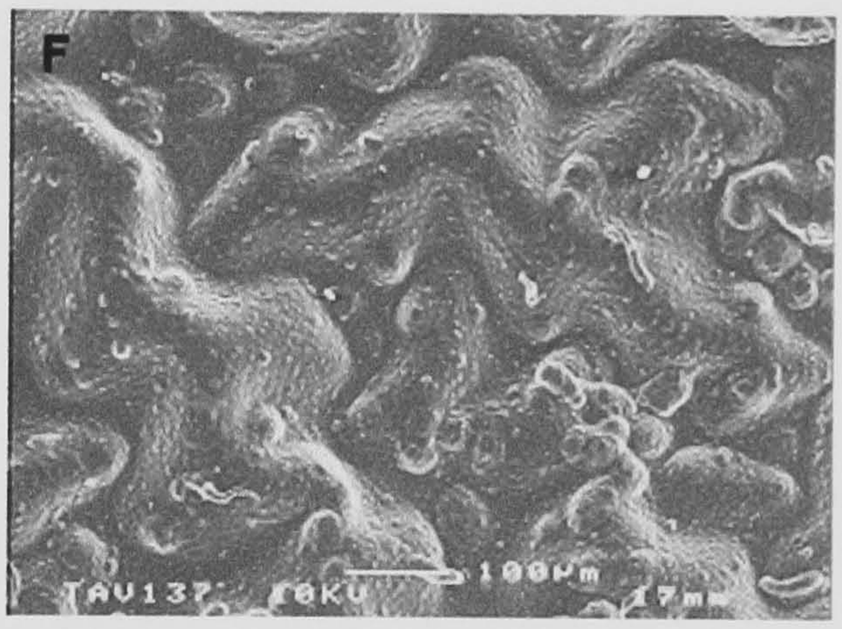

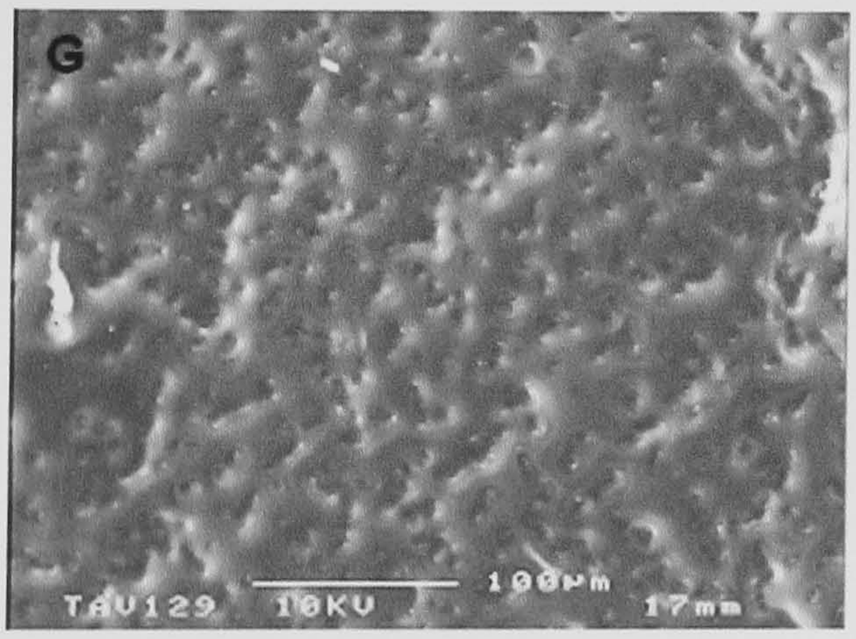

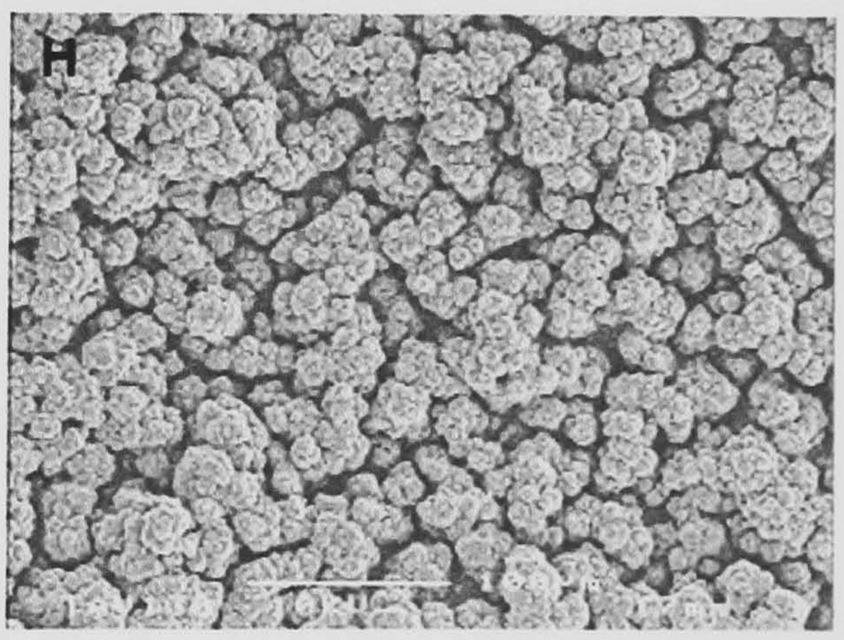

Figure 3.12: (A-B) PPy/Cl, (C-D) PPy/PVS, (E-F) PPy/Derm and (G-H) PPy/Col Thin Films (Left Column) and Thick Films (Right Column).

The chemical polymerisation of polypyrrole produced yet another type of distinct topography resembling the structure of coral (Fig 3.13). Essentially, the polypyrrole film consisted of aggregated powdery particles.

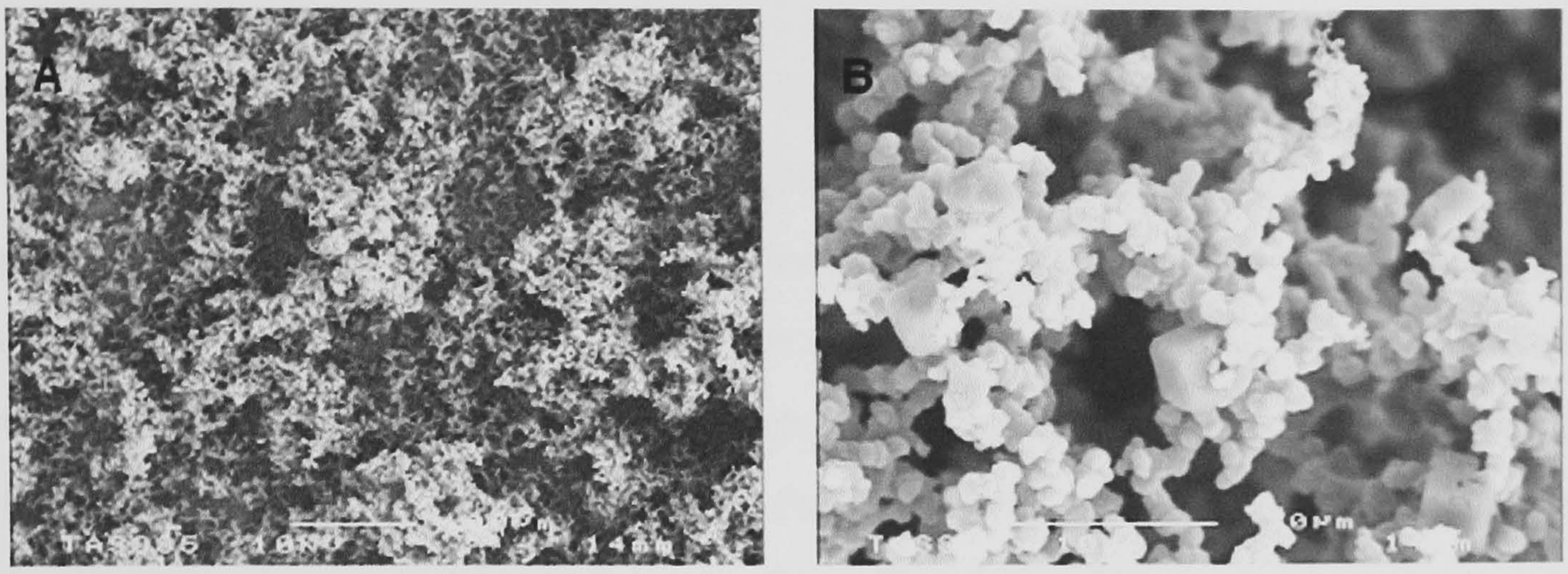

Figure 3.13: SEM of Chemically Polymerised Polypyrrole

(A) Low Magnification and (B) High Magnification.

3.4 Cyclic Voltammetry Studies of Polypyrrole Films

3.4.1 Cyclic Voltammetry

Cyclic voltammetry is often used to study redox processes including those of polypyrrole films (Fig 3.14). Voltammograms vary according to polymer loading and experimental conditions *i.e.* electrolyte composition, scan rate and potential limits. These curves generate a peak anodic current (I_{pa}) corresponding to peak oxidation potential (E_{pa}) and a peak cathodic current (I_{pc}) corresponding to peak reduction potential (E_{pc}). Other parameters such as the peak ratio, peak separation and the area under the curve equivalent to charge passed are also obtainable.

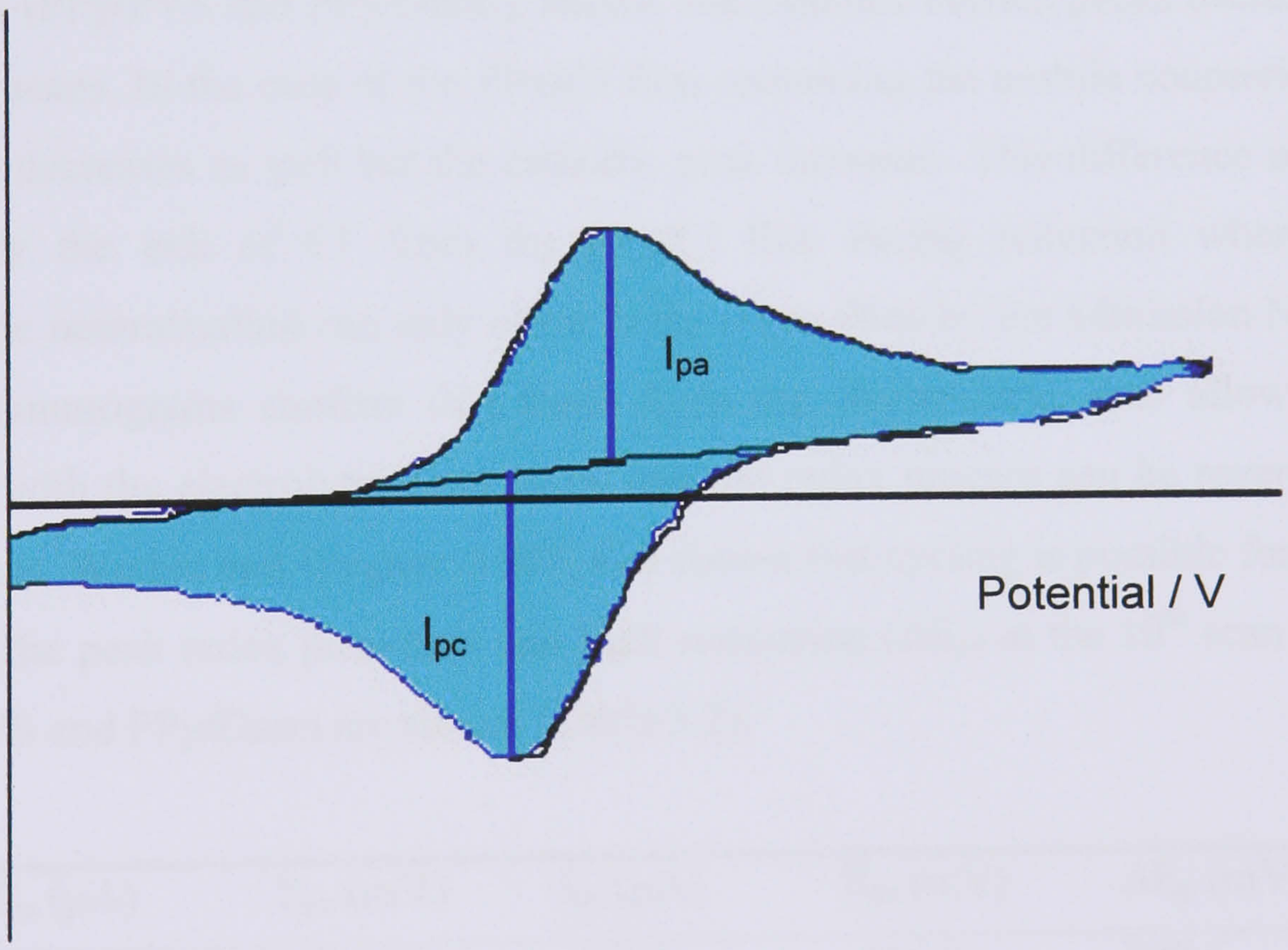

Figure 3.14: Model Cyclic Voltammogram for a Redox Active Species in Solution.

3.4.2 Cyclic Voltammetry of Selected Polypyrrole Films

Cyclic voltammetry was undertaken in a de-oxygenated monomer free 50 mM NaCl solution for all films at a scan rate of 50 mV/s. Potential limits were set between -0.8 V and +0.2 V *vs.* Ag/AgCl as to prevent overoxidation at higher positive potentials. Thin and thick PPy/Cl, PPy/PVS, PPy/Derm and PPy/Col films were studied (Fig 3.15 – 3.16). For each thin film except PPy/Col, redox peaks were easily identified. The absence of peaks in PPy/Col could be due to poor polymerisation resulting in poor electroactivity. For similar reasons, it is also difficult to distinguish peaks in the thick films. However, it can be seen from the areas under the curves that more charge is passed compared with thin films. Colour shifts between green, brown and black, characteristic of polypyrrole were also observed during cyclic voltammetry.

Repetitive cycling showed minor changes in peak position with increasing scans. This is more pronounced with initial scans. It is interesting to note that with the immobile counterion films (PPy/PVS and PPy/Derm), anodic and cathodic current peaks decrease with increasing scans. In the case of the PPy/Cl film containing the mobile counterion, the anodic peak decreases as well but the cathodic peak increases. This difference may be explained by the exit of Cl^- from the PPy/Cl film during reduction whereas equivalent charge neutralisation can only occur in the other films by the admission Na^+. The cyclic voltammograms confirm that these films are electroactive thus allowing ionic exchange with the electrolyte. They show that the redox process can be reversed for repeated scans, Wernet and Wegner (1987) had shown that cycling is possible for up to 4000 scans. The peak redox potentials and peak separation (ΔE_p) at the 10^{th} scan for PPy/Cl, PPy/PVS and PPy/Derm are shown (Table 3.2).

	I_{pa} (μA)	E_{pa} (mV)	I_{pc} (μA)	E_{pc} (mV)	ΔE_p (mV)
PPy/Cl	364.5	-152.3	-459.8	-551.9	399.6
PPy/PVS	285.8	-116.3	-376.2	-537.9	421.6
PPy/Derm	73.51	-182.4	-215.5	-441.9	259.5

Table 3.2: Cyclic Voltammetry Data for Thin Polypyrrole Films

(50 mV/s; 10^{th} Scan; electrolyte: 50 mM NaCl in dH_2O).

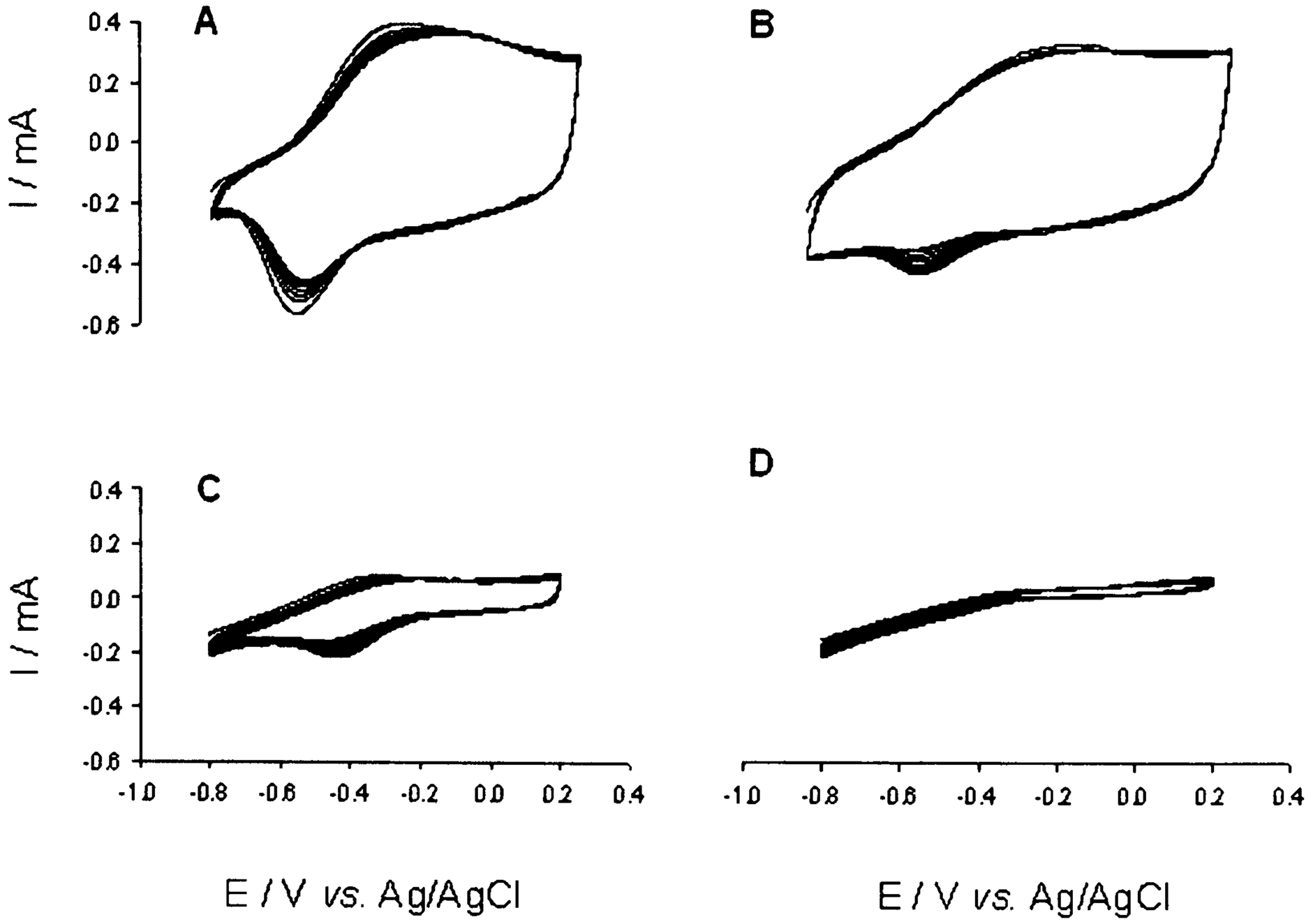

Figure 3.15: Cyclic voltammograms of thin PPy films *(50 mV/s vs. Ag/AgCl; 10 scans; 50 mM NaCl electrolyte). (A) PPy/Cl (B) PPy/PVS (C) PPy/Derm and (D) PPy/Col (synthesis electrolyte: 1 M pyrrole and 50 mM NaCl or 0.2 mg/ml PVS, Derm or Col).*

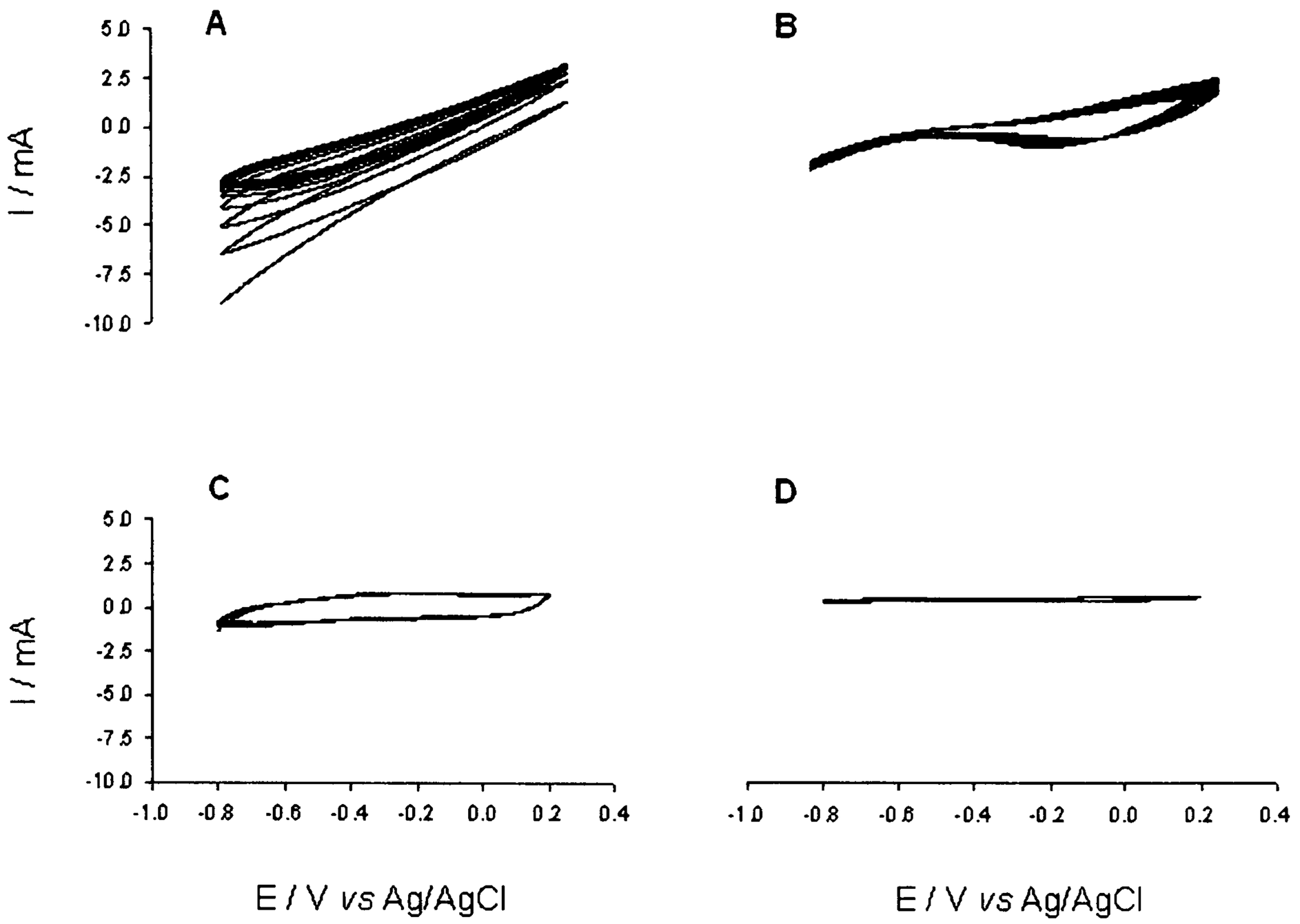

Figure 3.16: Cyclic voltammograms of thick PPy films*(50 mV/s vs. Ag/AgCl; 10 scans; 50 mM NaCl electrolyte). (A) PPy/Cl (B) PPy/PVS (C) PPy/Derm and (D) PPy/Col (synthesis electrolyte: 1 M pyrrole and 50 mM NaCl or 0.2 mg/ml PVS, Derm or Col).*

3.5 Impedance Spectroscopy Studies of Polypyrrole Films

3.5.1 In-Plane Two-Electrode Impedance

The results presented here are of chloride and dodecyl sulfate-loaded films deposited on gold IDEs. They are included to demonstrate the value of EIS as a characterisation technique for the material in its numerous configurations (*i.e.* redox states and counterion composition). Interdigitated electrodes were used in the two-electrode format as this forces most of the current to flow across the film thus recording in-plane impedance data. Theoretical analysis of electric fields at unmodified interdigitated electrodes used for impedimetric biosensing similar to those employed by this study (Gerwen *et al.*, 1998), demonstrated that the amount of current flow away from the plane was dependent on the spacing between the digits in addition to other factors such as the applied potential or solution resistance (Fig 3.17). Chapter 5 discusses data collected in the three-electrode format where impedance was sampled out-of-plane *i.e.* through the film.

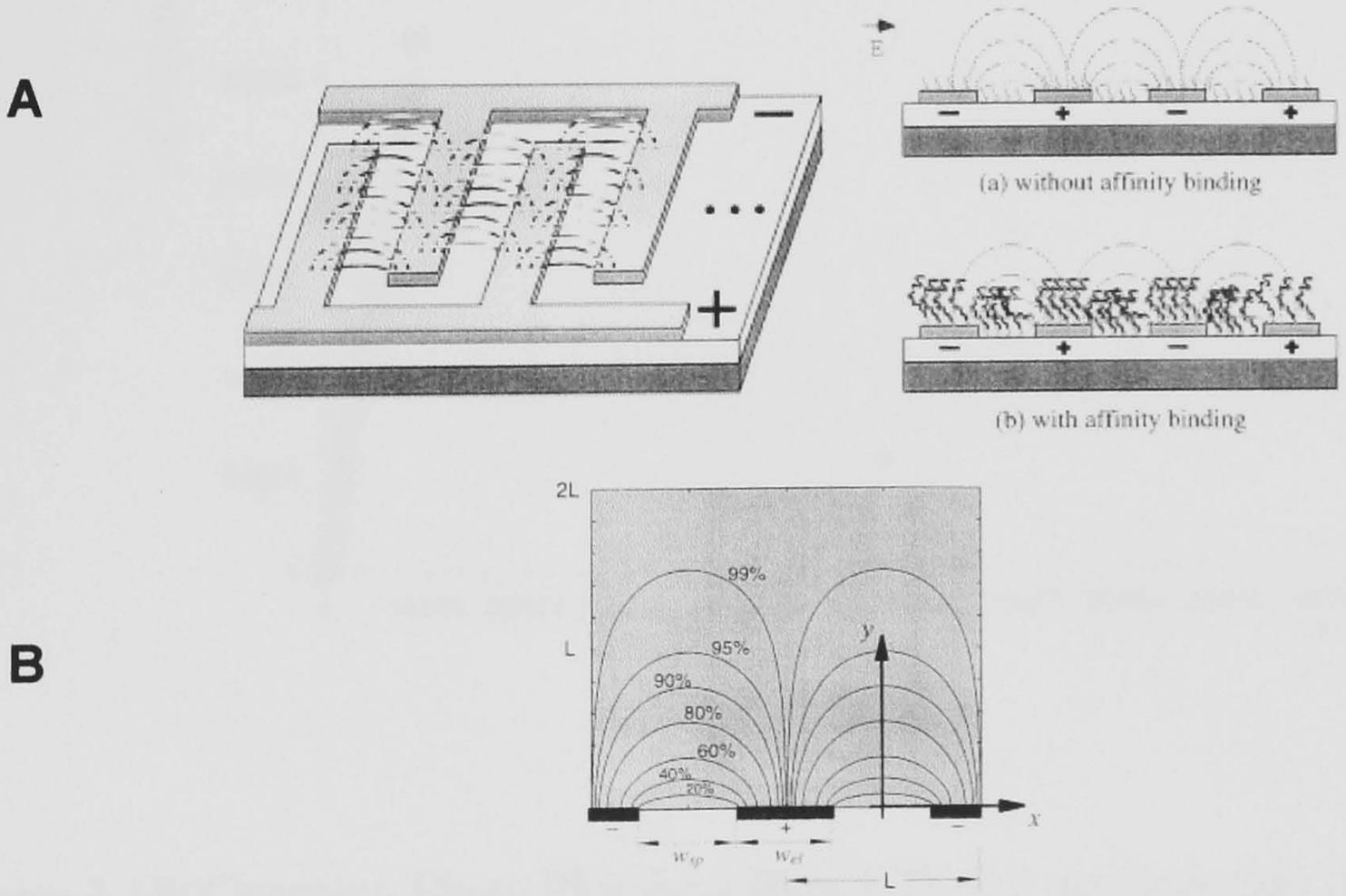

Figure 3.17: Unmodified Nanoscaled IDE

(A) Impedimetric Sensing and (B) Current Flow above IDE Plane

(Taken from Gerwen *et al.*, 1998).

3.5.2 Counterion Effect

Impedance spectra represented on complex planes (out-of phase impedance, Z'' against the in-phase impedance, Z') for a bare gold IDE and polypyrrole loaded with either chloride or dodecyl sulfate are shown in figures 3.18 – 3.20. Corresponding Bode plots are presented in figures 3.21 – 3.22. These films were analysed in a reduced state (or possibly partially reduced) since the last polymerisation scan was terminated at a -0.9 V *vs.* Ag/AgCl. As the chloride anions are highly mobile, they would have exited the film upon reduction. Conversely the immobile dodecyl sulfate anions would have remained bound within the film. The PPy/Cl film did not bridge the digits to the same extent as PPy/DS for an equivalent number of polymerisation cycles, explaining the increased impedance observed compared to the PPy/DS film at lower frequencies.

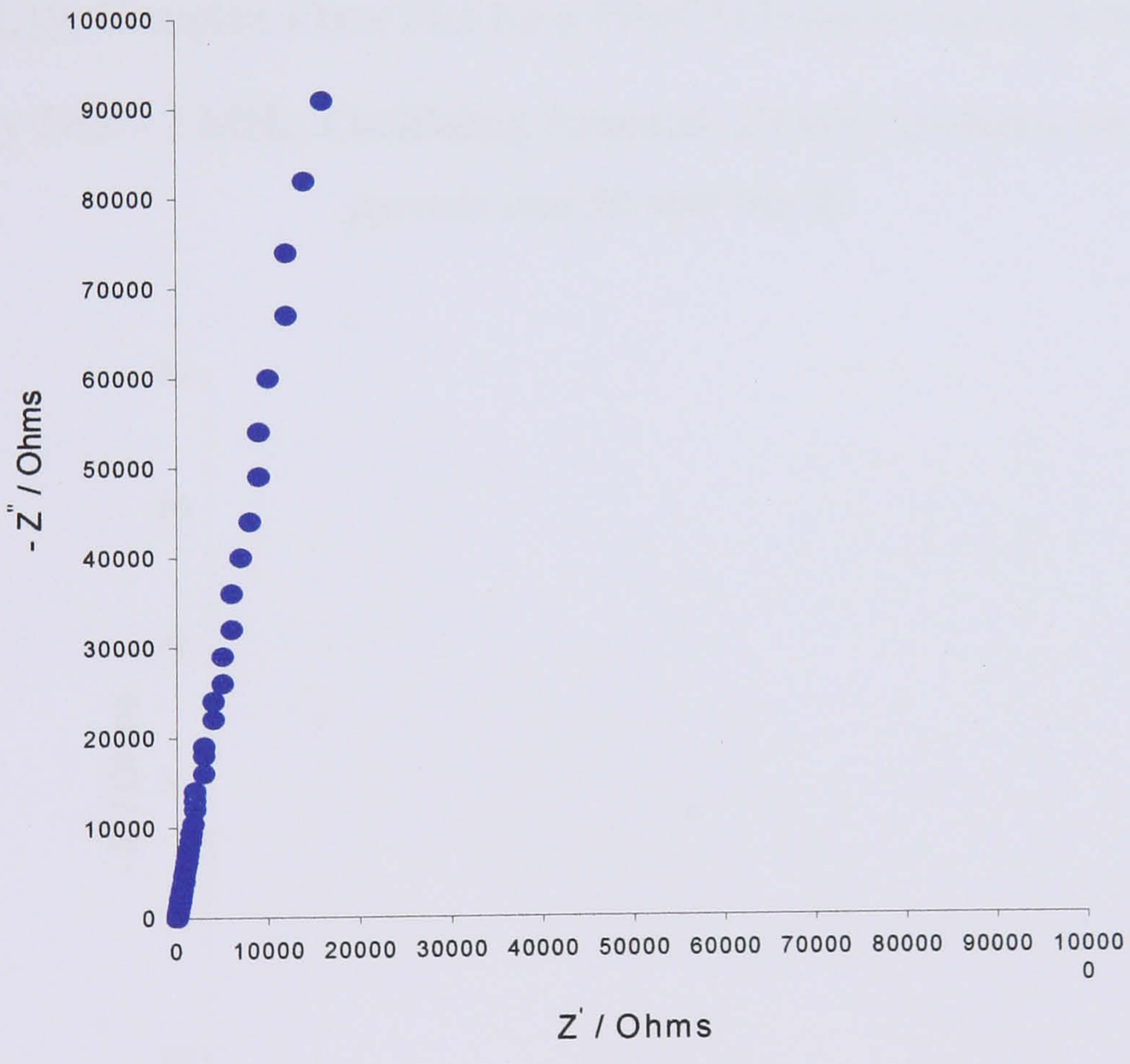

Figure 3.18: Complex Plane Plot for a Bare IDE (15 μm Spacing) in PBS (Buffer)

Frequency 5Hz – 1 MHz, Oscillating Potential: 20 mV

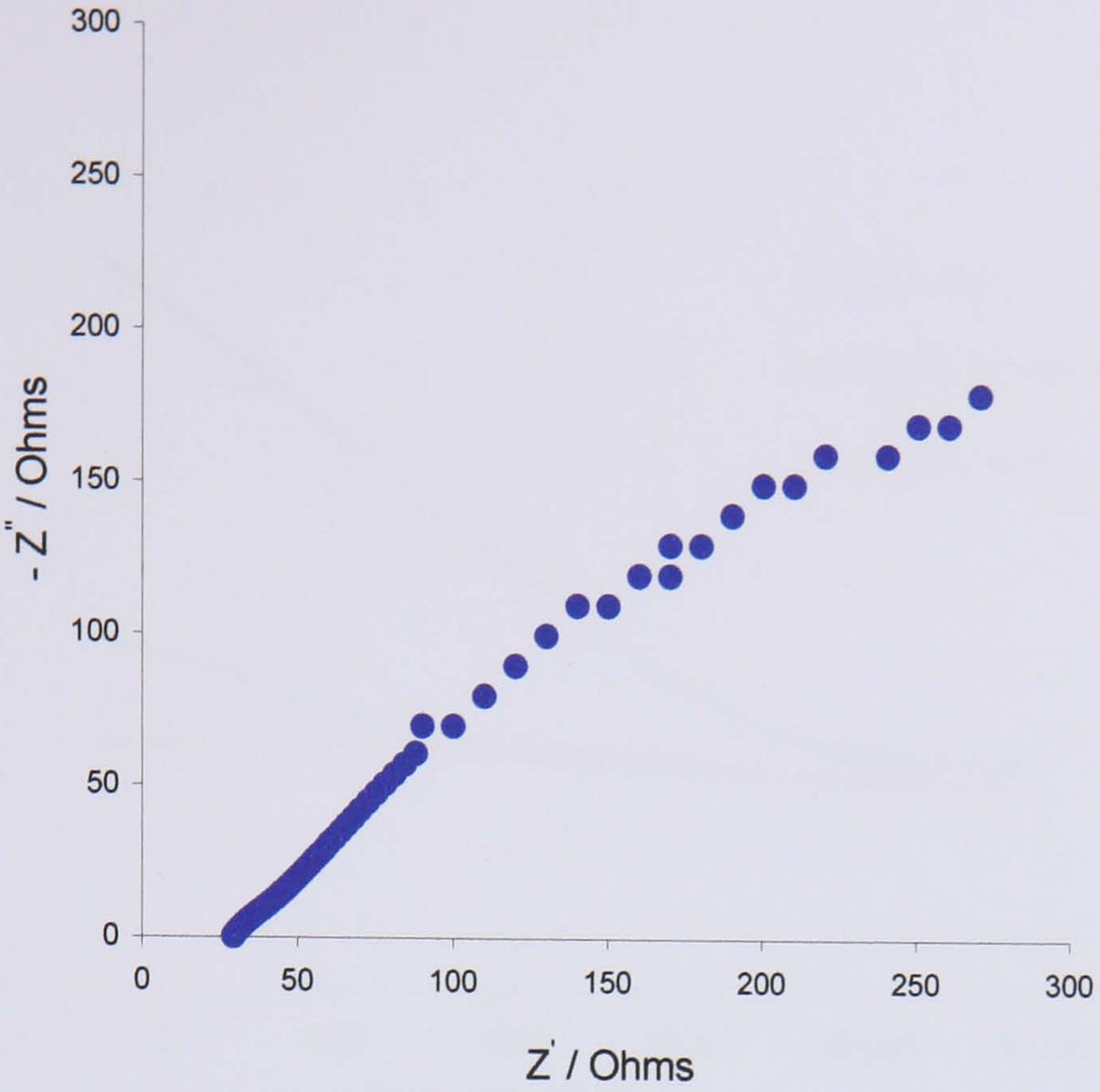

Figure 3.19: Complex Plane Plot for a PPy/Cl (Reduced State) in PBS (Buffer)

Frequency 5Hz – 1 MHz, Oscillating Potential: 20 mV *(synthesis electrolyte: 1 M pyrrole and 50 mM NaCl).*

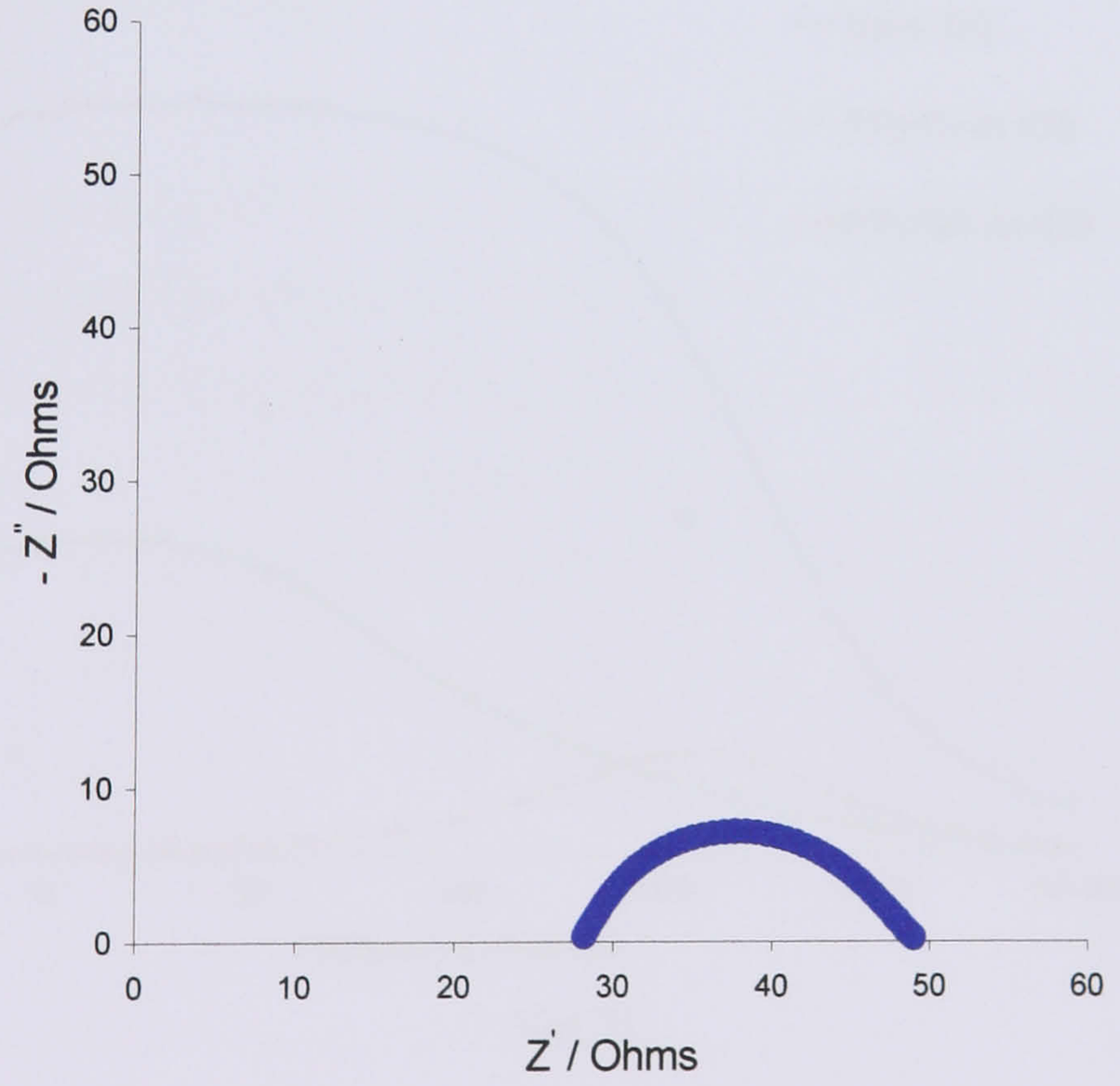

Figure 3.20: Complex Plane Plot for a PPy/DS (Reduced State) in PBS (Buffer)

Frequency 5Hz – 1 MHz, Oscillating Potential: 20 mV *(synthesis electrolyte: 1 M pyrrole and 50 mM NaCl).*

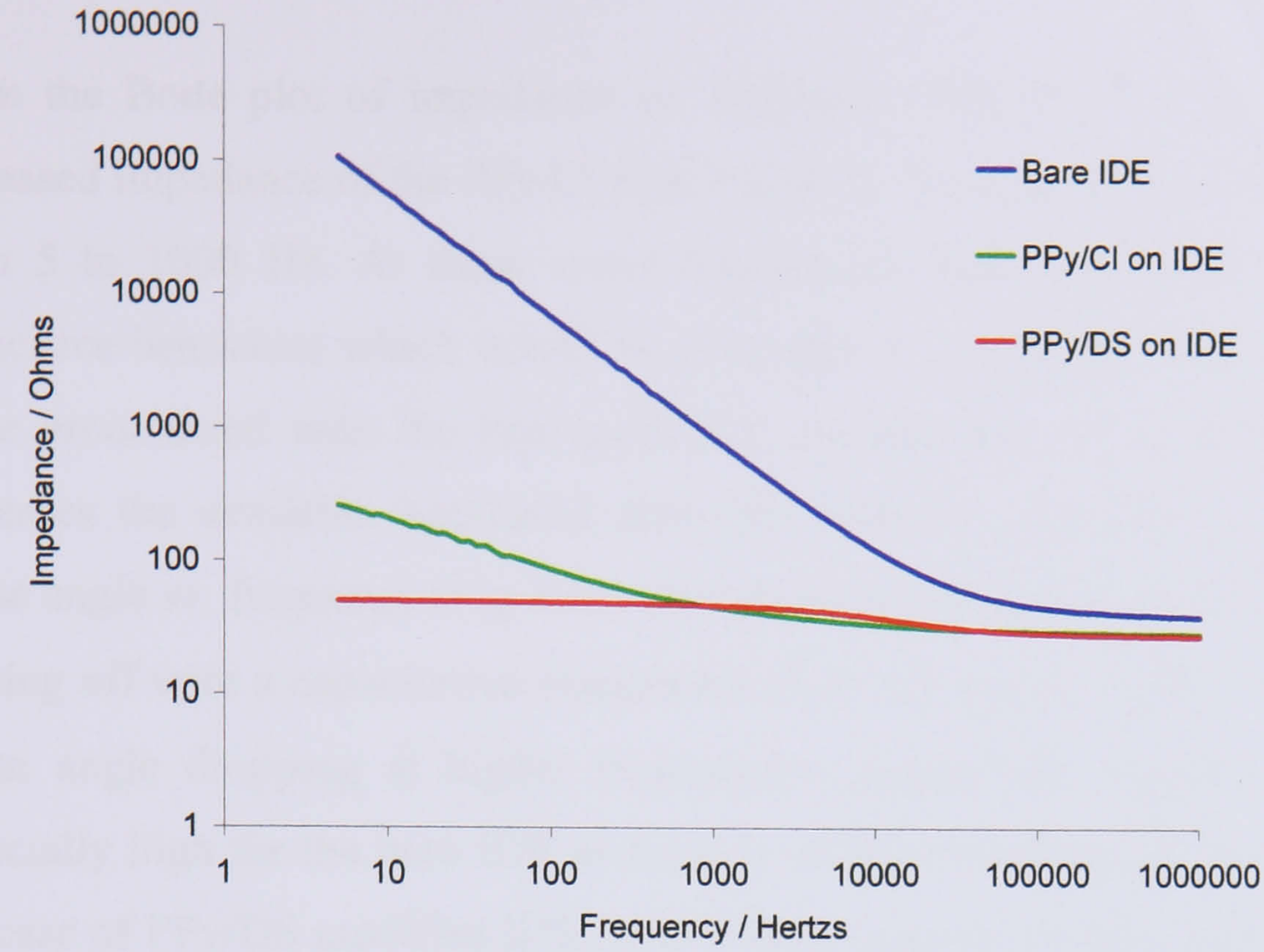

Figure 3.21: Bode Plot (Impedance *vs.* Frequency) in PBS (Buffer) Frequency 5Hz – 1 MHz, Oscillating Potential: 20 mV *(synthesis electrolyte: 1 M pyrrole and 50 mM NaCl).*

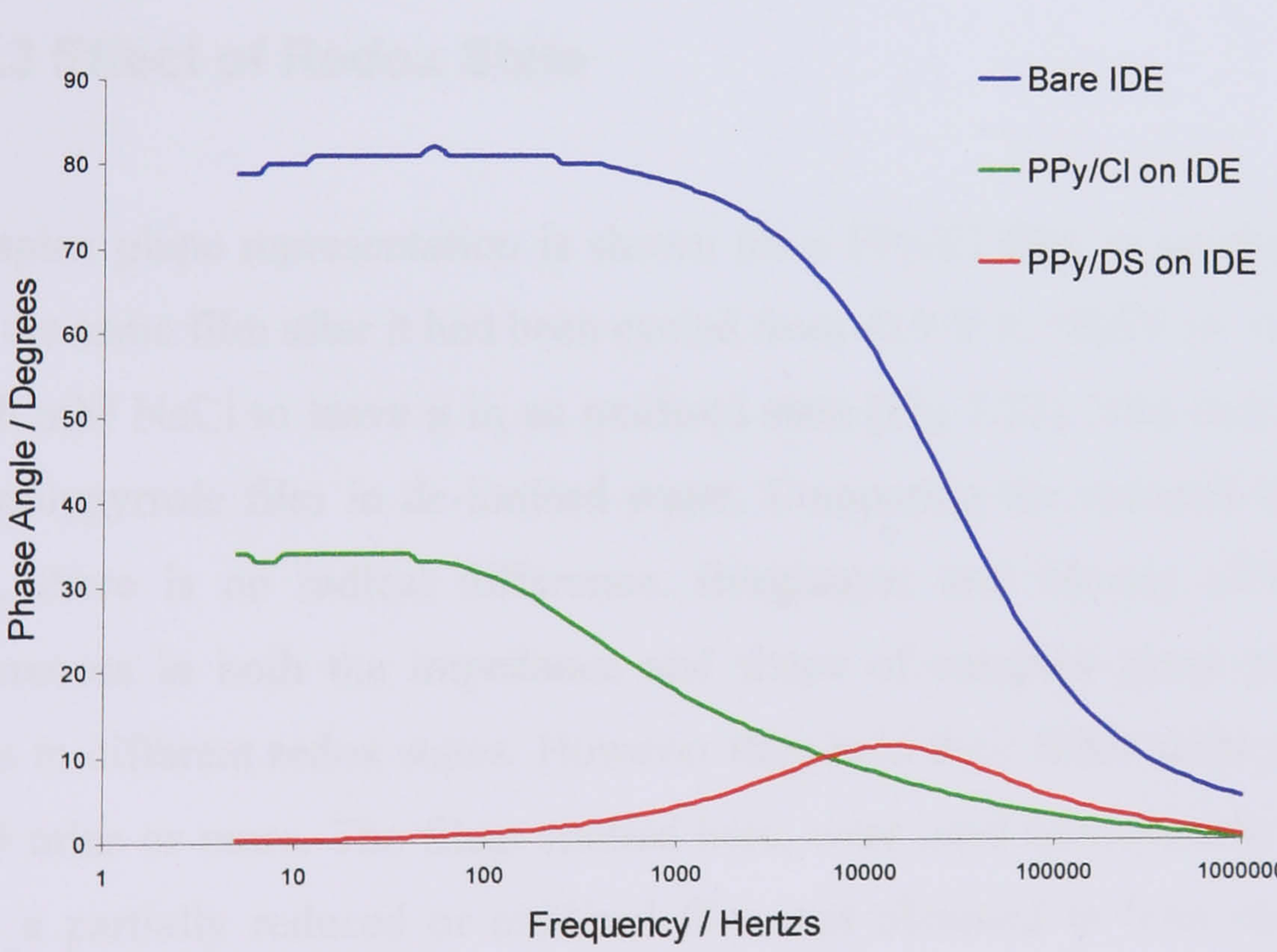

Figure 3.22: Bode Plot (Phase Angle *vs.* Frequency) in PBS (Buffer) Frequency 5Hz – 1 MHz, Oscillating Potential: 20 mV *(synthesis electrolyte: 1 M pyrrole and 50 mM NaCl).*

From the Bode plot of impedance *vs.* frequency (Fig 3.21) it may be seen that the increased impedance of the PPy/Cl film is mainly observed in the low frequency region, from 5 to 1000 Hz. At these lower frequencies high impedance is associated with capacitive behaviour which would be dominant in an incompletely bridged IDE and is more pronounced with the bare gold IDE. In addition, the polypyrrole modification increases the available interfacial area thus lowering impedance. The Bode plot for phase angle *vs.* frequency (Fig 3.22) also shows the bare IDE and PPy/Cl modified IDE starting off with a capacitative component (*N.B.* for a pure capacitor $\theta = 90°$) with the phase angle dropping at higher frequencies. Again, this capacitative component is especially high for the bare IDE as there is no polymer bridging between the digits. In the case of PPy/DS modified IDE, where there is good bridging between the digits, the material displays resistive behaviour (*N.B.* for a pure resistor $\theta = 0°$) especially at very low and very high frequencies. The phase angle rises to a peak of *ca* 11° around 15 kHz showing somewhat mixed behaviour.

3.5.3 Effect of Redox State

Complex plane representation is shown for a PPy/Cl film as produced (reduced state) and the same film after it had been cycled from -0.9 V to +0.6V *vs.* Ag/AgCl at 50 mV/s in 50 mM NaCl to leave it in an oxidised state (Fig 3.23). This data was recorded with the polypyrrole film in de-ionised water. Comparing the reduced film to the oxidised film, there is no radical difference. Burgmayer and Murray (1986) reported large differences in both the impedance and shape of complex plane plots of polypyrrole films in different redox states. However they held their films at the specified potentials for 5 mins or more. The films studied here, were used immediately. This suggests that only a partially reduced or oxidised film was obtained in both cases, explaining the similar spectra. However, subtle differences are observable between the two traces. These include the development of two semicircles before the transition to a straight slope in the case of the oxidised film compared to the reduced film where a linear slope is predominant.

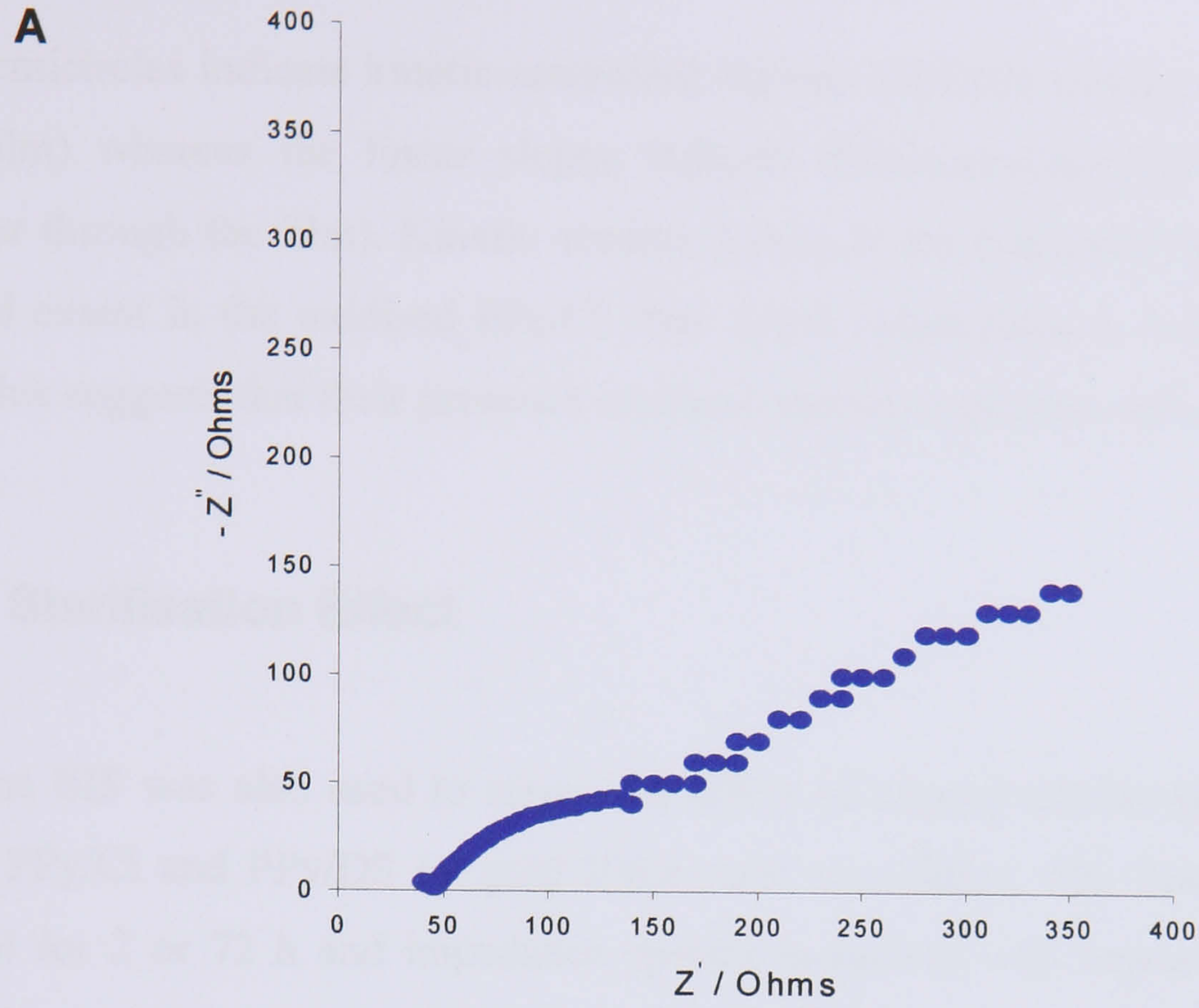

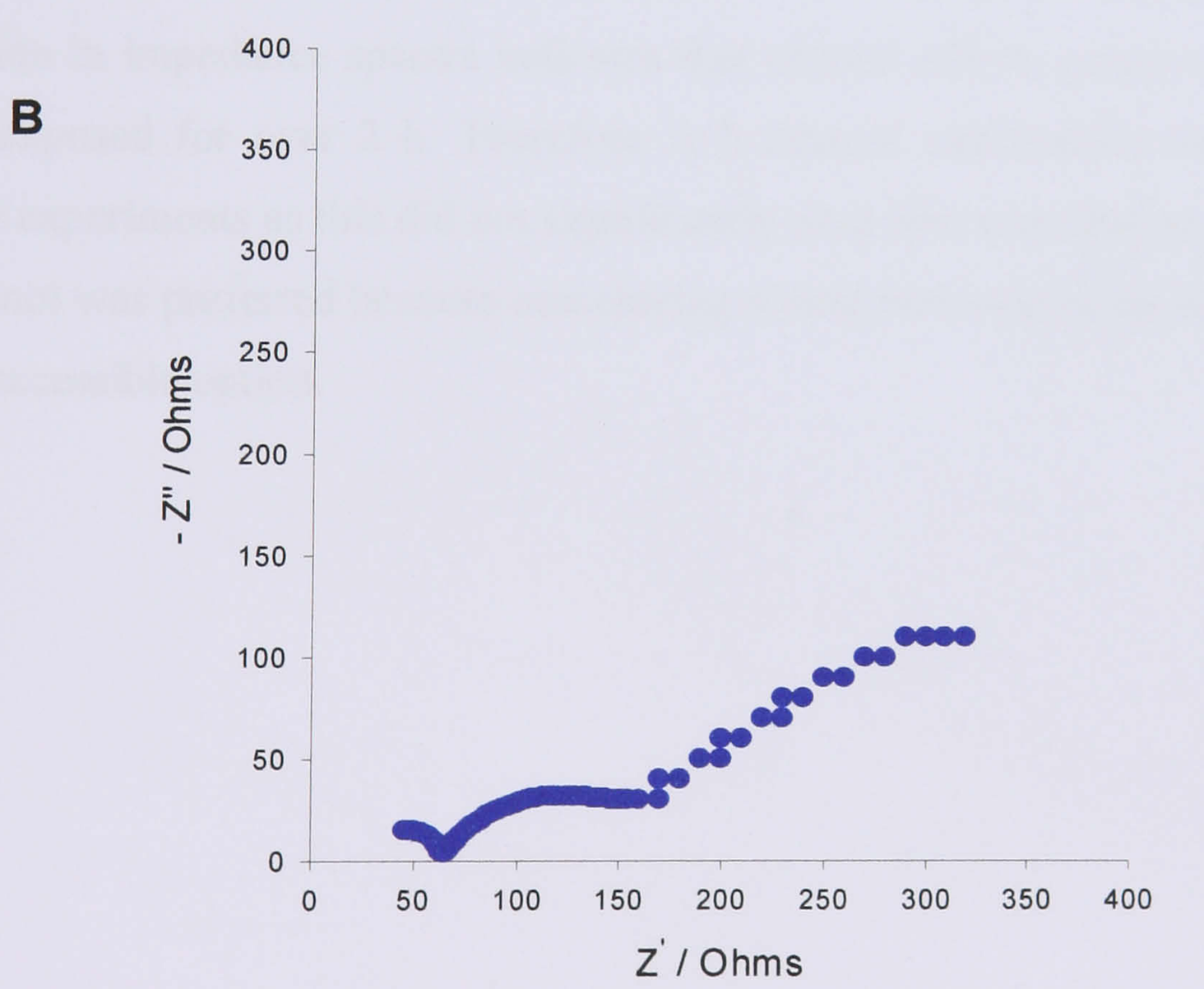

Figure 3.23: Complex Plane Plot for PPy/Cl (A) Reduced and (B) Oxidised in dH_2O Frequency 5Hz – 1 MHz, Oscillating Potential: 20 mV *(synthesis electrolyte: 1 M pyrrole and 50 mM NaCl).*

The semicircles indicate kinetic-controlled regions (electron transfer between electrode and film) whereas the linear slopes indicate diffusion-controlled regions (electron transfer through the film). Kinetic control is seen in the reduced PPy/DS film and to a limited extent in the oxidised PPy/Cl film. Since counterions in both cases are in the film, this suggests that their presence mediates electron transport within the film.

3.5.4 Sterilisation Effect

In-plane EIS was also used to assess the effect of ethanol sterilisation on polypyrrole films. PPy/Cl and PPy/DS on gold IDEs were considered. The films were soaked in ethanol for 2 or 72 h and impedance spectra compared with unmodified films in de-ionised water (Fig 3.24 – 3.25). At 2 h in ethanol, films are not altered significantly, but at 72 h, impedance spectra for both films are altered. For the PPy/DS film, no data could be recorded at all as impedance behaviour was out of the analyser's range. This alteration in impedance spectra indicates that ethanol affects polypyrrole film integrity when exposed for over 2 h. Therefore ½ h ethanol sterilisation was used for tissue culture experiments as this did not significantly alter film constitution. Cold sterilisation in ethanol was preferred because autoclaving would melt coverslips and γ-radiation was a less accessible option.

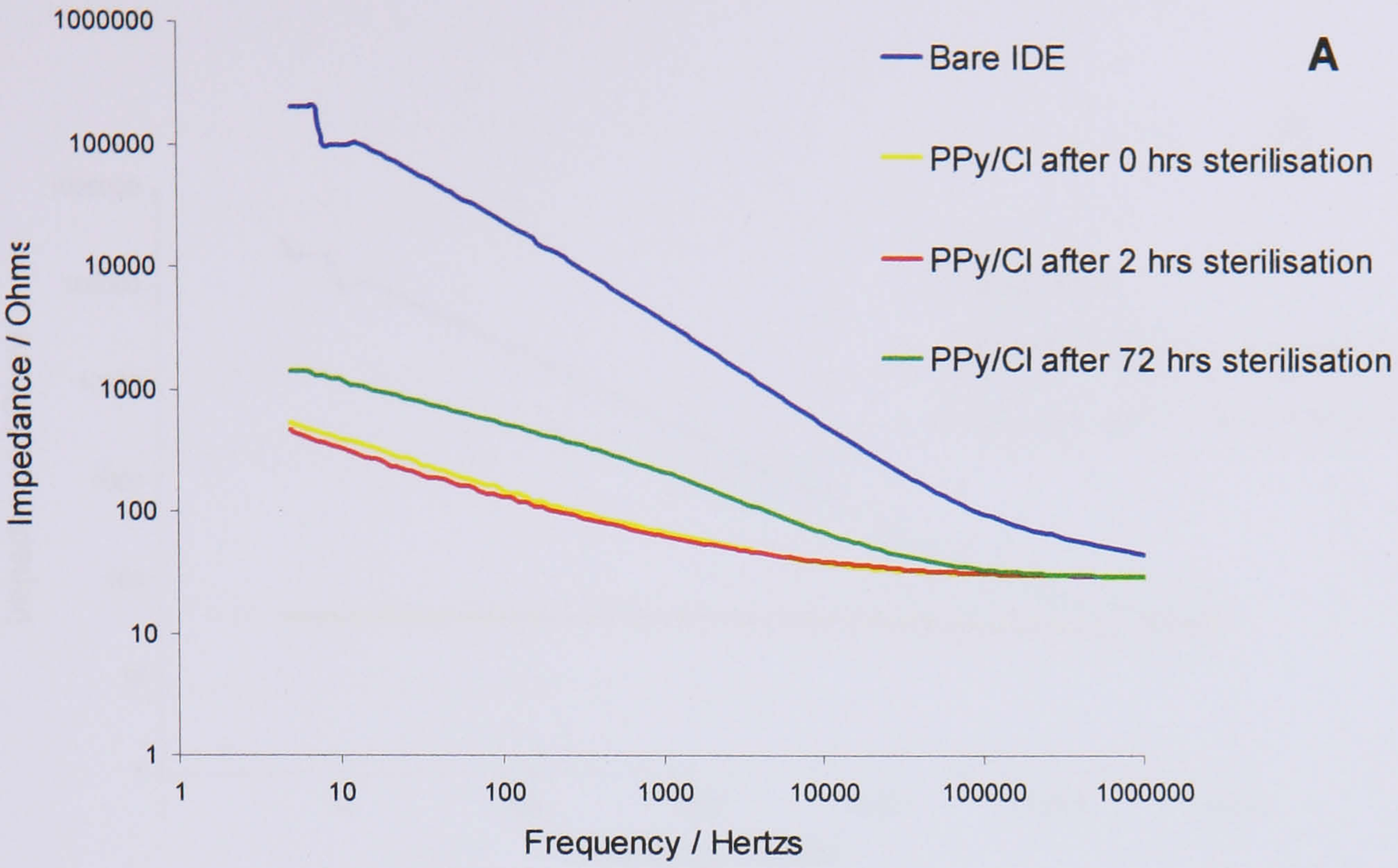

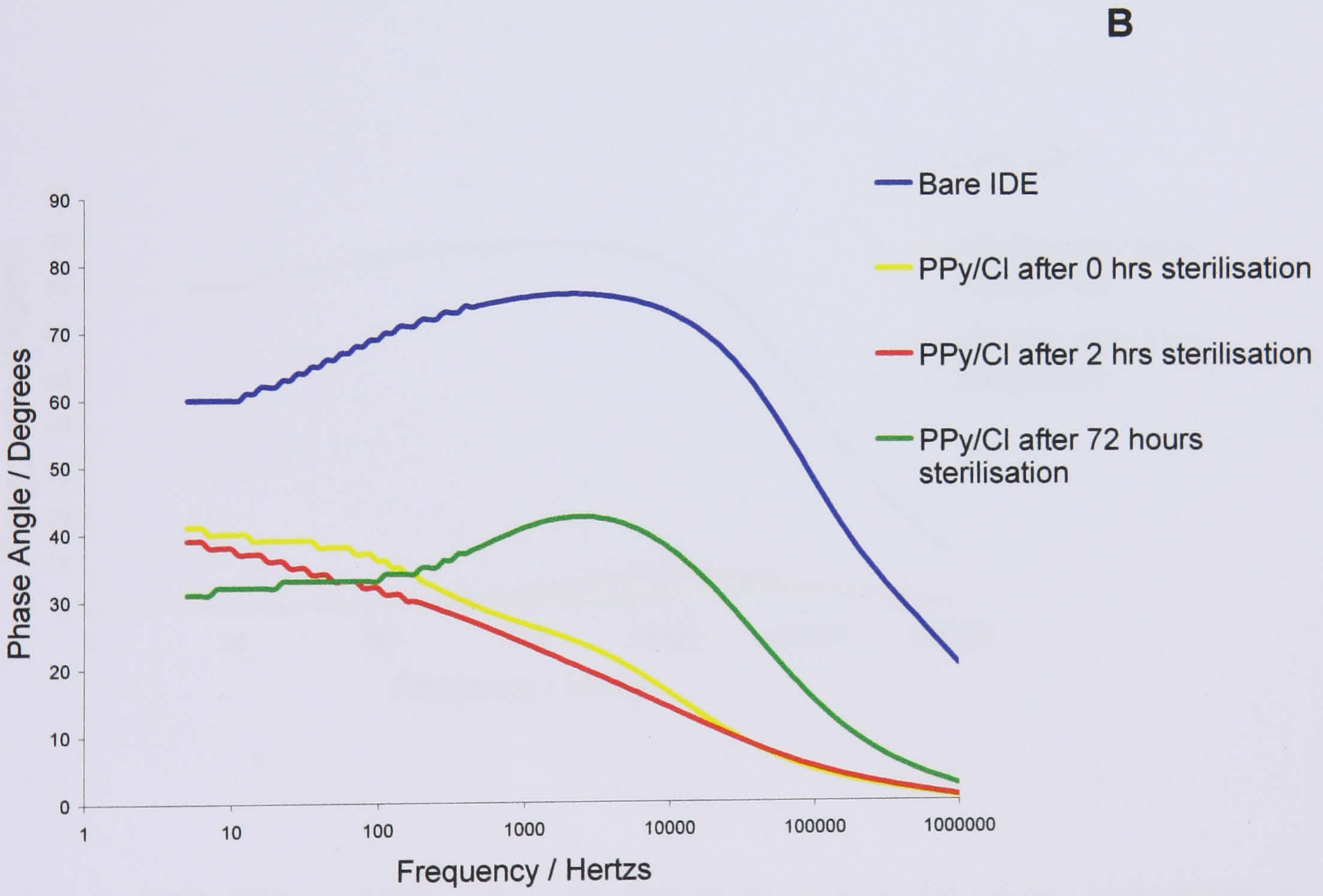

Figure 3.24: Effect of Ethanol on PPy/Cl Bode Plot (in dH_2O) (A) Impedance *vs.* Frequency and (B) Phase Angle *vs.* Frequency *(synthesis electrolyte: 1 M pyrrole and 50 mM NaCl).*

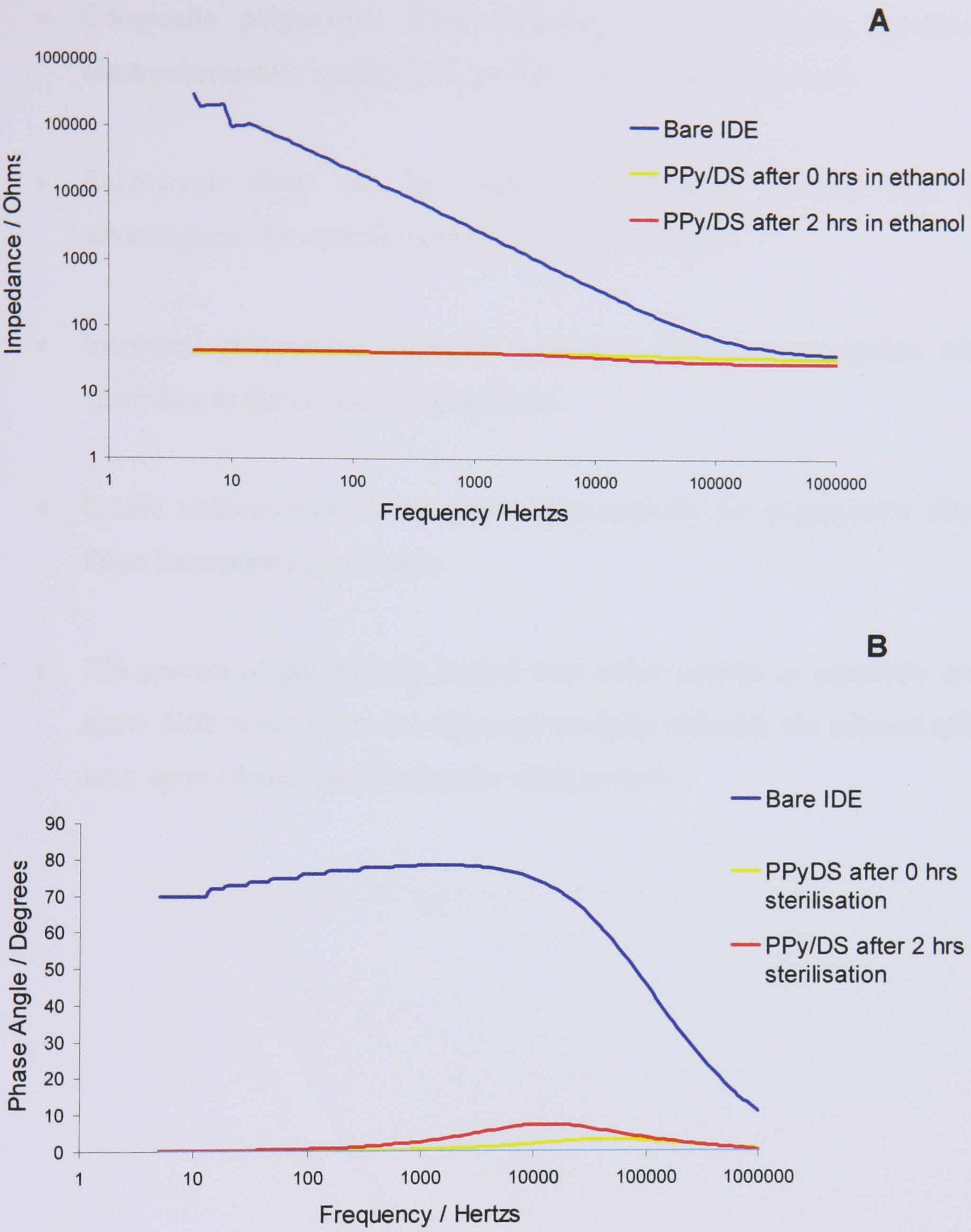

Figure 3.25: Effect of Ethanol on PPy/DS Bode Plot (in dH_2O) (A) Impedance *vs.* Frequency and (B) Phase Angle *vs.* Frequency *(synthesis electrolyte: 1 M pyrrole and 50 mM NaCl).*

3.6 Summary

- Composite polypyrrole films including those containing proteins can be electrochemically synthesised, preferentially potentiostatically.

- Polypyrrole films can be made transparent by limiting their thickness, advantageous for optical monitoring of cell cultures.

- Increased polypyrrole thickness generates distinct topographies which vary according to the counterion employed.

- Cyclic voltammetry shows good electroactivity for polypyrrole films except those incorporating collagen.

- EIS spectra of polypyrrole loaded with either mobile or immobile counterions show differences when the films are partially reduced. No adverse effects were seen upon ethanol sterilisation for short periods.

Chapter 4

Growth of Cells on Polypyrrole Films

4.1 Introduction

Successful synthesis and characterisation of a range of polypyrrole substrates enabled progression to the next step of investigations. The various polypyrrole substrates needed to be evaluated for their ability to support epithelial cell growth. This would not only enable the identification of preferential substrates but also provide insight into cell-material interactions. Here, the results for these studies, including biochemical assay and immunocytochemistry evidence, are presented. Studies into the use of polypyrrole as a tissue engineering substrate for the growth of primary skin cells and the challenges involved are also presented. The work in this Chapter facilitates the main project objective of studying epithelial cells on polypyrrole substrates using EIS, since impedimetric responses can be compared to viability data collected by alternative means.

4.2 SVK14 Keratinocytes

4.2.1 Viability and Proliferation Studies

Measuring Viability and Proliferation

The viability and proliferation of the immortalised SVK14 keratinocyte cell line was studied on differently-loaded polypyrrole films and on other control surfaces. The relatively new AlamarBlue™ assay, based on the transformation of an aqueous fluorescent dye, was used to determine cell viability and proliferation. This was preferred to the MTT assay as AlamarBlue™ is non-toxic to cells, allowing them to be reused. AlamarBlue™ is available in its oxidised, blue, non-fluorescent form. Upon exposure to cells, it is reduced to a pink fluorescent form by cellular metabolic activity; absorbance or fluorescence can be monitored in direct relation to cell activity.

O'Brien *et al* (2000) compared AlamarBlue™ and MTT for cell cytotoxicity and proliferation. They concluded that AlamarBlue™ gave 'a very simple, fast, sensitive and accurate cell viability measurement' if precautions were taken. Firstly, they advised that cross-reactivity of AlamarBlue™ with any compound should be tested in the absence of cells. Secondly, the reduction rate by cells in culture needed to be tested for optimising concentration and incubation time; it is necessary to avoid over-reduction, to the colourless and non-fluorescent hydroresorufin. Finally they suggest that the assay is better used as an end point measure rather than a kinetic measure for cell growth.

Ojeh (2002) previously studied SVK14 keratinocytes in tissue culture well plates to compare the AlamarBlue™ and MTT assays. One of the conclusions was that AlamarBlue™ was a suitable assay for SVK14 keratinocyte proliferation with the added advantage of non-toxicity. The results and the manufacturer's guidelines were used to establish the initial experimental conditions. AlamarBlue™ results were verified by both microscopy and other assays; quantitative cell protein and ATP analysis. Also, immunocytochemistry was performed.

AlamarBlue™ Assays and Optical Microscopy

Continuous Measurements

Results for one of the first studies of SVK14 keratinocytes proliferation on polypyrrole are shown in figure 4.1. PPy/Cl films are compared with a TCPS control. AlamarBlue™ was added at the beginning of the assay and left in the media for the duration of the study. Cells grown on TCPS are seen to have adhered by day 1 and confluent by day 7 (Fig 4.2); for PPy/Cl they are rounded, a sign of cell death (Fig 4.3). However, the AlamarBlue™ data fails to pick up this loss of cells, showing instead an increase in fluorescence. This is presumably because dye conversion which occurred before cell death was retained throughout.

These results indicated that it was important to sample specific time-points as recommended by O'Brien *et al* (2000). The poor growth of cells on polypyrrole was contrary to previous literature reports (Chapter 1). However, the fact that culture media was not replenished during the experiments may have contributed. The next experiments were carried out using single point AlamarBlue™ testing. This involved incubating cells in media without AlamarBlue™, then on measurement days only, exposing them to dye containing media for a fixed period after which samples were collected for analysis. The remaining solution was then aspirated and replaced with fresh media.

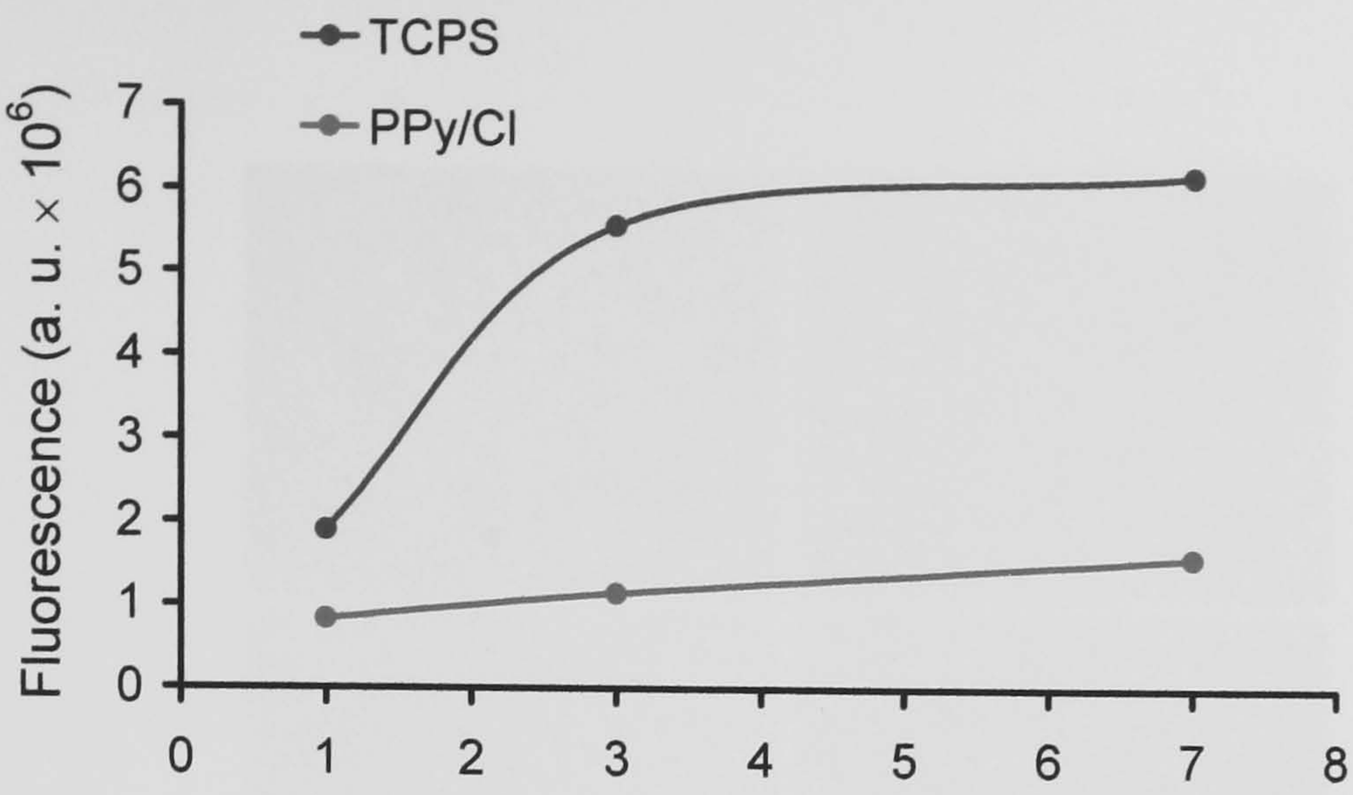

Figure 4.1: SVK14 Keratinocytes AlamarBlue™ Proliferation Assay

(Continuous Measurement)

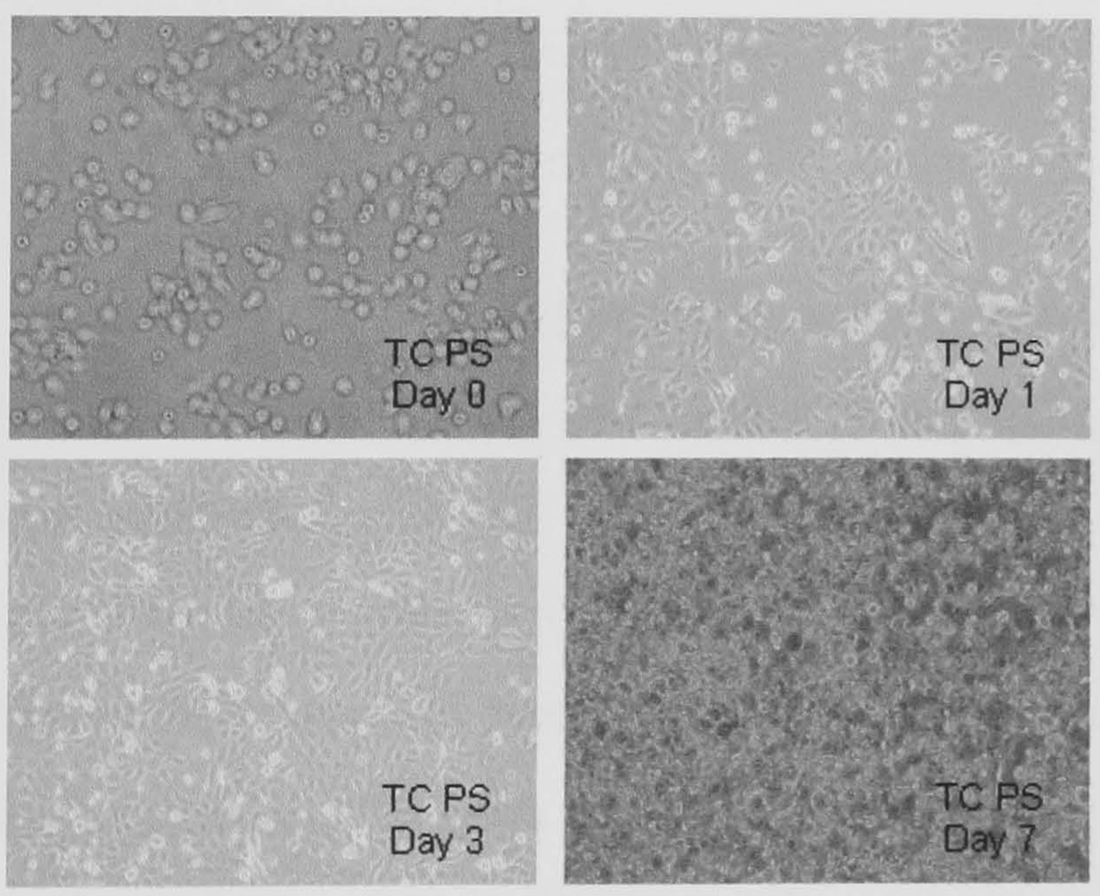

Figure 4.2: Micrographs of SVK14 Keratinocytes on TCPS. *Keratinocytes are starting to flatten out on day 0 and by day 1 they have fully adhered to the substrate and started to form colonies. On day 3 they have nearly covered the surface of the substrate and by day 7 full coverage as occurred with cells seen floating above those adhered to the substrate indicative of stratification as seen in skin.*

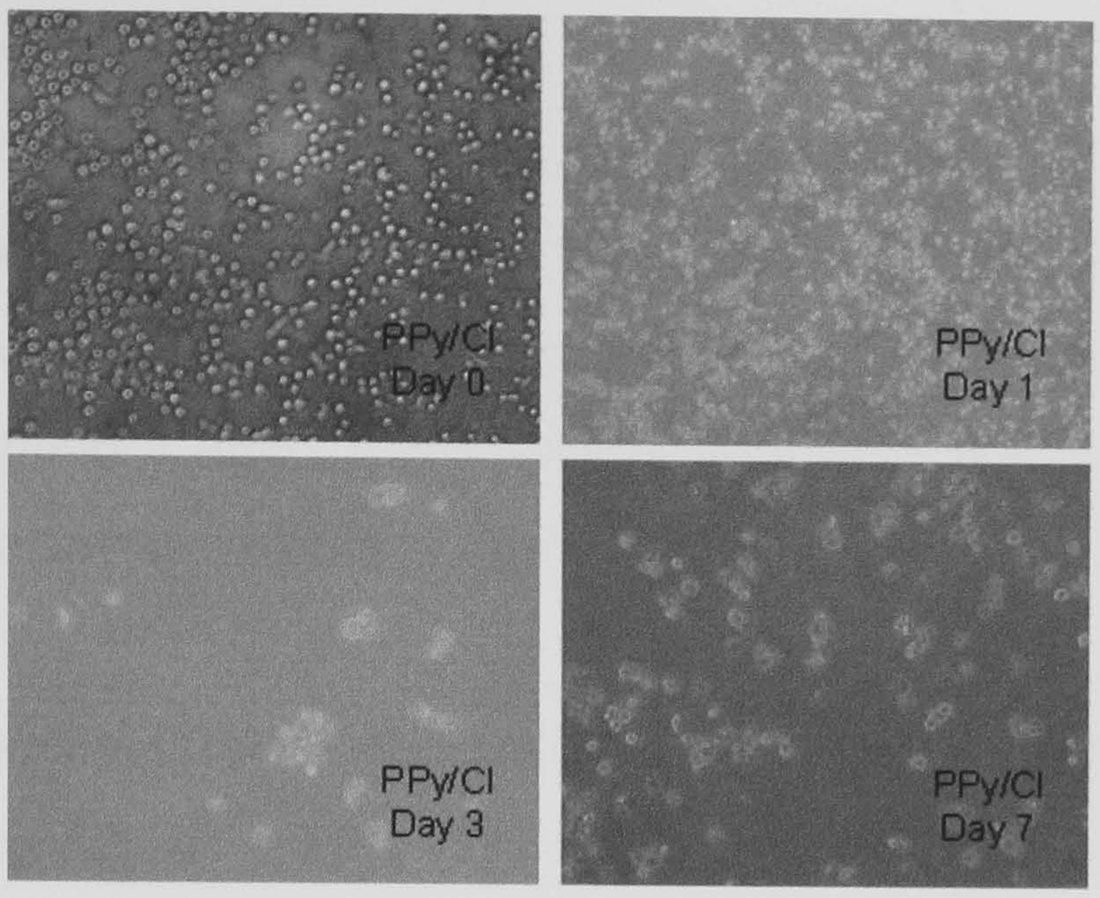

Figure 4.3: Micrographs of SVK14 Keratinocytes on PPy/Cl. *Keratinocytes on this substrate are still rounded after 4 h on day O and appear impaired by day 1. On subsequent days there are very few keratinocytes to be seen and they appear dead.*

Point Measurements

In addition to point measurements, later experiments looked at a range of counterions and control substrates for 15 days. These included chloride (Cl), polyvinyl sulphate (PVS), heparin (Hep), dermatan (Derm), fibrinogen (Fbri), fibronectin (FN) and Collagen (Col). Standard tissue culture polystyrene (TCPS), polycarbonate coverslips (PC) and bare gold-coated PC coverslips were used as controls. The AlamarBlue™ assay showed an increase in fluorescence for each substrate (Fig 4.4); this was in parallel with the appearance of confluent layers (Fig 4.5). For each substrate, keratinocyte colonies formed by day 4 and fully confluent layers established by day 8. It is difficult to observe any morphological differences between the substrates. However, differences were present 4 hours after the cells were seeded (Fig 4.5).

A predominantly rounded morphology was found for TCPS, PC, gold, PPy/PVS, PPy/Hep and PPy/Fbri. This shows poorer initial cell adhesion compared with other substrates. In the case of PPy/Cl, PPy/Derm, PPy/FN and PPy/Col more cells were seen

to spread on the surface. Most of the surfaces exhibiting good initial cell adhesion were those incorporating biological molecules. The role of fibronectin and collagen in promoting cell adhesion is well established (Alberts *et al.*, 2002; Grinnell, 2003; Shin *et al.*, 2003). Despite being the most abundant GAG in skin, dermatan is less well studied. There is evidence that it plays a role in stimulating keratinocyte growth by ligand binding to keratinocyte growth factor (Trowbridge *et al.*, 2002) and in other cellular behaviour (Trowbridge and Gallo, 2002; Sugahara *et al.*, 2003). However, there is no data available to support a direct role in cell adhesion although its abundance within skin suggests it has many as yet unidentified functions.

There were also polymers incorporating biological molecules which showed poor initial cell adhesion. In particular, cells on PPy/Hep and PPy/Fbri films had a rounded morphology. Incorporation of heparin into polypyrrole films has conferred affinity to thrombin in the oxidised polymer (Zhou *et al.*, 1999). PPy/Hep films also support endothelial cell attachment (Garner *et al.*, 1999b). However, there is evidence for heparin having an inhibitory effect on the proliferation of other cell types. These include cultured mesangial cells (Castellot *et al.*, 1985), murine mammary adenocarcinoma cells (Bertolesi *et al.*, 1994) and rat smooth muscle cells (Kazi *et al.*, 2002). Fibrinogen plays an essential role during blood clotting through conversion fibrin. It has mainly studied as a fouling agent after blood contact with medical implants and devices such as biosensors. Seeger *et al.* (2002) showed that endothelial cells grown on culture dishes pre-coated with fibrinogen had poor adherence compared to those coated with gelatin or fibronectin. In addition, the authors observed 'disorganised, retracted' cell morphology on fibrinogen substrates compared with 'cobblestone' organisation on the other proteins.

Scanning electron microscopy was used to study SVK14 keratinocytes on the various substrates after 5 days in culture. Cells were well represented on all substrates except PC where cells appear to have detached during processing (Figs 4.5). Cells presented an irregular polygonal shape with membrane ridges indicative of maturation (Merrick *et al.*, 1990). Morphologically there were no differences between the various substrates except for TCPS *vs.* other substrates; cells were found qualitatively to have more folds in their membranes than those on other substrates. Colony edges appeared similar for all substrates and examples of cells attached through extension of processes were found. Some isolated cells were also found that appeared necrotic. Steinberg *et al.* (1983)

compared SV40 infected to normal human keratinocytes by SEM. They reported that infected cells displayed progressively less ridging than their normal counterparts with an increase in villi. They also pointed out that mature cells, as found in higher passage cells, did loose their villi. In this study, the latter structures were not commonly found on the cell surfaces. The SEM analysis provides more support for the positive growth of cells on polypyrrole as well as for interaction between the substrate with active cell processes seen for attachment.

The fact that PPy/Cl allowed for better cell adhesion suggests that the effect with other films cannot be interpreted solely due to the activity of biological molecules. The surface and physical quality of films is also important, *e.g.* more efficient polymerisation with the small chloride anion. The initial effect appeared not to be indicative of later behaviour, as all films subsequently supported cell growth, with loss of any significant differences (Ateh, 2003). However, observed cell growth proved also to be due to well surfaces (Fig 4.6). This meant that they contributed to AlamarBlue™ dye reduction. To avoid this, substrates were transferred to new wells before each measurement. Nevertheless, the initial cell responses to the various substrates remained valid.

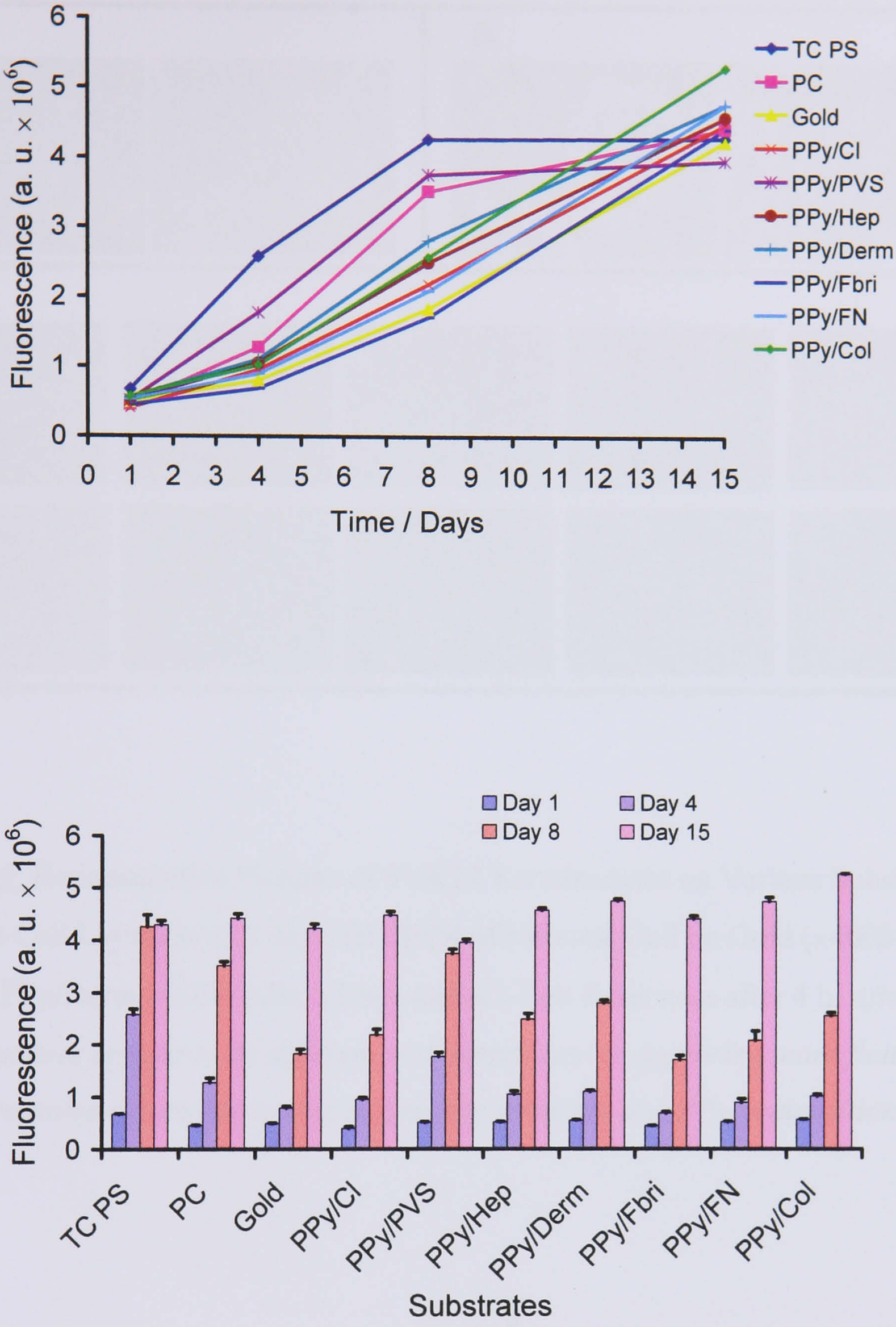

Figure 4.4: SVK14 Keratinocytes AlamarBlue™ Proliferation Assay

(Point Measurement)

(A) Scatter Chart and (B) Bar Chart (± SE, n = 9)

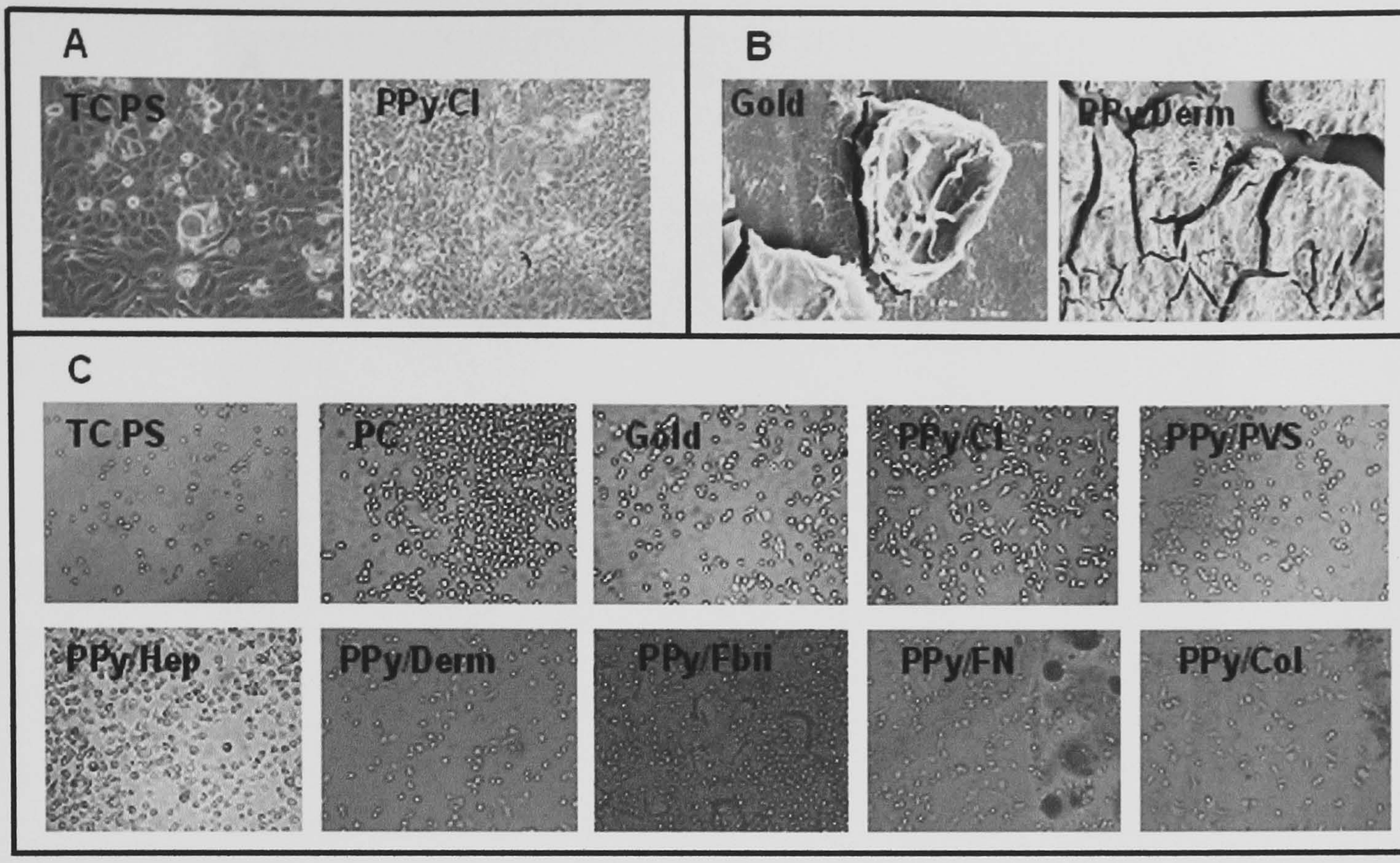

Figure 4.5: Representative Pictures of SVK14 Keratinocytes on Various Substrates (A) Confluent Cell Layers after 4 days, (B) SEM of Necrotic Cell on Gold (×4000) and Cell Layer on PPy/Derm (×500) after 5 Days and (C) Cell Responses after 4 h. *After 4 hours cell responses appear to be different with kerationcytes appearing more flattened or rounded depending on the supporting substrate and PPy composition.*

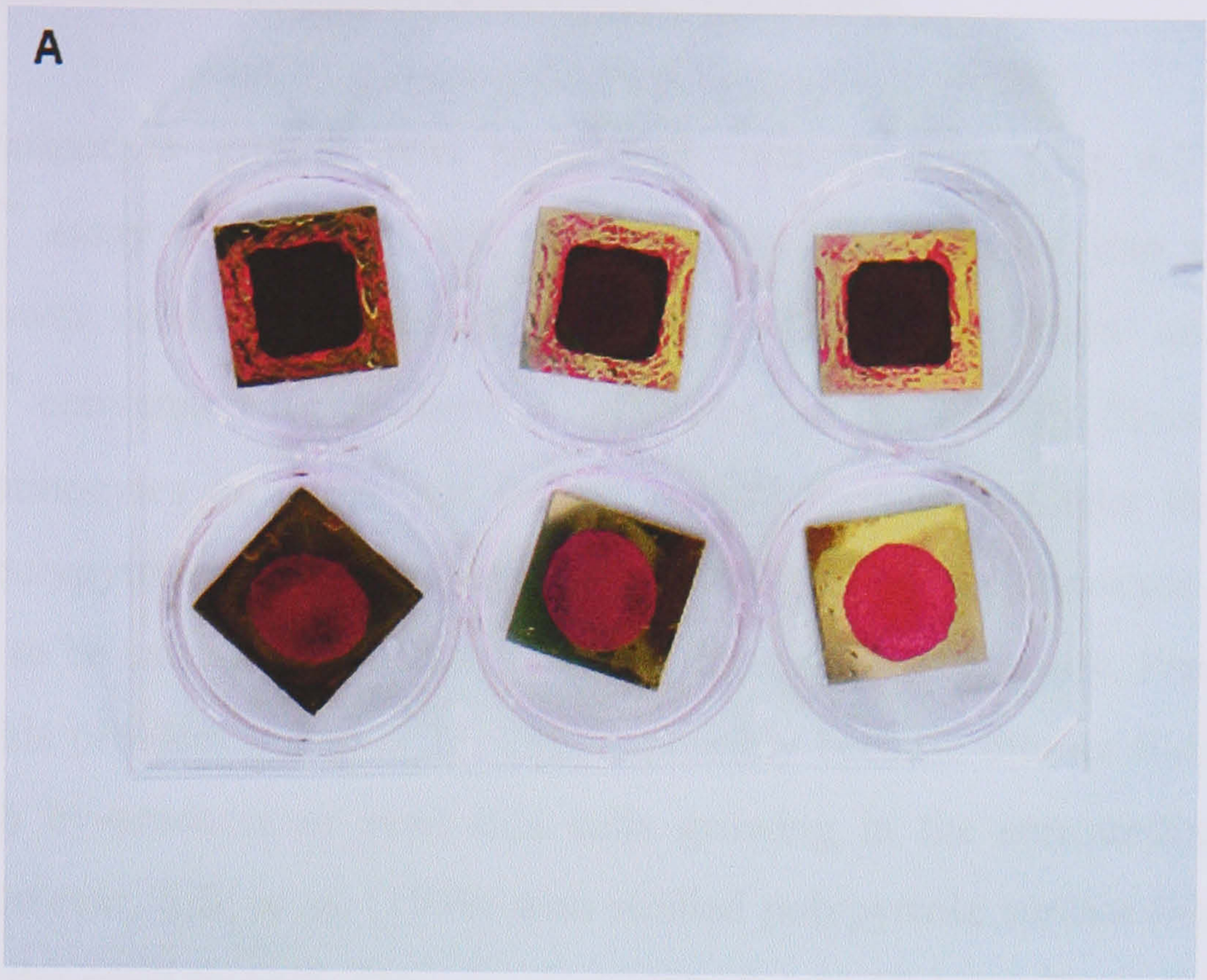

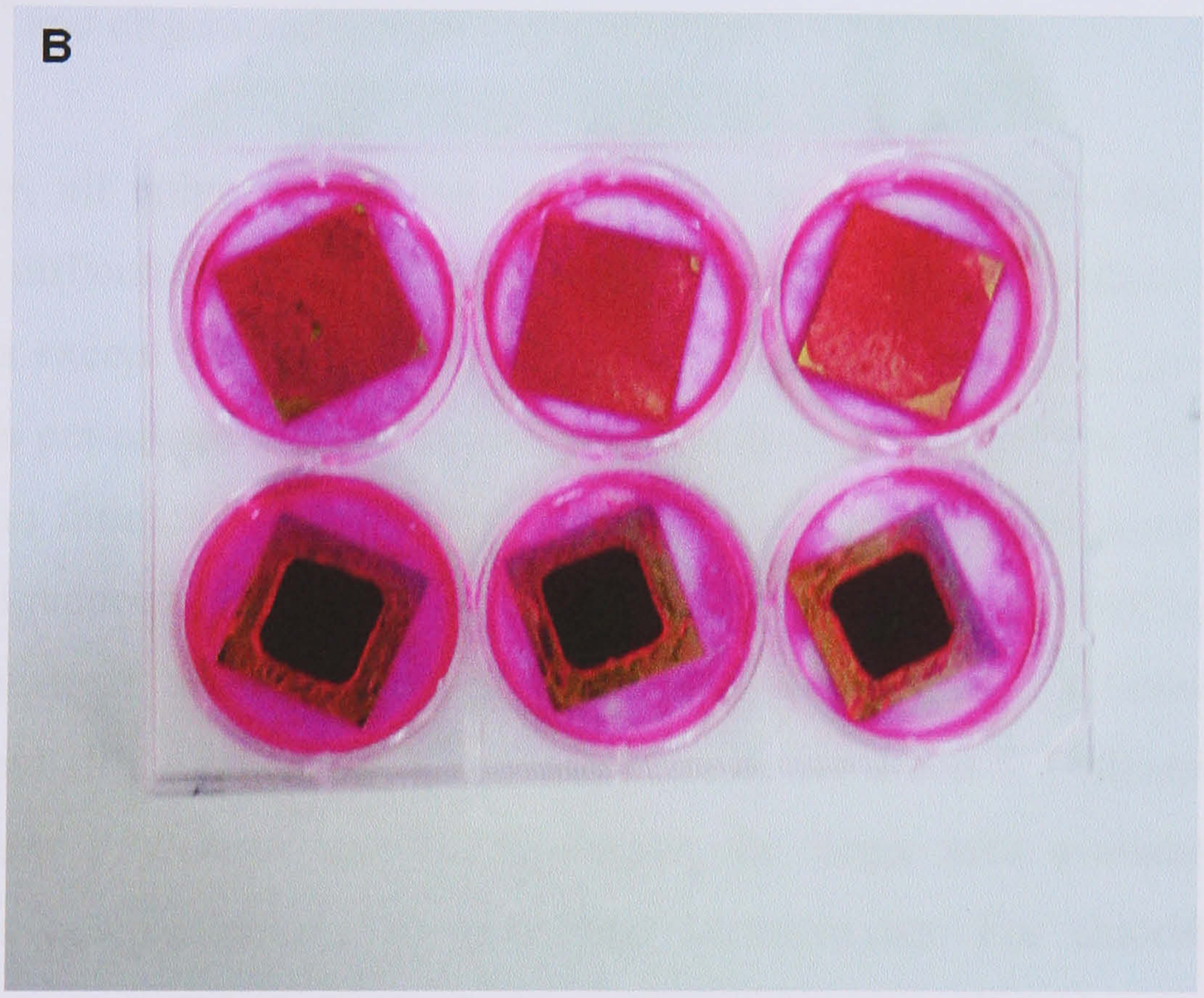

Figure 4.6: Rhodamine B Stained Keratinocytes in Substrate Containing Wells (A) After 3 Days in Culture and (B) After 14 Days in Culture. *This shows that keratinocytes did not grow exclusively on the desired substrate but after some time in culture expanded around the well. Therefore, for this experimental design, the results for the AlamarBlue™ Proliferation Assay at later days are unreliable since they incorporate the activity of cells growing on the surrounding TCPS well.*

Point Measurements with Substrate Transfer to New Wells

SVK14 keratinocyte growth was monitored over 5 days (Fig 4.7). Here, the AlamarBlue™ assay was carried out after transferring substrates into new wells to measure growth only on the intended surface. The results show an increase in AlamarBlue™ conversion for the control substrates but not for PPy films. Microscopy showed keratinocytes on films and limited colony formation. Under these stringent conditions, polypyrrole films were shown to be inhibitory to keratinocyte growth. This was thought to be caused by monomer and oligomer remnant toxicity. Previous reports do not cite this problem (Chapter 1). This is possibly because thinner films were used, limiting such by-products or even that cells growing in the surrounding well were included. However, Silk *et al.* (1998) who studied polypyrrole surface morphology by AFM stated the need to soak films in electrolyte for 24-30 h to eliminate by-products including H^+ and oligomers.

Subsequently, all polypyrrole films were soaked in distilled water for 3 days. This resolved the difficulties of cell growth (Fig 4.8). Positive cell proliferation was found on all substrates except PPy/Col. This was not expected since better cell growth occurred on substrates pre-coated with collagen compared to dermatan or bare TCPS (Fig 4.9). The poor film formation with collagen (Chapter 3), however, could result in more by-products and reduced mechanical integrity. PPy/Derm provided the best surface for cell growth. Statistical analysis showed there was a significant difference between PPy/Derm and all the other PPy based substrates at day 2 and 5. Differences were not found between PPy/Derm and TCPS, despite the larger area available on TCPS, suggesting a comparable ability to support keratinocytes. For chloride, polyvinyl sulphate, dermatan sulphate and collagen-loaded polypyrrole films, bare polycarbonate and gold substrates, keratinocyte viability was respectively 47%, 60%, 88% and 23%, 75% and 61% of tissue culture polystyrene controls after 5 days.

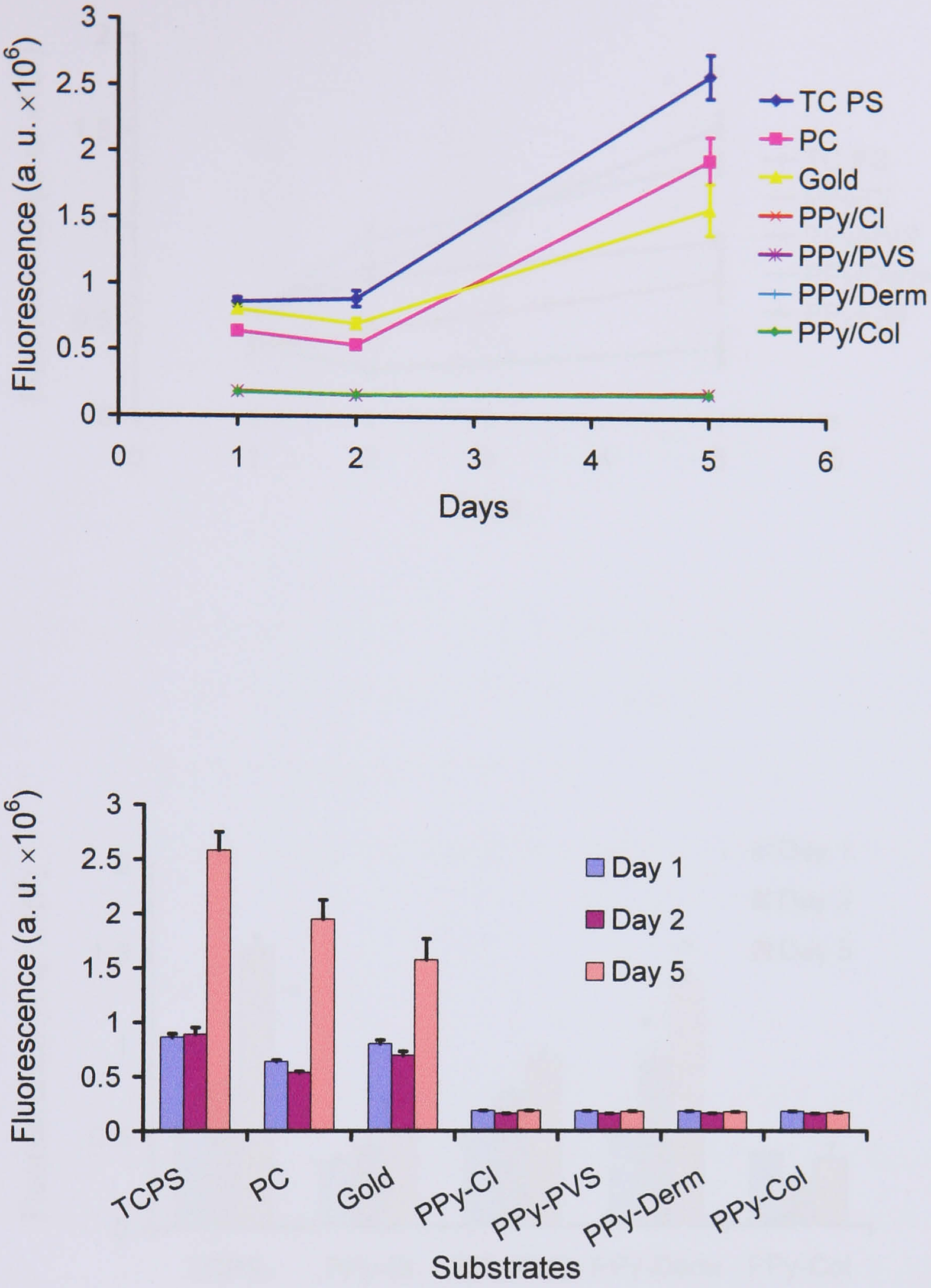

Figure 4.7: SVK14 Keratinocytes AlamarBlue™ Proliferation Assay (Point Measurement/New Wells).

(A) Scatter Chart and (B) Bar Chart (± SE, n = 9).

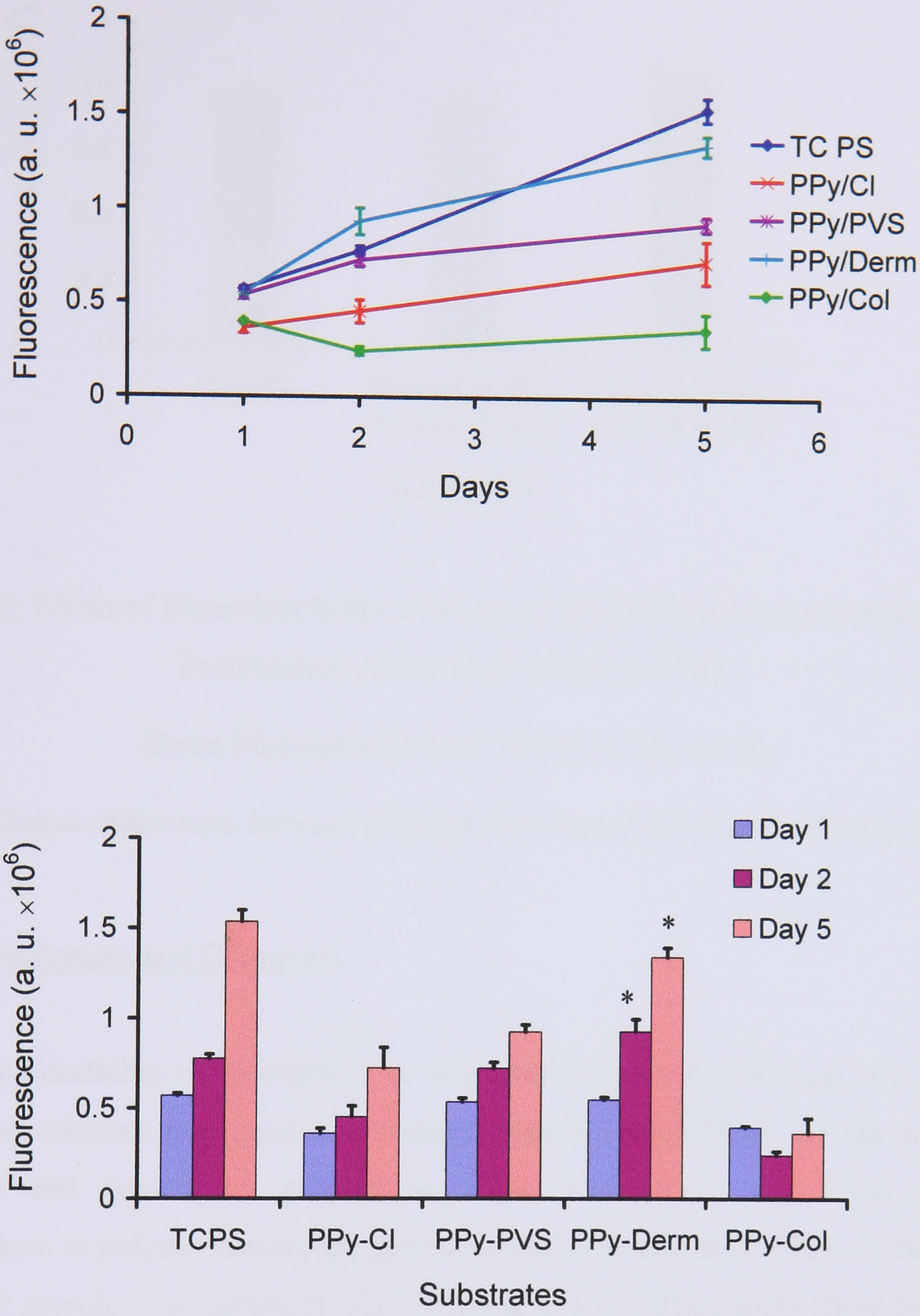

Figure 4.8: SVK14 Keratinocytes AlamarBlue™ Proliferation Assay

(Point Measurement/New Wells/Washed Films).

(A) Scatter chart and (B) bar chart (± SE, n = 9).

** Significant differences between PPy/Derm and other PPy substrates ($p<0.05$).*

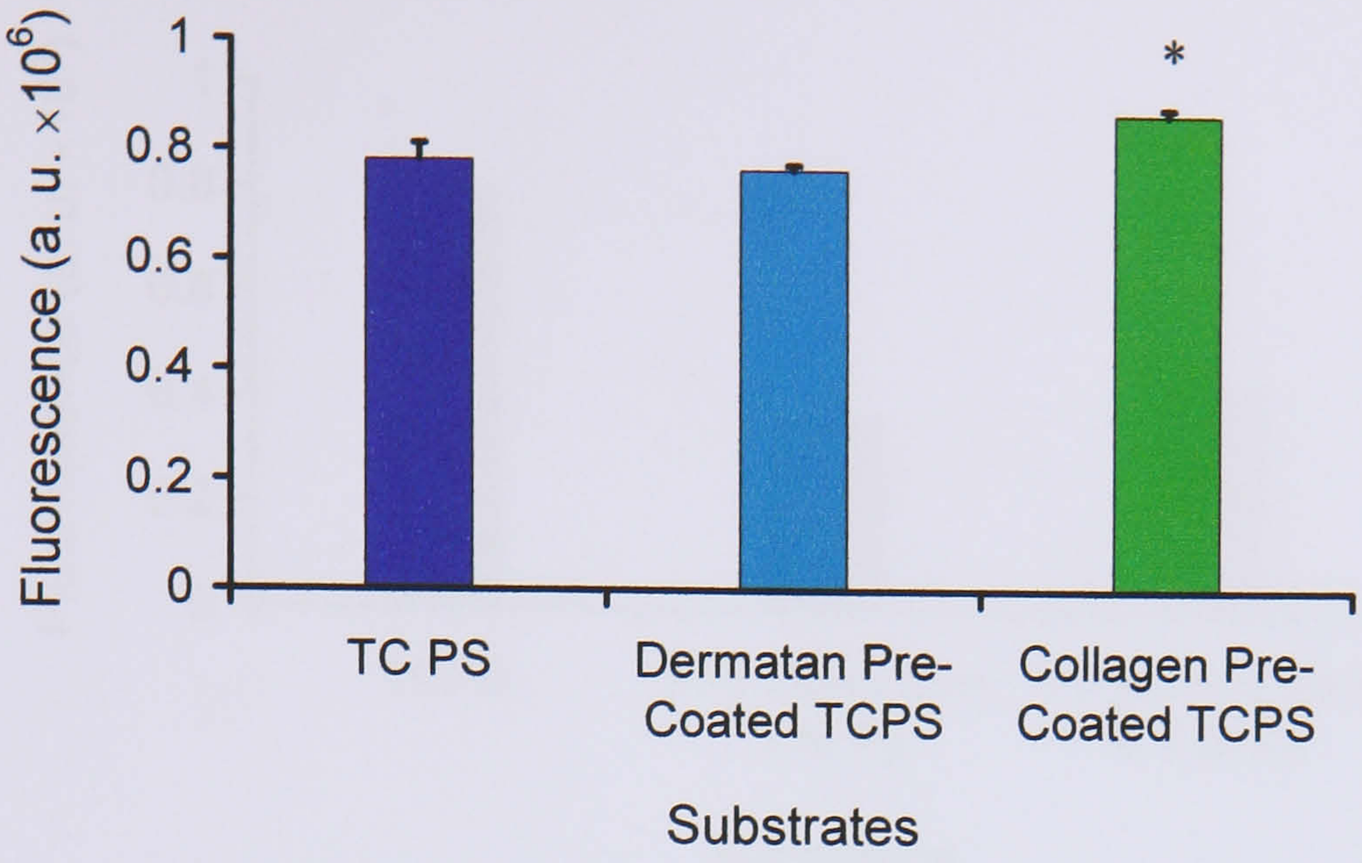

Figure 4.9: Effect of Biomolecule Pre-Coating on SVK14 Keratinocytes AlamarBlue™ Proliferation Assay after 24 hrs on TCPS.

(Point Measurement/New Wells) (± SE, n = 9).

** Significant differences between collagen pre-coated TCPS and others ($p<0.05$).*

Effect of Monomers and Oligomers

To test the possibility of monomeric or oligomeric remnant effects on cell growth, a series of experiments was conducted using dermatan-loaded films. As the majority of reports of cell growth on polypyrrole films (Chapter 1) use lower monomer concentrations at polymerisation, the growth of cells on unwashed films made from 0.1 M and 1 M pyrrole was compared after 24 hrs (Fig 4.10). The results show that in both cases cell proliferation is poor, so high monomer concentrations at polymerisation is not the cause of the inhibitory effect. When unwashed thick PPy/Derm films were exposed to culture media for 16 h and the media transferred to a TCPS well, there was no inhibitory effect on cells (Fig 4.11). Therefore, the toxicity effect requires the direct contact of cells with polypyrrole. This could be due to increased concentrations of toxic factors at the surface or local cell activity promoting their release. It is difficult to postulate a mechanism for the latter; possibilities are a local pH fall, released cell enzymes or mechanical disruption. The effect of pyrrole concentration in culture media was also studied (Fig 4.12); at 24 h cell viability is reduced with increasing monomer concentration. All cells died at pyrrole concentrations above 100 mM.

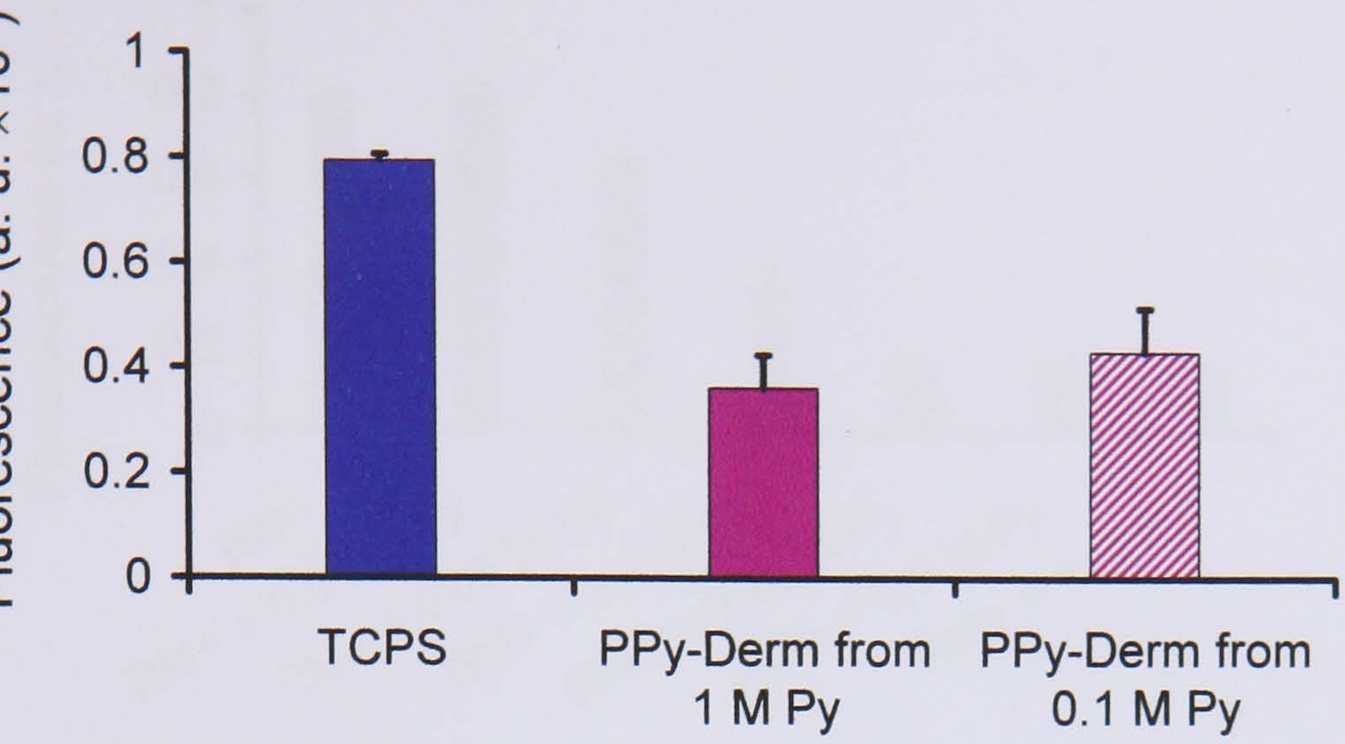

Figure 4.10: Effect of Pyrrole Concentration in Polymerisation Solution on SVK14 Keratinocytes AlamarBlue™ Proliferation Assay after 24 hrs on PPy/Derm.

(Point Measurement/Fresh Wells) (± SE, n = 9).

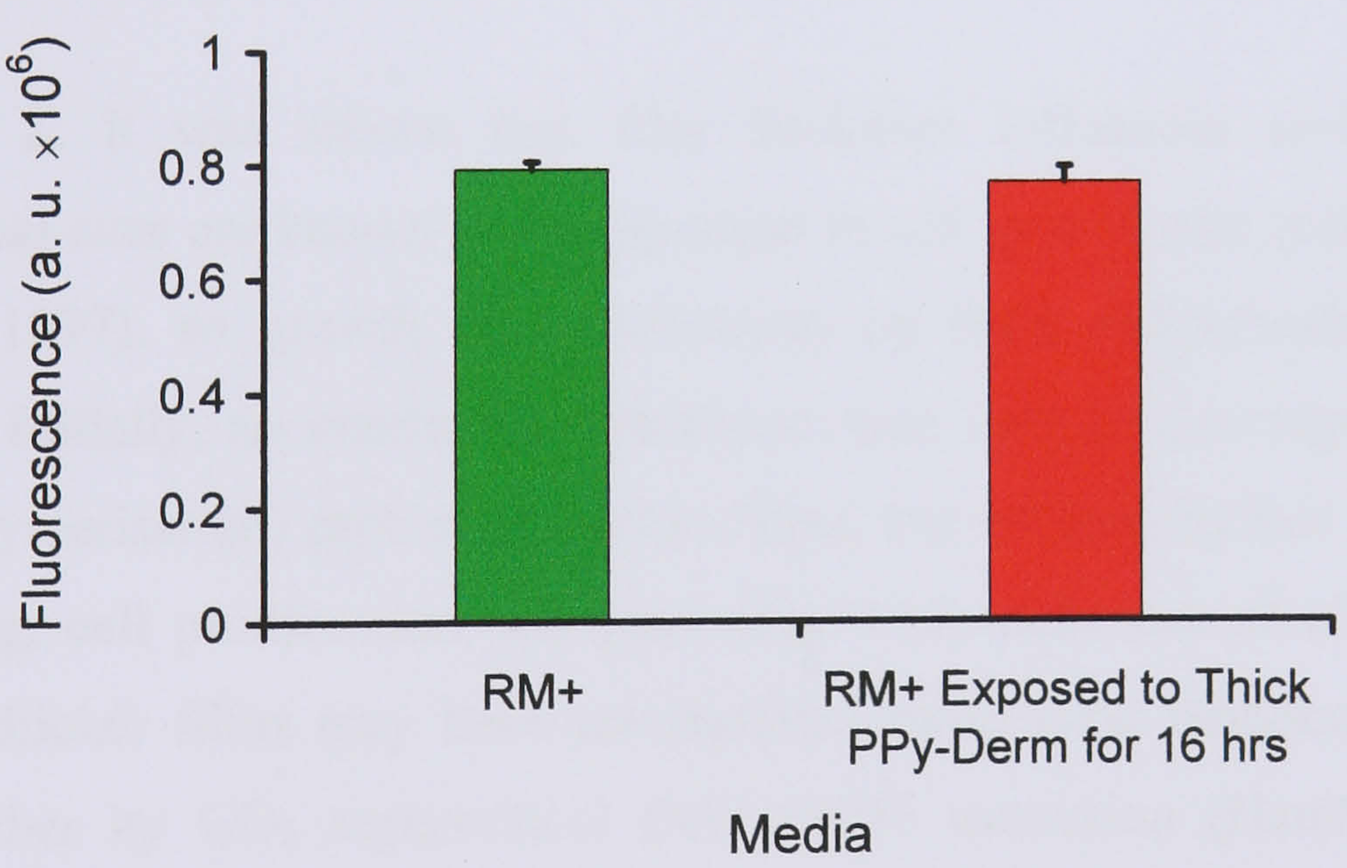

Figure 4.11: Effect of Culture Media Pre-Exposure to Thick PPy/Derm on SVK14 Keratinocytes AlamarBlue™ Proliferation Assay after 24 hrs on TCPS.

(Point Measurement) (± SE, n = 9).

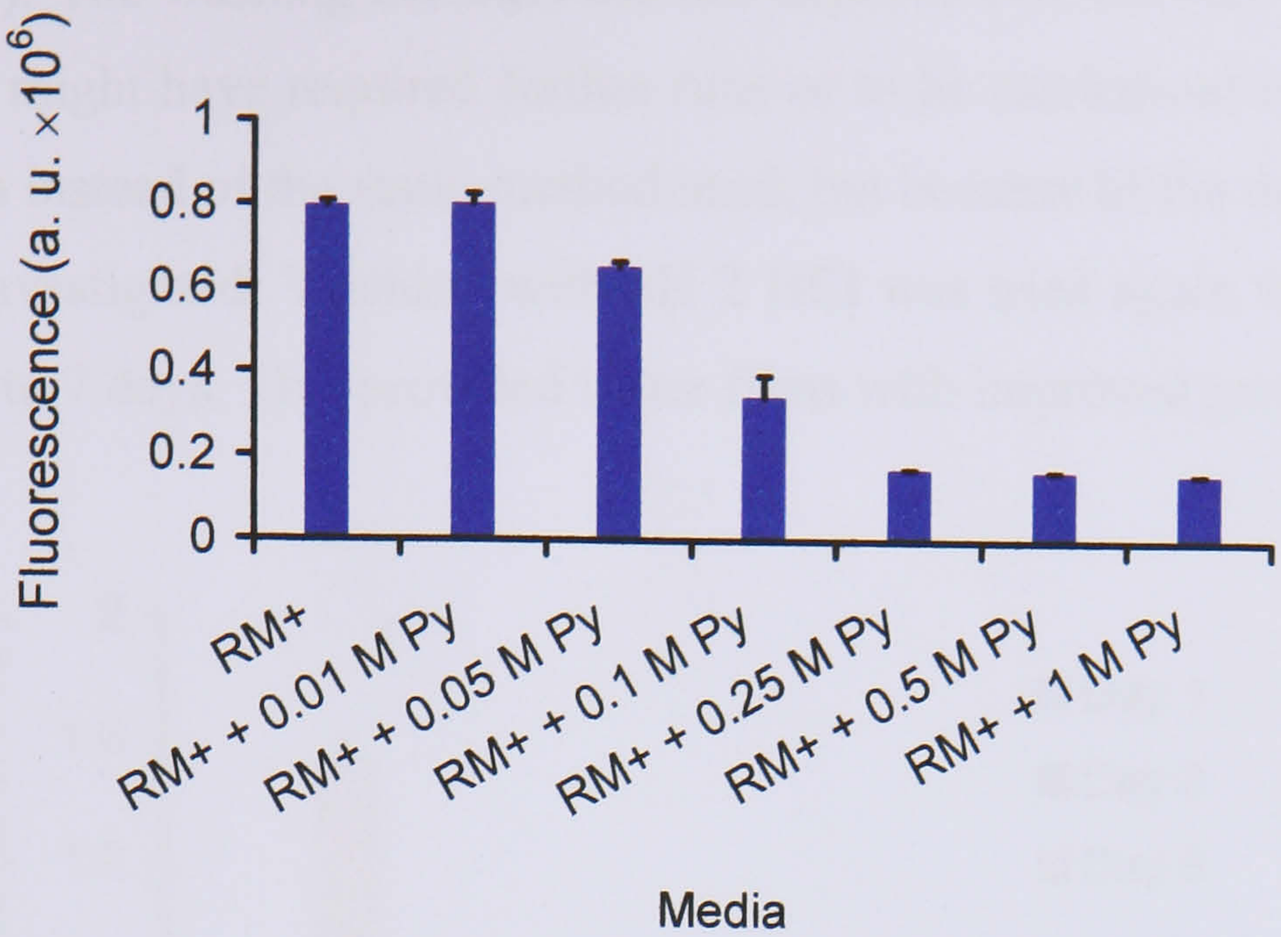

Figure 4.12: Effect of Pyrrole Concentration in Culture Media on SVK14 Keratinocytes AlamarBlue™ Proliferation Assay after 24 hrs on TCPS.

(Point Measurement) (± SE, n = 9).

Effect of Film Thickness

In Chapter 2, it was shown that film thickness influences surface topography. Topographical cues are known to be important in cell growth and guidance (Curtis and Wilkinson, 1997), so growth of keratinocytes on thick polypyrrole films was also undertaken. Initially, an intermediate thickness was used to investigate toxicity alone (45 min polymerisation) providing thicker films, but without surface features. Despite film washing, cell proliferation was poor (Fig 4.13) with loss of all cells by day 5. Again, the thicker films may have accumulated more toxic monomers or oligomers. Washing either by CO_2 supercritical fluid (SCF) extraction (Hauthal, 2001) or by soaking in HCl at pH 2 for 2 days was tried next.

The former involved maintaining CO_2 above its critical pressure and temperature in a pressure vessel containing the thick films for 2 hours. In this supercritical state, CO_2 becomes a powerful solvent with high diffusivity and low viscosity. It was hoped this could be a fast method for the extraction of unreacted monomer and loose oligomers. Electron microscopy showed the effects of these treatments on the film surfaces (Fig 4.14). Washing in HCl at pH 2 did not affect the surface whereas defects were created using the SCF method. The growth of cells on these surfaces was considered after 24

hrs (Fig 4.15). The washing methods did not improve cell viability on thick films. The SCF method might have required further runs or to be carried-out in a continuous flow configuration instead of the static method used, but because of the defects created it was not further investigated. Washing with pH 2 HCl was tried again with an extension of film soaking to 7 days. This provided better films with improved growth (Fig 4.16).

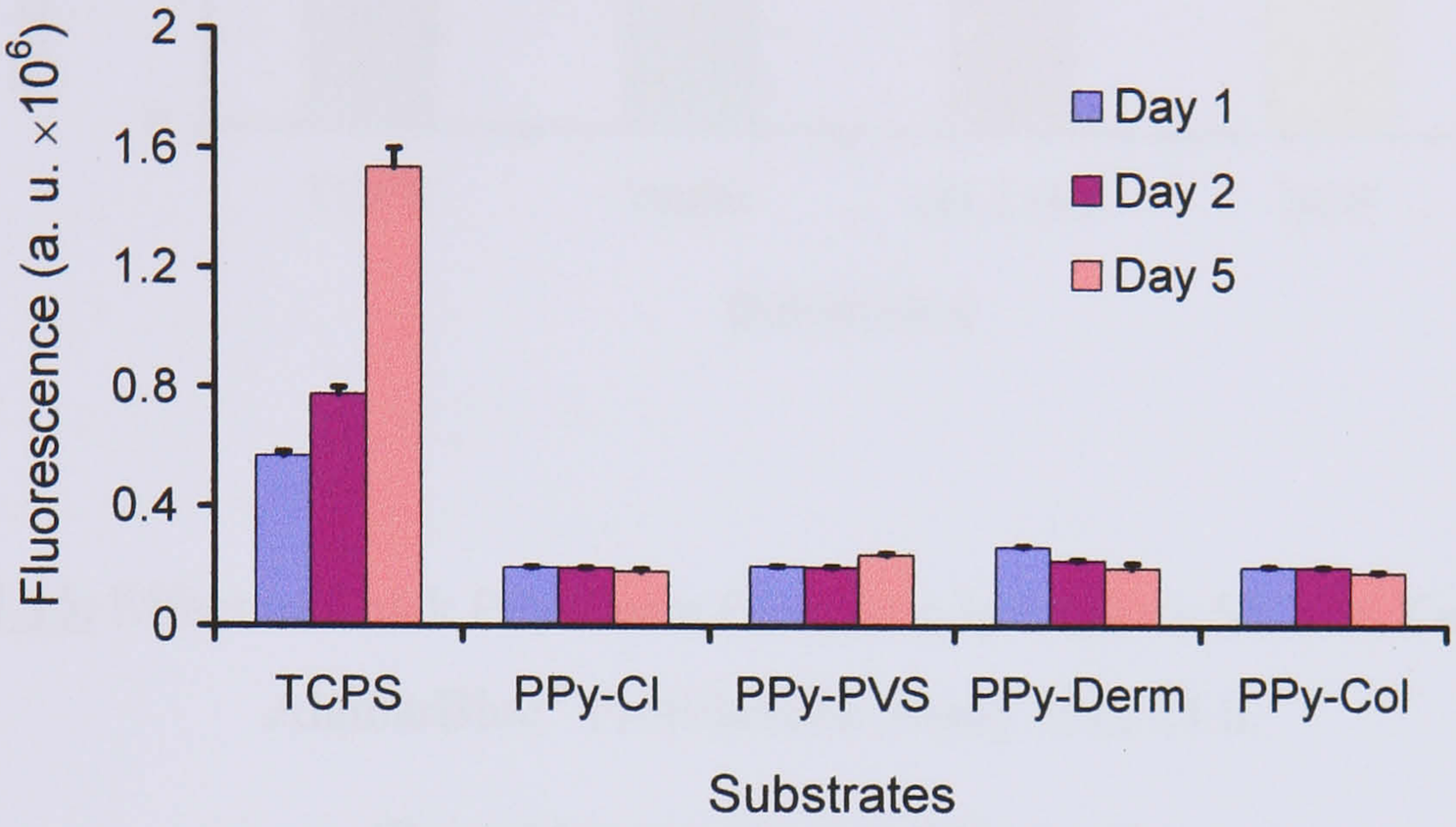

Figure 4.13: SVK14 Keratinocytes AlamarBlue™ Proliferation Assay (Point Measurement/Fresh Wells/Washed Films/Thick Films) (± SE, n = 9).

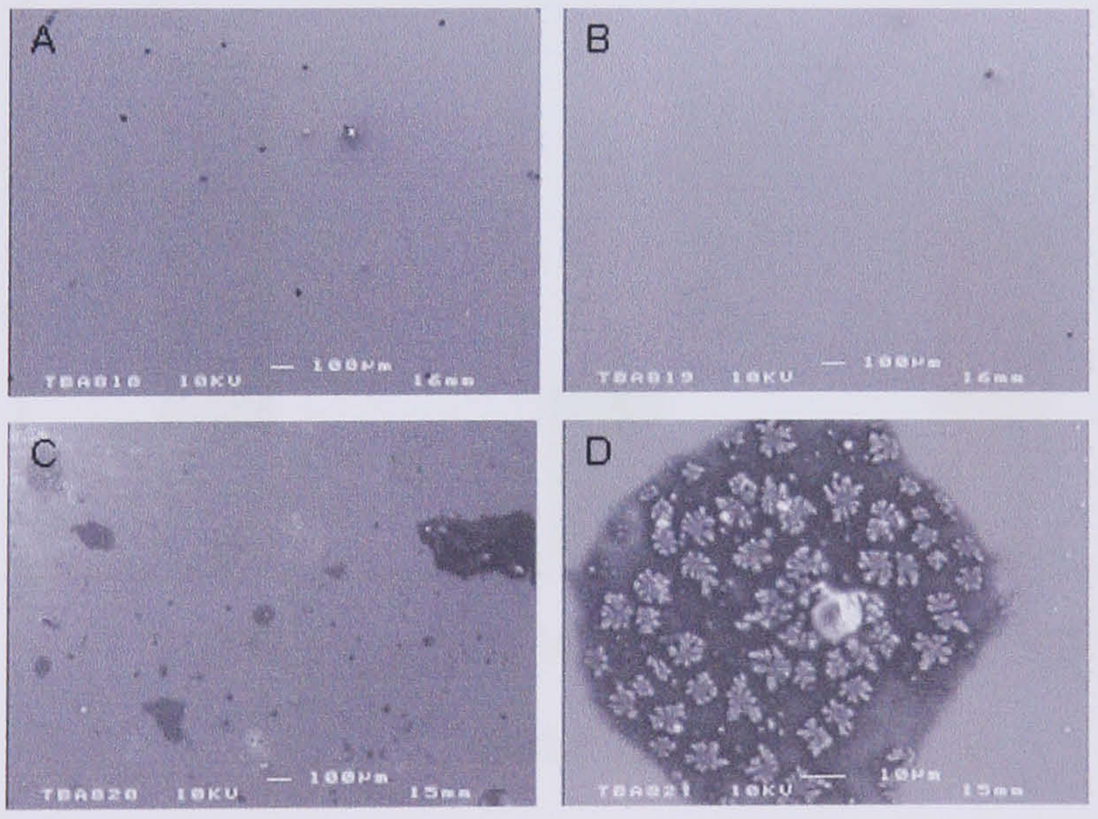

Figure 4.14: SEM of Thick PPy/Derm after Treatments

(A) Unwashed, (B) pH 2 HCl (C) CO_2 SCF and (D) defect on CO_2 SCF. *Panel C and D show defects caused at the surface of the polymer when treated using the SCF method whereas this does not happen with acid treatment seen in panel B.*

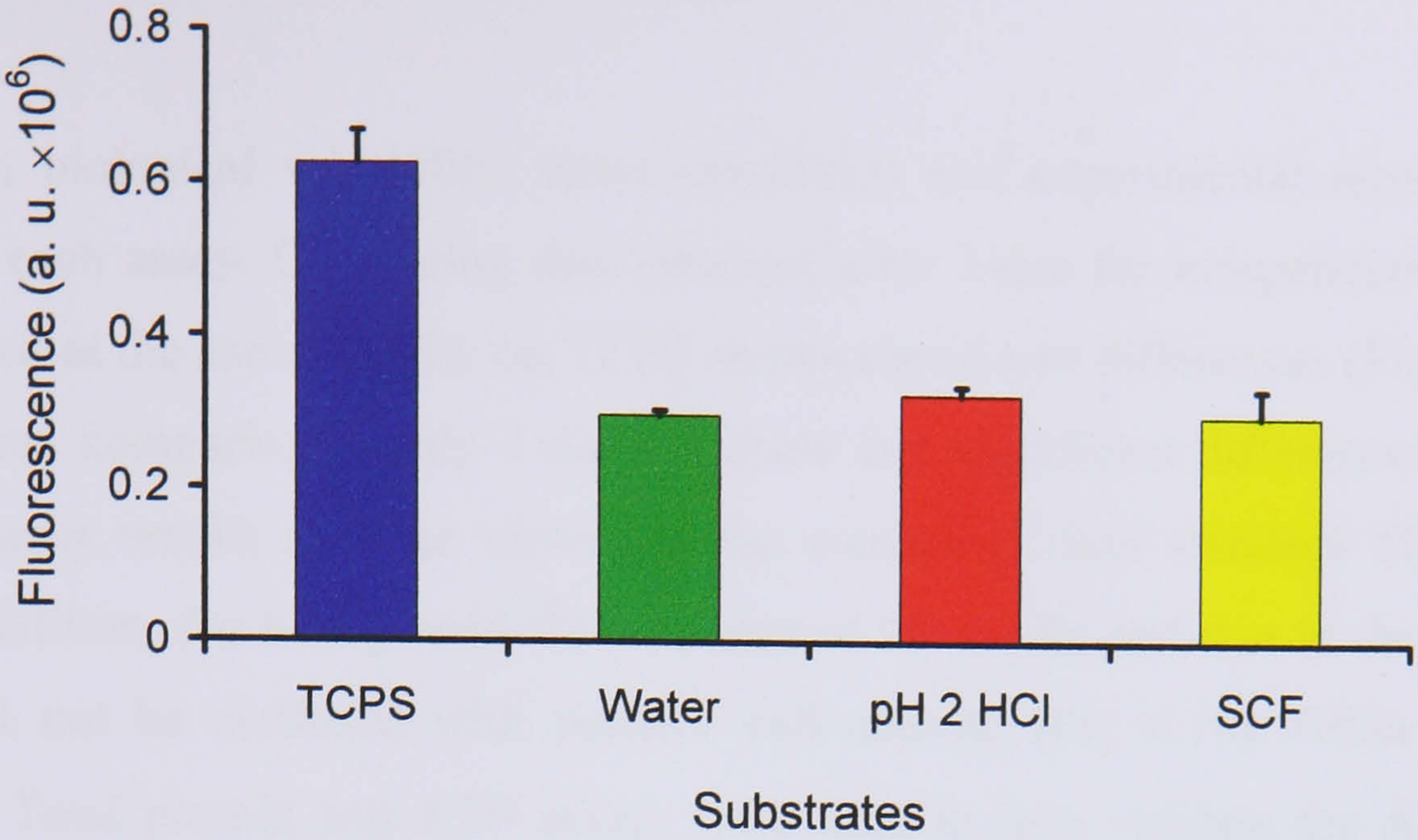

Figure 4.15: Effect of Thick PPy/Derm Cleansing Method on SVK14 Keratinocytes AlamarBlue™ Proliferation Assay after 24 h.

(Point Measurement) (± SE, n = 9).

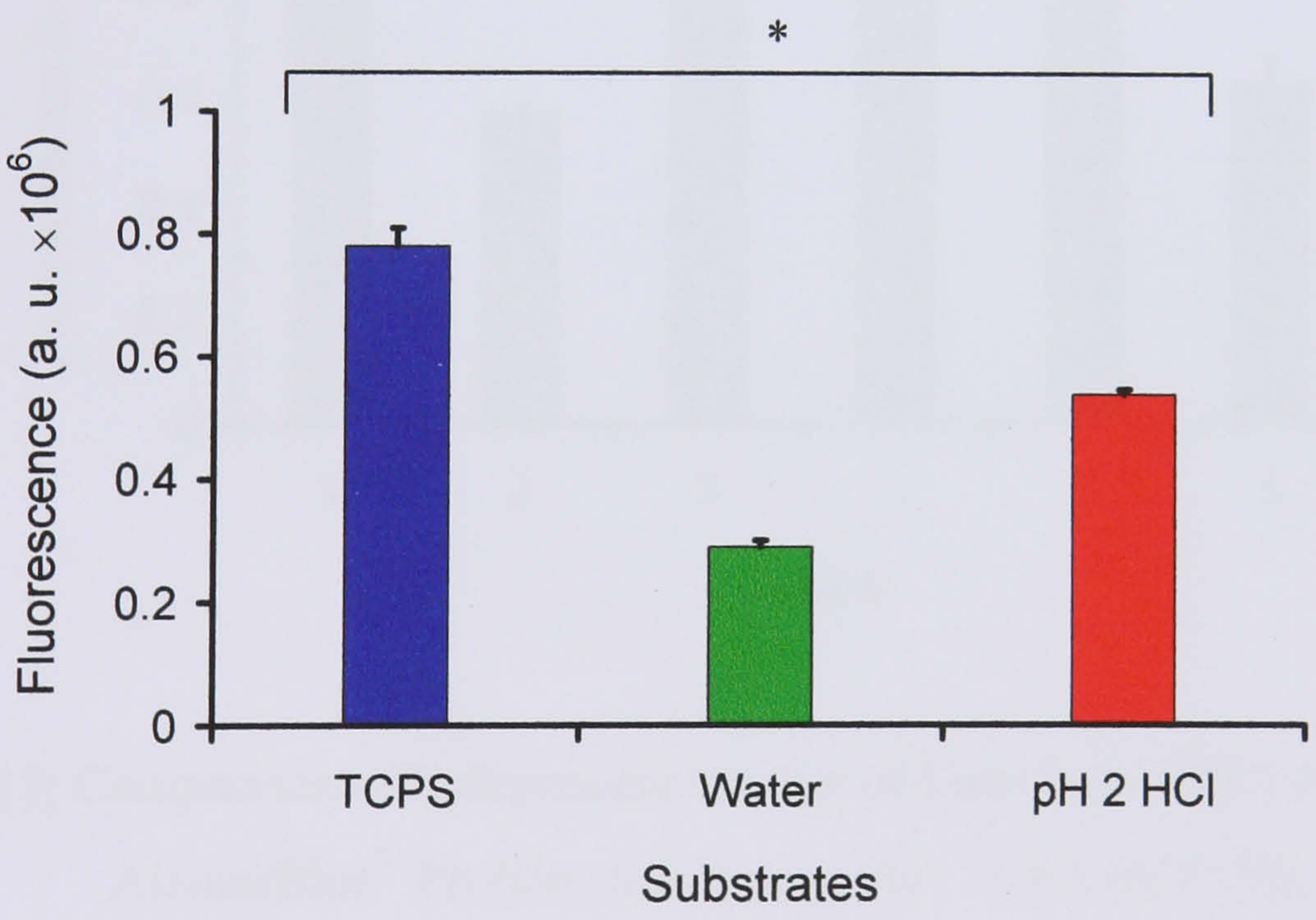

Figure 4.16: Effect of Longer (7 Days) pH 2 HCl Thick PPy/Derm Wash Time on SVK14 Keratinocytes AlamarBlue™ Proliferation Assay after 24 h.

(Point Measurement) (± SE, n = 9).

** Significant differences between all substrates ($p<0.05$)*

Reproducibility of AlamarBlue™ Assays

Inevitably, biological variability, exact conditions and experimental error affect the results of each assay. Comparing data obtained after 24hrs for independent batches of cells seeded at the same density on TCPS shows significant differences (Fig 4.17). Out of 15 paired comparisons, only 4 did not show any significant differences. For these reasons, assay results must be viewed in the context of their standard TCPS control data. In addition, the background fluorescence of the media and dye in the absence of cells must not be confused with positive cell activity (Fig 4.18). Other techniques including Total protein and ATP assays were used to help validate the AlamarBlue™ assay. SEM and immunocytochemistry were also used to assess cell proliferation and differentiation of SVK14 keratinocytes on polypyrrole films.

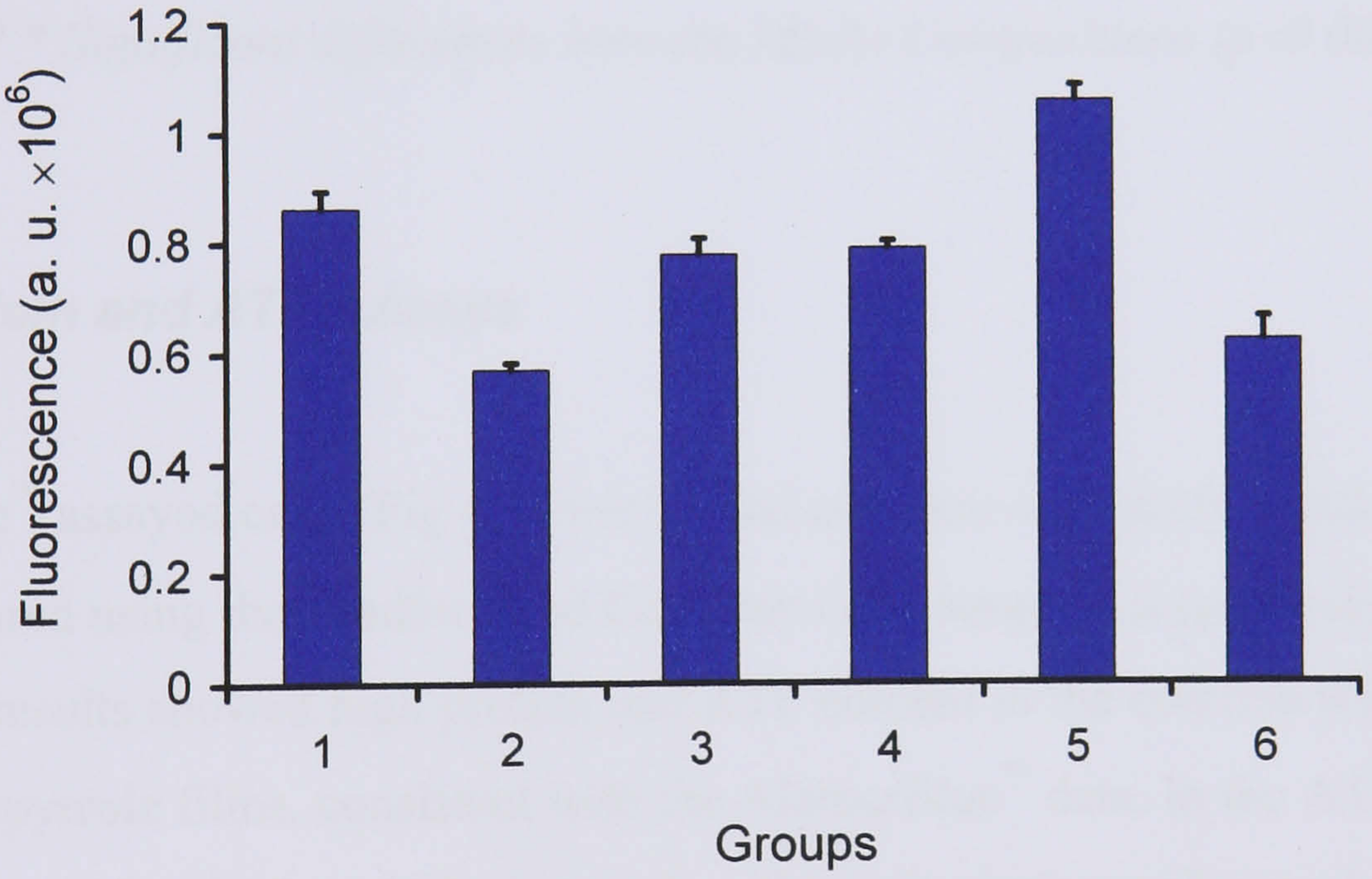

Figure 4.17: Comparison of Independent Groups of Data from SVK14 Keratinocytes AlamarBlue™ Proliferation Assay after 24 hrs on TCPS.

(Point Measurement) (± SE, n = 9).

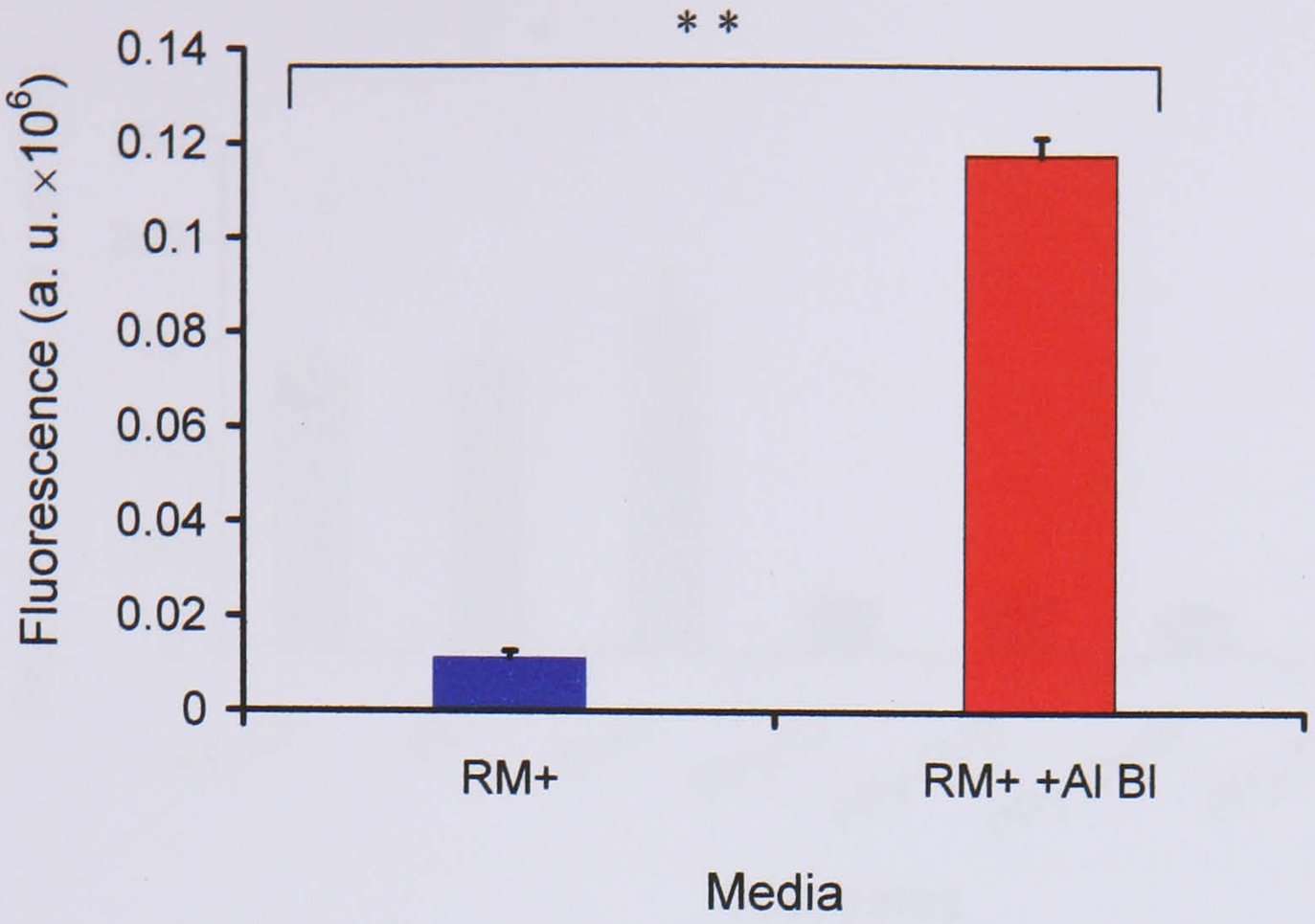

Figure 4.18: Fluorescence of RM+ Culture Media *vs*. RM+ + AlamarBlue™ without the Presence of SVK14 Keratinocytes (Point Measurement) (± SE, n = 9).

* * *Significant differences between Media Compositions ($p<0.001$)*

Total Protein and ATP Assays

AlamarBlue™ assayed cells (Fig 4.7) were lysed and their total protein and ATP content were measured using the Bradford and CellTiter-Glo™ reagents respectively (Figs 4.19 – 4.20). The results showed high protein and ATP content in the controls with low values for the polypyrrole films, consistent with the AlamarBlue™ data. In the ATP assay, cells from the PPy/Cl had higher ATP content than those from other polypyrrole films. These differences were not seen in the AlamarBlue™ assay but are explained by the higher sensitivity of the CellTiter-Glo™ luminescent assay at lower cell numbers. The fact that cells on PPy/Cl films fared better, reinforces the earlier consideration that by-products of polymerisation cause cell death because chloride is assumed to provide the most efficient polypyrrole polymerisation with minimum leachable products.

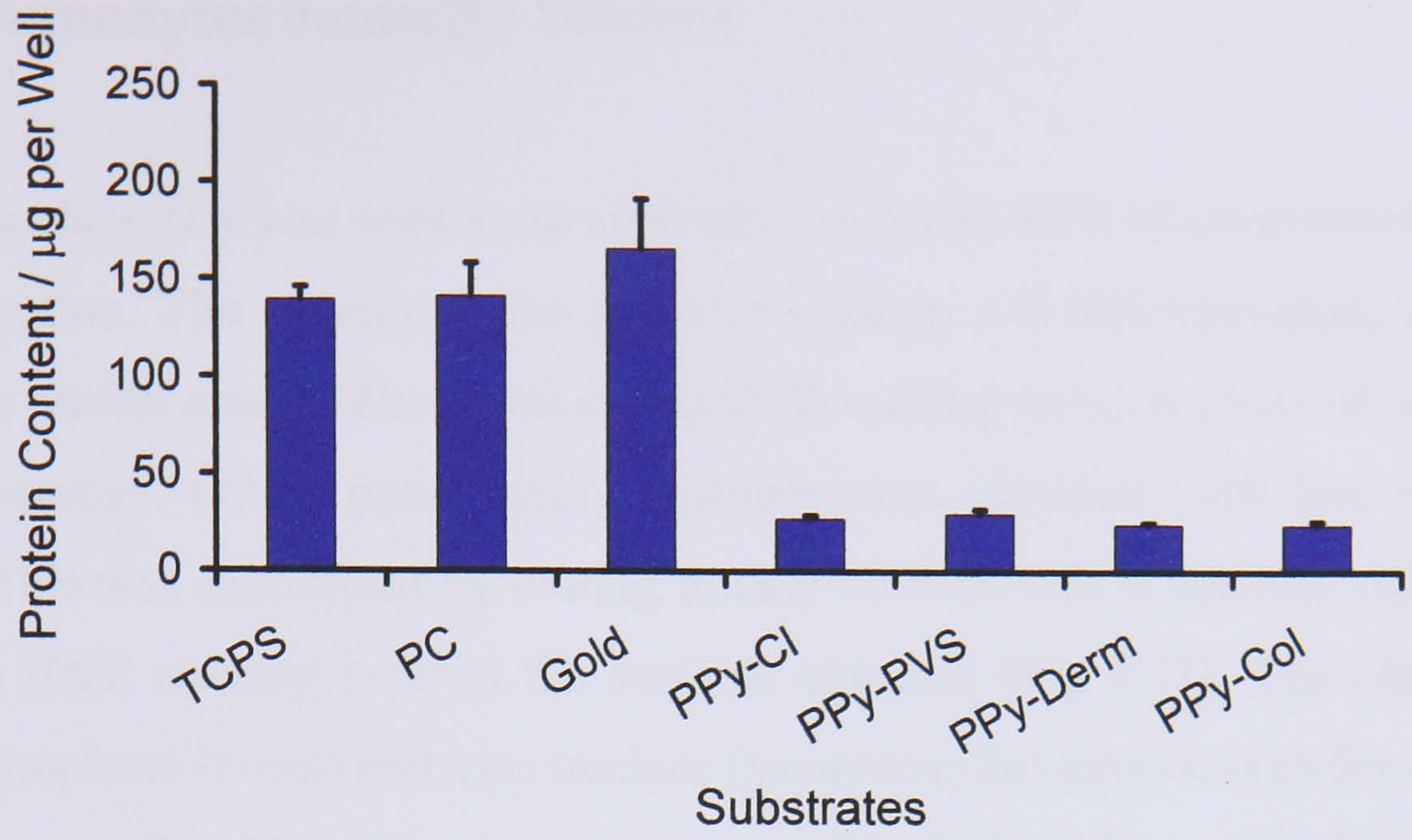

Figure 4.19: Protein Content of SVK14 Keratinocytes on Various Substrates after 5 Days of Culture (± SE, n = 6).

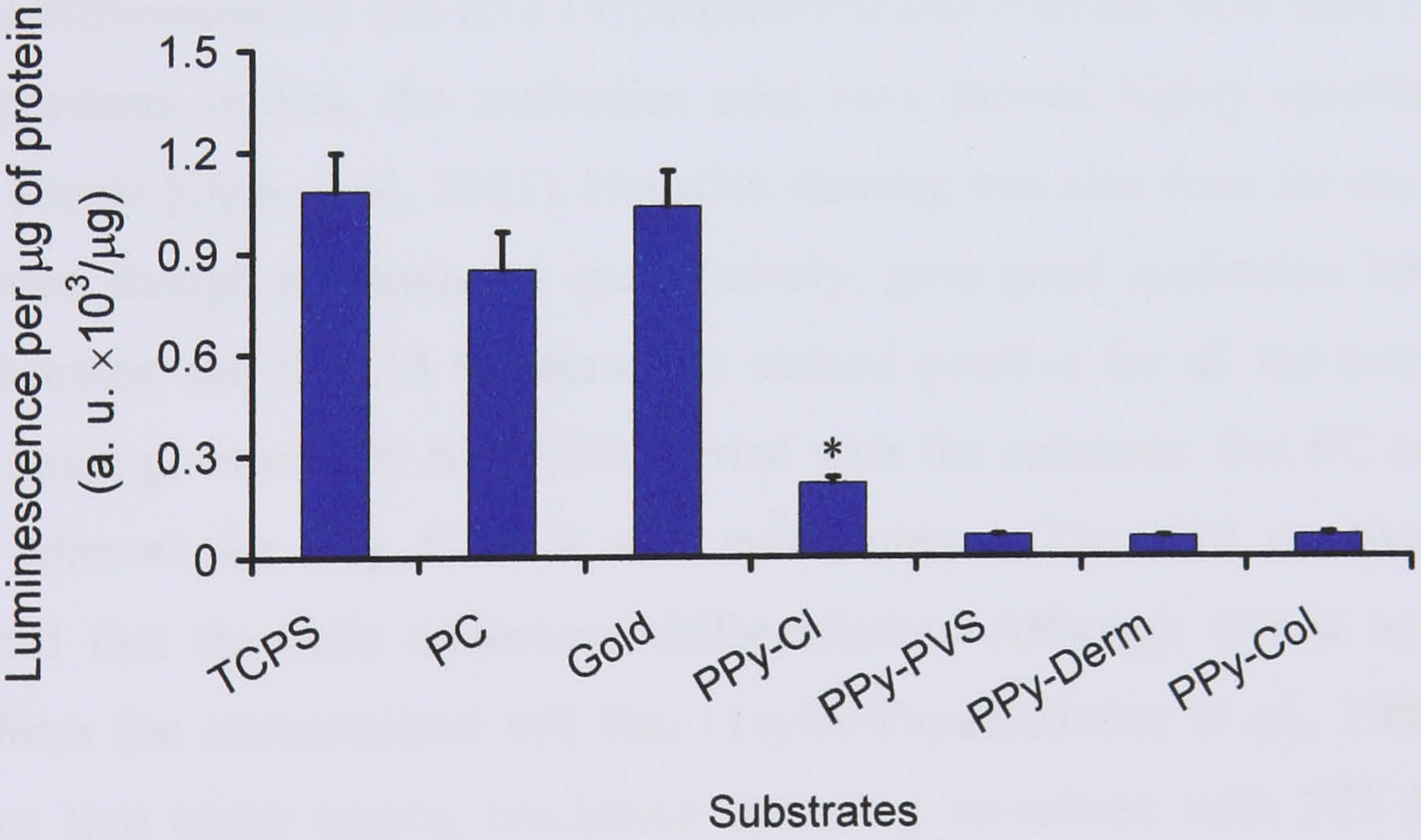

Figure 4.20: Relative Content of ATP in SVK14 Keratinocytes on Various Substrates after 5 Days of Culture (± SE, n = 6).

** Significant differences PPy/Cl and other PPy substrates ($p<0.05$).*

4.2.2 Immunocytochemistry Studies

Immunocytochemistry was used as an alternative to verify SVK14 keratinocyte viability and proliferation. The technique also provided data on cell differentiation, not readily accessed by earlier assays. There was difficulty in making cross-sections of cells coated on PC coverslips. Often, poor quality sections were obtained with loss of cells or substrate. This was minimised by cutting thicker sections and frequently replacing the blade. The H&E staining typifies the sections obtained (Fig 4.21). The characteristic pink cell cytoplasm (eosin) and blue nucleus (haematoxylin) may be seen for cells on all substrates except PPy/Col. On numerous repeats, PPy/Col sections were devoid of cells and usually showed a series of black spots suggesting the polymer had a powdery consistency. This is consistent with poor film formation and cell growth seen in previous experiments. For this reason further staining was not carried out on PPy/Col substrates. TCPS substrates were also not considered as they were too thick for cutting and attempts at examining pellets were unsuccessful.

Further staining was carried out on the other substrates. PCNA (proliferation), K10 (suprabasal differentiation) and K16 (hyperproliferation) markers were used (Fig 4.22–4.26). In previous studies, the antibodies used have proved highly specific to their respective targets (Ojeh *et al.*, 2001). Negative staining was also done for each section. Stained slides, though not analysed quantitatively, gave good qualitative information. For all substrates, the SVK14 keratinocytes stained positive for all the markers. The degree of staining, especially for PCNA varied with the substrate. For PC and gold it was poor whereas for PPy films it was more intense. The K10 positive sections demonstrated that the cells underwent differentiation. Although this is not initially expected from the immortalised cell line (Taylor-Papadimitriou *et al.*, 1982), others have shown that under certain conditions including co-culture with 3T3 fibroblasts (Kamalati *et al.*, 1989a), in the presence of IGF I stimulation (Kamalati *et al.*, 1989b) or Ca^{2+} modulated EGF receptor expression (Boonstra *et al.*, 1985) SVK14 keratinocytes differentiation does occur. The differentiation of cells here was therefore possibly not induced by the substrates but more likely by the components of RM+ media.

Morphologically, individual cell membranes and nuclei were distinguishable on every substrate. PCNA staining was localised to the nucleus whereas K10 and K16 were

cytoplasmic as expected. Cells were mainly in monolayers as is typical for a submerged cell line culture, but occasional areas of multilayering were observed. This was more particular to polypyrrole films especially dermatan loaded films compared with PC or gold substrates. No sign of terminally differentiated cells *i.e.* cornified cells was observed. This may be expected for the short incubation period, in any case only partial differentiation is expected with this cell line.

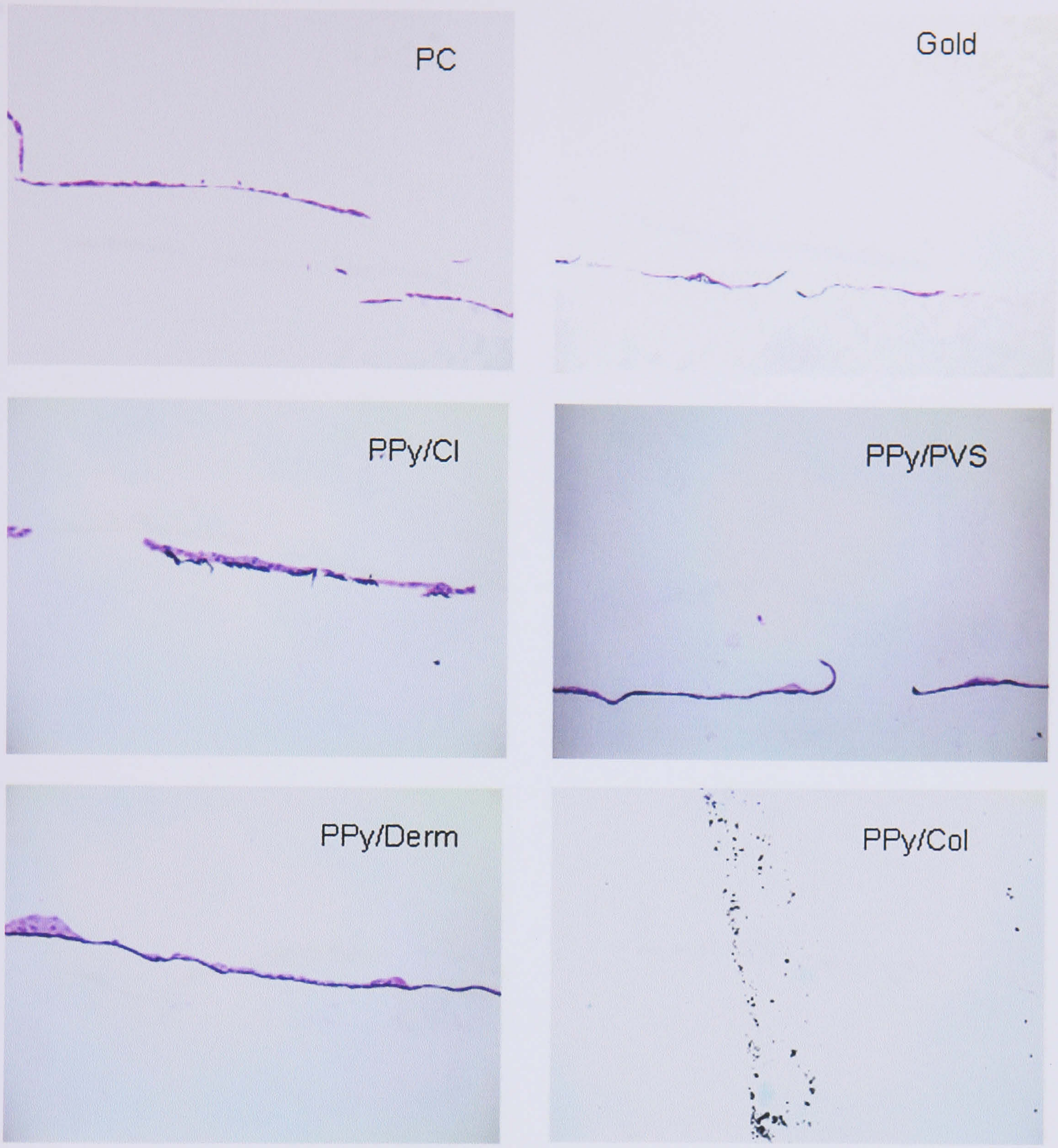

Figure 4.21: H & E for SVK14 Keratinocytes on Substrates after 5 Days. *Eosin (pink), an acidic dye, stains basic structures and is therefore cell body prominent whereas haematoxylin (blue) stains negatively charged molecules and is concentrated in the nucleus. From the low magnification images (×20 objective lens) in these panels, it can be seen that except for PPy/Col, viable cells were observed for all substrates with some evidence of multilayering especially inn the case of PPy/Derm. The substrates, especially those that were polypyrrole based are seen as a fine black strip.*

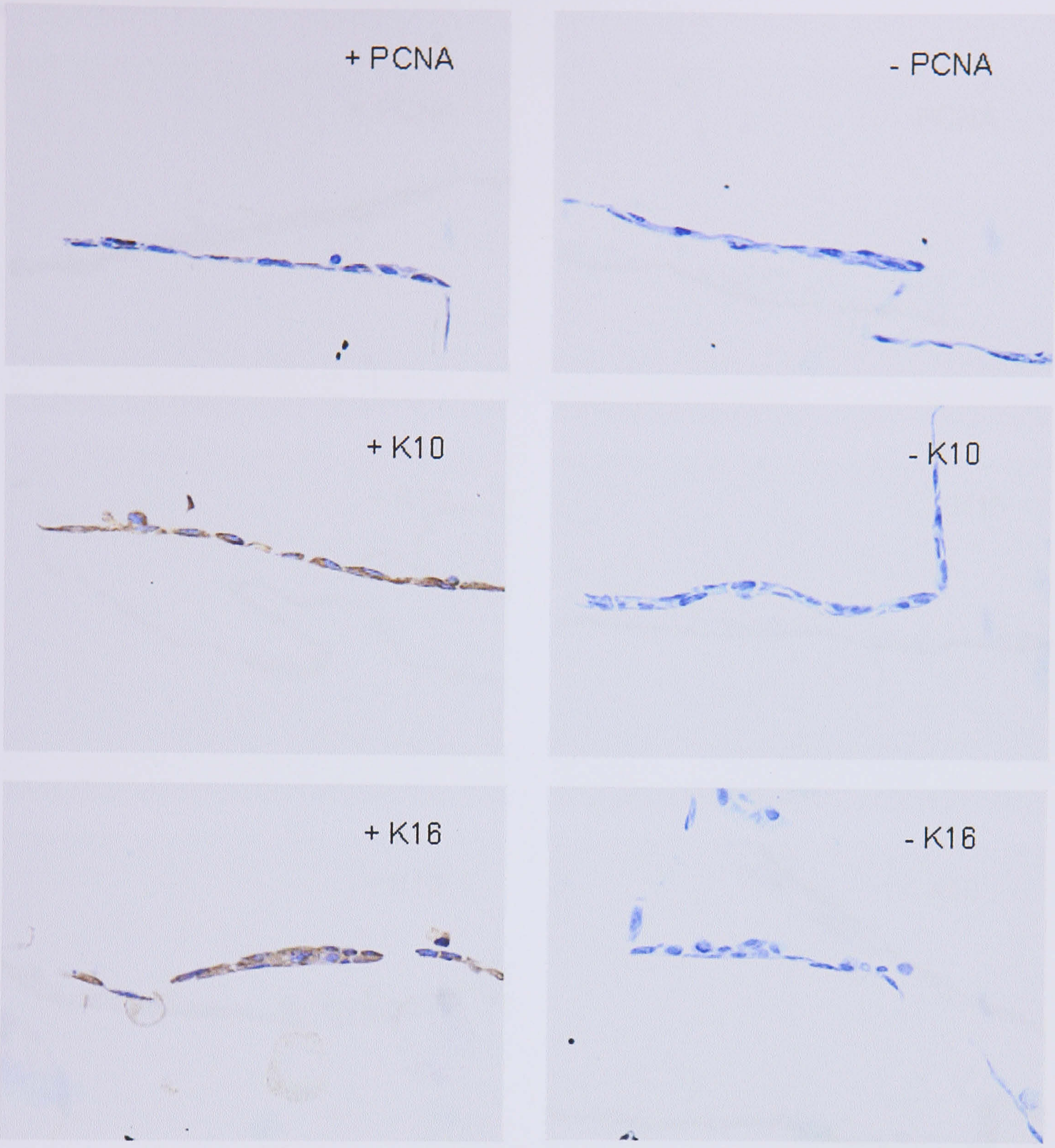

Figure 4.22: Stained SVK14 Keratinocytes on PC after 5 Days. *The brown colour in the left panels, absent from controls (right) shows that keratinocytes on PC were positive for the markers considered. From the high magnification images (×60 oil objective lens) in these panels, PCNA staining, indicative of cell proliferation was weak whereas K10 (suprabasal differentiation) and K16 (hyperproliferation) were strongly expressed and cell body prominent as expected.*

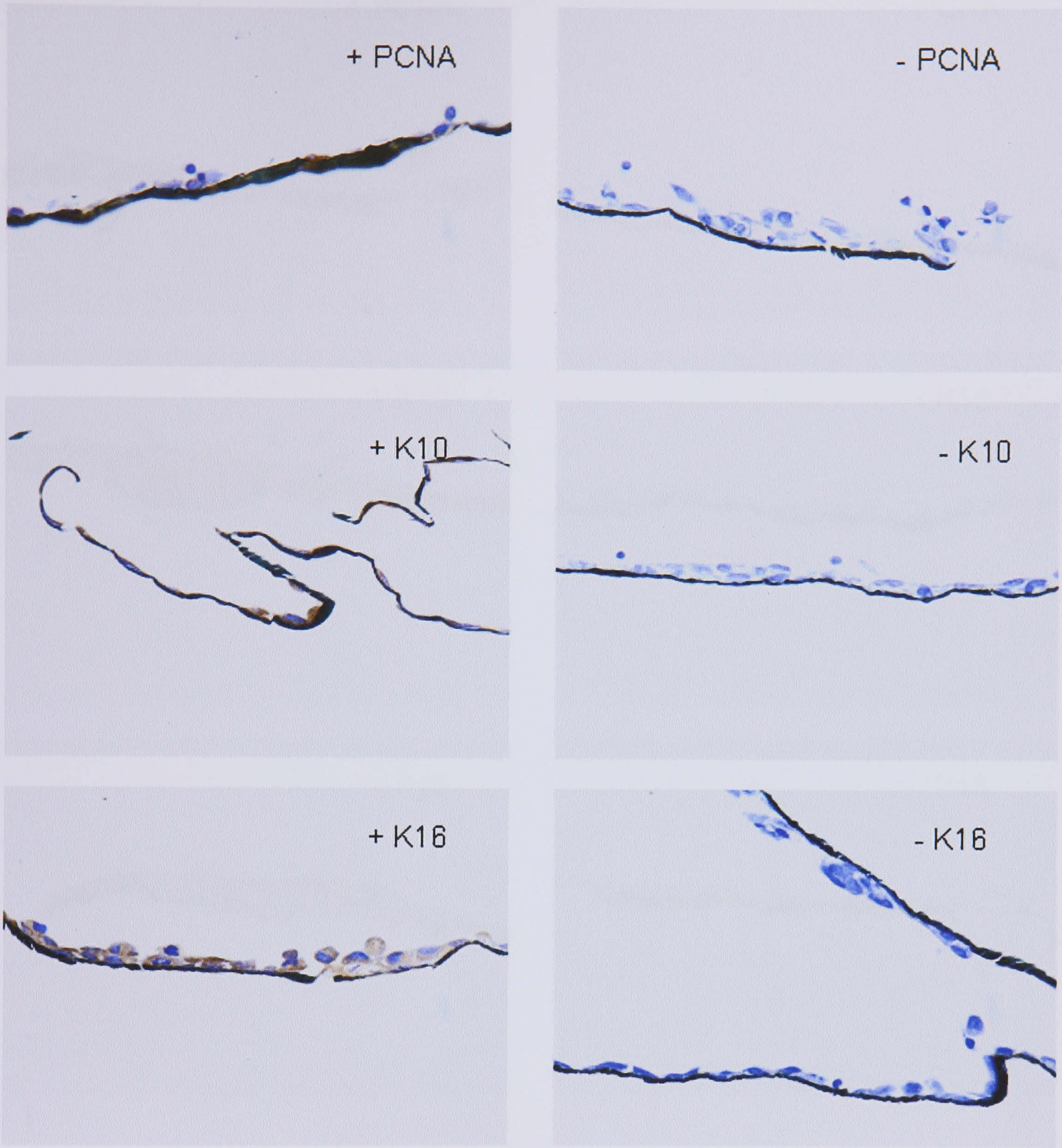

Figure 4.23: Stained SVK14 Keratinocytes on Gold after 5 Days. *The brown colour in the left panels, absent from controls (right) shows that keratinocytes on gold were positive for the markers considered. From the high magnification images (×60 oil objective lens) in these panels, PCNA staining, indicative of cell proliferation was moderate whereas K10 (suprabasal differentiation) and K16 (hyperproliferation) were strongly expressed and cell body prominent as expected. From all panels, there is also some evidence that keratinocytes did not strongly adhere to the gold substrate since some delamination and more rounded morphology may be observed.*

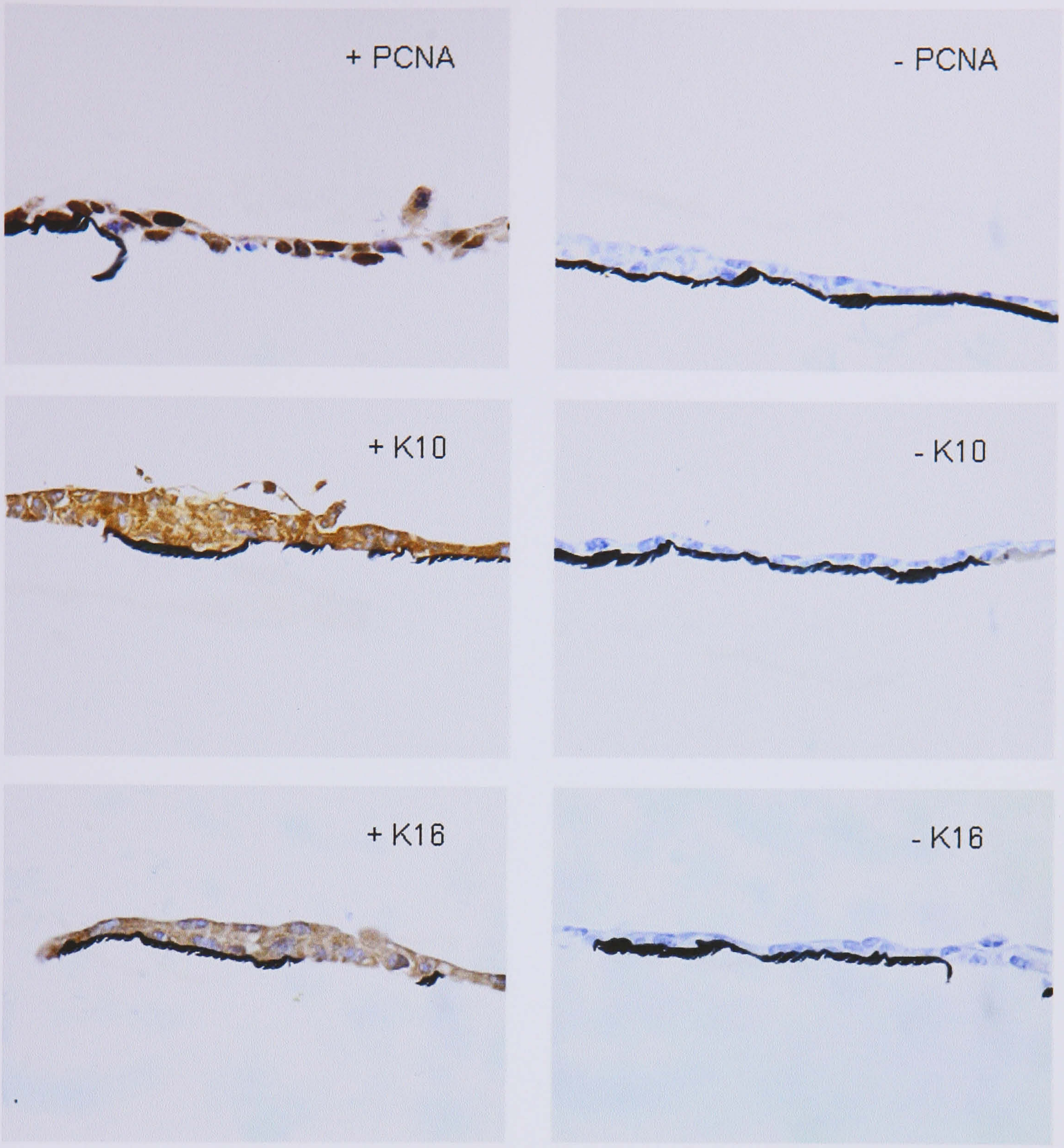

Figure 4.24: Stained SVK14 Keratinocytes on PPy/Cl after 5 Days. *The brown colour in the left panels, absent from controls (right) shows that keratinocytes on PPy/Cl were positive for the markers considered. From the high magnification images (×60 oil objective lens) in these panels, PCNA staining, indicative of cell proliferation was very strong and localised to the nucleus as expected. K10 (suprabasal differentiation) and K16 (hyperproliferation) were strongly expressed and cell body prominent as expected. These panels also show that cell good adhesion and multilayering occurred on PPy/Cl.*

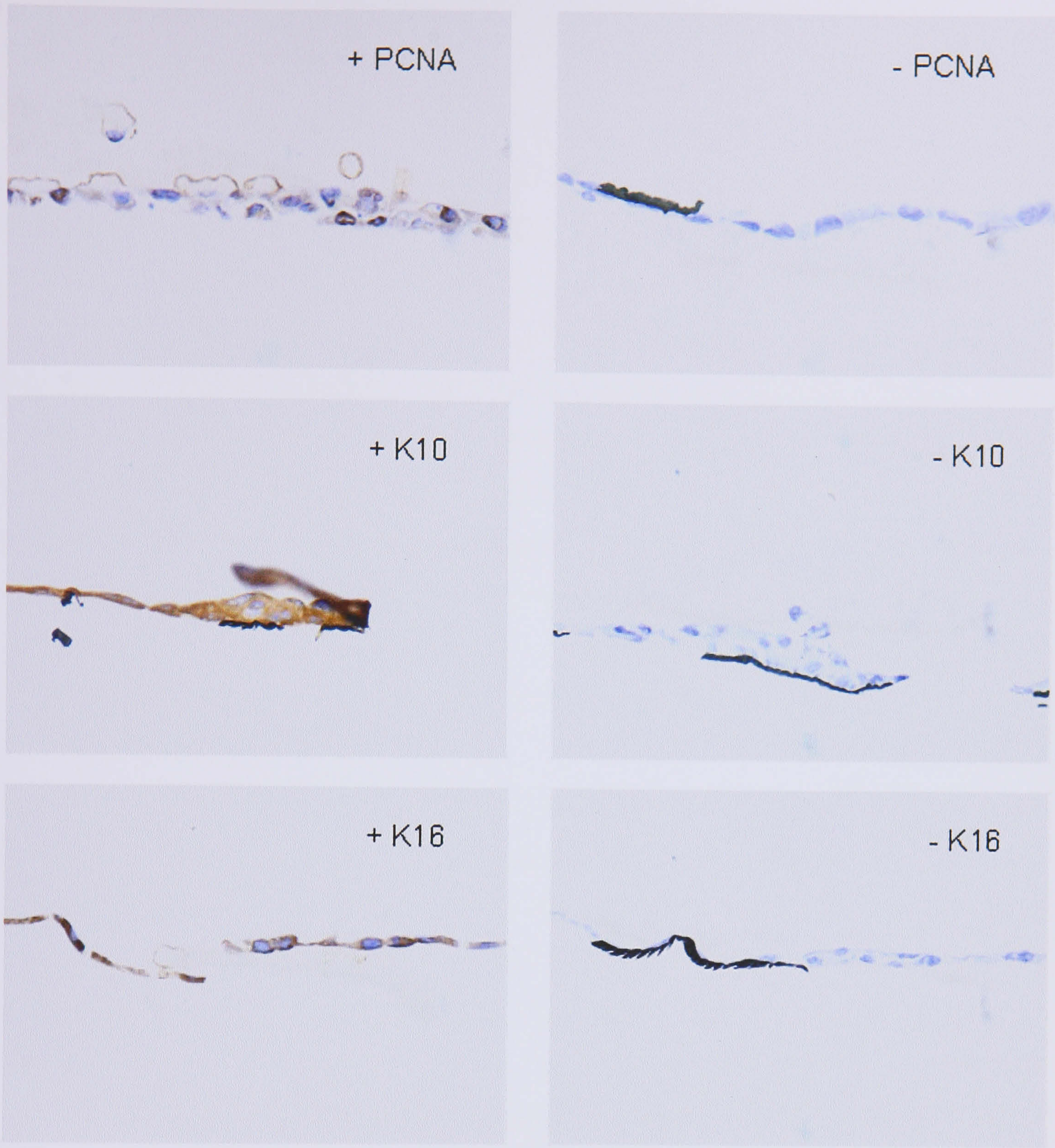

Figure 4.25: Stained SVK14 Keratinocytes on PPy/PVS after 5 Days. *The brown colour in the left panels, absent from controls (right) shows that keratinocytes on PPy/PVS were positive for the markers considered. From the high magnification images (×60 oil objective lens) in these panels, PCNA staining, indicative of cell proliferation was weak with some non nuclear localisation with K10 (suprabasal differentiation) and K16 (hyperproliferation) strongly expressed and cell body prominent as expected.*

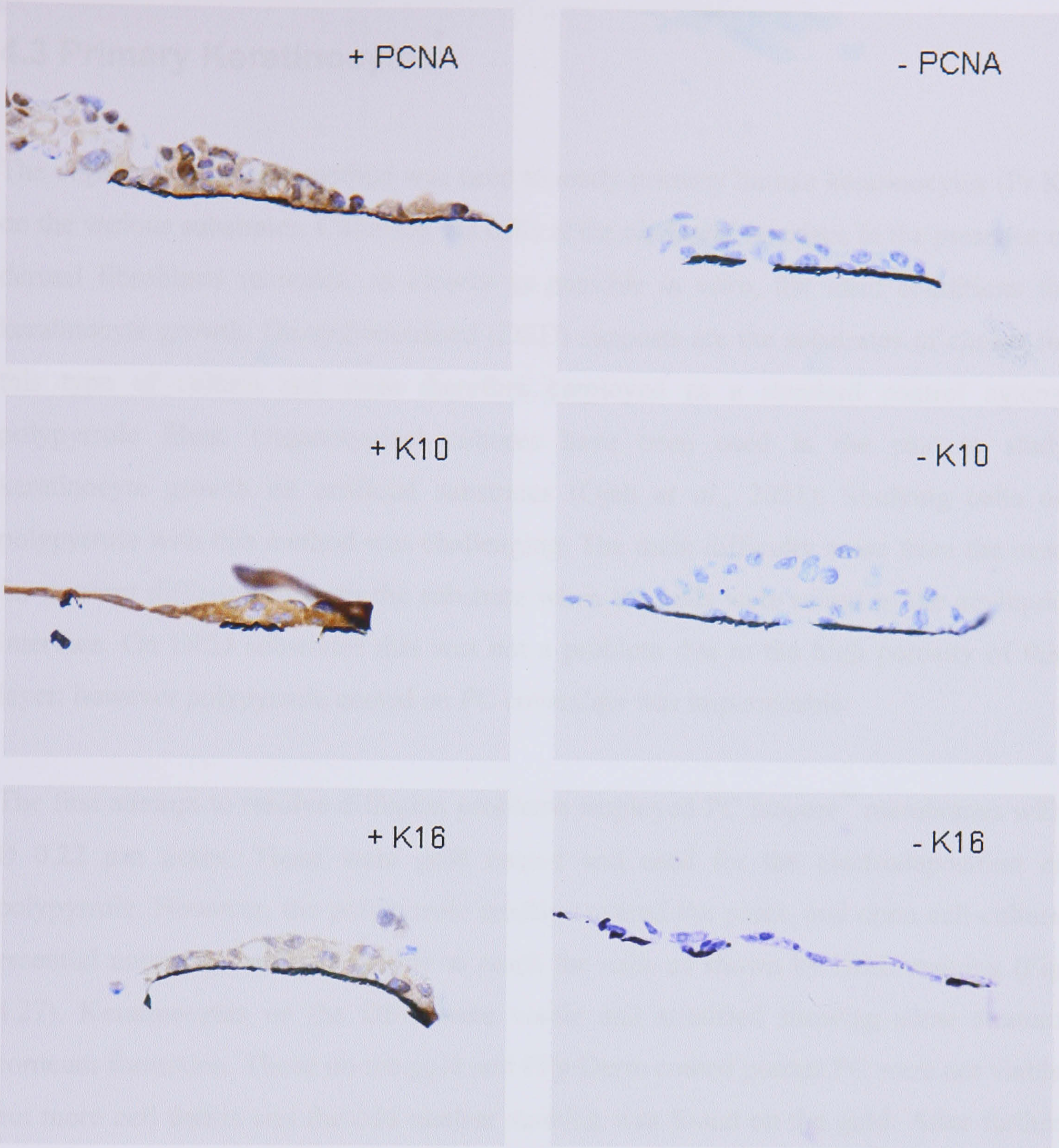

Figure 4.26: Stained SVK14 Keratinocytes on PPy/Derm after 5 Days. *The brown colour in the left panels, absent from controls (right) shows that keratinocytes on PPy/PVS were positive for the markers considered. From the high magnification images (×60 oil objective lens) in these panels, PCNA staining, indicative of cell proliferation was strong with K10 (suprabasal differentiation) strongly expressed and K16 (hyperproliferation) staining weak. These panels show that cells adhered well to PPy/Derm and formed multiple layers during culture.*

4.3 Primary Keratinocytes

The organotypic culture method was used to study primary human keratinocytes (Pr K) on the various substrates. Culturing the cells at the air-liquid interface in the presence of dermal fibroblasts recreates, as closely as possible *in vitro*, the ideal conditions for keratinocyte growth. De-epidermalised (DED) supports are the substrates of choice for this type of culture and were therefore employed as a standard control against polypyrrole films. Organotypical cultures have been used in the past to study keratinocyte growth on artificial substrates (Ojeh *et al.*, 2001). Studying cells on polypyrrole with this method was challenging. The main difficulty arose from the need for nutrient diffusion through the substrate when the cells were raised to the air-liquid interface. On DED substrates this was not a problem due to the high porosity of this layer; however polypyrrole coated on PC coverslips was impermeable.

The first attempt to resolve diffusion problems employed PC Isopore™ membranes with Ø 0.22 μm pores. These were gold coated and used for the electrodeposition of polypyrrole. However, the polypyrrole readily covered the pores, and upon cell culture essential nutrients were still unable to reach the cells as shown by H&E staining (Fig 4.27). Keratinocytes on the DED were viable and stratified showing some stratum corneum formation. Those on the gold and PPy/Derm coated porous PC were not viable but more cell debris and the odd nuclear staining was found on the gold. After further trials it was found best to use the original PC coverslips, but to physically pierce holes through the cell seeded substrate prior to air-liquid interface exposure. Additionally, media needed to be added slightly above the cell layer for best results.

The H&E of cells grown on DED, thin and thick PPy/Derm using this method are shown in Figure 4.28. They show cell viability using this method although with poorer morphological quality compared to DED. Stratification on the PPy/Derm substrates was limited. Nevertheless, all the substrates were stained for PCNA, K10 and K16 (Fig 4.29). The results showed that keratinocytes were positive for these markers on all substrates. However, this was to a lesser intensity than found with the SVK14s. When the staining of an ideal organotypic *i.e.* with keratinocytes grown at a proper air-liquid interface was compared to the experimental DED control where media was slightly above cells, morphology and localisation of staining was improved.

These results demonstrate the viability of primary keratinocytes on thin and thick PPy/Derm without discernable differences. However, differentiation was very poor on these substrates as often found in artificial dermal equivalents (Ojeh *et al.*, 2001). In this case, a number of reasons could be cited including poor nutrient diffusion, poor access to the air interface, flat contact compared with the rutted dermal surface or the lack of basement membrane proteins. These could be tested with the design of PPy coatable substrates of similar geometry to the papillary dermis surface with adequately sized and distributed pores for effective nutrient delivery.

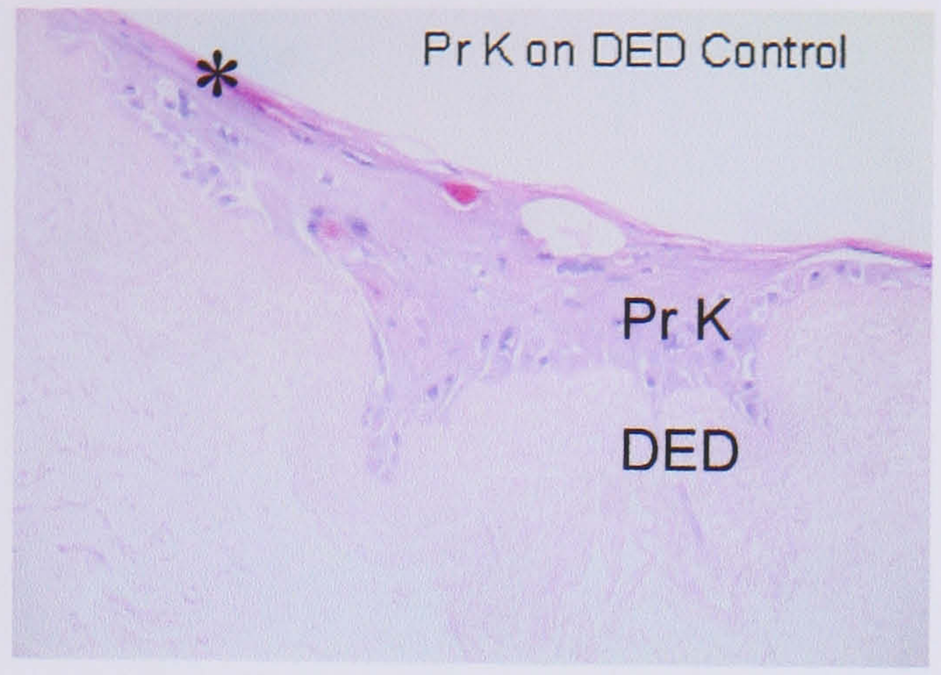

Figure 4.27: H & E for Primary Keratinocytes on Porous PC. *Eosin (pink), an acidic dye, stains basic structures and is therefore cell body prominent whereas haematoxylin (blue) stains negatively charged molecules and is concentrated in the nucleus. From the low magnification images (×20 objective lens) in these panels, it can be seen that primary keratinocytes grow well on DED with stratification ending in a visible stratum corneum layer (asterix). This is not the case for cells on gold-coated porous PC where poor morphology and very little nuclear staining indicates dead cells. This is even worse for the PPy/Cl coated substrate as pore blockage probably totally inhibited the diffusion of nutrients from the underlying media.*

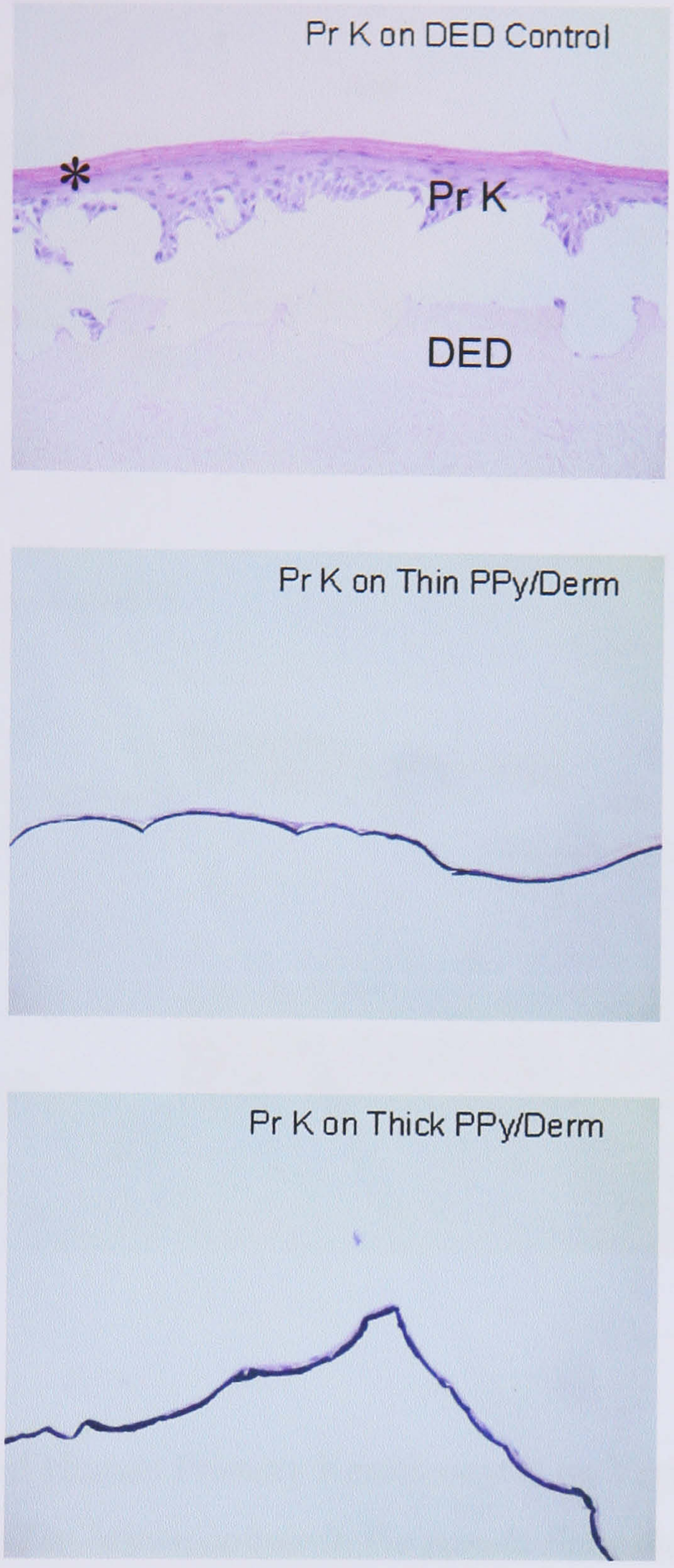

Figure 4.28: H & E for Primary Keratinocytes on PC Coverslips. *Eosin (pink), an acidic dye, stains basic structures and is therefore cell body prominent whereas haematoxylin (blue) stains negatively charged molecules and is concentrated in the nucleus. From the low magnification images (×20 objective lens) in these panels, it can be seen that primary keratinocytes grow well on DED with stratification ending in a visible stratum corneum layer (asterix) (delamination between epidermis and dermis occurred during tissue processing). Poor stratification is seen for cells on both thin and thick PPy/Derm although there is evidence of a living cell layer from morphology and intact nuclear staining seen at the surface of the polymer (black strip on bottom two panels) undoubdetly due to the fact that the cells were slightly submerged with culture media.*

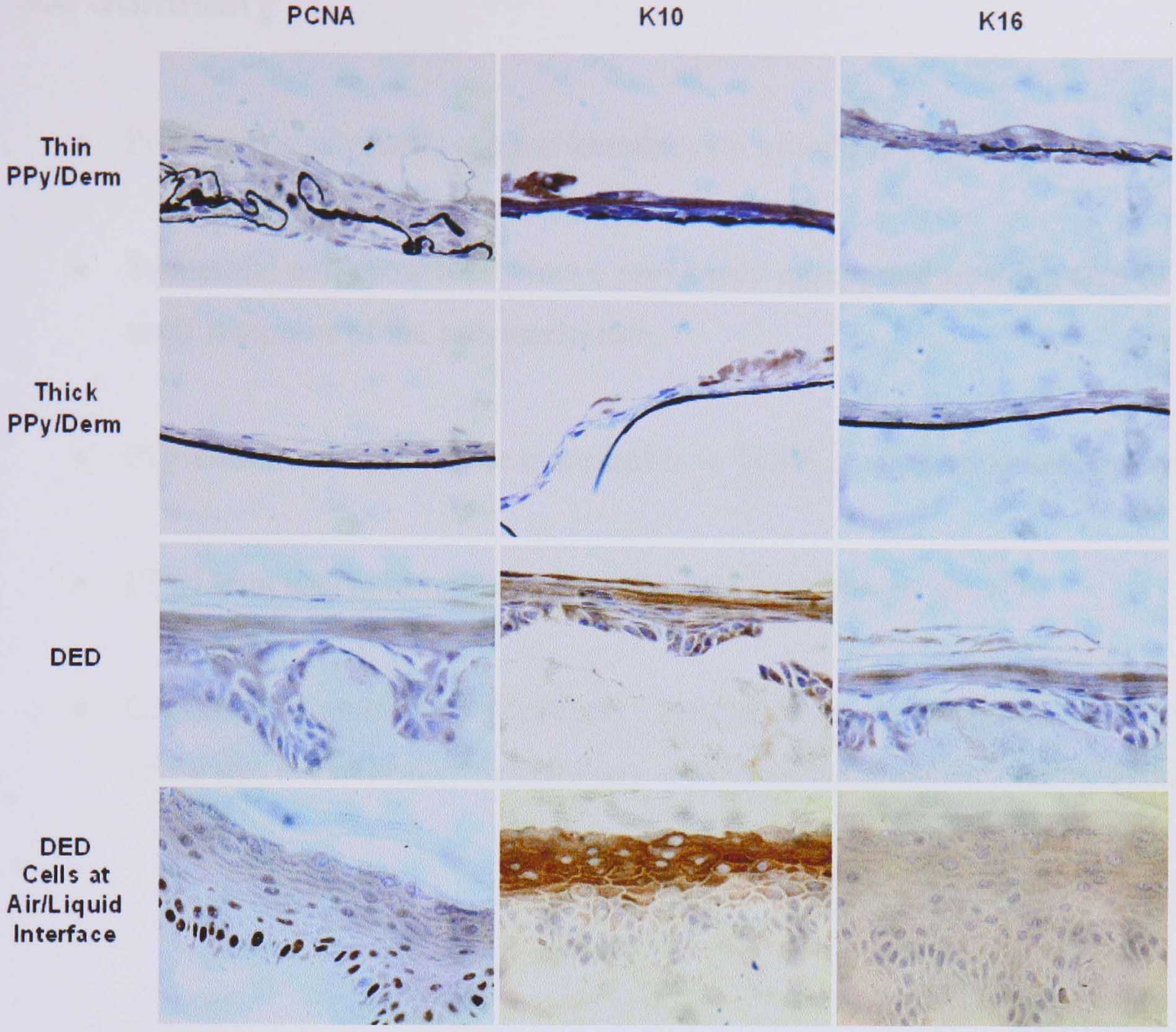

Figure 4.29: Stained Human Primary Keratinocytes on Various Substrates after Organotypical Culture. *The brown colour in the panels show that primary keratinocytes were positive for the markers considered. From the high magnification images (×60 oil objective lens) in these panels, it may be seen that when the cells are slightly submerged in culture media, staining is weaker even for the DED substrate (top three panels) although there is better stratification and morphology in the latter. The bottom panels, where primary keratinocytes were grown under optimal conditions, including an air/liquid interface, show intense PCNA staining localised to basal layer nuclei as expected. K10 (suprabasal differentiation) was also strongly expressed at the granular layer as expected and K16 (hyperproliferation) was weakly expressed at all layers.*

4.4 Summary

- Polypyrrole substrates support keratinocyte growth in a load dependent manner.

- Successful cell growth requires a previously unreported washing step to remove toxic remnants of the polymerisation.

- PPy/Derm was found to be comparable to TCPS in supporting keratinocytes.

- PPy/Derm was preferential to bare gold for keratinocyte growth.

- Organotypic cultures of primary keratinocytes were viable on PPy/Derm substrates but of poorer morphology than those on de-epidermalised dermis.

Chapter 5

Impedance Sensing of Cells on Polypyrrole Films

5.1 Introduction

The use of impedance to monitor cells has been investigated in the past using gold electrodes. This Chapter addresses the central theme for this project which is the study of cells on polypyrrole modified electrodes by impedimetric methods. This technique could provide an alternative means for monitoring cells in constructs or their reactions to the effects of drugs and environmental conditions. Currently literature reports for such studies do not exist and with PPy/Derm for instance found more suitable to cell growth than bare gold, it is worth studying cells on polypyrrole using impedance. Indeed, further advantages may be brought to light. Three approaches are presented for the study of cells on various substrates, a direct consideration of full EIS data, a more specific analysis at single frequencies and finally in terms of equivalent electric circuit parameters whose contributions may be directly mapped intracellular and intercellular spaces and membrane components of cells.

5.2 Impedance Spectroscopy Monitoring

5.2.1 Growth of SVK14 Keratinocytes in Culture

Figures 5.1 and 5.2 show the changes in impedance spectra for SVK14 keratinocytes cultured on either gold or PPy/Derm over 7 days for different initial cell seeding densities. In the control groups, without cells, no significant changes were noted over the experiment duration except for a small difference for PPy/Derm substrates between the day 0 data set and others. This small difference was possibly due to the hydration of the PPy/Derm films after 24 h immersed in culture media. Comparing the spectra of the bare gold and PPy/Derm substrates, it can be seen that polypyrrole reduces total impedance at the lower frequencies as seen earlier with in-plane, two-electrode analysis (Figs 3.22-3.23). Impedance spectra of SVK14 keratinocytes on gold and PPy/Derm substrates showed changes over 7 days for all cell seeding densities (4×10^4, 4×10^5 and 4×10^6 cells) in a frequency and time dependent manner, not seen for the controls.

Impedance spectra for gold substrates (Fig 5.1) show significant changes from day 1 for the mid and highest cell seeding densities on gold substrates whereas for the lowest seeding density this occurs only on day 7. On PPy/Derm substrates (Fig 5.2) changes are seen across all the initial cell seeding densities. These changes are also distributed along the frequency spectrum compared to gold where the changes are confined to the higher frequencies (*ca* 1-100 kHz). Complex plane representations of imaginary versus real impedance show how the cell-induced impedance signal is associated with the partial formation of a semicircle at higher frequencies, absent in controls. The high frequency semi-circle indicates an interfacial transfer process that is slow enough to observe (Cui *et al.*, 2001), in this case caused by plasma membrane charging. After 7 days in culture, microscopy showed a cell layer on all substrates with an excess of cells on the substrates with mid and high seeding densities (Fig 5.3). The variation of impedance spectra as a function of frequency, seeding density and substrate material for these results are further discussed through single frequency analysis (section 5.3).

Control (0 Cells)

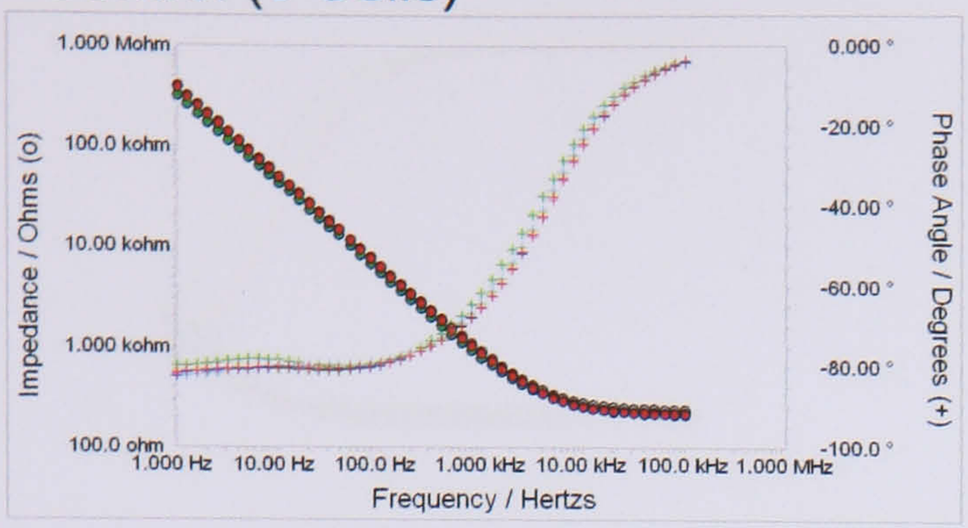

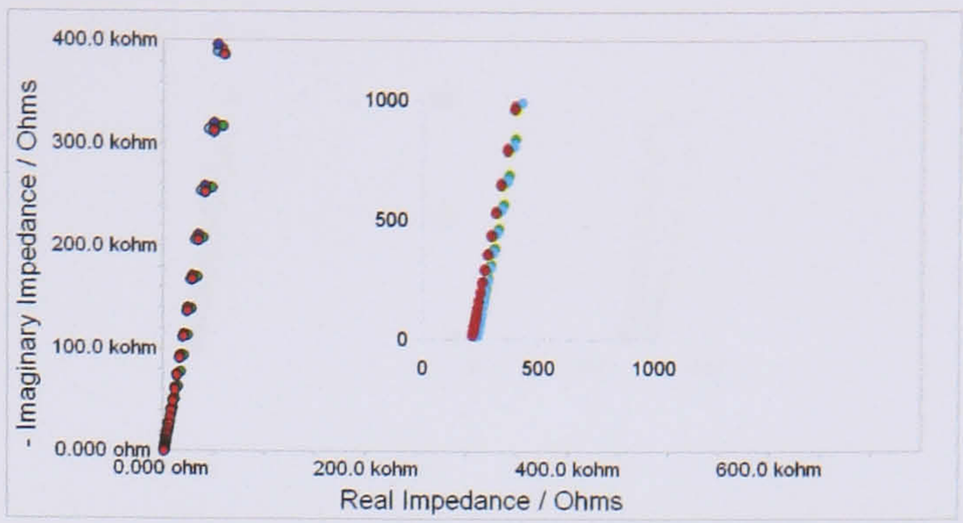

4×10^4 Cells Seeded

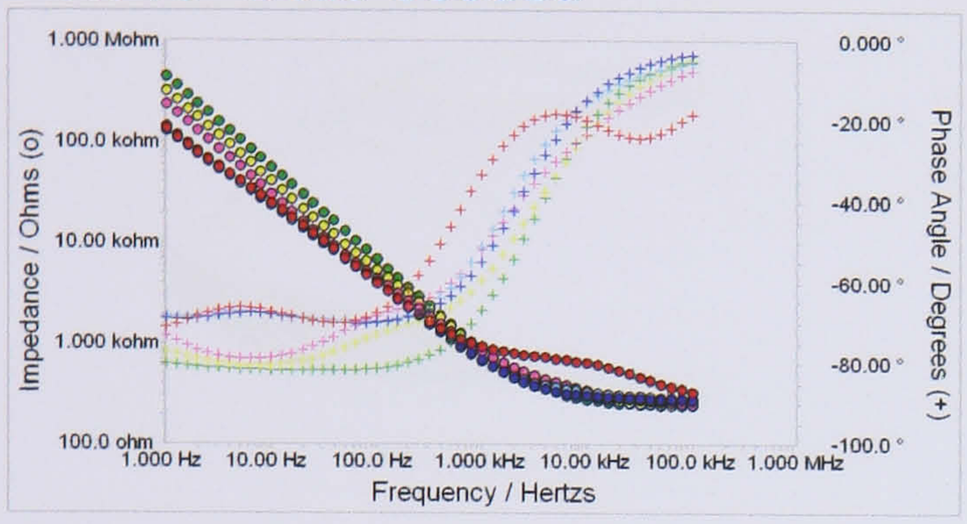

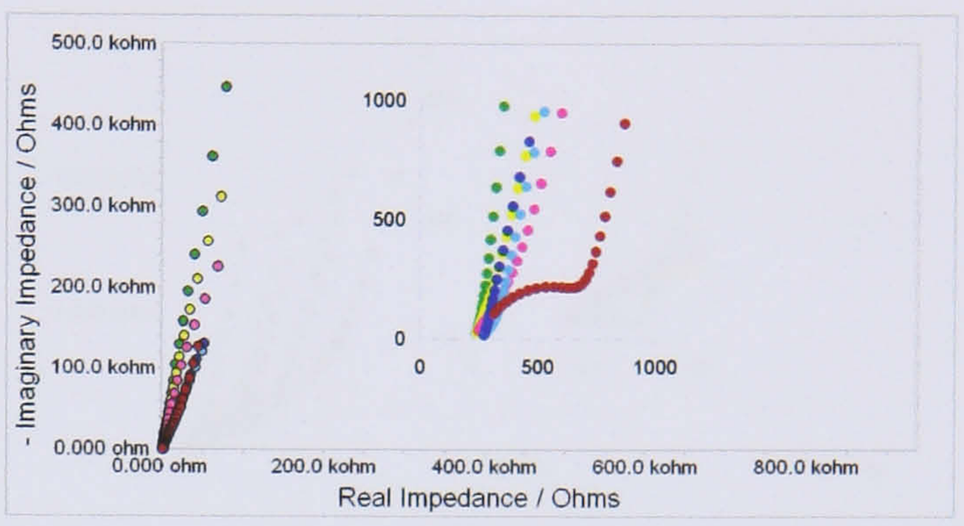

4×10^5 Cells Seeded

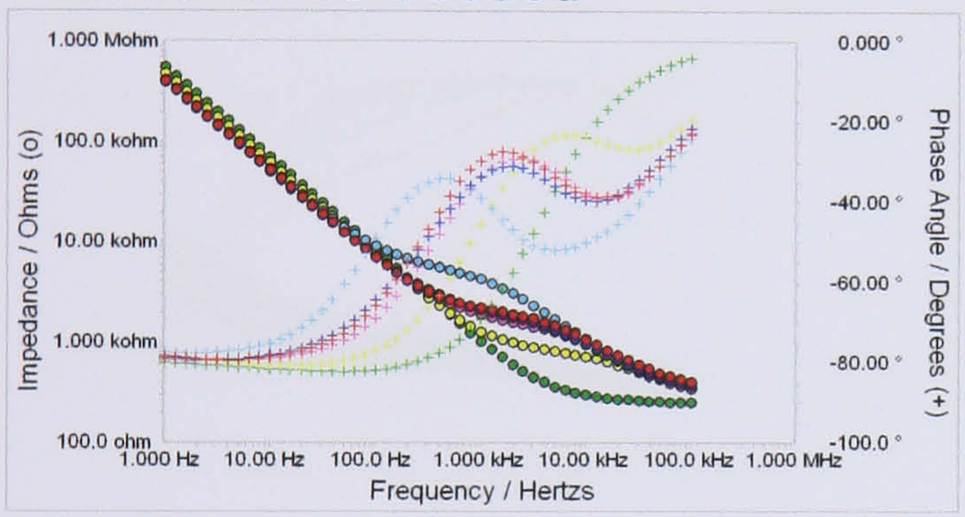

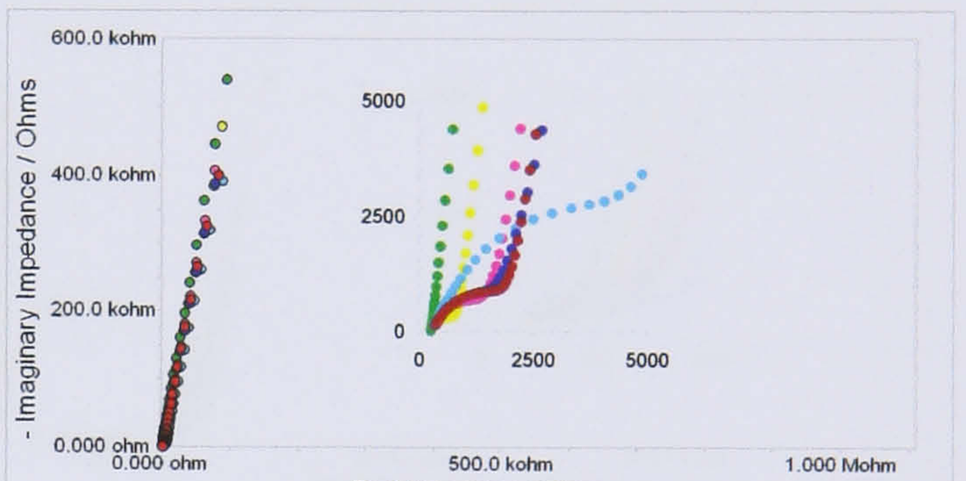

4×10^6 Cells Seeded

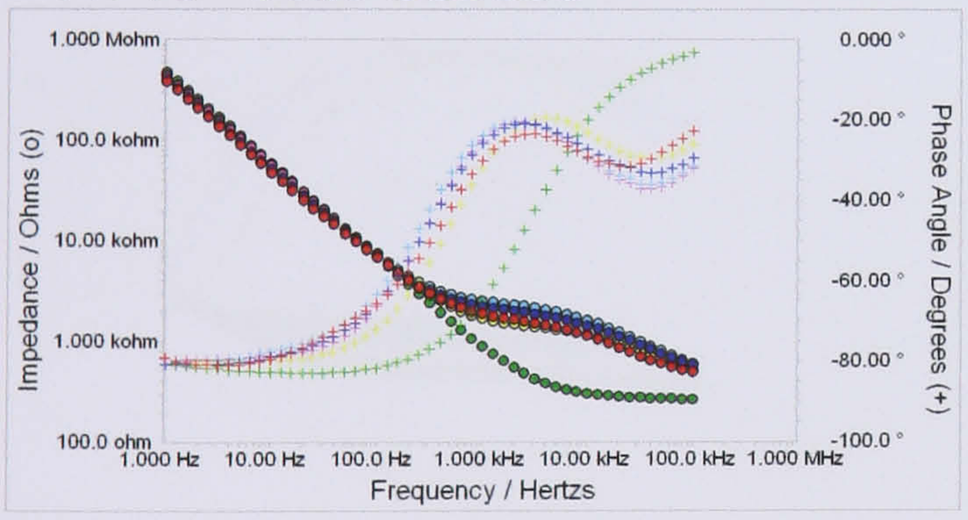

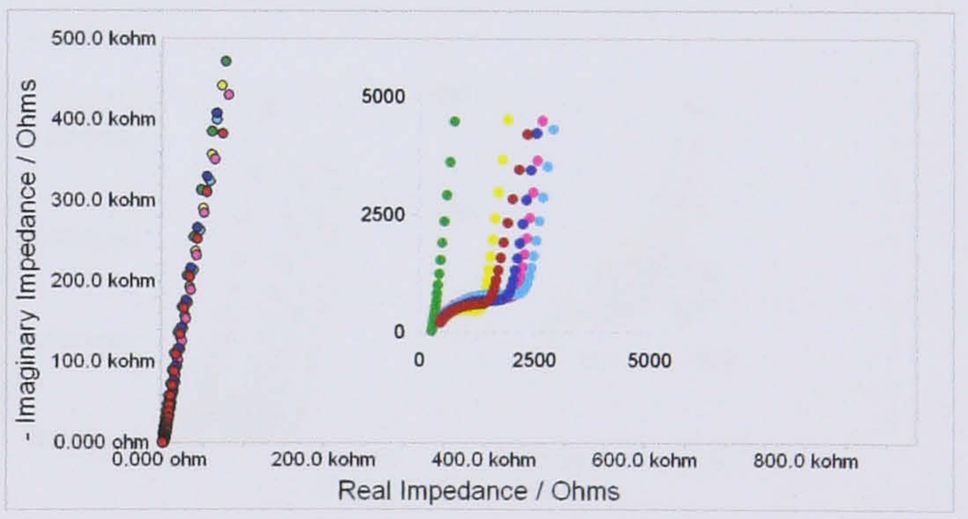

Figure 5.1: Representative Bode Plots (Left) and Complex Plane Plots (Right) of SVK14 Keratinocytes on Gold digit-Coated PC Coverslips. *The control plots (without cells) show no change in impedance over 7 days whereas changes are seen when cells are added. These changes occur more reapidly with higher cell seeding densities and are characterised by increases in impedance at specific frequencies on the Bode plot and the appearance of a semi-circle at low frequencies in the complex plane.*

Control (0 Cells)

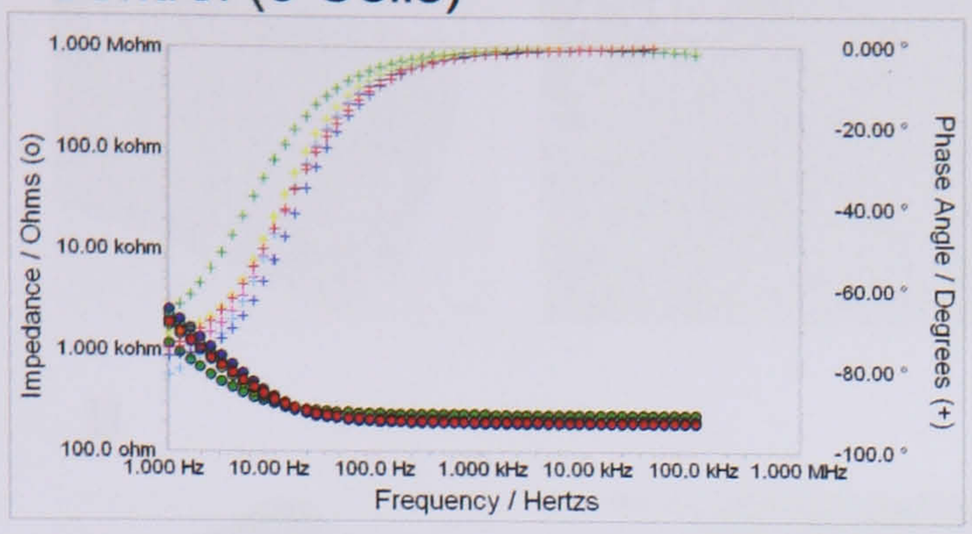

4×10^4 Cells Seeded

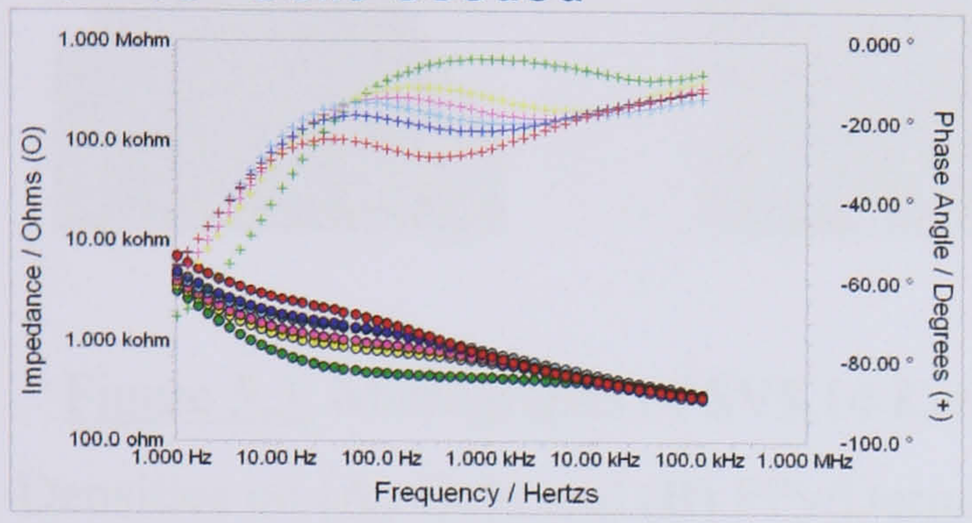

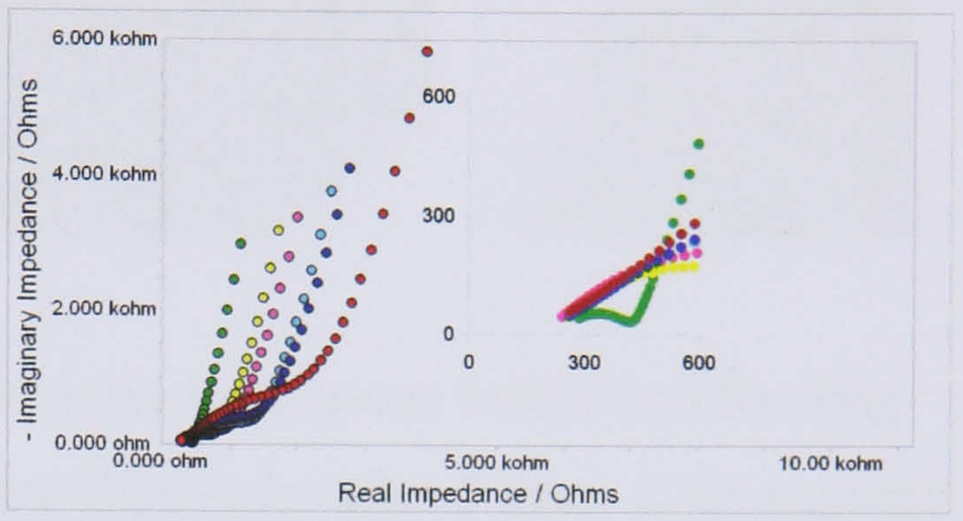

4×10^5 Cells Seeded

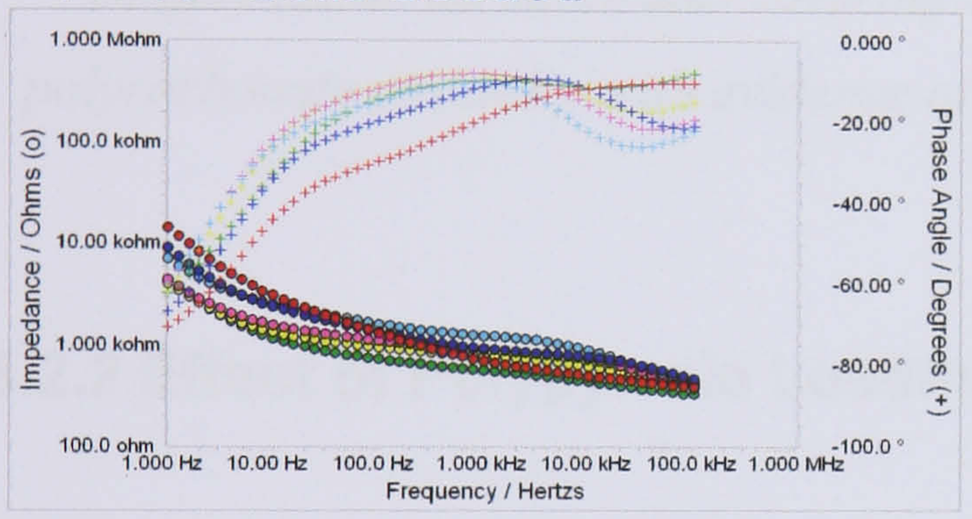

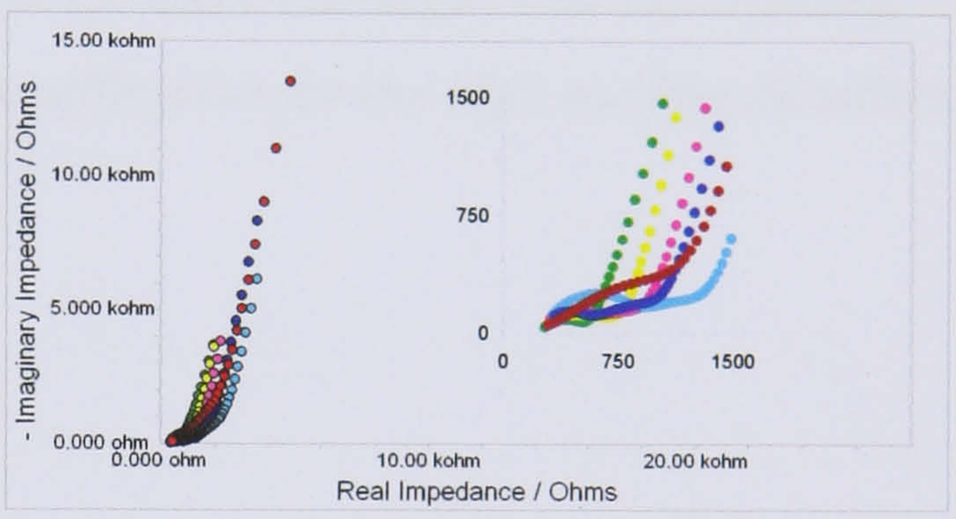

4×10^6 Cells Seeded

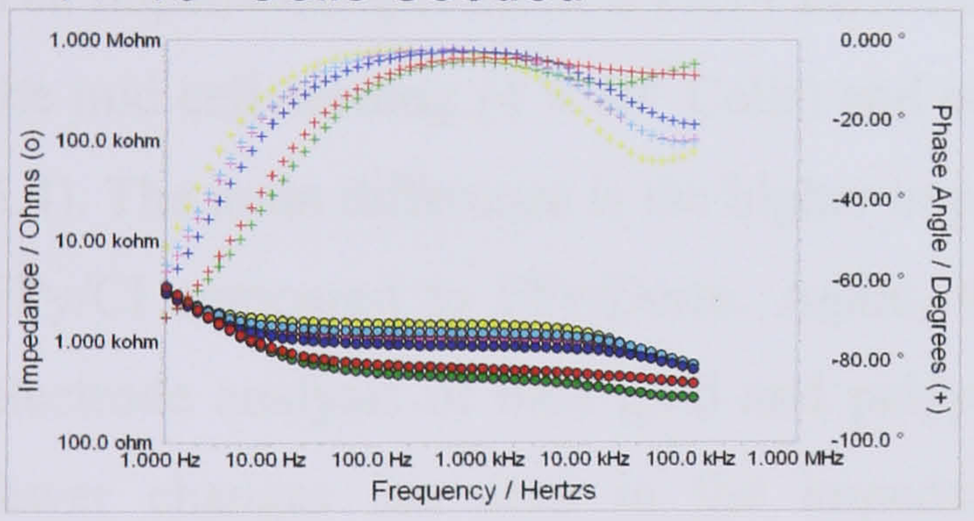

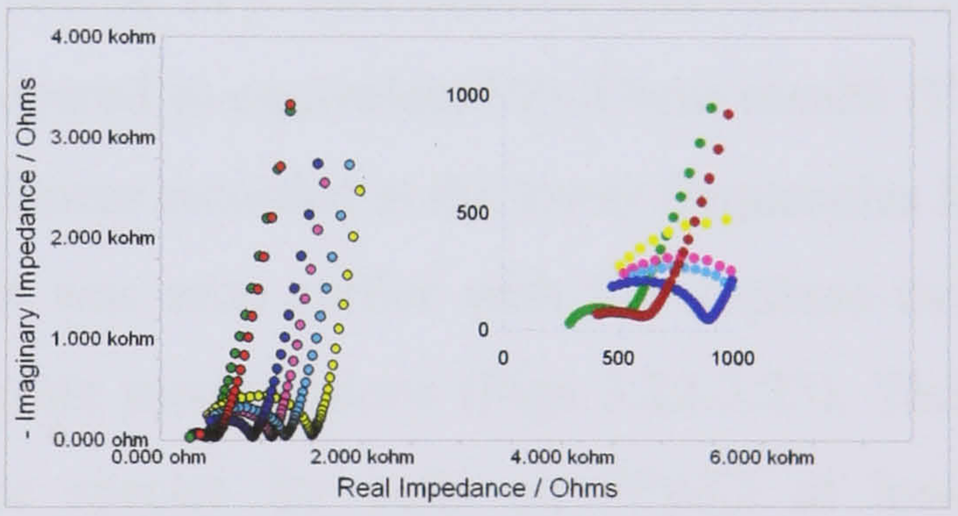

Day 0 Day 1 Day 2 Day 3 Day 4 Day 7

Figure 5.2: Representative Bode Plots (Left) and Complex Plane Plots (Right) of SVK14 Keratinocytes on Washed PPy/Derm digit-Coated PC Coverslips. *The control plots (without cells) show a small change in impedance after day 0 (probably due to polymer hydration) but are otherwise similar over 7 days. When cells are added changes are seen between the different spectra and are characterised again by increases in impedance at specific frequencies on the Bode plot and the appearance of a semi-circle at low frequencies in the complex plane.*

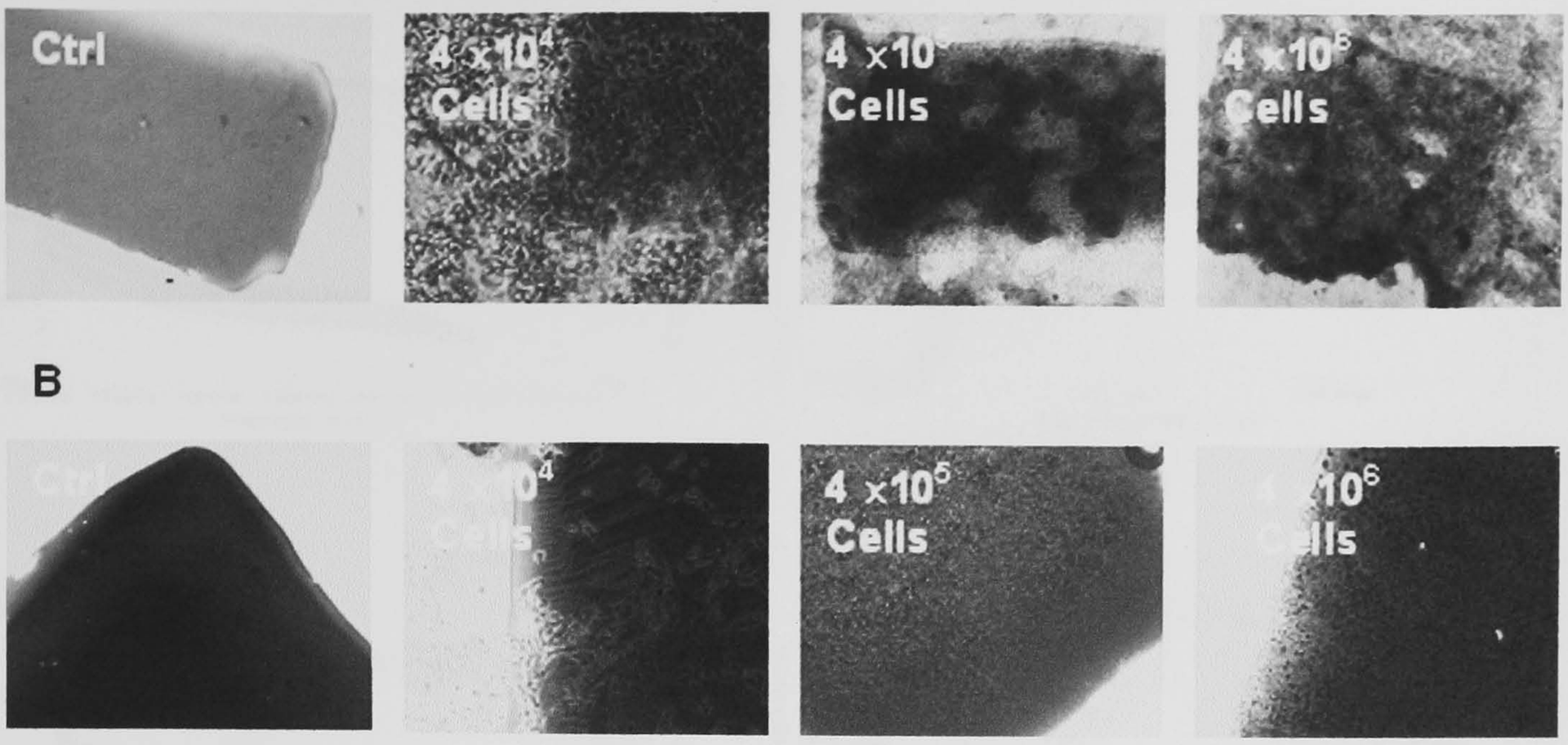

Figure 5.3: Micrographs of SVK14 Keratinocytes for Various Initial Cell Seeding Densities on (A) Gold and (B) PPy/Derm-Digit Electrodes after 7 days. *Cells reached confluence on all substrates covering both the electrode digits and surrounding polycarbonate coverslip with evidence of stratification for the high seeding densities.*

5.2.2 Effect of Polypyrrole Loading

The impedance spectra of SVK14 keratinocytes on PPy with chloride was recorded for the mid cell seeding (4×10^5 Cells) and compared to equivalent PPy/Derm results (Fig 5.4). The main difference is the higher impedances recorded at the lower frequencies for PPy/Cl compared to PPy/Derm. Again, this was seen earlier with the in-plane two-electrode analysis of bare gold and polypyrrole modifications (Figs 3.22-3.23). Thus, fewer changes are seen in the impedance spectra for cells on PPy/Cl at lower frequencies compared to PPy/Derm. Also of note when considering the phase angle data, is the shift towards -90° on the left side of the Bode plots for cells on PPy/Cl. These differences are due to the different electrochemical behaviour of these films due to their counterion loadings (section 3.5.2). The changes in impedance normalised against controls at selected frequencies for cells on both types of PPy are presented in Section 5.3.

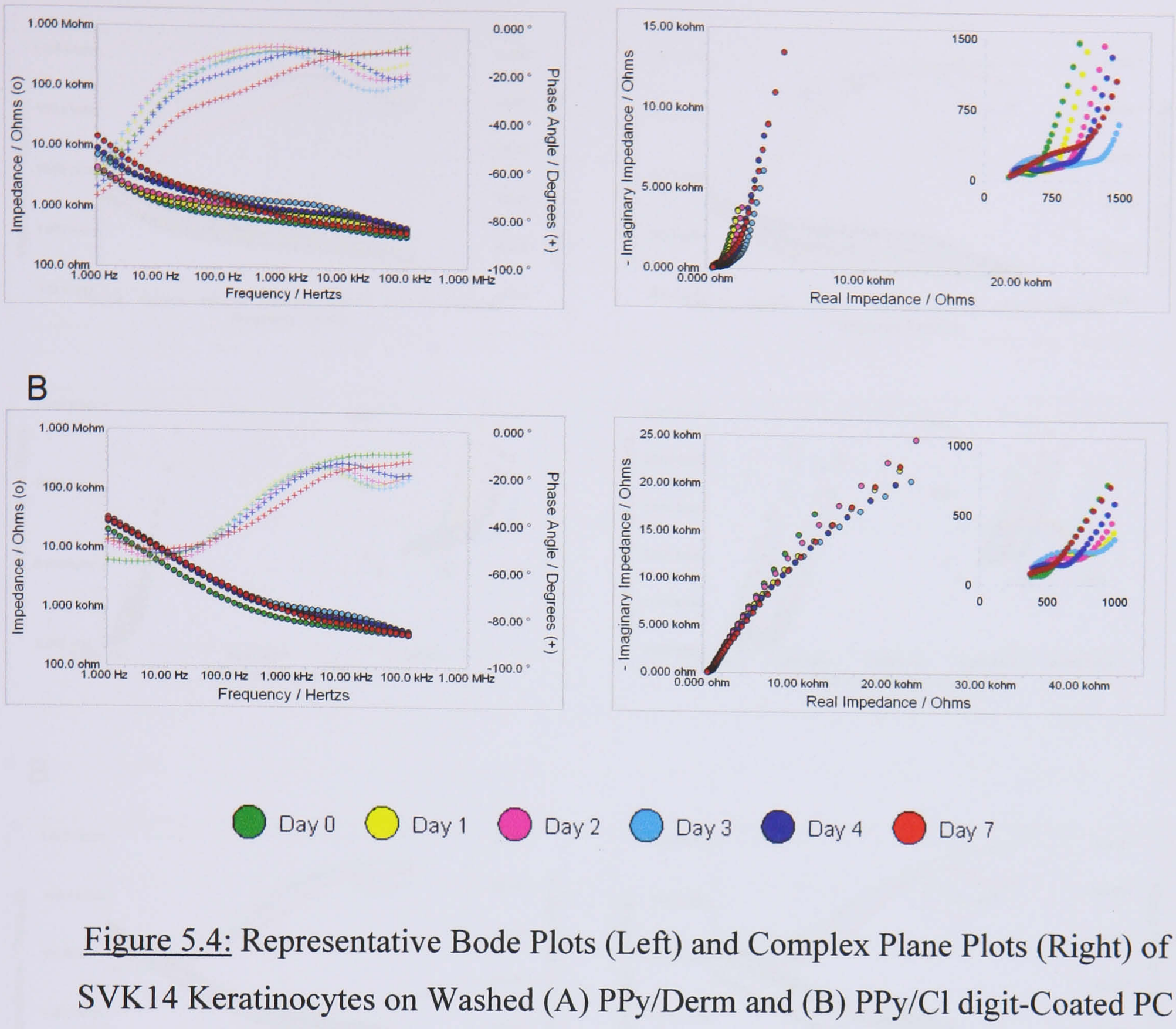

Figure 5.4: Representative Bode Plots (Left) and Complex Plane Plots (Right) of SVK14 Keratinocytes on Washed (A) PPy/Derm and (B) PPy/Cl digit-Coated PC Coverslips (4×10^5 Cells Seeded).

5.2.3 Effect of wash

The PPy films used for cell-induced impedance studies presented in this section were water washed to prevent the cytotoxic effect observed for unwashed films (Chapter 3). Figure 5.5 shows impedance spectra recorded for cells on PPy/Derm and PPy/Cl compared to those for their unwashed counterparts. It is useful to note that there are some differences between earlier experiments where unwashed PPy toxicity was studied and the set-up used for impedance measurements. Previously, the cells were only in contact with the PPy surface whereas for impedance measurements the surface only occupied small electrode areas surrounded by polycarbonate which was cell compatible. Therefore, any toxic effect would be lessened in addition to a constant supply of new cells available from the surrounding polycarbonate. After 7 days in culture, viable cells were seen on the PPy-coated electrodes (Fig 5.6).

A

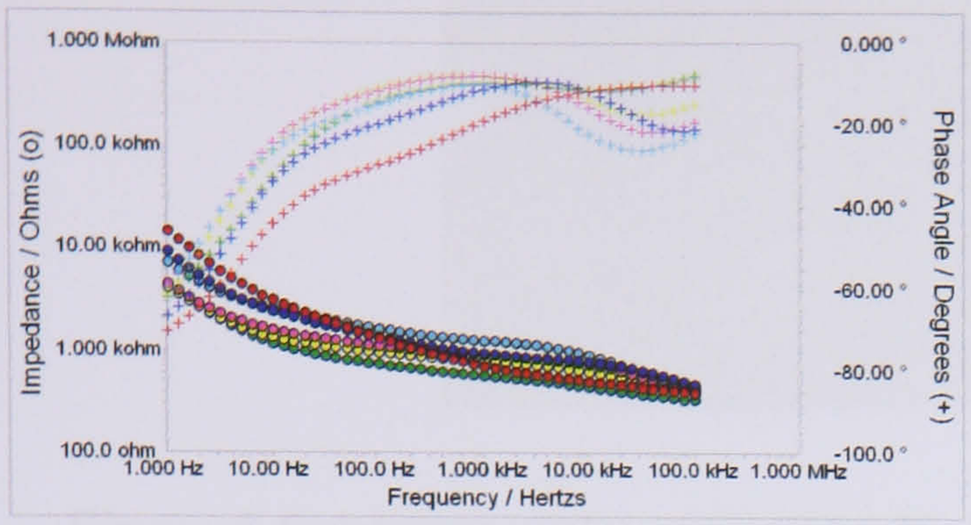

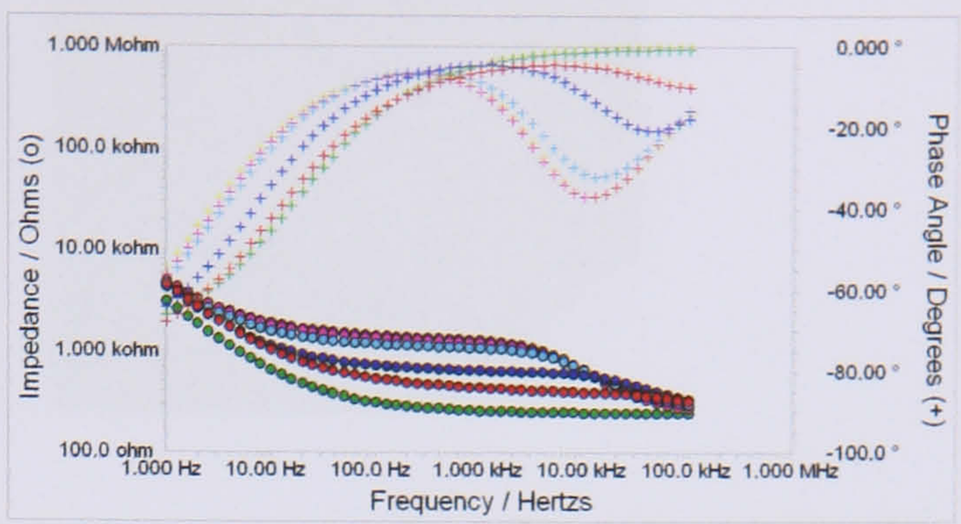

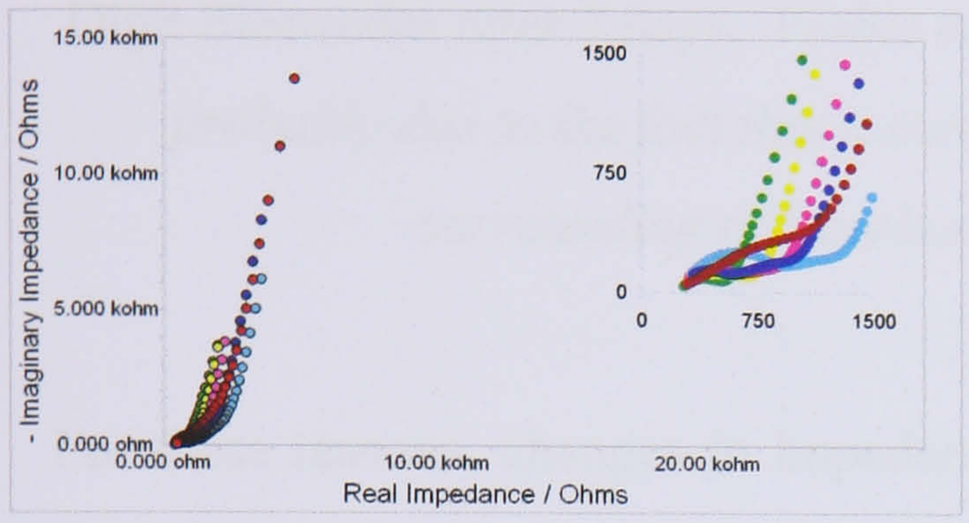

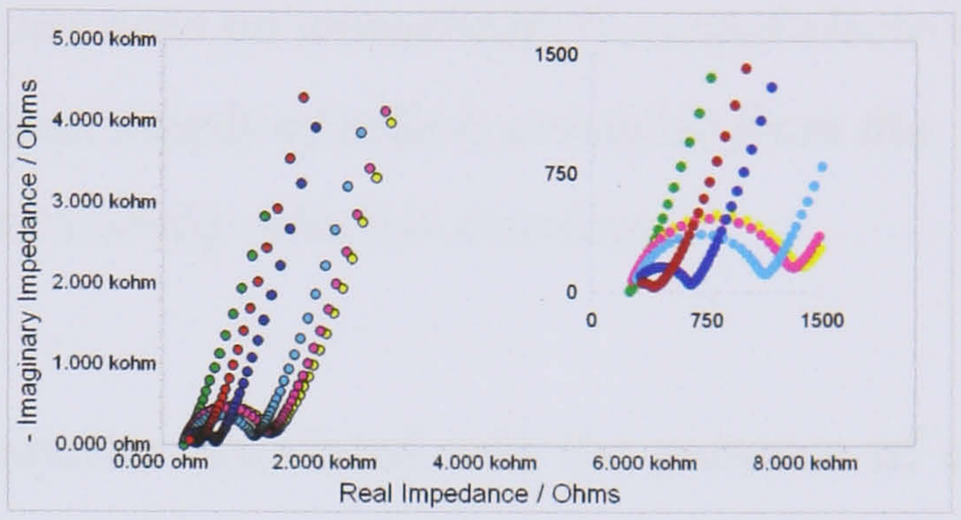

B

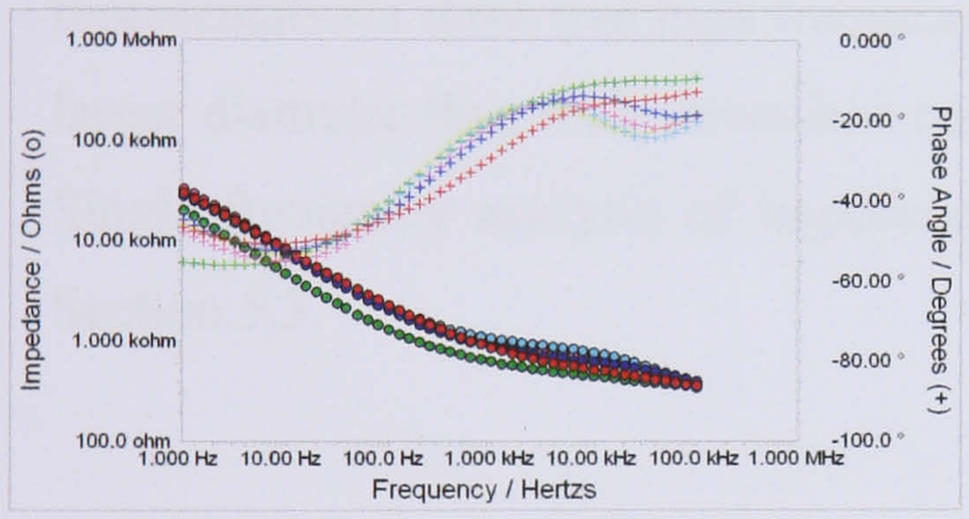

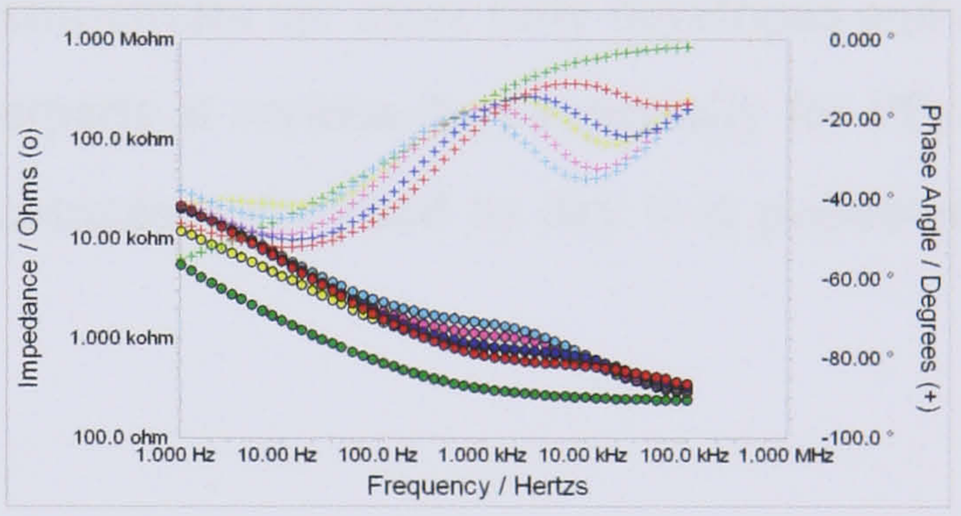

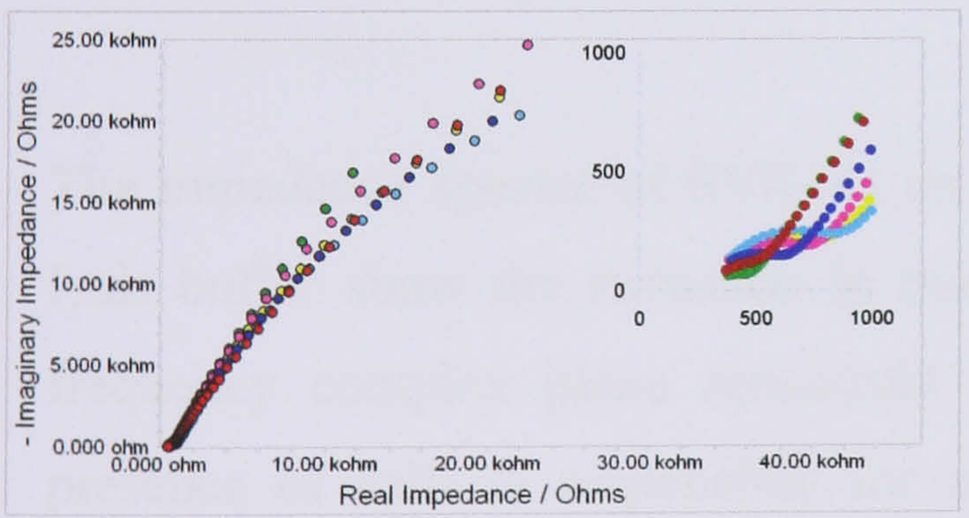

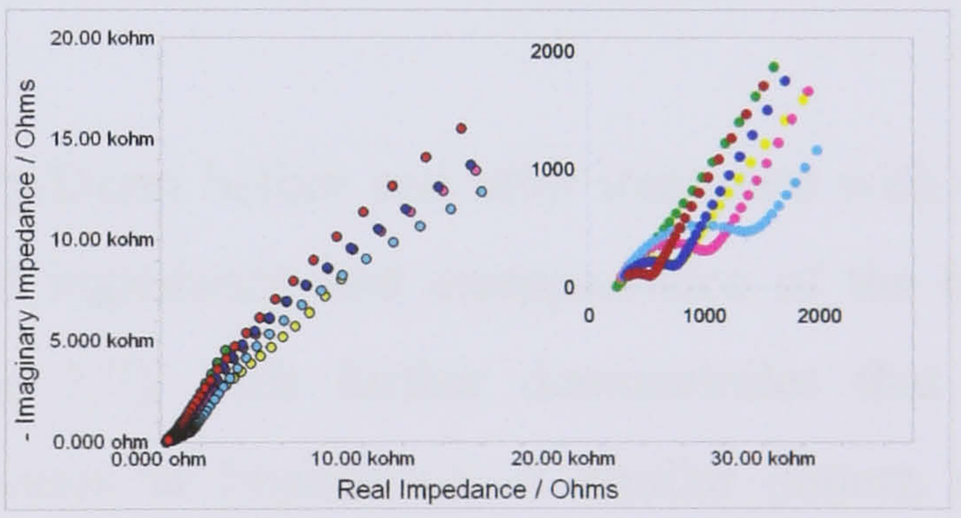

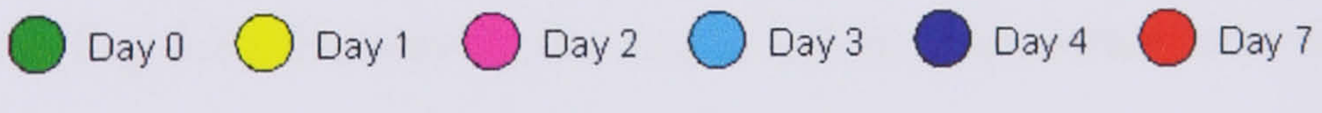

Figure 5.5: Representative Bode and Complex Plane of SVK14 Keratinocytes on Washed (Left) and Unwashed PPy films (Right).

(A) PPy/Derm and (B) PPy/Cl digit-Coated PC Coverslips (4×10^5 Cells Seeded).

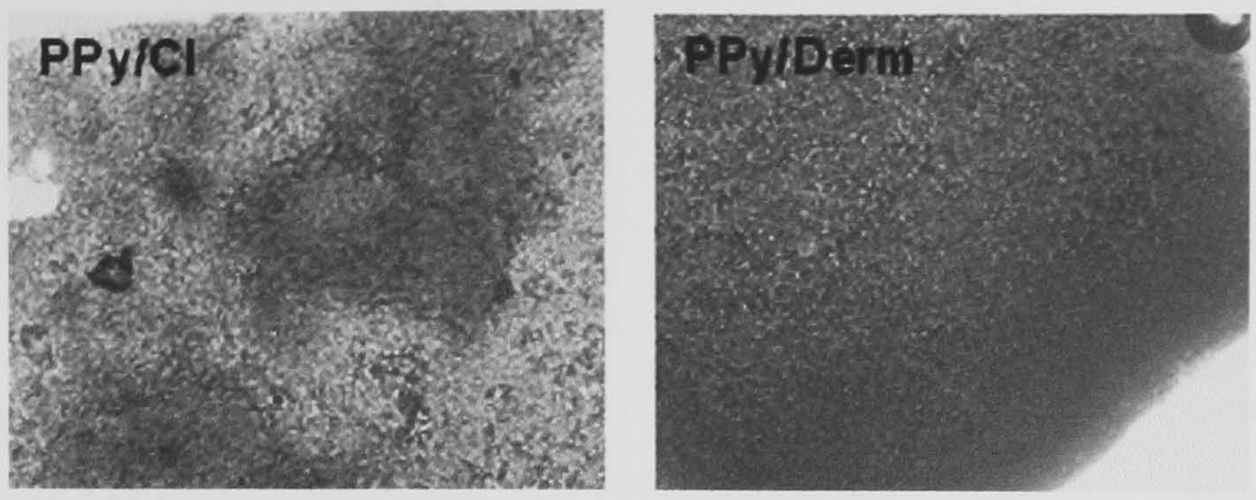

Figure 5.6: Micrographs of SVK14 Keratinocytes on unwashed PPy/Cl and PPy/Derm-Digit Electrodes after 7 days. *Viable cells are seen on unwashedPPy coated electrodes probably due to the fact that a continuous supply of cells is available from the surrounding polycarbonate coverslip which is non-toxic.*

For these reasons, changes in impedance spectra associated with the presence of cells were also seen on unwashed films. Impedance increases between day 0 and day 1 on unwashed films were large compared to washed films. Also, the complex plane representations show that high frequency semi-circles are more fully developed and of a larger diameter than their unwashed counterparts at various days especially for PPy/Cl. Single frequency analysis of impedance changes normalised to day 0 is presented in Section 5.3.

5.2.5 Effect of Lysis Buffer, Trypsin and Paraformaldehyde

The impedance spectra of SVK14s on PPy/Derm before and after treatment with cell lysis buffer show the reduction in overall impedance and disappearance of the high frequency complex plane semicircle (Fig 5.7). This further demonstrates that the presence of cells is responsible for increases in impedance. A similar pattern was obtained after treatment with trypsin, an enzyme regularly used in cell culture to release cell monolayers (Fig 5.8). However, the reduction in impedance was not as significant as that observed with the lysis buffer treatment; some cells were still found on the PPy/Derm substrate (Fig 5.9). This is because trypsin treatment was only carried-out at room temperature whereas it operates optimally at 37°C with substrate physical tapping often required for cell release not applied here. For cells treated with fixative (4% w/v paraformaldehyde), Bode and complex plots remain similar to those observed for live cells (Fig 5.10) confirming that physical obstruction by the cell produces the impedance signal seen.

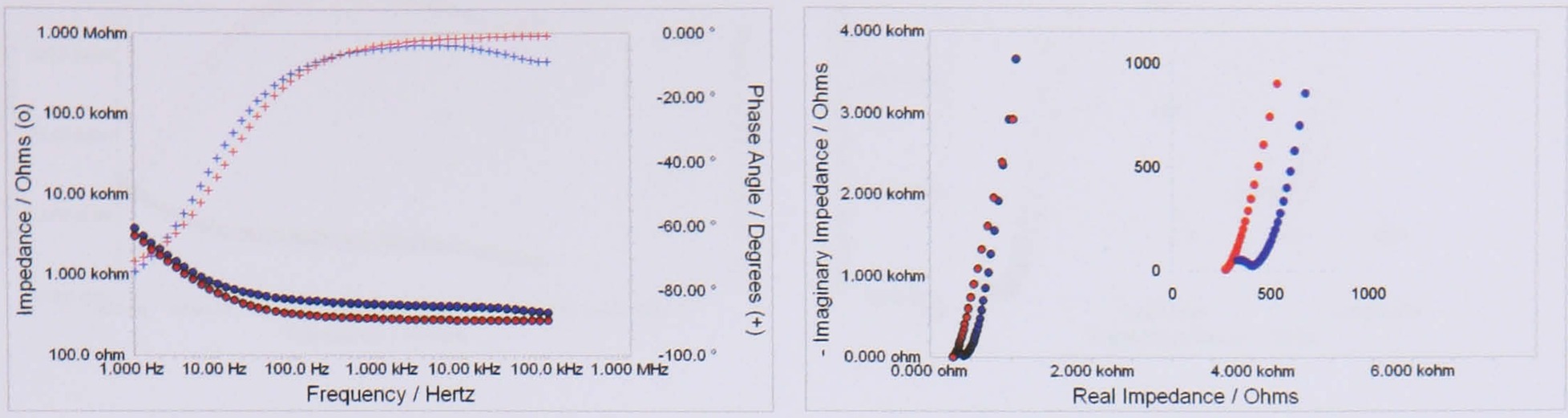

Figure 5.7: Representative Bode and Complex Plane Plots of Impedance Changes for SVK14 Keratinocytes on PPy/Derm Before (Blue) and After (Red) Treatment with Cell Lysis Buffer for 5 mins. *After treatment with cell lysis buffer, the semi-circle present at low frequencies in the complex plane (blue) dissapears (red).*

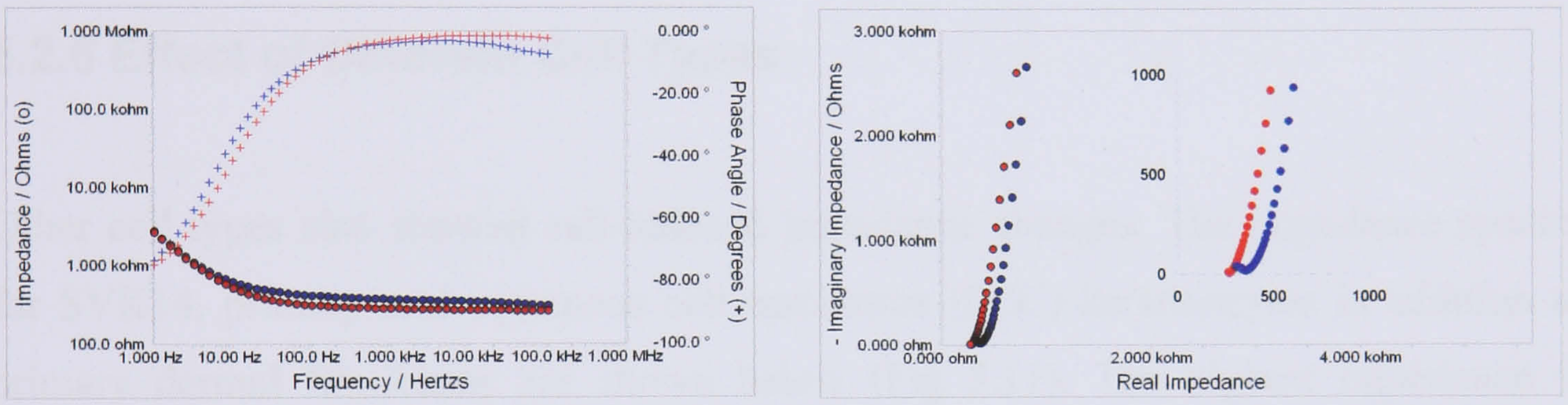

Figure 5.8: Representative Bode and Complex Plane Plots of Impedance Changes for SVK14 Keratinocytes on PPy/Derm Before (Blue) and After (Red) Treatment with 0.05% Trypsin for *ca* 24 mins. *After treatment with cell lysis buffer, the semi-circle present at low frequencies in the complex plane (blue) dissapears (red).*

Figure 5.9: Micrographs of SVK14 Keratinocytes Remaining on PPy/Derm after Treatment with 0.05% Trypsin for *ca* 24 mins.

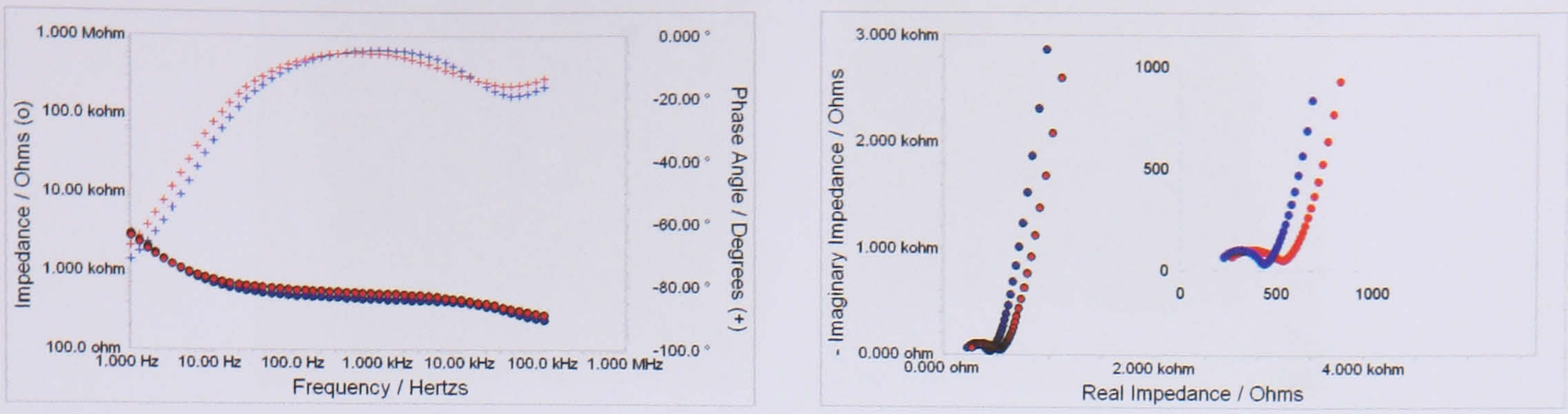

Figure 5.10: Representative Bode and Complex Plane Plots of Impedance Changes for SVK14 Keratinocytes on PPy/Derm Before (Blue) and After (Red) Treatment with 4% Paraformaldehyde for 10 mins. *After treatment with paraformaldehyde, the semi-circle present at low frequencies in the complex plane (blue) remians (red).*

5.2.6 Effect of Different Cell Types

Other cell types also showed cell-induced impedance changes. The impedance spectra for SVK14, primary and squamous cell carcinoma (SCC) keratinocytes in addition to primary dermal fibroblasts are shown below (Fig 5.11). The highest impedance is recorded for the SVK14 cell line with primary keratinocytes also high. The primary fibroblasts caused the smallest impedance rise since these cells form fewer cell-cell junctions than keratinocytes, thus causing less of an obstruction to current flow. Microscopy showed viable cells (Fig 5.12). The fact that SCC keratinocytes, despite forming confluent layers over the electrode as in the SVK14 case, also exhibit relatively low impedance suggests they also form less cell-cell adhesion junctions.

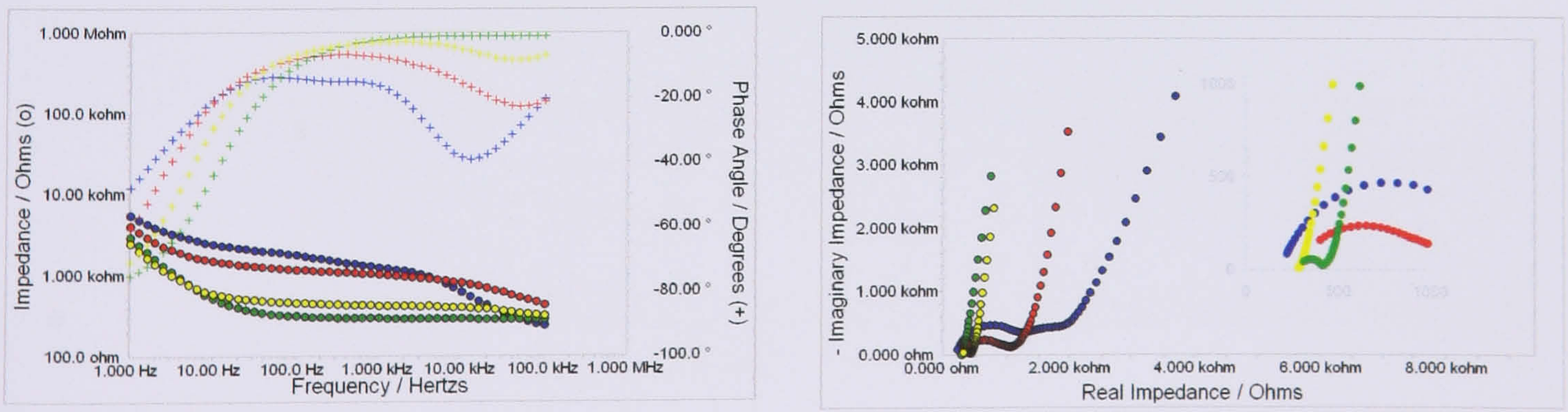

Figure 5.11: Representative Bode and Complex Plane Plots of Impedance for SVK14 (Blue), Primary (Red), SCC (Yellow) Keratinocytes and Primary Fibroblasts (Green) on PPy/Derm (after 24 hrs from 4×10^5 Cells Initially Seeded).

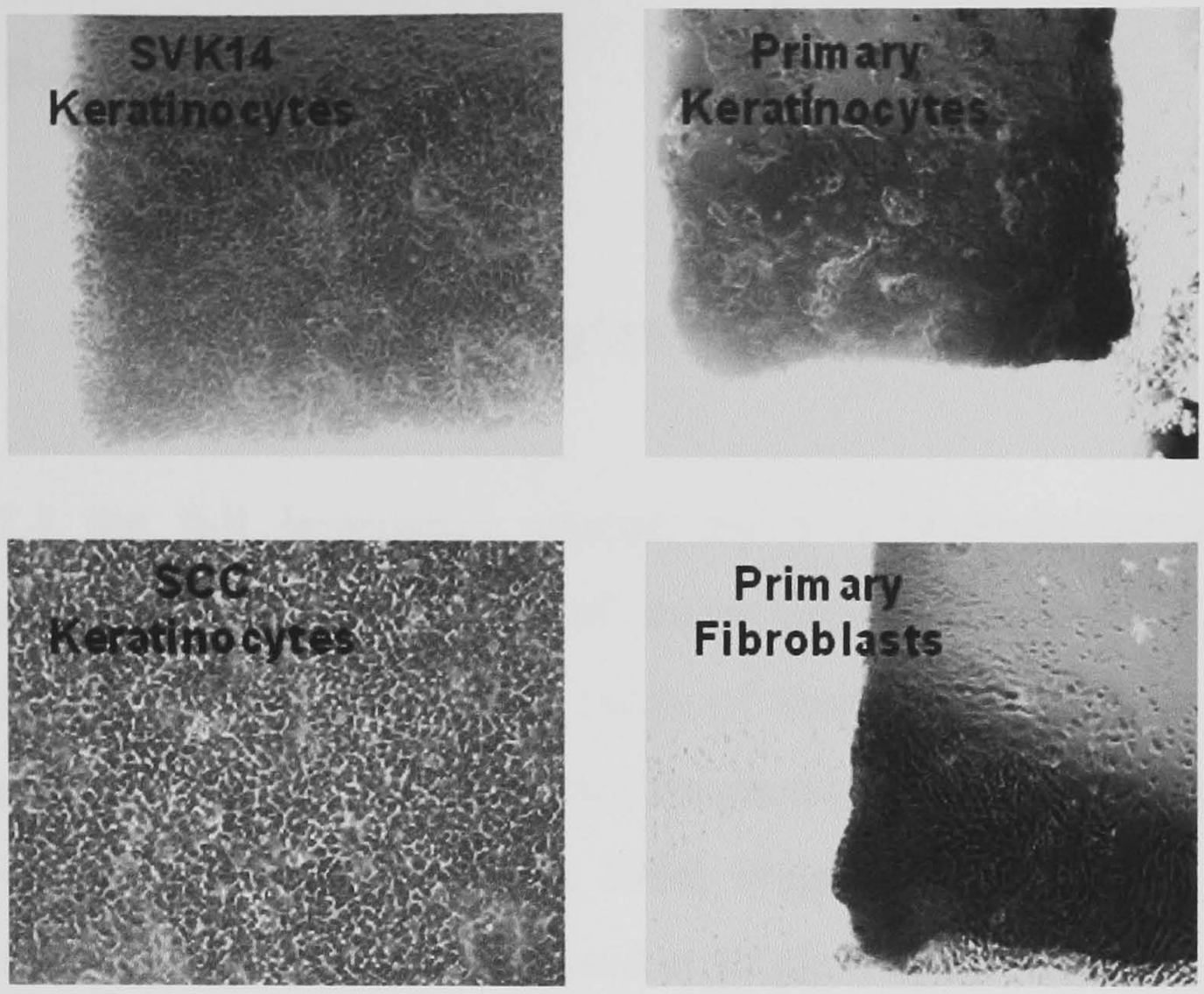

Figure 5.12: Micrographs of Different Cells on PPy/Derm

(after 24 hrs from 4×10^5 Cells Initially Seeded). *SVK14, primary and SCC keratinocytes have similar morphologies characterised by flat polygonal shapes whereas primary fibroblasts are thin and spindle like.*

5.3 Single Frequency Analysis

5.3.1 Growth of SVK14 Keratinocytes in Culture

In section 5.2.1 the full impedance spectra for SVK14 keratinocytes on various substrates were presented. Observation of these spectra (Fig 5.1-5.2) showed that impedance changes occurred over a wide range of frequencies. It has been shown that for cells cultured on gold electrodes, certain frequencies may be particularly suited to follow these changes (Giaever and Keese, 1986; Wegener *et al.*, 2000). Therefore, the impedance spectra for SVK14s were analysed at single frequencies. This included 4, 40 and 400 Hz (data not shown) where impedance changes normalised against day 0 readings were small in the case of the gold substrates and relatively large for PPy/Derm. However, these changes at low frequencies are not discussed further, although the better resolution for PPy was noted. Three dielectric relaxation mechanisms (Table 5.1) were established by Schwan in 1957 upon examination of the electrical properties of biological tissues (Grimnes and Martinsen, 2000). The frequencies discussed here are at the high and low end of the α- and β-dispersion respectfully.

Dispersion Type	Characteristic Frequency	Mechanism
α	mHz-kHz	Counterion effects (perpendicular or lateral) near the membrane surfaces, active cell membrane effects and gated channels, intracellular structures (*e.g.* sarcotubular system), ionic diffusion, dielectric losses (at lower frequencies the lower the conductivity)
β	0.1-100 MHz	Maxwell-Wagner effects, passive cell membrane capacitance, intracellular organelle membranes, protein molecule response
γ	0.1-100 GHz	Dipolar mechanisms in polar media such as water, salts and proteins

Table 5.1: Dielectric Dispersions of Biological Tissue

(Taken from Grimnes and Martinsen, 2000)

Large changes in normalised impedance were observed for SVK14s on all substrates at 4 and 40 kHz (Fig 5.13-5.16). The changes in normalised phase angle, real and imaginary impedances are also shown. Differences were seen according to the initial cell seeding density and the parameter considered. Wegener *et al.* (2000) studied epithelial MDCK-II (Madin-Darby canine kidney) cells on gold using impedance and concluded that capacitance measurements at 40 kHz were particularly suited to follow cell attachment and spreading. The phase angle and imaginary impedance parameters are particularly sensitive to capacitive components and were seen to have the largest normalised increases with imaginary impedance for SVK14s on gold at 40 kHz recording the highest (Fig 5.14 D). Imaginary impedance at 40 kHz showed that a peak was reached for cells seeded at the highest density on gold at day 3 and on PPy/Derm at day 1 followed by a decline. A similar pattern, of initial increases followed by decline, had also been previously reported for the impedance analysis of MDCK-II cells on gold studied over 6 days (Wegener *et al.*, 1996). This could be related to the dynamics of cell-cell junction formation, plasma membrane permeability and intracellular space.

In general, impedance changes were at their maximum for the highest cell seeding and smallest for the lowest cell seeding. Minimal changes were seen between the lowest cell seeding and controls until day 7 on gold, but there was a difference from day 1 on PPy/Derm. This was especially so for phase angle or imaginary impedance parameters at 4 kHz (Fig 5.17). This shows that the polypyrrole modification enables the detection of cell-induced changes for lower cell numbers. However, this increased sensitivity for the polypyrrole modification and better cell viability results in AlamarBlue™ assays (Chapter 4) seems at odds with the fact that the highest cell-induced impedance changes were recorded on the gold substrates. It is possible that higher cell turnover may occur on gold compared to PPy/Derm, resulting in higher amounts of plasma membrane remnants, in turn explaining the larger increases in impedance changes. To test this hypothesis, single frequency impedance changes in unwashed PPy/Cl and PPy/Derm known to show cell toxicity were compared to those for washed films (section 5.3.3).

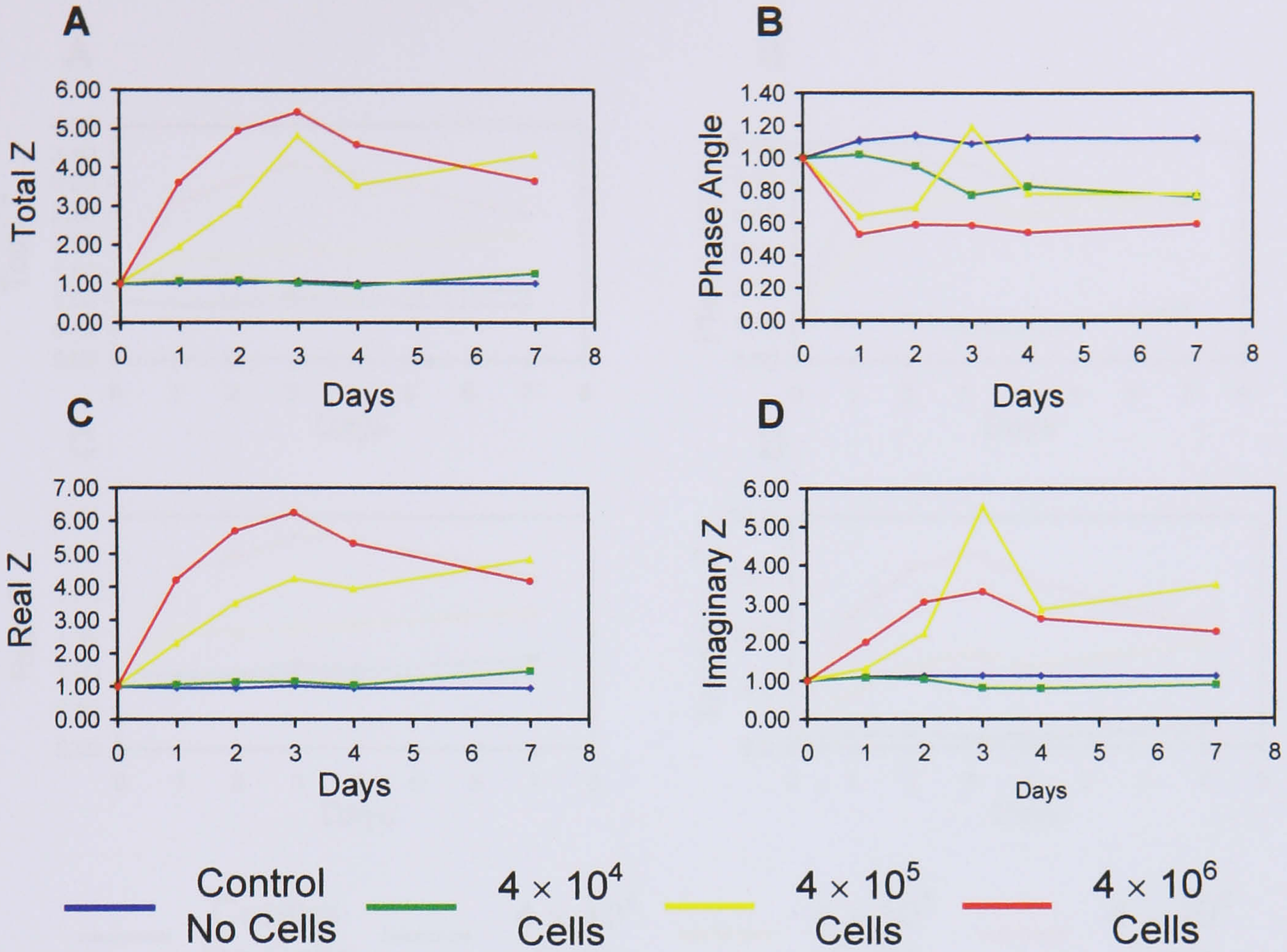

Figure 5.13: Normalised (A) Total Impedance, (B) Phase Angle, (C) Real Impedance and (D) Imaginary Impedance *vs.* Time for SVK14 Keratinocytes on Gold digit-Coated PC Coverslips at 4 kHz (n = 3).

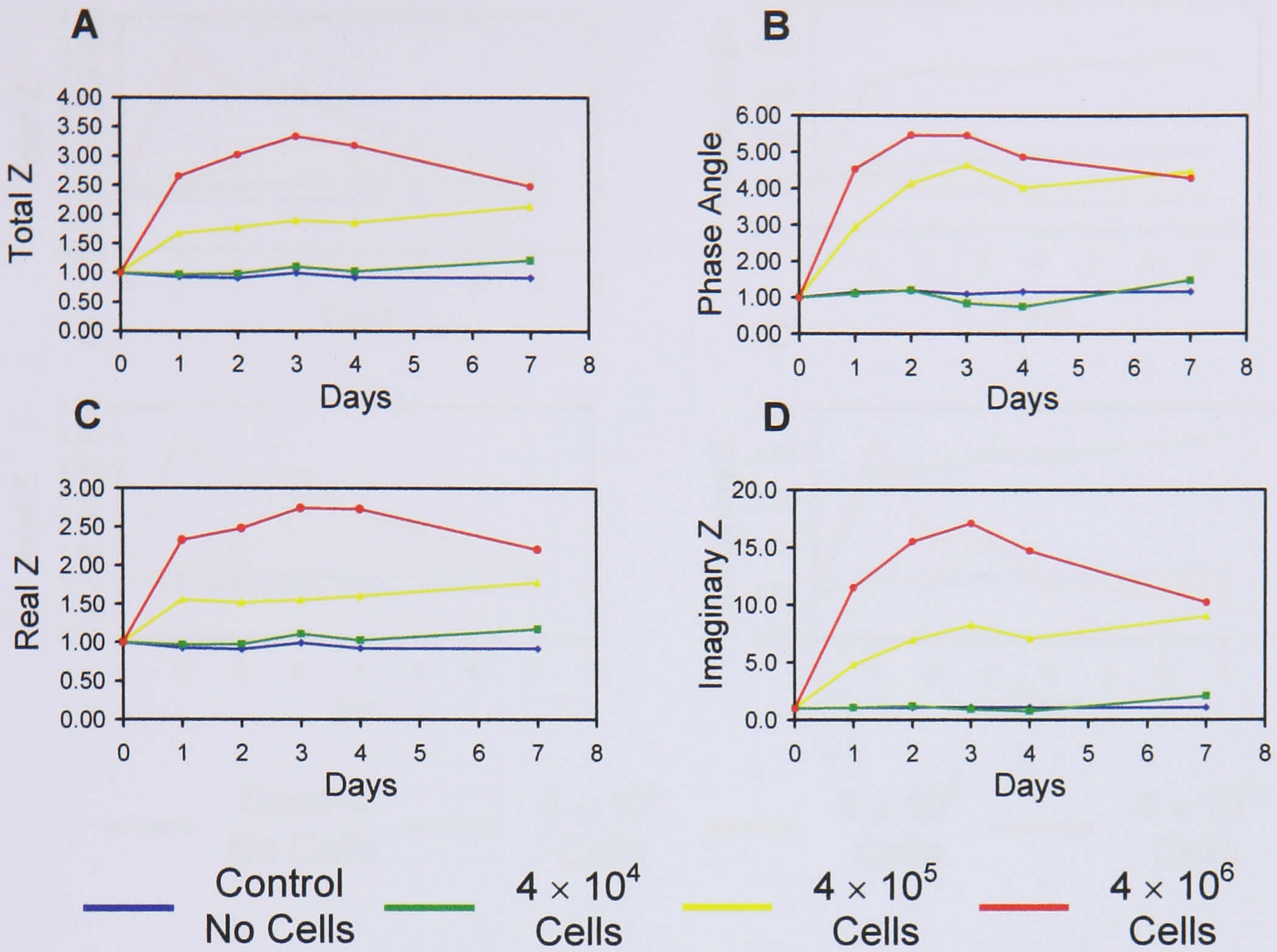

Figure 5.14: Normalised (A) Total Impedance, (B) Phase Angle, (C) Real Impedance and (D) Imaginary Impedance *vs.* Time for SVK14 Keratinocytes on Gold digit-Coated PC Coverslips at 40 kHz (n = 3).

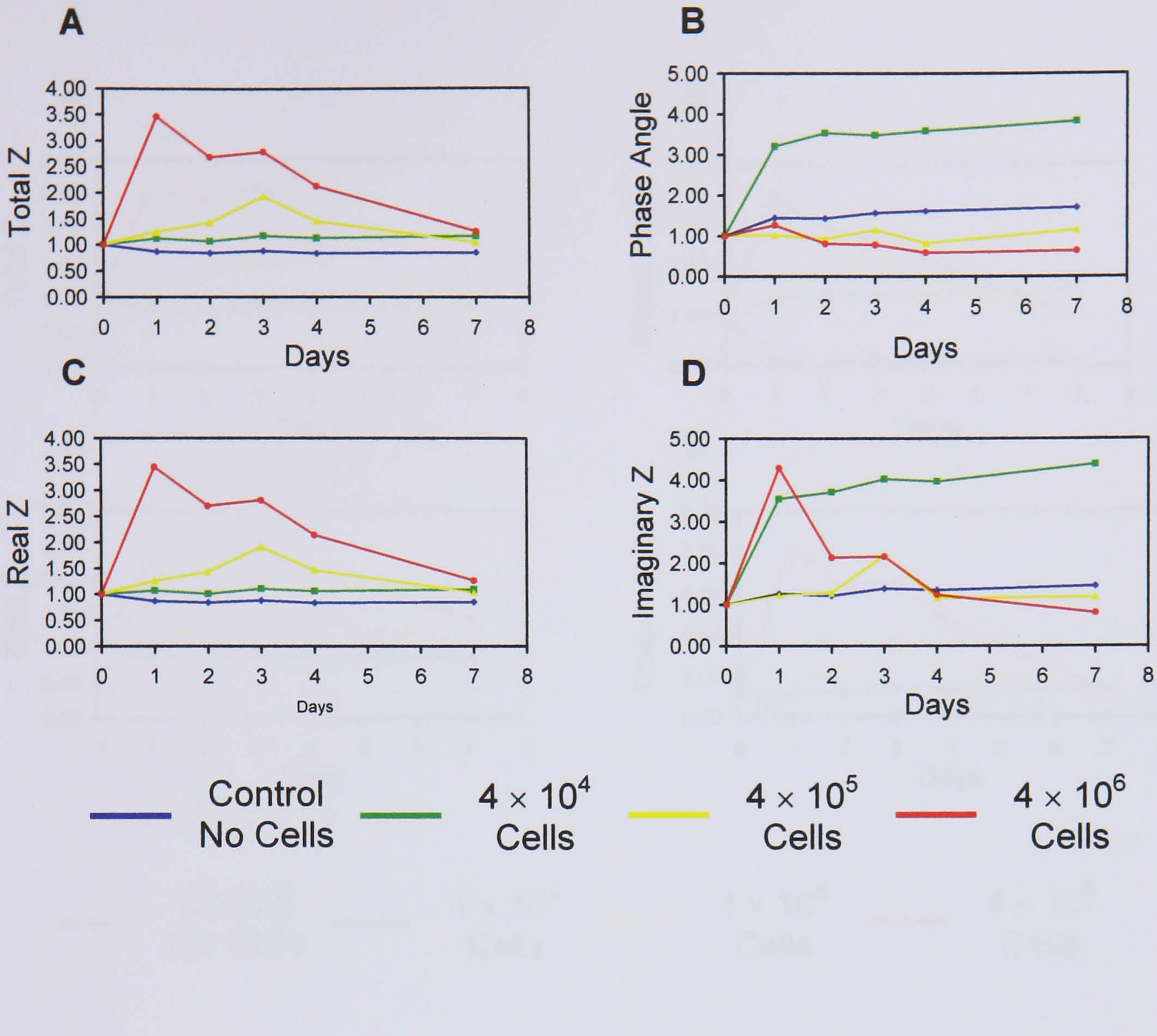

Figure5.15: Normalised (A) Total Impedance, (B) Phase Angle, (C) Real Impedance and (D) Imaginary Impedance *vs.* Time for SVK14 Keratinocytes on Washed PPy/Derm digit-Coated PC Coverslips at 4 kHz (n = 3).

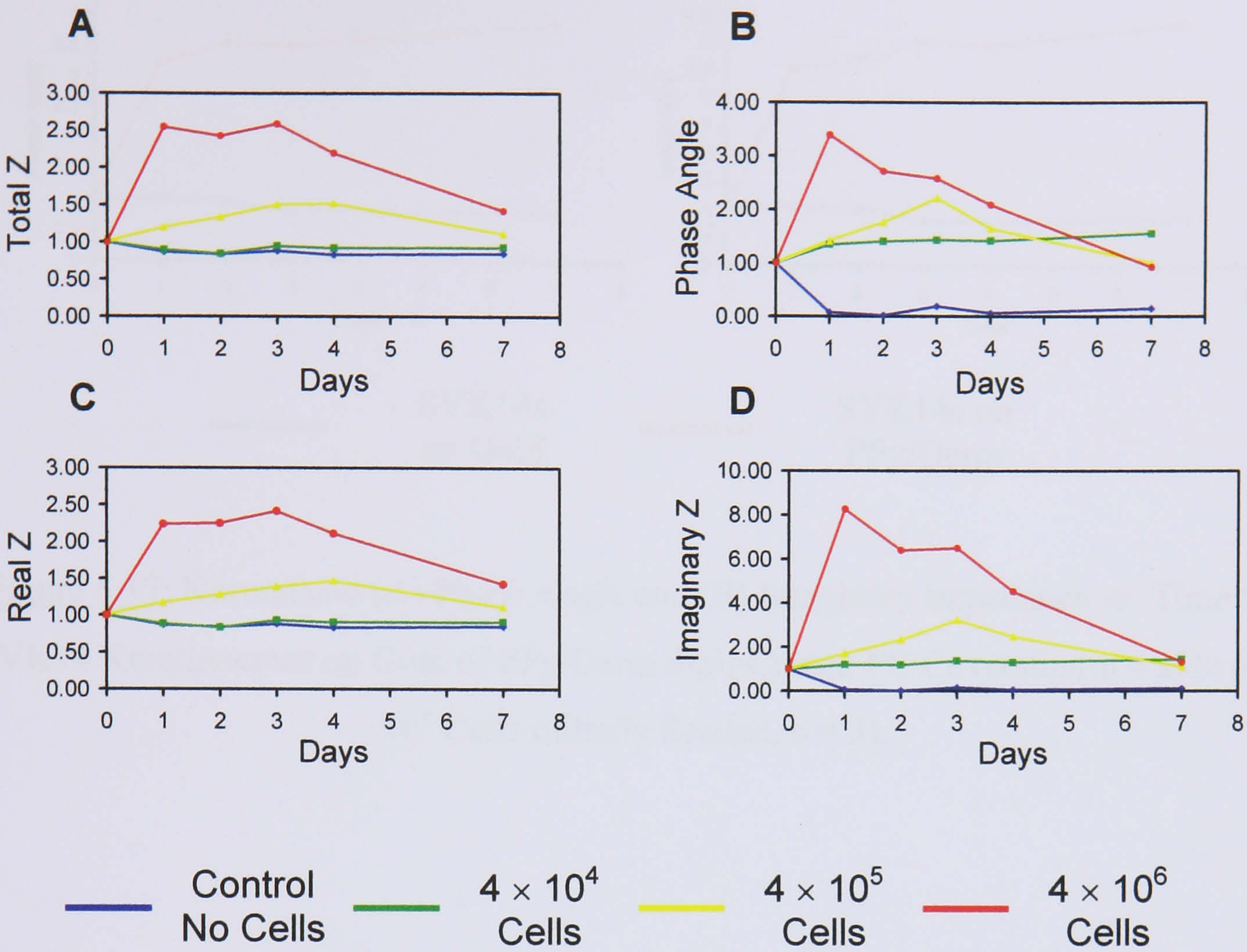

Figure 5.16: Normalised (A) Total Impedance, (B) Phase Angle, (C) Real Impedance and (D) Imaginary Impedance *vs.* Time for SVK14 Keratinocytes on Washed PPy/Derm digit-Coated PC Coverslips at 40 kHz (n = 3).

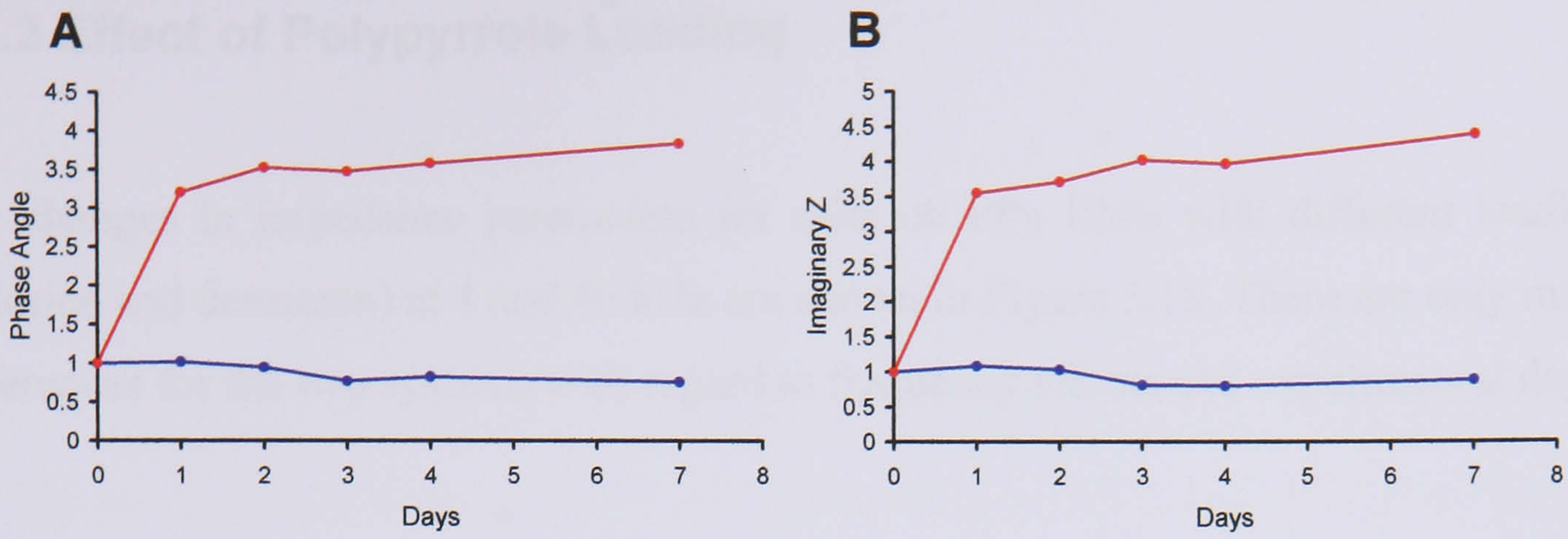

Figure 5.17: Normalised (A) Phase Angle and (B) Imaginary Impedance *vs.* Time for SVK14 Keratinocytes on Gold or PPy/Derm digit-Coated PC Coverslips at 4 kHz (4×10^4 Cells Initially Seeded, n = 3).

5.3.2 Effect of Polypyrrole Loading

The changes in impedance parameters for cells on PPy films with different loadings (chloride and dermatan) at 4 and 40 kHz are shown in Figure 5.18. There are only minor differences for the two systems with regard to frequency effects and experimental day.

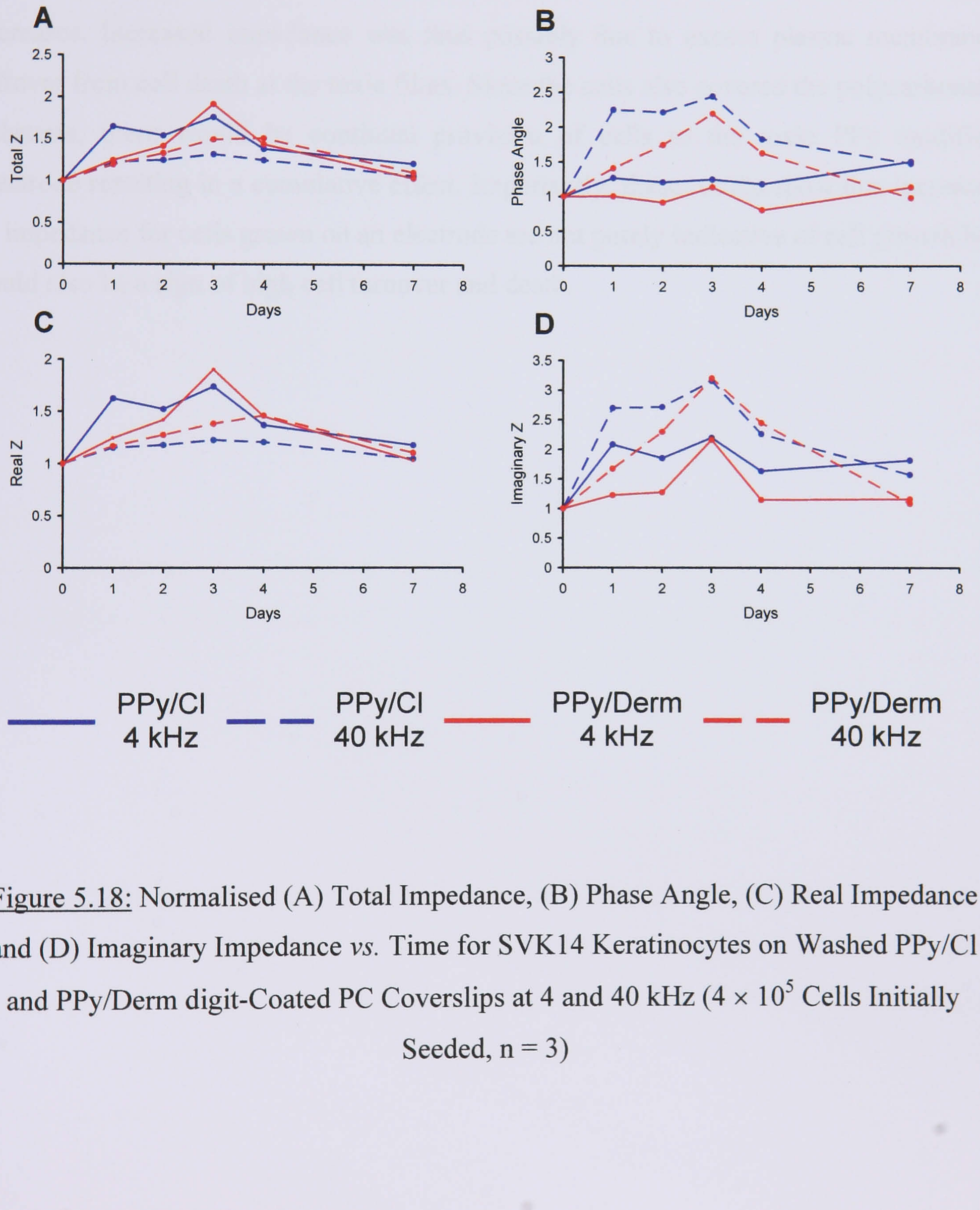

Figure 5.18: Normalised (A) Total Impedance, (B) Phase Angle, (C) Real Impedance and (D) Imaginary Impedance *vs.* Time for SVK14 Keratinocytes on Washed PPy/Cl and PPy/Derm digit-Coated PC Coverslips at 4 and 40 kHz (4×10^5 Cells Initially Seeded, n = 3)

5.3.3 Effect of wash

Normalised cell-induced impedance changes for washed and unwashed PPy films were found to be markedly different at 4 and 40 kHz (Fig 5.19-5.20). SVK14 keratinocytes on unwashed films were found to produce substantially higher changes for all the parameters considered. This was especially high for imaginary impedance measured at 40 kHz in the case of cells on PPy/Derm. These changes are not explained by film re-hydration in the presence of culture media, as unwashed control films did not show such increases. Increased impedance was thus possibly due to excess plasma membranes leftover from cell death at the toxic films. Since the cells also covered the polycarbonate substrate, there would be continual provision of cells to the toxic PPy modified electrode resulting in a cumulative effect. Importantly, these results show that increases in impedance for cells grown on an electrode are not purely indicative of cell growth but could also be a sign of high cell turnover and death.

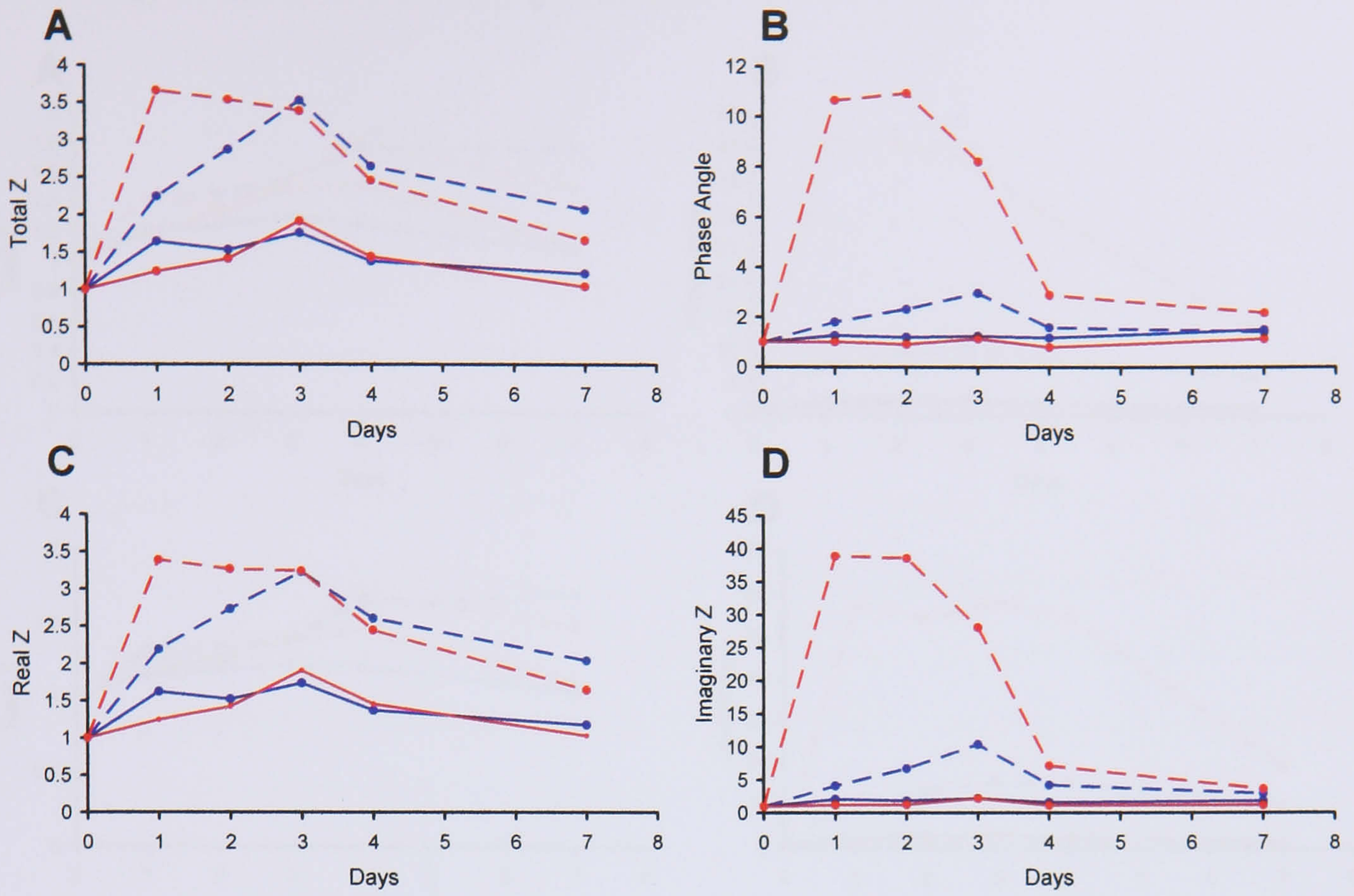

Figure 5.19: Normalised (A) Total Impedance, (B) Phase Angle, (C) Real Impedance and (D) Imaginary Impedance *vs.* Time for SVK14 Keratinocytes on Washed (W) and Unwashed (U) PPy/Cl and PPy/Derm digit-Coated PC Coverslips at 4 kHz (4×10^5 Cells Initially Seeded, n = 3).

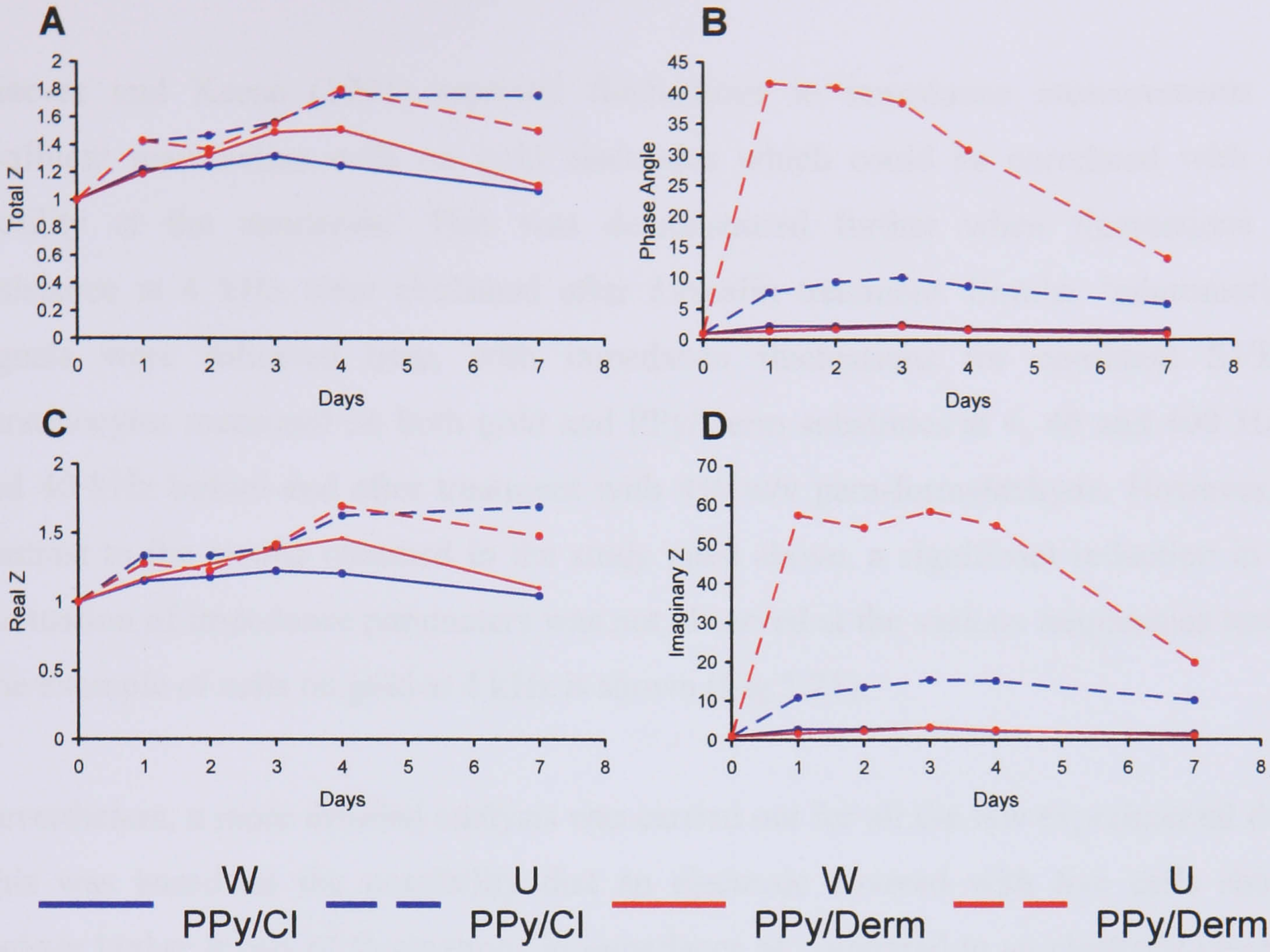

Figure 5.20: Normalised (A) Total Impedance, (B) Phase Angle, (C) Real Impedance and (D) Imaginary Impedance *vs.* Time for SVK14 Keratinocytes on Washed (W) and Unwashed (U) PPy/Cl and PPy/Derm digit-Coated PC Coverslips at 40 kHz (4×10^5 Cells Initially Seeded, n = 3).

5.3.4 Live and Fixed Cell Measurements

Giaever and Keese (1991) reported fluctuations in impedance measurements for confluent mammalian cells on gold electrodes which could be correlated with cell motility at the nanoscale. This was demonstrated further when fluctuations for resistance at 4 kHz were abolished after formalin treatment. Similar 'micromotion' signals were followed here, with impedance fluctuations for confluent SVK14 keratinocytes measured on both gold and PPy/Derm substrates at 4, 40 and 400 Hz, 4 and 40 kHz before and after treatment with 4% w/v para-formaldehyde. However, in contrast to the results obtained in the study cited above, a significant reduction in the fluctuation of impedance parameters was not observed at the various frequencies tested. The example of cells on gold at 4 kHz is shown (Fig 5.21).

Nevertheless, a more detailed analysis was carried out for all the raw experimental data. This was based on the possibility that an electrode covered with live cells should register higher levels of fluctuations in impedance as compared to an electrode covered by fixed cells. The impedance was measured at 6 s intervals giving 60 data points over 6 mins; the standard error of the mean of these points was used as an indicator of fluctuation, *i.e.* the greater the standard error, the greater the fluctuations. In the majority of cases, the expected trend of high errors in live cells compared with fixed cells was not observed to be statistically significant (Fig 5.22-5.23). Large standard errors overall were found in the case of SVK14s on Gold at 4 Hz compared to those on PPy/Derm due to the higher impedances recorded at lower frequencies for the former electrode. The lack of evidence for cell micromotions could be due to the comparatively large working electrodes used in this study (10 mm^2 *vs.* 1 mm^2 for Giaever and Keese, 1991). Also, the previous study considered a fibroblast cell line which may have enhanced micromotion capacity compared to the SVK14 keratinocytes studied here.

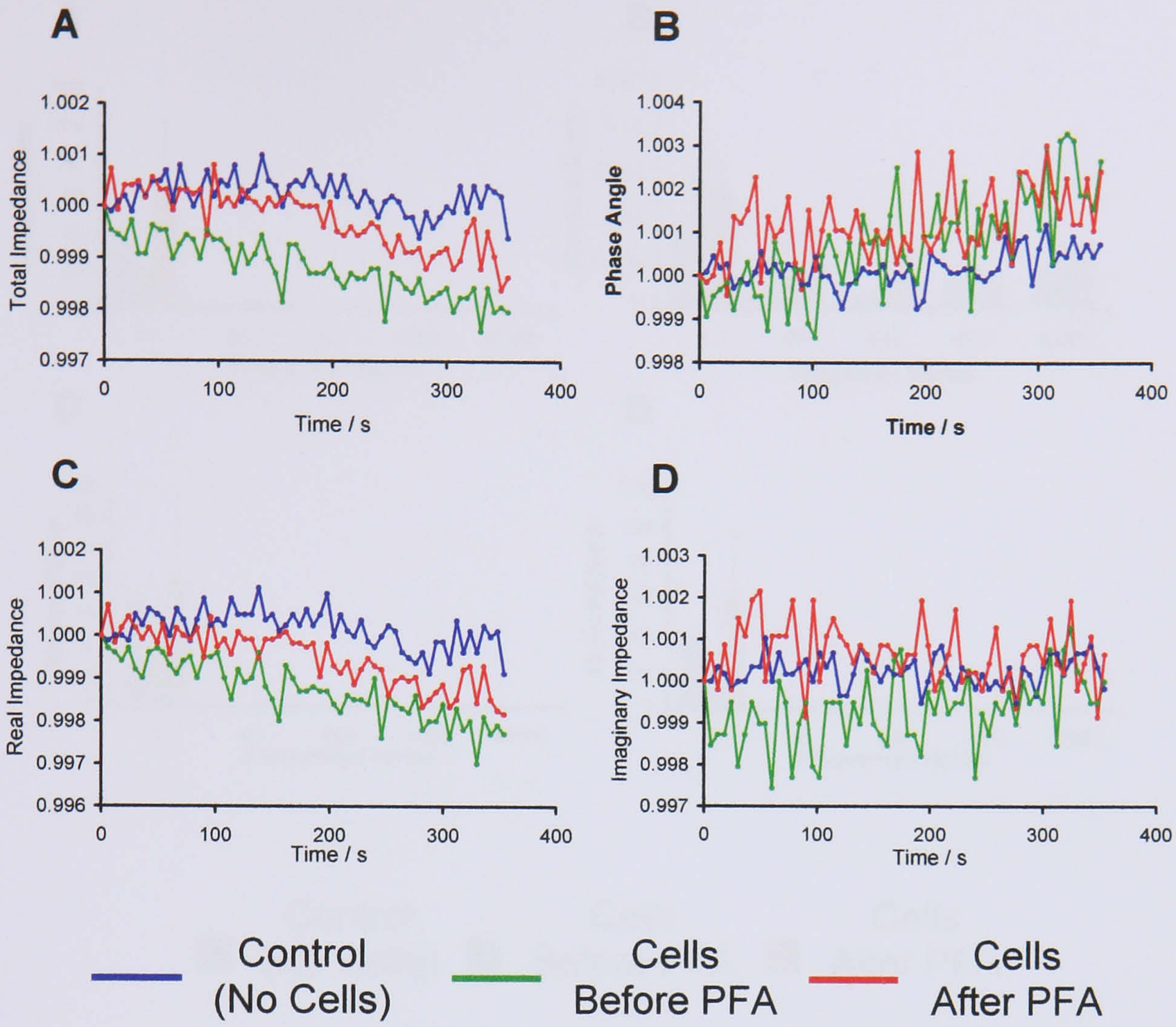

Figure 5.21: Normalised (A) Total Impedance, (B) Phase Angle, (C) Real Impedance and (D) Imaginary Impedance fluctuations *vs.* Time for Bare, SVK14 Keratinocytes Before and After Treatment with 4% Para-Formaldehyde on Gold digit-Coated PC Coverslips at 4 kHz over 6 mins (After 24 Hrs of 4×10^5 Cells Initially Seeded, n = 3).

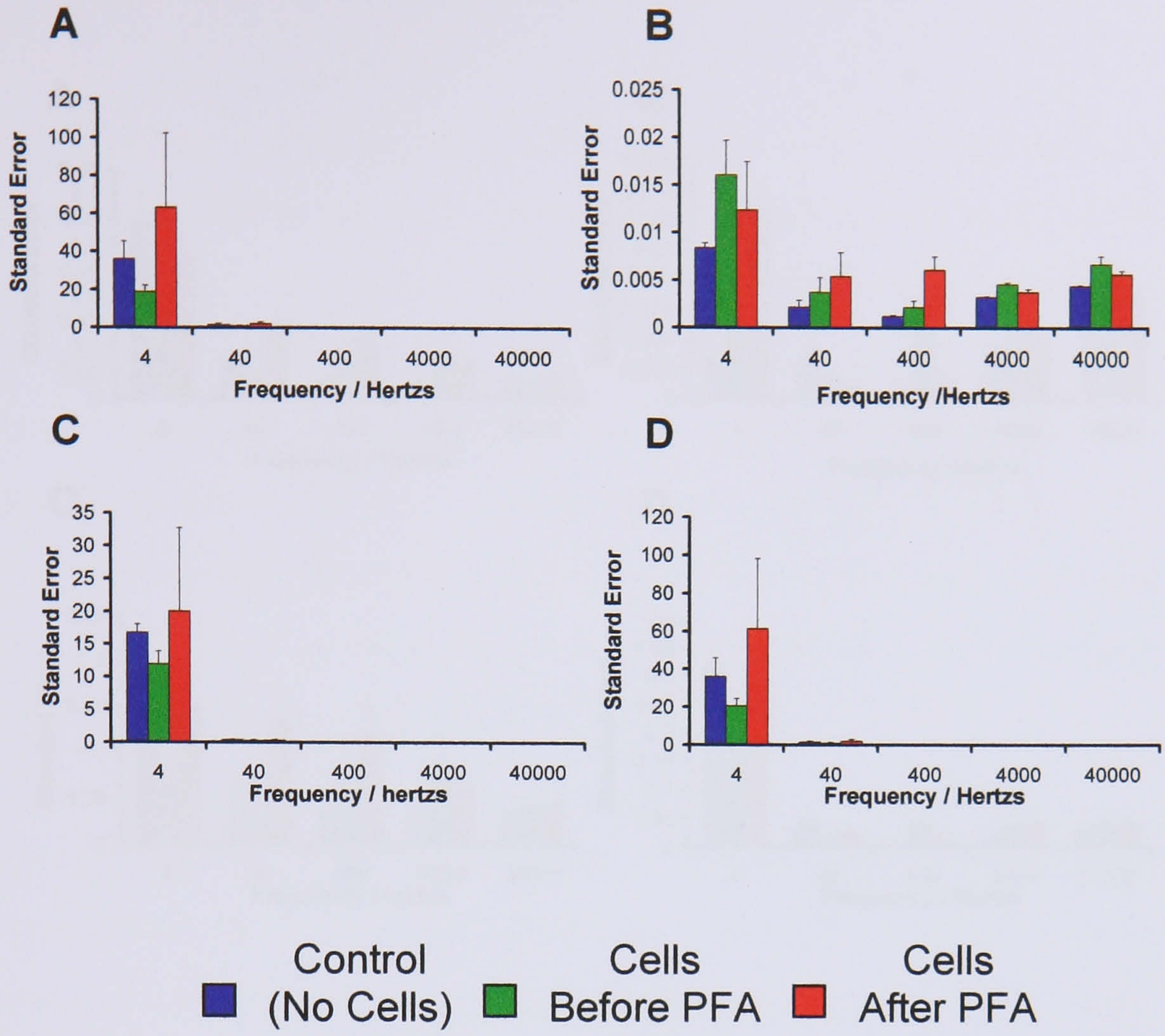

Figure 5.22: Standard Error (n = 60) for (A) Total Impedance, (B) Phase Angle, (C) Real Impedance and (D) Imaginary Impedance average fluctuations *vs.* Time for Bare, SVK14 Keratinocytes Before and After Treatment with 4% Para-Formaldehyde on Gold digit-Coated PC Coverslips.

(After 24 Hrs of 4×10^5 Cells Initially Seeded, n = 3).

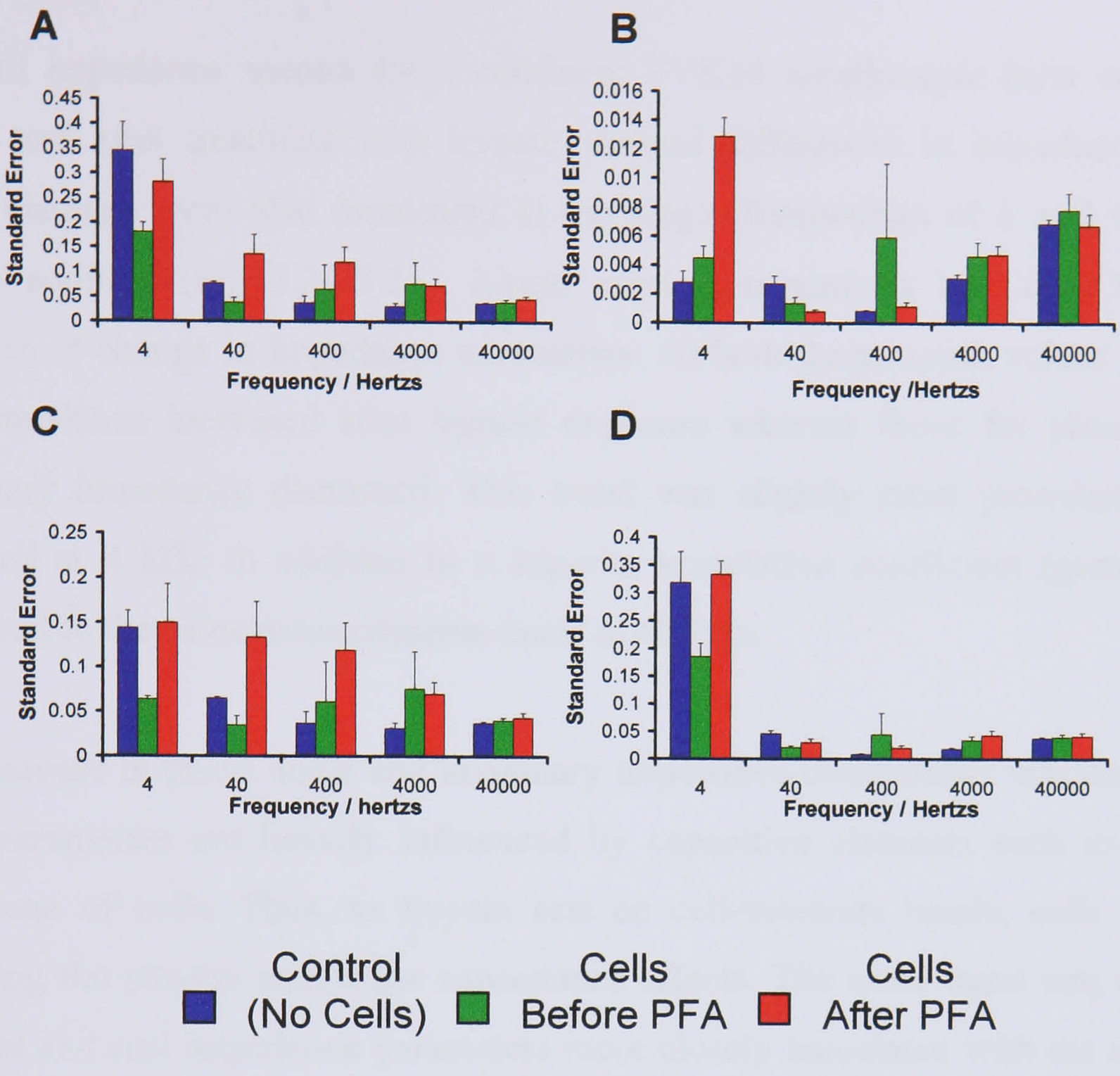

Figure 5.23: Standard Error (n = 60) for (A) Total Impedance, (B) Phase Angle, (C) Real Impedance and (D) Imaginary Impedance average fluctuations *vs.* Time for Bare, SVK14 Keratinocytes Before and After Treatment with 4% Para-Formaldehyde on PPy/Derm digit-Coated PC Coverslips.

(After 24 Hrs of 4×10^5 Cells Initially Seeded, n = 3).

5.3.5 Trypsinisation Measurements

The full impedance spectra for a confluent SVK14 keratinocyte layer on PPy/Derm before and after treatment with trypsin showed differences in impedance (Fig 5.8). These changes were also monitored at the single frequencies of 4 and 40 kHz after trypsin addition (Fig 5.24-5.25). Linear regression analysis was used to show the direction of change in impedance parameters. At both frequencies, values for total and real impedance increased after trypsin exposure whereas those for phase angle and imaginary impedance decreased. This trend was slightly more pronounced for data collected at 4 kHz in addition to a superior correlation coefficient (goodness of fit) compared to the same measurements made at 40 kHz.

The decrease in phase angle and imaginary impedance components was expected since these parameters are heavily influenced by capacitive elements such as the plasma membrane of cells. Thus, as trypsin acts on cell-substrate bonds, cells are released removing the plasma membrane capacitance effects. The same trend was expected for the total and real impedance parameters more closely associated with the restriction of intercellular current (*i.e.* the presence of cell-cell junctions). However, this was not the case at either 4 or 40 kHz although there is an initial decrease for around 3 mins in the latter. This could possibly be due to the fact that measurements were carried out at room temperature and there could have been a background increase in impedance due to the reduction in electrolyte temperature masking the trypsin effect (Barron and Aston, 2005). Indeed, temperature changes for culture media from the 37°C incubator recorded a drop to 32.47°C (±0.18, n = 3) after 1 min, 25.23°C (±0.33, n = 3) after 30 mins and 24.37°C (±0.20, n = 3) after 2 hours showing a significant drop over the time-course of the experiment. In the next section, study of the adhesion of cells (the reverse scenario) is presented using 40 kHz over a longer time-period at a constant temperature of 37°C.

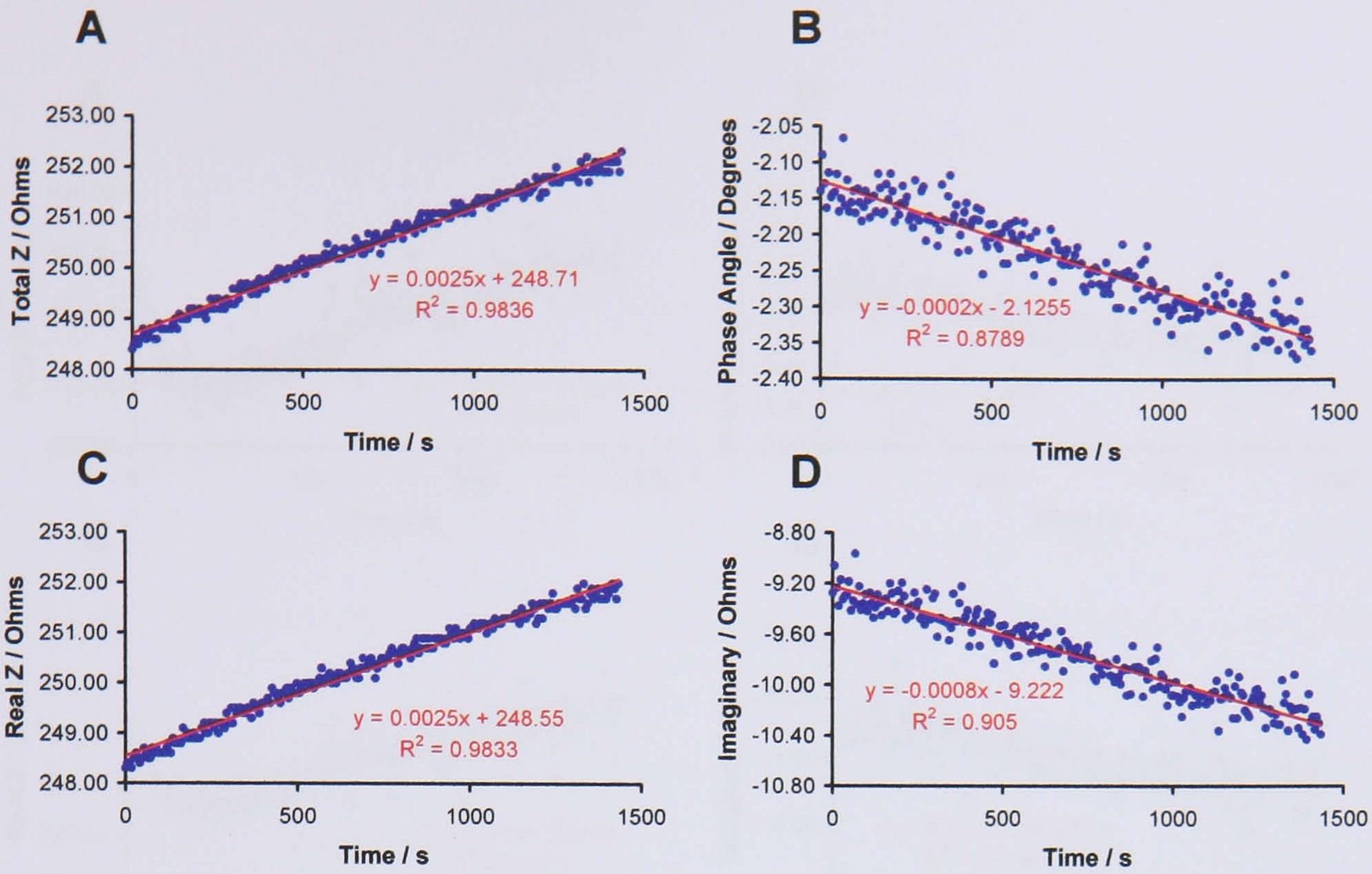

Figure 5.24: (A) Total Impedance, (B) Phase Angle, (C) Real Impedance and (D) Imaginary Impedance (Blue) and Linear Regression Analysis (Red) *vs.* Time for SVK14 Keratinocytes on PPy/Derm during Treatment with 0.05% Trypsin at 4 kHz. (After 24 Hrs of 4×10^5 Cells Initially Seeded, n = 3).

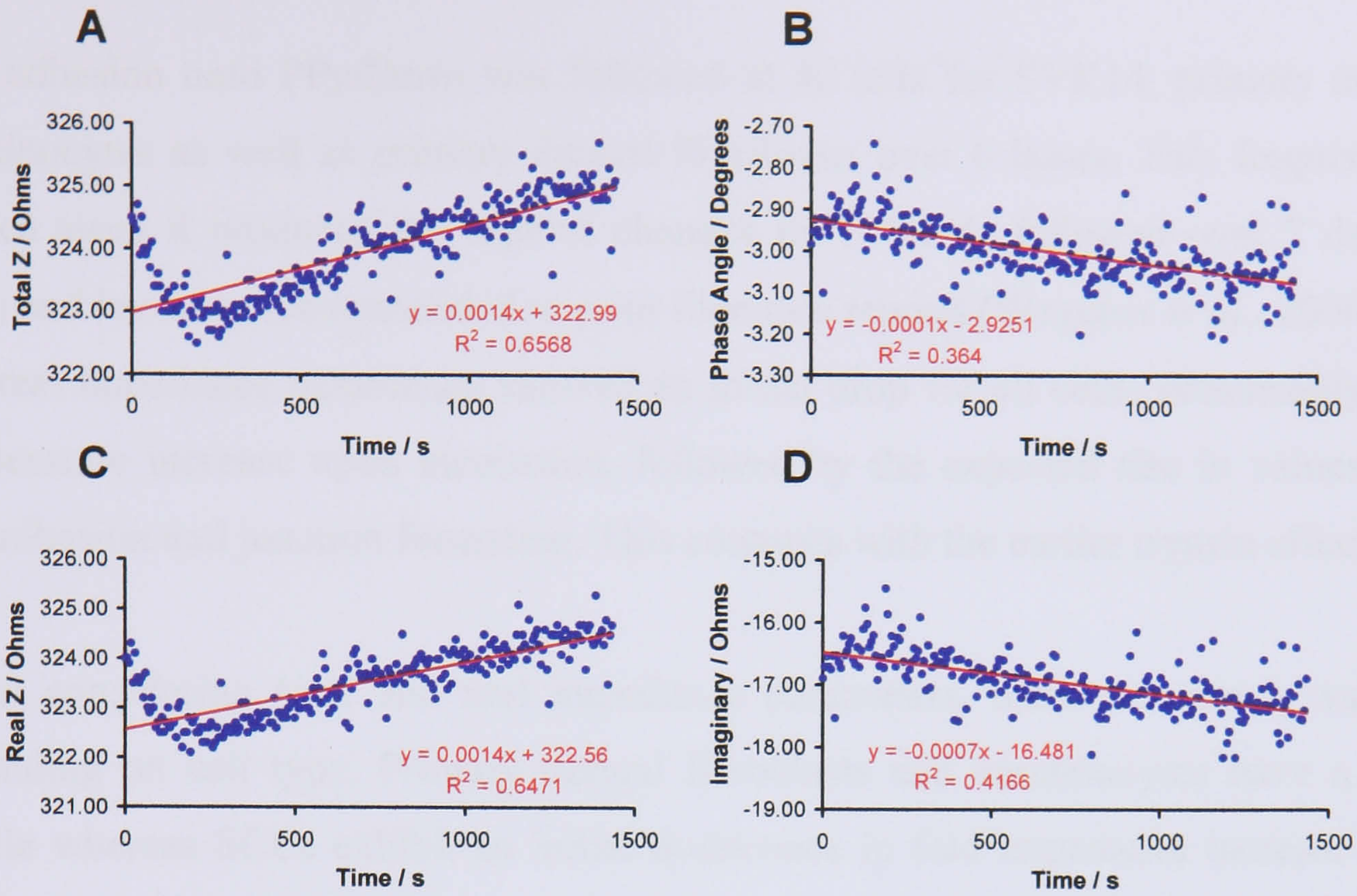

Figure 5.25: (A) Total Impedance, (B) Phase Angle, (C) Real Impedance and (D) Imaginary Impedance (Blue) and Linear Regression Analysis (Red) *vs.* Time for SVK14 Keratinocytes on PPy/Derm during Treatment with 0.05% Trypsin at 40 kHz.

(After 24 Hrs of 4×10^5 Cells Initially Seeded, n = 3).

5.3.6 Different Cell Type Measurements

Cell adhesion onto PPy/Derm was followed at 40 kHz for SVK14, primary and SCC keratinocytes as well as primary dermal fibroblasts over 6 hours. This frequency was chosen since it produced the highest changes for SVK14s followed over 7 days (Fig 5.16) and has been recommended in prior literature reports (Wegener *et al.*, 2000). Total and real impedance parameters showed an initial drop for all cells, presumably due to temperature increase upon incubation, followed by the expected rise in values due to cell adhesion and junction formation. This contrasts with the earlier trypsin effect.

When considering total and real impedance parameters, there are clearly variations depending on cell type. Primary dermal fibroblasts and keratinocytes have a similar profile whereas SCCs exhibit an initial dominance in fold impedance increase but are overtaken by SVK14s *ca* 5 hours into the experiment. Phase angle and imaginary impedance parameters, associated with the presence of cell membranes, showed the most interesting changes. Here, the SVK14 and primary keratinocytes shared a similar profile with primary fibroblast showing a slight increase over them. However, there was a large difference between the fold increase in phase angle and imaginary impedance for SCC keratinocytes compared to all other cells. This shows that these cells proliferated the fastest, a key characteristic of cancer cells.

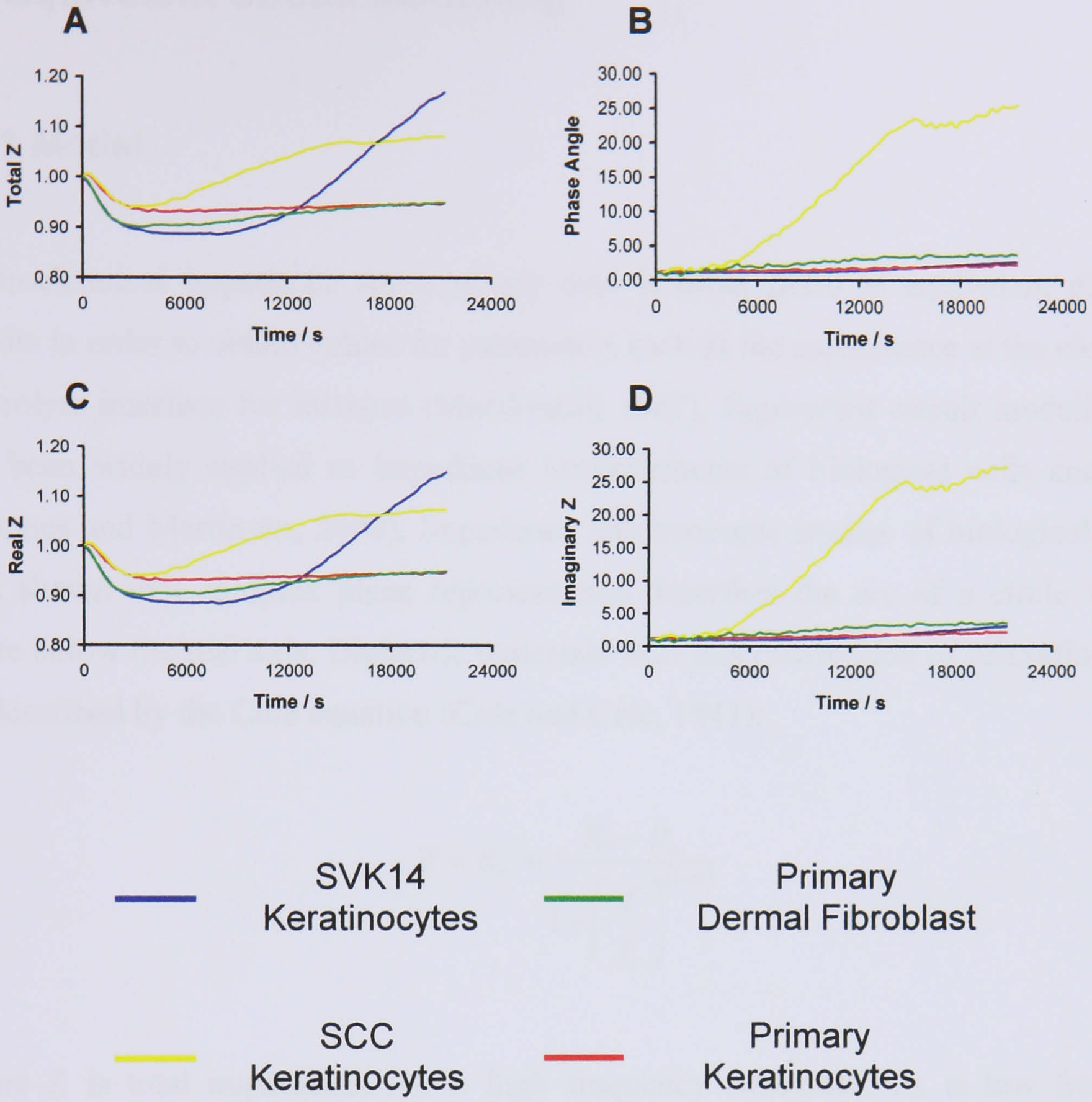

Figure 5.26: Normalised (A) Total Impedance, (B) Phase Angle, (C) Real Impedance and (D) Imaginary Impedance *vs.* Time for Different Cells on PPy/Derm digit-Coated PC Coverslips at 40 kHz over 6 hrs (4×10^5 Cells Initially Seeded).

5.4 Equivalent Circuit Modelling

5.4.1 Model

Electrochemical impedance spectroscopy data is often fitted to equivalent electrical circuits in order to obtain values for parameters such as the capacitance at the electrode-electrolyte interface for instance (Macdonald, 1987). Equivalent circuit modelling has also been widely applied to impedance measurements of biological cells and tissue (Grimnes and Martinsen, 2000). Impedance spectroscopic studies of biological tissues have shown that complex plane representation describes the arc of a circle with its centre below the real axis. Dielectric materials with this distribution of relaxation times are described by the Cole equation (Cole and Cole, 1941):

$$Z = R_\infty + \frac{R_0 - R_\infty}{1 + \left(\frac{if}{f_c}\right)^{(1-\alpha)}}$$

Where Z is total impedance, R_∞ is high frequency resistance, R_0 is low frequency resistance, f is frequency and f_c is the characteristic frequency at the centre of the dispersion. α is a constant that increases with tissue inhomogeneity, 0.1 was used for this study.

The Cole equation is therefore commonly used in the analysis of impedance measurements of biological tissue. In an equivalent electrical circuit, cells in tissue may be represented as a resistance, R (intercellular fluid), a capacitance, C (plasma membrane), and another resistance, S (intracellular fluid) (Fig 5.27). These parameters can be mapped to a circuit of equal frequency response representing the Cole equation parameters. The impedance spectra data (over frequencies representative of the semi-circle arc) for this project were fitted by a complex non-linear least square method (Waterworth, 2000) to the Cole equation in order to derive values for cell membrane capacitance, intracellular and intercellular resistance.

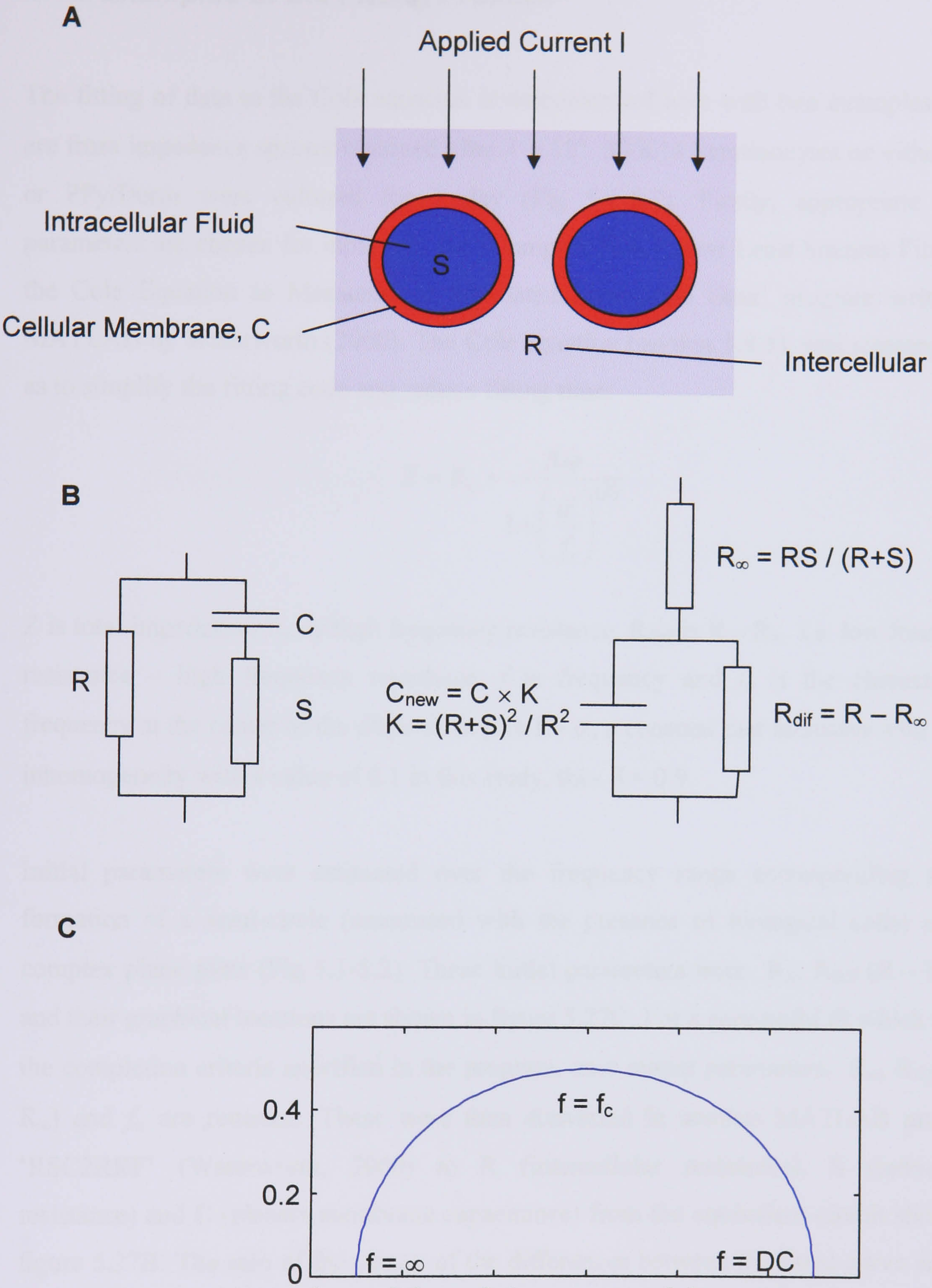

Figure 5.27: (A) Schematic of Cells in Tissue and Equivalent Electrical Components, (B) Equivalent Circuit for Tissue Model and Circuit of Equal Frequency Response Showing Relationship to (C) Cole Equation Parameters on Complex Plane Representation (Adapted from Waterworth, 2000).

5.4.2 Examples of the Fitting Process

The fitting of data to the Cole equation is demonstrated here with two examples. They are from impedance spectra obtained after 4×10^6 SVK14 keratinocytes on either gold or PPy/Derm were cultured for 1 day (Fig 5.1-5.2). Firstly, appropriate initial parameters are chosen for input into the 'Complex Non-Linear Least Squares Fitting of the Cole Equation to Measured or Simulated Impedance Data' program written in MATLAB by Waterworth (2000). The Cole equation (section 5.4.1), was rearranged so as to simplify the fitting code and reduce fitting time:

$$Z = R_\infty + \frac{R_{diff}}{1 + \left(\frac{if}{f_c}\right)^{(\beta)}}$$

Z is total impedance, R_∞ is high frequency resistance, R_{diff} is $R - R_\infty$ *i.e.* low frequency resistance – high frequency resistance, f is frequency and f_c is the characteristic frequency at the centre of the dispersion. β is $1 - \alpha$, a constant that increases with tissue inhomogeneity with a value of 0.1 in this study, thus $\beta = 0.9$.

Initial parameters were estimated over the frequency range corresponding to the formation of a semi-circle (associated with the presence of biological cells) on the complex plane plots (Fig 5.1-5.2). These initial parameters were R_∞, R_{diff} ($R - R_\infty$), f_c and their graphical locations are shown in figure 5.27C. For a successful fit which meets the completion criteria specified in the program, new output parameters, R_∞, R_{diff} ($R - R_\infty$) and f_c, are returned. These were then converted in another MATLAB program 'RSC2RRF' (Waterworth, 2000) to R (intercellular resistance), S (intracelllar resistance) and C (plasma membrane capacitance) from the equivalent circuit shown in figure 5.27B. The sum of the square of the differences between the fitted curve and the data (LS) which gives a goodness of fit for each experiment is also obtained. For the two examples used here, figure 5.28 shows the data curves and their fits. Table 5.3 summarises the input and output data and their errors for three repeat experiments in each example. Only R, S and C values along with their errors are shown for the results discussed in the rest of this chapter.

A

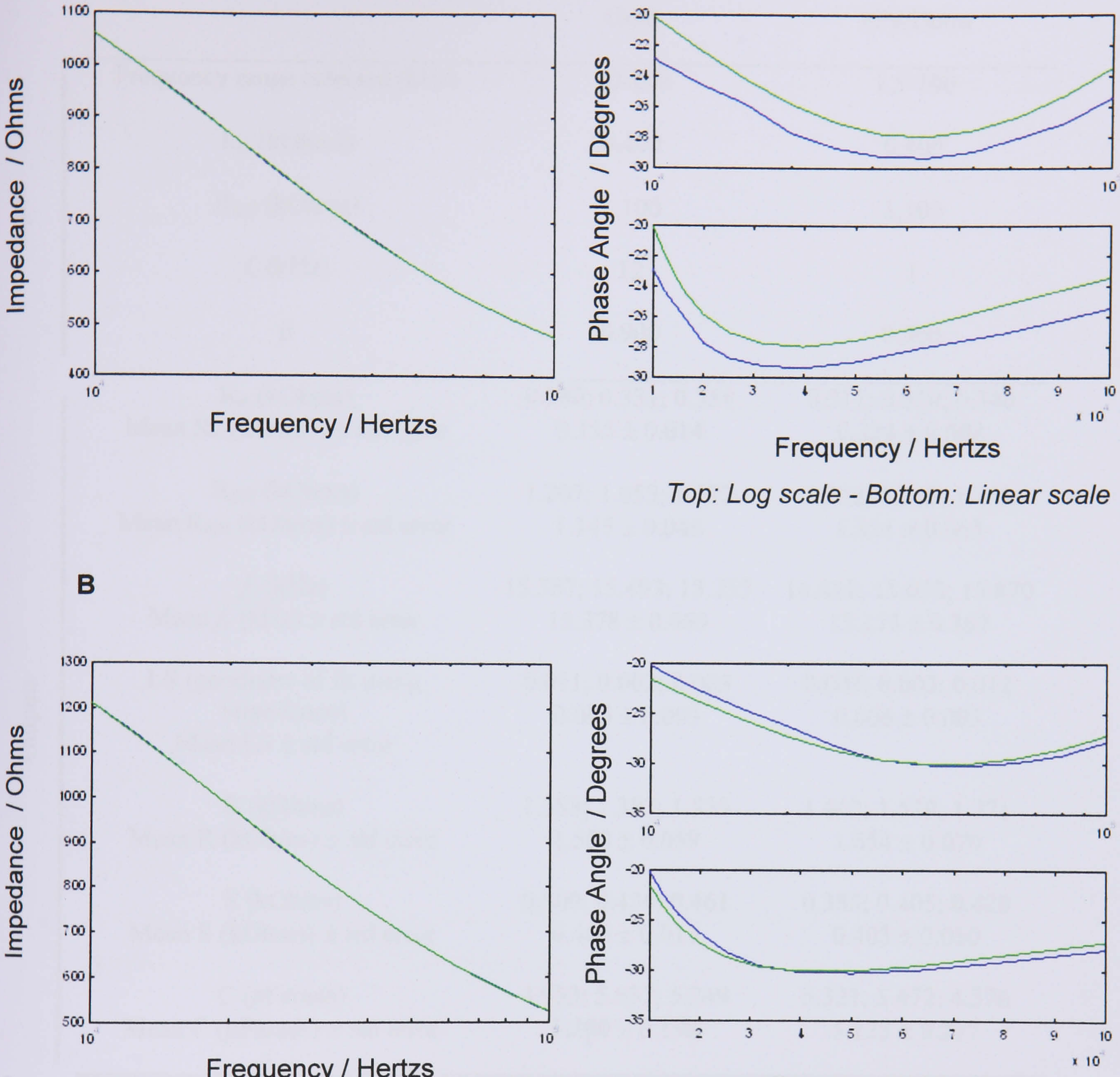

Top: Log scale - Bottom: Linear scale

B

Top: Log scale - Bottom: Linear scale

Figure 5.28: Representative Bode Plots of Data Curves (Blue) and Fitted Curves (Green) for 4×10^6 SVK14 Keratinocytes on Gold (A) and PPy/Derm (B) after 1 Day in Culture. *The fits appear very good with respect to impedance. However, there is a mismatch with the phase angle data for cells on gold but not in the case of PPy/Derm.*

		SVK14 keratinocytes substrate	
		Gold	PPy/Derm
Inputs	Frequency range selected (kHz)	10-100	1.5-100
	R_∞ (kOhms)	0.400	0.400
	R_{diff} (kOhms)	1.100	1.100
	f_c (kHz)	12	1
	β	0.900	0.900
Outputs	R_∞ (kOhms) Mean R_∞ (kOhms) ± std error	0.380; 0.331; 0.354 0.355 ± 0.014	0.311; 0.320; 0.340 0.324 ± 0.008
	R_{diff} (kOhms) Mean R_{diff} (kOhms) ± std error	1.207; 1.055; 1.172 1.145 ± 0.046	1.352; 1.209; 1.431 1.331 ± 0.065
	f_c (kHz) Mean f_c (kHz) ± std error	15.387; 15.493; 15.255 15.378 ± 0.069	14.621; 15.033; 15.870 15.175 ± 0.367
	LS (goodness of fit using impedance) Mean LS ± std error	0.011; 0.002; 0.003 0.005 ± 0.003	0.003; 0.003; 0.012 0.006 ± 0.003
	R (kOhms) Mean R (kOhms) ± std error	1.588; 1.387; 1.525 1.500 ± 0.059	1.663; 1.529; 1.771 1.654 ± 0.070
	S (kOhms) Mean S (kOhms) ± std error	0.500; 0.436; 0.461 0.466 ± 0.019	0.383; 0.405; 0.420 0.403 ± 0.010
	C (*p*Farads) Mean C (*p*Farads) ± std error	4.953; 5.637; 5.249 5.280 ± 0.198	5.321; 5.472; 4.576 5.123 ± 0.277

Table 5.2: Modelling Input and Output Parameters. *It may be seen that for each of the three repeat experiments, reproducibility is good with low errors for resulting outputs. In addition, the closeness of LS to zero confirms that fits were good.*

5.4.3 Growth of SVK14 Keratinocytes in Culture

The impedance spectra for SVK14 keratinocytes grown on gold and PPy/Derm were fitted to the Cole equation for equivalent circuit values (Fig 5.29). A fit was obtained for all data except in the case of cells on PPy/Derm at day 7. This was because of the substantial reduction in the semi-circle arc from the spectrum at that time-point (Fig 5.2). For SVK14s on Gold, changes were seen in intercellular resistance (R) and plasma membrane capacitance (C) with intracellular resistance (S) remaining relatively constant. Peaks for both R and C were seen at day 3. For SVK14s on PPy/Derm, R and S are relatively constant with C showing differences. Plasma membrane capacitances for cells on gold were found to be between a maximum of 0.2 $\mu F/cm^2$ and a minimum of 0.09 $\mu F/cm^2$. On PPy/Derm these were 0.1 $\mu F/cm^2$ and 0.036 $\mu F/cm^2$. These values are lower than those quoted in the literature which vary between 0.5 $\mu F/cm^2$ and 2.9 $\mu F/cm^2$ (Walker, 2001).

Comparing cells on gold to those on PPy/Derm, they are found to have similar intracellular resistance, but higher intercellular resistance and plasma membrane capacitance. This is in agreement with the results analysed at single frequencies (section 5.3.1), and supports the possibility of high cell membrane turnover in the case of cells on gold. However, the difference in values could also indicate polypyrrole mediated reduction in overall impedance since these results are inclusive of impedance through the polypyrrole layer as well as cell behaviour on polypyrrole.

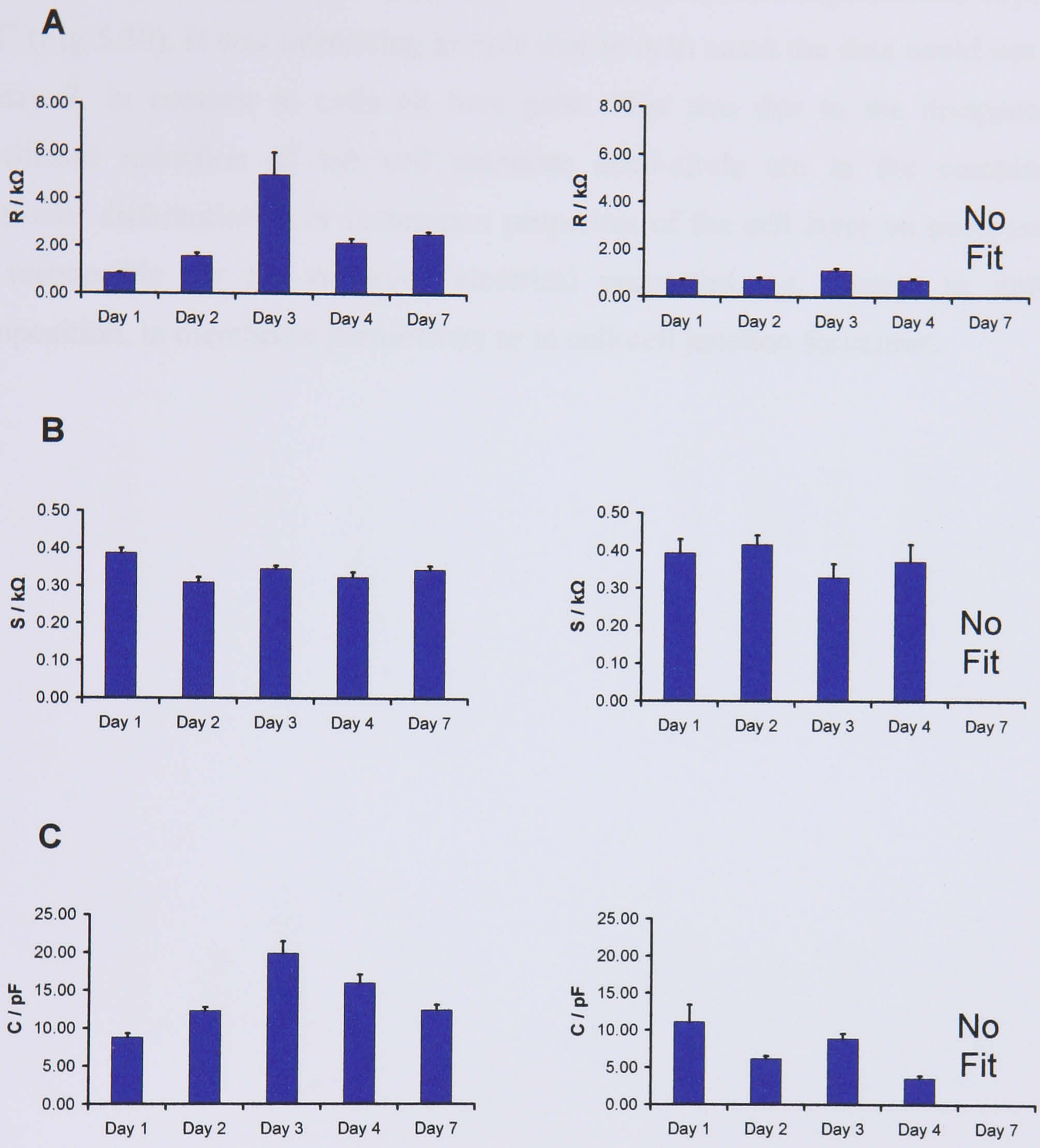

Figure 5.29: Equivalent Circuit Analysis for SVK14 Keratinocytes on (left) Gold compared to (Right) PPy/Derm (A) Intercellular Resistance, R, (B) Intracellular Resistance, S and (C) Plasma Membrane Capacitance, C (4×10^5 Cells Seeded).

5.4.4 Effect of Polypyrrole Loading

In good agreement with single frequency analysis of the effect of polypyrrole loading (section 5.3.2) no large differences were seen on the various experimental days for R, S or C (Fig 5.30). It was interesting to note that in both cases the data could not be fitted at day 7, in contrast to cells on bare gold. This was due to the disappearance or significant reduction of the cell associate semi-circle arc in the complex plane. Particular differentiation or maturation properties of the cell layer on polypyrrole may be responsible for the observed electrical properties *e.g.* change in intracellular composition, in membrane permittivity or in cell-cell junction formation.

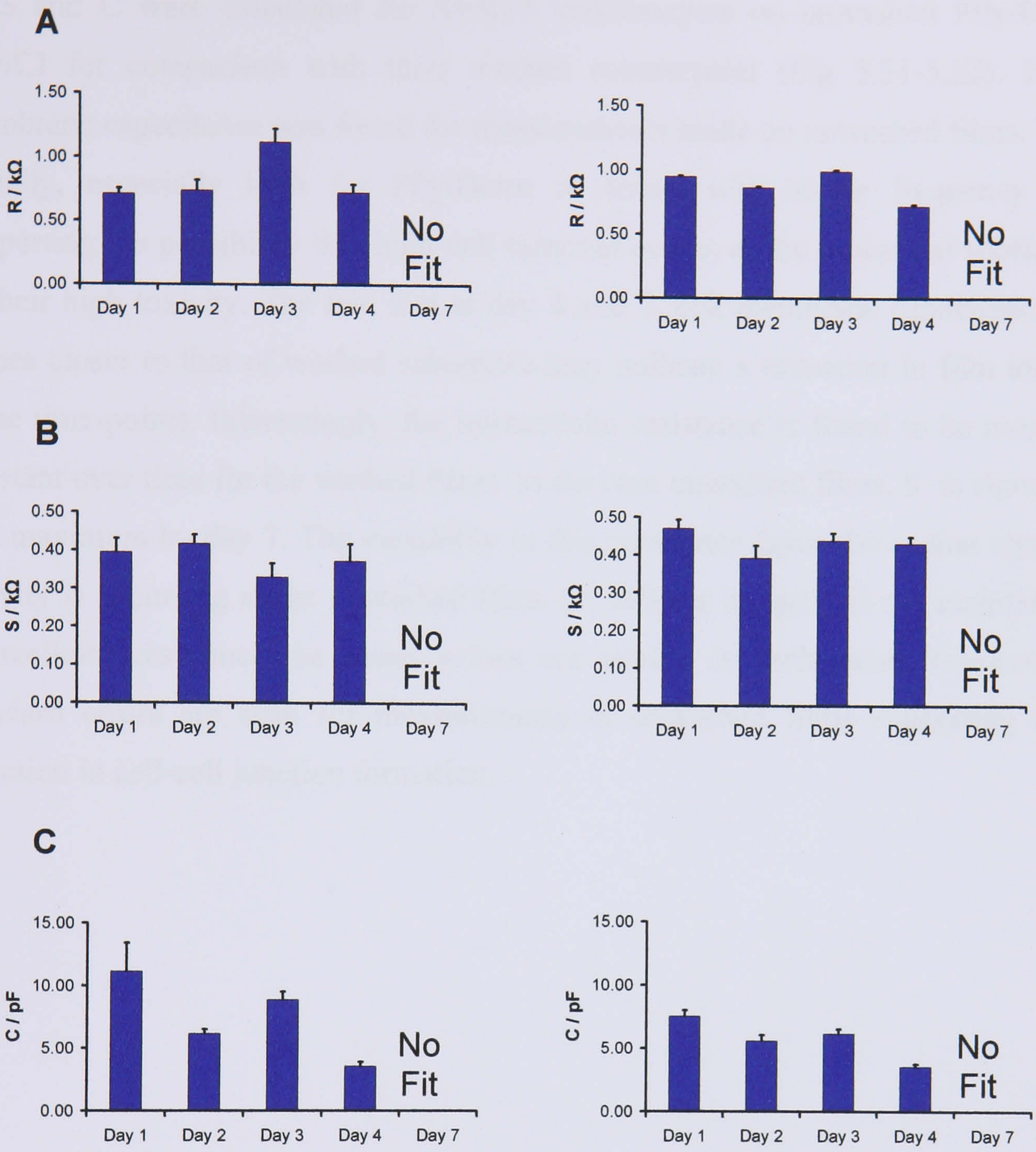

Figure 5.30: Equivalent Circuit Analysis for SVK14 Keratinocytes on (left) PPy/Derm compared to (Right) PPy/Cl (A) Intercellular Resistance, R, (B) Intracellular Resistance, S and (C) Plasma Membrane Capacitance, C.

(4×10^5 Cells Seeded).

5.4.5 Effect of wash

R, S and C were calculated for SVK14 keratinocytes on unwashed PPy/Derm and PPy/Cl for comparison with their washed counterparts (Fig 5.31-5.32). High cell membrane capacitance was found for measurements made on unwashed films. This was initially, especially high for PPy/Derm as found with single frequency analysis supporting the possibility that high cell turnover occurs at the unwashed substrates due to their high toxicity. The fact that at day 4 and 7, cell membrane capacitance falls to values closer to that of washed substrates may indicate a reduction in film toxicity by those time-points. Interestingly, the intracellular resistance is found to be more or less constant over time for the washed films. In the case unwashed films, S is shown to rise to a maximum by day 7. The variability in this parameter again shows that atypical cell activity is occurring at the unwashed films *i.e.* cellular integrity is not maintained. For intercellular resistance the mean values are similar in both cases; however higher standard errors are seen for measurements of unwashed films suggesting a higher variation in cell-cell junction formation.

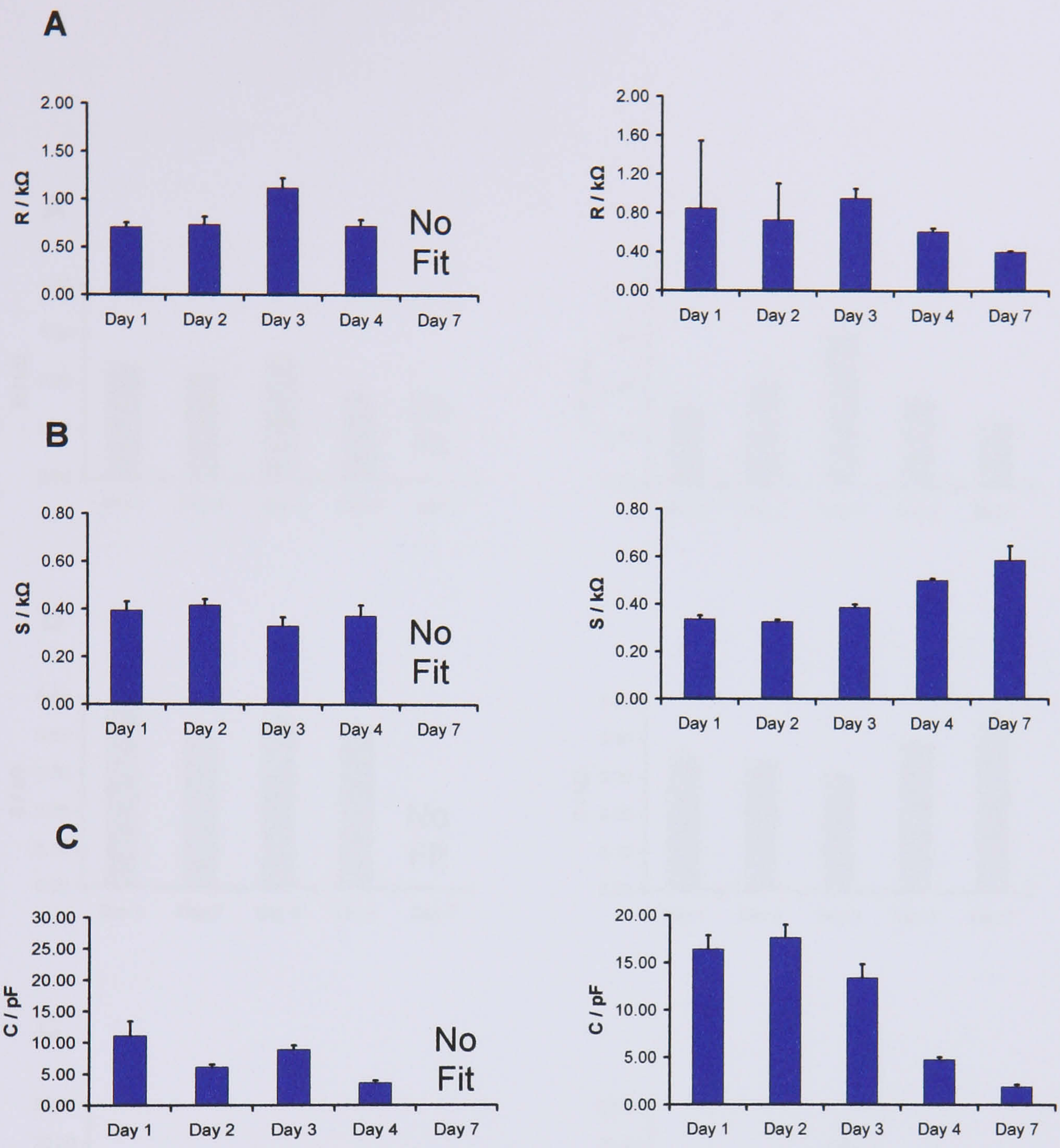

Figure 5.31: Equivalent Circuit Analysis for SVK14 Keratinocytes on (left) Washed PPy/Derm compared to (Right) Unwashed PPy/Derm (A) Intercellular Resistance, R, (B) Intracellular Resistance, S and (C) Plasma Membrane Capacitance, C.

(4×10^5 Cells Seeded).

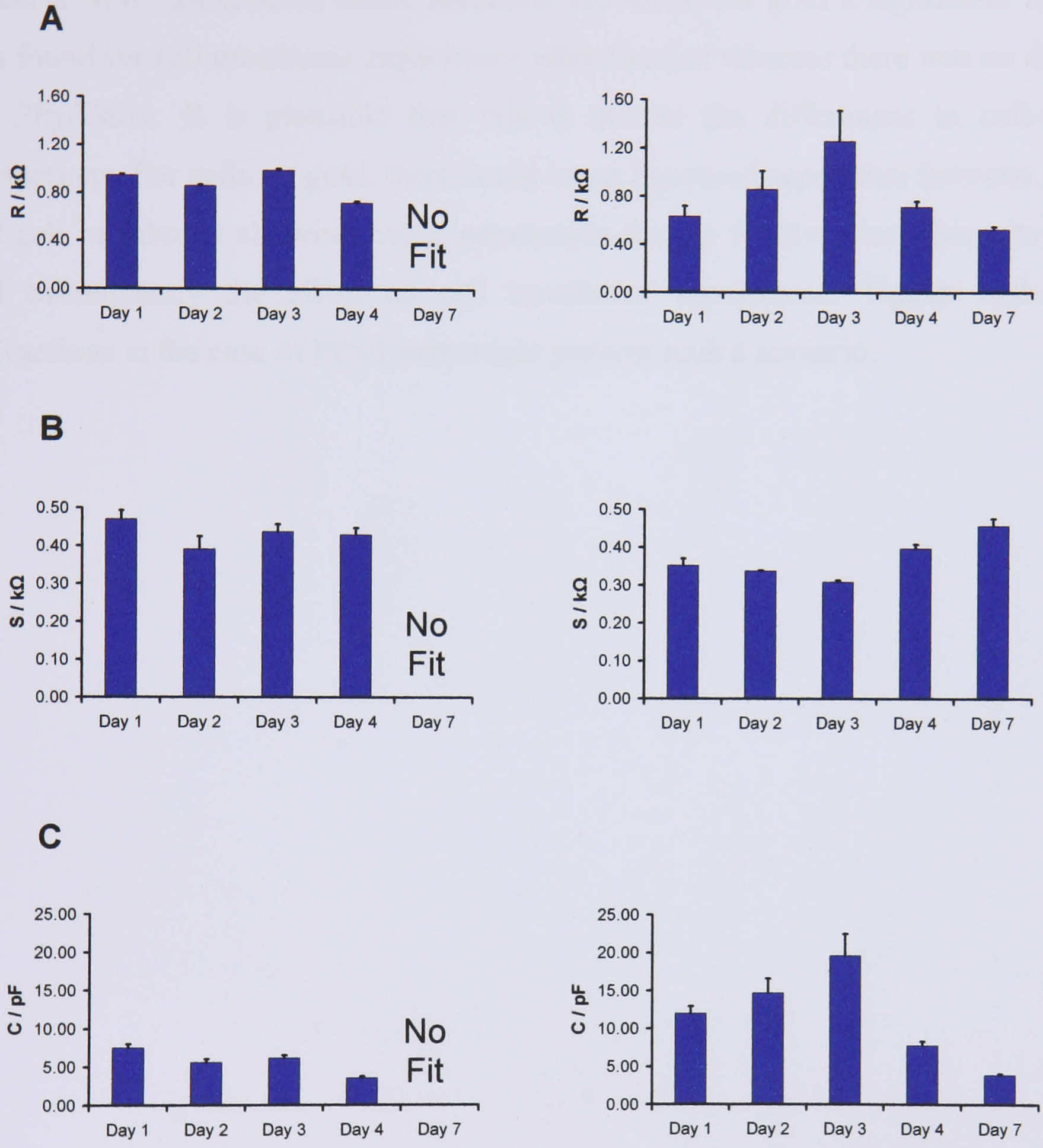

Figure 5.32: Equivalent Circuit Analysis for SVK14 Keratinocytes on (left) Washed PPy/Cl compared to (Right) Unwashed PPy/Cl (A) Intercellular Resistance, R, (B) Intracellular Resistance, S and (C) Plasma Membrane Capacitance, C.

(4×10^5 Cells Seeded).

5.4.6 Effect of Fixation

The change in R, S and C was considered for SVK14 keratinocytes on PPy/Derm and bare gold after exposure to 4% w/v para-formaldehyde (Fig 5.33). Major differences in R and S were not seen on either substrate. However, for gold a significant difference was found for cell membrane capacitance after fixation whereas there was no difference for PPy/Derm. It is plausible that this is due to the differences in cell-substrate interactions. For cells on gold, there could be an increased separation between substrate and cell membrane allowing better penetration for the fixative, increasing its efficacy and subsequently the effect on cell membrane capacitance. Tighter cell-substrate interactions in the case of PPy/Derm might prevent such a scenario.

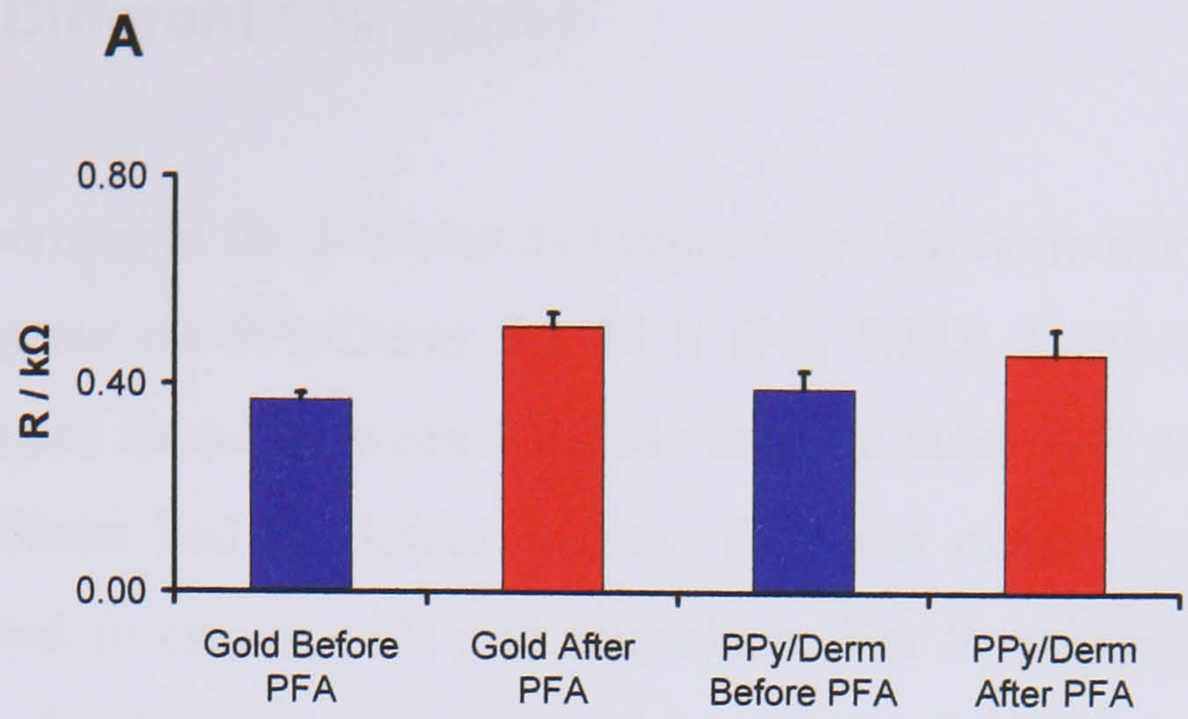

Figure 5.33: Equivalent Circuit Analysis for SVK14 Keratinocytes on Gold and PPy/Derm Before and After Treatment with 4% Para-Formaldehyde (A) Intercellular Resistance, R, (B) Intracellular Resistance, S and (C) Plasma Membrane Capacitance, C (4×10^5 Cells Seeded).

* * *Significant differences after treatment ($p<0.001$).*

5.4.7 Effect of Different Cell Types

R, S and C were compared for different cell types after the same initial number of cells were allowed to grow on PPy/Derm for 24 h (Fig 5.34). There were a number of significant differences found between SVK14s and the other cell types. For R, SCCs and primary fibroblasts had the lowest values. This was expected since less cell-cell junctions are formed in cancer cells and fibroblasts. For S, primary fibroblasts had a high value compared to SVK14s, primary keratinocytes and SCCs which were at similar magnitudes. This again could be explained by differences in cell morphology, size and intracellular composition of fibroblasts compared to keratinocytes. Fibroblasts are slender shaped, have a smaller cytoplasmic volume and do not undergo keratinisation. Significant differences were found between SVK14s and all other cell types for C. This could be because of membrane permittivity differences due to differential ion channel expression between the cell types or cell-substrate interactions. These results show that with this approach, it could be possible to have a signature parameter and value that enables discrimination between cell types on polypyrrole substrates.

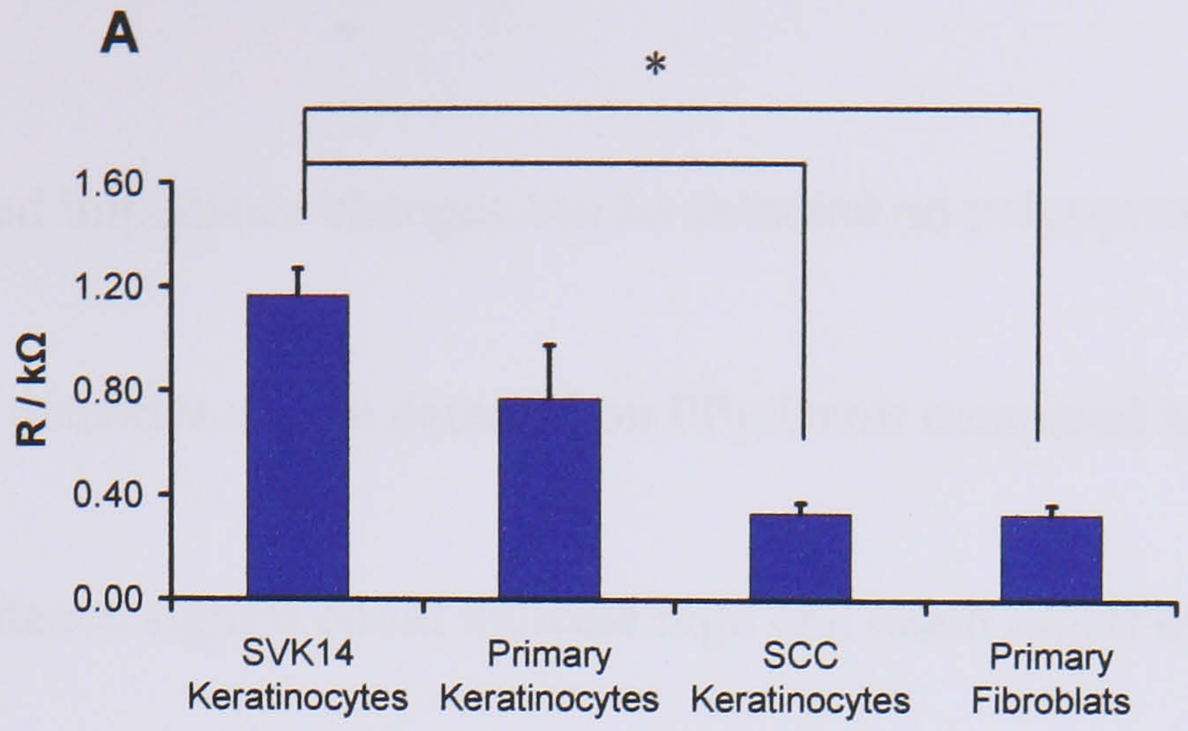

Figure 5.34: Equivalent Circuit Analysis for Various Cells on PPy/Derm

(A) Intercellular Resistance, R, (B) Intracellular Resistance, S and (C) Plasma Membrane Capacitance, C (4×10^5 Cells Seeded).

** Significant differences between SVK14s and other cells ($p<0.05$).*

5.4 Summary

- Cell-induced impedance changes can be detected on polypyrrole.
- Lower cell densities can be detected on PPy/Derm compared to gold.
- High impedance signals could indicate high cell death rather than viability.
- Single frequency analysis can be used to follow cells in a continuous manner.
- Different cell types can be discriminated by impedance.

Chapter 6

General Discussion, Future Work and Conclusions

6.1 General Discussion

6.1.1 Cell Compatible Polypyrrole Films

The first Chapter reviewed research in which PPy films were developed as substrates for cell growth. In most of those, non-biological counterions such as polystyrene sulphonate (Schmidt *et al.*, 1997) or polysaccharides such as hyaluronic acid (Collier *et al.*, 2000) were employed. The co-entrapment of proteins in PPy films has mainly been explored for biosensors (Sun and Tachikawa, 1992; Lillie *et al.*, 2001) although there are reports of post-film synthesis protein adsorption for cell growth applications (Kotwal and Schmidt, 2001). In this study, PPy films were developed for cell growth including those that incorporate proteins. The synthesis of films with negative counterions (chloride, dodecyl sulphate, polyvinyl sulphate, heparin and dermatan) was straightforward. The incorporation of various proteins (fibrinogen, fibronectin and collagen) was also shown to be feasible in the sole presence of monomer. The polymerisation reaction probably required the presence of negative charges on the protein. This was supported by the fact that alkaline pH was required for successful PPy/Col film formation (collagen is negatively charged only at alkaline pH). Electrochemical analysis as well as physical examination including electron microscopy showed that film properties varied according to the counterion loading.

Collagen-loaded PPy films which were studied in depth compared with other protein-loadings showed poor electroactivity (Fig 3.5-3.6, 3.15-3.16). In addition, a powdery 'cauliflower' like topography was noted for thicker films (Fig 3.12) which were fragile to the touch as evidenced with attempts to cut wax embedded cross-sections (Fig 4.21). PPy/Col was then shown to be unsuitable for keratinocyte growth (Fig 4.8) possibly because of the presence of toxic debris due to poor film integrity. This may stem from the particular aggregation properties of collagen during polymerisation since other protein-loaded films did not appear as brittle. Those other films were not studied here in sufficient depth for definite claims to be made over cell response; there are also no literature reports of cell growth on PPy-protein composites. All other PPy films were of superior integrity and found to be suitable for keratinocyte growth with some

divergence. In particular, PPy/Derm was found to be significantly better than other PPy films, bare polycarbonate and gold but similar to TCPS (Fig 4.8).

This was a surprising result, not least because no advantage was found for dermatan pre-coated TCPS (Fig 4.9). However, GAG coating of culture surfaces is not routine practice, unlike proteins, and it is conceivable that adsorption was compromised. It is possible that regardless of any dermatan biological effect, PPy/Derm films were simply of better mechanical integrity, thus explaining preferential growth data. Though this is unlikely, since they were observationally similar to other PPy films in terms of integrity and in any case films with a simple chloride anion provided the most efficiently polymerised films. The sharpest redox peaks were indeed seen for PPy/Cl (Fig 3.15) although it must be noted that for each counterion-loading, a unique environment for the electroactive group results accounting for differences seen in peak potential values.

Additional evidence of better film quality was shown by the significantly higher ATP content compared with other PPy films for keratinocytes grown on unwashed PPy/Cl (Fig 4.20). This suggests that although cell survival was far from ideal (the ATP assay was simply more sensitive than AlamarBlue™ at lower cell numbers) it improved for PPy/Cl, the most efficiently polymerised film with probably fewer toxic products. For these reasons, it is plausible that advantages seen for PPy/Derm are due to dermatan mediated biological interactions. This is an important result as dermatan's role in skin is poorly understood with only the few studies and reviews cited earlier (Chapter 4) exploring its functions. Trowbridge and Gallo (2002) tabulated dermatan sulphate binding proteins. Their list included collagen and fibronectin also known to bind membrane integrins and could form a paradigm for cell growth on PPy/Derm (Fig 6.1).

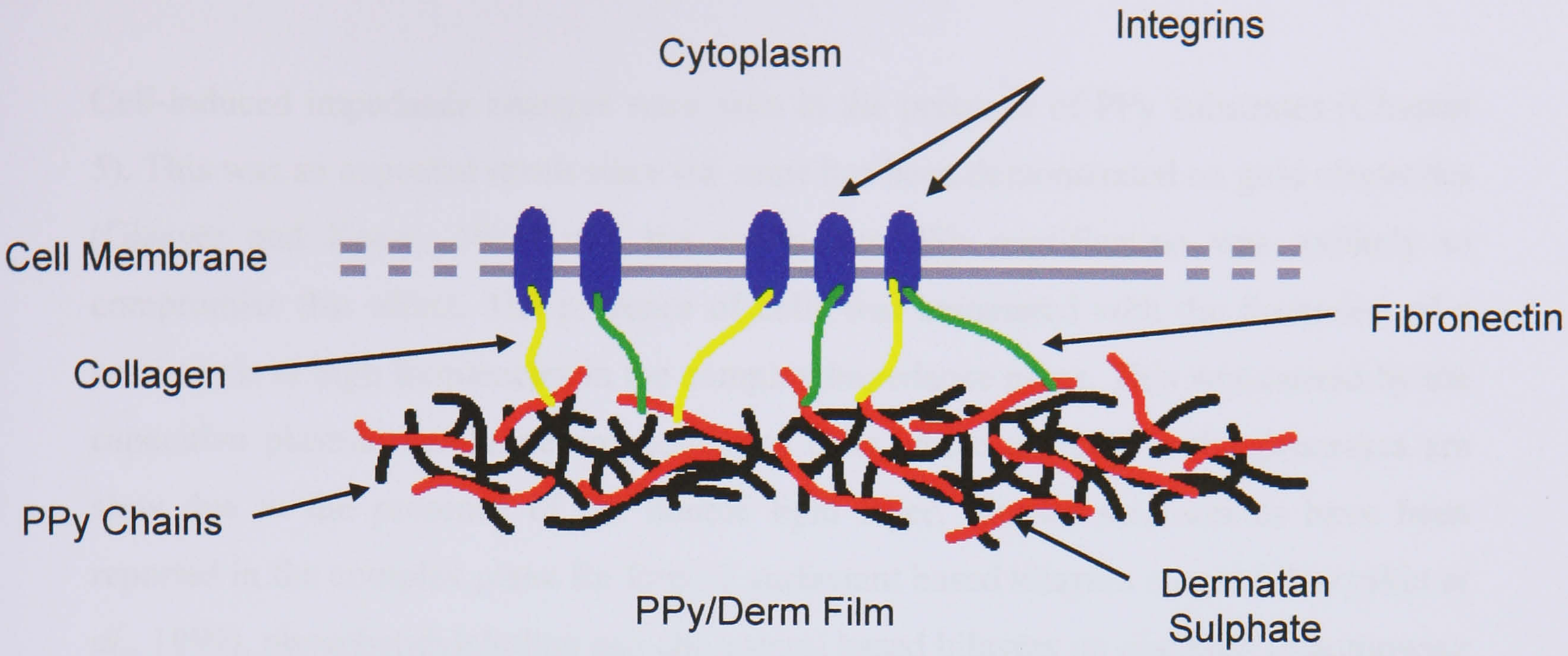

Figure 6.1 Proposed Model for Cell Interactions with PPy/Derm.

Dermatan Sulphate Chains Protrude from PPy Matrix and Bind Collagen and/or Fibronectin which then Bind to Cell Surface Integrin Receptors.

Importantly, it was found during the course of this research that a washing step was required prior to successful cell growth (Fig 4.7-4.8). This was a key discovery since it has not been previously reported in the literature and could explain previous poor adhesion (Mattioli-Belmonte, 2003) and culture away from PPy surface (Pu *et al*., 2001) for keratinocytes. Lakard (2005) recently investigated the culture of neural cells on a variety of materials including PPy and found that cell numbers increased with time except for PPy where numbers reached a plateau after 20 h. Again, this cell growth discrepancy with other substrates could be due to the authors overlooking the need to wash PPy. In this research, subsequent investigations of primary keratinocytes on washed PPy/Derm films grown in an organotypical fashion showed decreased quality compared to those grown on DED although viable cells were still seen (Fig 4.29). Possible reasons for this were elaborated earlier (Chapter 4) and further research could improve the prospects for producing functional tissue engineered epidermis on PPy substrates. Nevertheless, this study has arrived at a selection of keratinocyte compatible PPy substrates which could serve as a platform in future research efforts.

6.1.2 Cell-Induced Impedance on Polypyrrole Films

Cell-induced impedance changes were seen in the presence of PPy substrates (Chapter 5). This was an expected result since the same has been demonstrated on gold electrodes (Giaever and Keese, 1984) and the conductive PPy modification was unlikely to compromise this effect. The presence of cells was associated with the formation of a semi-circle at high frequencies in the complex impedance plane. This was caused by the capacitive plasma membrane component of cells where charge transfer processes are slow due to the presence of the double lipid layer. Similar semi-circles have been reported in the complex plane for Brij-52 surfactant based bilayers on gold (Karyakin *et al.*, 1999), phosphatidylcholine and cholesterol based bilayers on platinum (Naumowicz *et al.*, 2005), also dimyristoyl-$_L$-alpha-phophatidylcholine and dimyristoyl-$_L$-alpha-phophatidyl-$_L$-serine based bilayers on PPy modified gold (Shao *et al.*, 2005). The presence of a PPy modification was expected to provide differences compared to measurements made on bare gold since their properties are dissimilar and cell behaviour diverged (Fig 4.8). For comparable cell seeding densities, differences were indeed seen in the full impedance spectra, at single frequencies and for equivalent circuit values between cells on gold and those on PPy/Derm (Chapter 5).

The PPy modification was shown to enable visualisation of cell-induced changes at lower frequencies, although these are difficult to interpret since they involve polarisation of membrane bound molecules. Notably, it enabled impedimetric detection at lower cell densities (Fig 5.17). This could be due to increases in contact surface area from intimate association between PPy/Derm and cells, ease of current obstruction on ion-porous PPy, and/or cell-induced changes within the polymer. In support of the latter point, it is known that decreasing pH increases PPy impedance (Lillie *et al.*, 2001). Well characterised substrates, in terms of their ability to support cell growth, are necessary to correctly interpret impedance data since it was shown that higher impedances were recorded on unwashed PPy of known cytotoxicity (Fig 5.19-5.20). This was ascribed to the large presence of discarded plasma membrane from lysed cells constantly replenished by neighbouring cells on non-toxic polycarbonate (Fig 6.2). It was interesting to find that in support of the ATP assay results (Fig 4.20), impedance increases were lower on unwashed PPy/Cl compared to PPy/Derm indicating lower toxicity (Fig 5.19D). There remains the possibility that the intracellular resistance

component seen to vary for cells on unwashed films (Fig 5.31) could provide a means of determining cell viability.

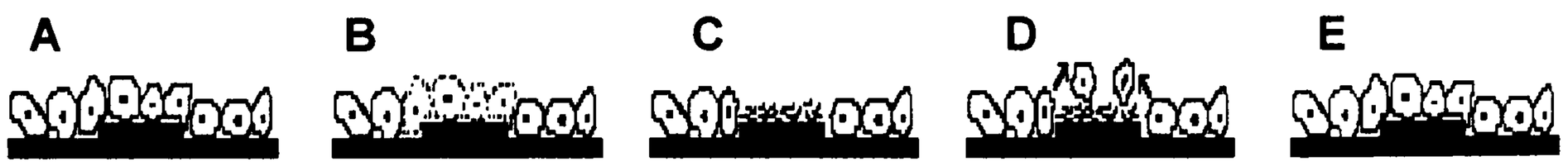

Figure 6.2 Proposed Model for High Impedance Responses on Unwashed PPy.

Cells grow well on washed PPy digits (elevated surface) and surrounding PC (A). However, when on unwashed PPy (B), the cells perish due to PPy toxicity although intact cells may exist on the surrounding PC. Plasma membranes are thus discarded by dead cells on the unwashed PPy substrate (C), and intact cells migrate to PPy from surrounding PC (D) repeating the cycle and thus increasing the amount of discarded membrane present at the surface. This in turn explains the high impedance signals recorded. Eventually, PPy toxicity is depleted and intact cells exist on PPy digit (E).

For keratinocytes on PPy, it was also observed that measured at 40 kHz, an impedance peak was reached by day 1 rather than day 3 as for those on gold (Fig 5.14 & 5.16). This suggests that maximum confluence was reached faster on PPy rather than gold in agreement with Chapter 4 findings (Fig 4.8). The decline in impedance values after these respective peaks are possibly associated with changes in keratinocyte layer dynamics and are further discussed in the next section.

6.1.3 Keratinocytes Layer Dynamics in Relation to EIS

Impedimetric sensing of keratinocytes over time showed variations in response when full spectrum, single frequency or equivalent circuit data were considered (Chapter 5). For those seeded at the lower density of 4×10^4 cells per well, impedance increased until the final experimental day whether on bare gold or PPy/Derm (Fig 5.1-5.2, 5.13-5.16). This was most probably due to the cells reaching confluence on their substrates over time. For cells seeded at the mid and high densities (4×10^5 and 4×10^6 cells per well respectively) confluence was reached rapidly; seen using microscopy. The impedance response for those seeding densities was distinct from the lower seeding densities, maxima were reached at around 1 and 3 days on PPy/Derm and gold

respectively followed by a decline (Fig 5.1-5.2, 5.13-5.16, 5.29). Since confluence was rapidly established and no cytotoxic effect was observed, these changes may be explained in terms of layer dynamics when keratinocytes become confluent.

Thus changes in observed impedance may be correlated with intracellular (*e.g.* keratin expression and differentiation), intercellular (*e.g.* desmosomes expression) and cell membrane (*e.g.* ion channel expression) changes. From the results obtained, intercellular and cell membrane changes are likely to be dominant especially for cells on gold (Fig 5.29). Quantitative studies on the expression of desmosomes, adherens, tight junctions (different cell-cell junctions) or transmembrane ion channels for keratinocytes in culture over time have not been found in the literature. However using impedimetric techniques, Wegener *et al.* (1996) found the same rise and drop in impedance for MDCK-II epithelial cells and Pliquett and Pliquett (1996) showed a similar pattern for excised human skin. Although the models they investigated were different from this study, they do provide further confirmation that electrical properties in confluent epithelial cells are transient over time and most probably change because of the dynamic remodelling of the cell layer.

It is known that adherens (Lecuit, 2005) and desmosomes (Yin and Green, 2004) undergo remodelling during development and differentiation in epithelial cells. In fact the proteins that form desmosomes, namely the well studied desmosomal cadherins which are further subdivided into desmogleins (Dsg) and desmocollins (Dsc), are expressed in distinct isoforms depending on cell type and differentiation state for complex epithelia (Yin and Green, 2004; Getsios *et al.*, 2004). In the case of desmosomes, it is conceivable that the type of Dsg or Dsc isoform expressed determines strength and quantity within the epidermis. In basal layers desmosomes would be expected to be weaker and fewer to facilitate cell migration for stratification. This could explain the fall in impedance seen in this study after 1 and 3 days for keratinocytes on PPy/Derm and gold respectively; once keratinocytes reached confluence, cell-cell junctions were weakened to enable stratification. These results could provide a means of determining cell differentiation state in culture.

6.1.4 Continuous Cell Monitoring using EIS

Single frequency continuous real-time cell monitoring by impedance has been widely investigated on gold electrodes, often pre-coated with fibronectin, and some of these studies have been discussed earlier (Chapter 1). The technique has been used to elucidate the effect of histamine and thrombin on endothelial focal adhesions (Moy *et al.*, 1996), to assess the effect of cytotoxic agents on cells (Xiao *et al.*, 2002; Xiao and Luong, 2003; Xing *et al.*, 2005), to monitor changes in endothelial morphology during apoptosis (Wegener *et al.*, 2004) and to follow cell migration during wound healing (Keese *et al.*, 2004). In this study, continuous cell monitoring has been investigated for cells on PPy/Derm modified electrodes. Differences in impedance fluctuations, associated with cell movements on the nanometer scale (Giaever and Keese, 1991; Lo *et al.*, 1993), were not seen for SVK14 keratinocytes pre- and post-fixation (Fig 5.21-5.22). The fact that in addition, differences were not found with bare controls suggests that any background electrical noise masked keratinocyte-induced changes although the different cell type here could also have had an effect.

These hypotheses could be verified on less noisy microelectrodes and by testing different cell types. Continuous measurements following the adhesion of various cells showed behavioural differences, notably between cancer and normal cells (Fig 5.26). In the opposite case, a reduction in impedance (at least for the phase/imaginary components) was seen for SVK14 keratinocytes treated with trypsin (Fig 5.24-5.25). These experiments confirm that as for previous work on gold electrodes, it is also possible to monitor cells on PPy electrodes in a continuous fashion. The advantage here could be a preferential substrate for cell growth (Fig 4.8) with the added advantage of variable film inclusions for tailored surface properties.

6.1.5 Cell Discrimination using EIS

Having already observed differences through monitoring of various cell types during adhesion (Fig 5.26), it was of interest to test whether EIS could discriminate between cells on PPy/Derm after confluence. Differences were indeed seen in the full impedance spectra for SVK14, primary and SCC keratinocytes as well as primary fibroblasts. Also, equivalent circuit modelling proved to be an effective means of cell discrimination as

the combination of intercellular and intracellular resistances and membrane capacitance differed for each cell type (Fig 5.34). Variations on this model have been used in equivalent circuit analysis of cells or tissue including those taking interfacial resistance and capacitance between an electrode and electrolyte into account (Grimnes and Martinsen, 2000). This has usually been done by adding a series resistor and capacitor to the circuit used for the work presented in this study.

However, since cells dominate measured impedance, a less complex model discounting the electrode-electrolyte contribution was preferred and found to be sufficient here. The equivalent circuit model used here has been successfully applied to discriminate pre-cancerous and cancerous epithelium of the cervix from normal tissue in patients using a novel pencil probe for impedance measurements (Brown *et al.*, 2000). Other impedance based methodologies have also been applied to cell discrimination. This includes complex permittivity measurements to detect osteoblast and macrophage signatures (Bagnaninchi *et al.*, 2004) and impedance spectroscopy flow cytometry shown to differentiate between polystyrene beads, red blood cells, ghost cells and fixed cells (Cheung *et al.*, 2005).

6.2 Future Work

6.2.1 Improving Polypyrrole Films

Further to work presented here, PPy films could be improved for superior cell growth and electrochemical properties. This could include investigating the inclusion of other biomolecules and clarifying their entrapment state using surface characterisation methods (Castner and Ratner, 2002). Concomitantly, there is an argument to improve electrochemical properties as this would lead to more efficient film formation at polymerisation with subsequent advantages for electrical stimulation or impedimetric detection. This could possibly be done by co-entrapment of biological molecules with more efficient counter-ions and scouring the literature reveals promising candidates. For instance 'superatoms' where clusters of one atom can behave as another have recently been proposed to improve the conductivity of electroactive polymers (Ball, 2005). There is also room to consider the polymerisation of modified pyrrole monomers (*e.g.* methyl-pyrrole) and copolymers (*e.g.* pyrrole-thiophene).

The mechanical properties of the PPy films obtained also need to be investigated as resilience would be required in tissue engineering applications. The effect of various synthesis conditions such as temperature or reagent concentrations could be checked against subsequent mechanical properties such as tensile stress or modulus. Strategies to form porous films such as the entrapment of microparticles which could then be dissolved leaving a network of interconnected pores should be considered. Kim *et al.* (2004) have already shown that PPy may be electrogenerated in porous hydrogel scaffolds to produce distinct architectures. These developments need to be pursued in order to obtain tractable PPy films in a variety of geometries.

The synthesis of PPy films incorporating whole living cells would also be desirable. This has been achieved with red blood cells although their long term viability was unclear from the report (Campbell *et al.*, 1999). PPy incorporating viable dermal fibroblasts could have added value as a substrate in skin tissue engineering. Fibroblasts are found within the dermis *in vivo* and could promote better cell growth through basement membrane proteins or signal molecules expression in PPy constructs. This

study has shown that SVK14 keratinocytes can survive for 24 h in the presence of minimal pyrrole concentrations required for polymerisation (Fig 4.12) and future experiments can look at optimising the electropolymerisation process.

6.2.2 Electrical Stimulation of Cells on Polypyrrole Films

The electrical stimulation of cells on PPy is a major attraction for its use in tissue engineering. Studies have already been discussed (Chapter 1) showcasing advantages for cell control. Much work was carried-out in the late 80s by Aizawa's group at the Tokyo Institute of Technology. They found that electrochemical oxidation of PPy caused a large local pH change along with incorporation of anions from solution (Shinohara *et al.*, 1989b) and explored the rupture of erythrocyte cell membranes by applied potential (Shinohara *et al.*, 1989a). They attributed the pH change to local OH^- transfer between the electrolyte and the PPy film. In their work with erythrocytes, they found that cell lysis occurred on PPy-coated electrodes at *ca* +400 mV, whereas for uncoated (In_2O_3) electrodes, cell lysis was observed above +1200 mV. Preliminary studies during the course of this research suggest that electrical stimulation does have an effect on keratinocytes adhesion to PPy/Derm (Fig 6.3) although no effects were observed by microscopy when the experiment was repeated for a confluent cell layer.

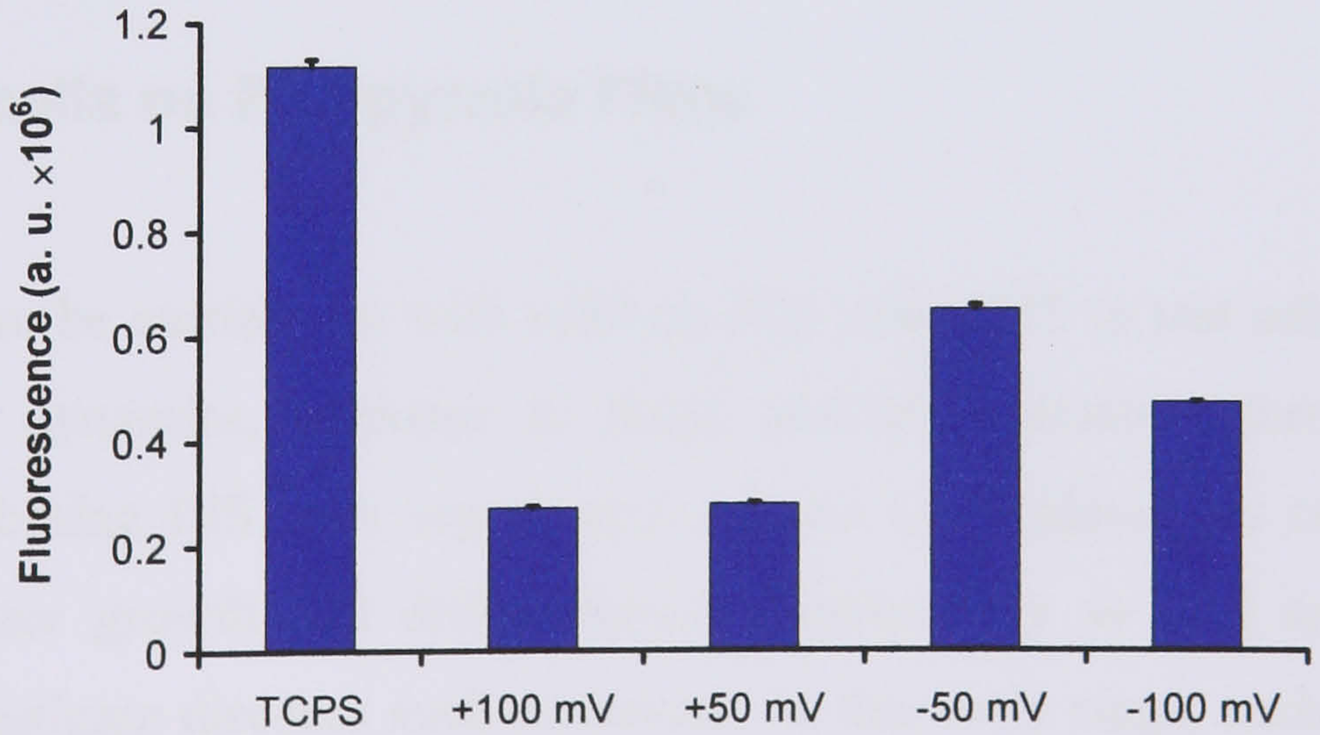

Figure 6.3: SVK14 Keratinocytes AlamarBlue™ Proliferation Assay on PPy/Derm Substrates Measured 24 h After Electrical Stimulation for 1 h Upon Addition of 4×10^6 Cells to Culture Media (± SE, n = 9 for single substrates).

For electrical stimulation on cell free PPy/Derm it was observed during this research that at overoxidising potentials, film integrity was destroyed revealing the bare polycarbonate support. If the same can be done in the presence of cells and shown not to affect viability this could be applied as a cell sheet release mechanism without the need of proteolytic enzymes. This has been shown for thermo-responsive polymers where conformational changes at lower temperatures induce cell detachment (Yamato and Okano, 2004). Another property that can be exploited with PPy is the fact that electrical stimulation also induces a volume change within the matrix as studied for artificial muscle applications (Otero and Sansinena, 1995). Substrate mechanics in addition to chemistry and topography are increasingly understood to be important factors in cell response (Wong *et al.*, 2004) as well as applied mechanical stress (Brown *et al.*, 1998; Lee and Knight, 2004). It would be interesting to investigate the feasibility of creating PPy surfaces with mechanical property gradients or capable of transmitting mechanical loading to cells through electrical stimulation.

Electrical stimulation of cells on PPy is a complex matter and any future studies would need to address the effect of PPy redox state, electrical charge, electrical field and transformation of culture media redox species (*e.g.* ascorbate) on the cells. This includes careful consideration of stimulatory voltage magnitude and configuration, *i.e.* continuous DC potential *vs.* continuous AC potential or pulsed potentials. However, such studies could uncover valuable methods for directing cell behaviour.

6.2.3 EIS of cells on Polypyrrole Films

More studies can be carried-out with cells on PPy using EIS to test adhesion profiles, wound healing dynamics, response to drugs and discrimination through cell type signature. Combining EIS with organotypic culture of keratinocytes could provide a means to monitor growth and differentiation continuously as well as to provide a platform to investigate diseases such as cancer. At this early stage, such studies would need to be preceded by investigations into the biology of the growing culture in order to establish the relationship between impedance data and cell expression profile. Studies charting gene expression at various stages of growth for a keratinocyte organotypic culture model have not yet been done. However, understanding cell-cell junction expression over time in a culture model for instance, would be vital in the interpretation

of impedimetric data. Incorporation of antibodies or enzymes within the PPy matrix to monitor specific cell interactions or products should also be considered.

An advance that could have a serious impact on this research would be the PPy modification of micro and nanoelectrodes. The reduced size of such electrodes would increase their sensitivity due to enhanced rates of mass transport to and from their surfaces compared with conventional electrodes. In addition, their size would enable single cell monitoring (microelectrode) or even single membrane channel monitoring (nanoelectrode) with the possibility of minimally invasive *in vivo* studies.

6.2.4 Drug Delivery

There are reports of controlled release from PPy films including ferrocyanide (Miller *et al.*, 1987), adenosine triphosphate (Pyo *et al.*, 1994) and heparin (Li *et al.*, 2005). Future work should consider exploring this area as it would be advantageous to have such capabilities integrated within a tissue engineering scaffold (Saltzman and Olbricht, 2002). A simple experiment could involve incorporating Ca^{2+} by reduction of an immobile counterion loaded PPy in its presence; Ca^{2+} mediated behaviour of cultures on such a substrate could be probed by controlled release of Ca^{2+} upon film oxidation.

6.3 Conclusions

This thesis has demonstrated the direct incorporation of biological macromolecules by means of overall negative charge into PPy films. The pre-treatment of formed PPy films was found to be necessary for successful cell growth. In particular, dermatan-loaded PPy was shown to be preferable for keratinocyte growth compared with bare gold and other PPy films. Taking advantage of the fact that PPy substrates are electrically addressable, it was shown that biological cells can be monitored by electrochemical impedance spectroscopy. This included continuous monitoring during adhesion or exposure to trypsin and cell type discrimination by equivalent circuit analysis. Advantages for the use of PPy were seen from reduced impedance at lower frequencies and the detection of lower cell numbers compared with gold.

This thesis has investigated novel concepts at the physical and life sciences interface and brought new knowledge to light. The research presented would serve well as a platform for further investigations as laid out under future work. Continued exploration of PPy biocomposites and their unique properties could lead to tissue engineering scaffolds that could both direct and report on cell activities.

Reference

Abatangelo G., Martelli M. and Vecchia P. Healing of Hyaluronic Acid-Enriched Wounds: Histological Observations. *Journal of Surgical Research*. **35**, 410-416 (1983)

Adejolu S. B. and Wallace G. G. Conducting Polymers and the Bioanalytical Sciences: New Tools for Biomolecular Communications – A Review. *Analyst*. **121**, 699-703 (1996)

Adejolu S. B., Shaw S. J. and Wallace G. G. Polypyrrole-Based Amperometric Flow Injection Biosensor for Urea. *Analytica Chimica Acta*. **323**, 107-113 (1996)

Alberts B., Johnson A., Lewis J., Raff M., Roberts K. and Walter P. (2002) Molecular Biology of the Cell. Garland Science

Alonso L. and Fuchs E. Stem Cells of the Skin Epithelium. *Proceedings of the National Academy of Sciences of the USA*. **100**, 11830-11835 (2003)

Armes S. P., Aldissi M., Hawley M., Beery J. G. and Gottesfeld S. Morphology and Structure of Conducting Polymers. *Langmuir*. **7**, 1447-1452 (1991)

Armes S. P. Optimum Reaction Conditions for the Polymerization of Pyrrole by Iron (III) Chloride in Aqueous Solution. *Synthetic Metals*. **20**, 365-371 (1987)

Arndt S., Seebach J., Psathaki K., Galla H-J. and Wegener J. Bioelectrical Impedance Assay to Monitor Changes in Cell Shape during Apoptosis. *Biosensors and Bioelectronics*. **19**, 583-594 (2004)

Assoian R. K. Anchorage-Dependent Cell Cycle Progression. *Journal of Cell Biology*. **136**, 1-4 (1997)

Ateh D. D. (2003) Polypyrrole Based Conducting Polymers as Substrates for Skin Tissue Engineering (Transfer Report). IRC in Biomedical Materials/Centre for Cutaneous Research, QMUL

Bagnaninchi P-O., Dikeakos M., Veres T. and Tabrizian M. Complex Permittivity Measurement as a New Noninvasive Tool for Monitoring *In Vitro* Tissue Engineering and Cell Signature Through the Detection of Cell Proliferation, Differentiation, and Pretissue Formation. *IEEE Transactions on Nanobioscience*. **3**, 243-250 (2004)

Ball P. A New Kind of Alchemy. *New Scientist*. **186** (2495), 30-33 (2005)

Barber D. C. and Brown B. H. Applied Potential Tomography. *Journal of Physics E: Scientific Instruments*. **17**, 723-733 (1984)

Barron J. J. and Ashton C. (2005) The Effect of Temperature on Conductivity Measurement. http://www.reagecon.com/techpapers.shtml

Bertolesi G. E., Lauria de Cidre L. and Eijan A. M. Growth Inhibition In Vitro of Murine Mammary Adenocarcinoma Cells by Heparin and Chemically Modified Heparins. *Tumor Biology*. **15**, 275-283 (1994)

Bhattacharya A., De A. and Das S. Electrochemical Preparation and Study of Transport Properties of Polypyrrole Doped with Unsaturated Organic Sulfonates. *Polymer*. **34**(19), 4375-4382 (1996)

Boonstra J. De Laat S. W. and Ponec M. Epidermal Growth Factor Receptor Expression Related to Differentiation Capacity in Normal and Transformed Keratinocytes. *Experimental Cell Research*. **161**, 421-433 (1985)

Bousse L. Whole Cell Biosensors. *Sensors and Actuators B*. **34**, 270-275 (1996)

Bowden P. E., Quinlan R. A., Breitkreutz D. and Fueng N. E. Proteolytic Modification of Acidic and Basic Keratins during Terminal Differentiation of Mouse and Human Epidermis. *European Journal of Biochemistry*. **142**, 29-36 (1984)

Brett C. M. A. and Brett A. M. O. (1993) Electrochemistry – Principles, Methods and Applications. Oxford University Press

Briggaman R. A., Yoshiike T. and Cronce D. J. In: Goldsmith L.A. Ed. (1991) Physiology, Biochemistry and Molecular Biology of the Skin Vol. II. Oxford University Press

Brown B. H., Tidy J. A., Boston K., Blackett A. D., Smallwood R. H. and Sharp F. The Relationship between Tissue Structure and Imposed Electrical Current Flow in Cervical Neoplasia **355**, *Lancet*. 892-895 (2000)

Brown R. A., Prajapati R., McGrouther D. A., Yannas I. V. and Eastwood M. Tensional Homeostasis: Mechanical Responses to Mechanical Loading in Three-Dimensional Substrates. *Journal of Cellular Physiology*. **175**, 323-332 (1998)

Burgmayer P. and Murray R. W. In: Skotheim T. A. (1986) Handbook of Conducting Polymers (Vol 1). Marcel Dekker, Inc.

Buxton P. K. (2003) ABC of Dermatology. BMJ Publishing Group Ltd.

Campbell T. E., Hodgson A. J. and Wallace G. G. Incorporation of Erythrocytes into Polypyrrole to form the Basis of a Biosensor to Screen for Rhesus (D) Blood Groups and Rhesus (D) Antibodies. *Electroanalysis*. **11**, 215-222 (1999)

Castellot J. J. Jr, Hoover R. L., Harper P. A. and Karnovsky M. J. Heparin and Glomerular Epithelial Cell-Secreted Heparin-Like Species Inhibit Mesangial-Cell Proliferation. *American Journal of Pathology*. **120**, 427-435 (1985)

Castner D. G. and Ratner B. D., Biomedical Surface Science: Foundations to Frontiers, *Surface Science*. **500**, 28-60 (2002)

Cell Applications Inc. (2004) http://cellapplications.com/HDF.htm

Cheung A. H. and Luna G. K. Cadaveric Organ Donor Availability: Regional Trauma Centre *vs.* Community Hospital. *Journal of Trauma*. **30**, 1366-1371 (1990)

Cheung K., Gawad S. and Renaud P. Impedance Spectroscopy Flow Cytometry: On-Chip Label-Free Cell Differentiation. *Cytometry Part A*. **65A**, 124-132 (2005)

Chien F., Kashimori Y. and Nishimoto K. Simulations on Soliton Dynamics in Polyacetylene Systems. *Chemical Physics*. **125**, 269-278 (1988)

Clark L. C. and Lyons C. Electrode Systems for Continuous Monitoring in Cardiovascular Surgery. *Annals of the New York Academy of Sciences*. **102**, 29-45 (1962)

Clark P., Connolly P., Curtis A. S. G., Dow J. A. T. and Wilkinson C. D. W. Cell Guidance by Ultrafine Topography *In Vitro*. *Journal of Cell Science*. **99**, 73-77 (1991)

Cole K. S. and Cole R. H. Dispersion and Absorption in Dielectrics. Alternating Current Characteristics. *Journal of Chemical Physics* **9**, 341-351 (1941)

Collier J. H., Camp J. P., Hudson T. W. and Schmidt C. E. Synthesis and Characterization of Polypyrrole-Hyaluronic Acid Composite Biomaterials for Tissue Engineering Applications. *Journal of Biomedical Material Research*. **50**, 574-584 (2000)

Crow D. R. (1994) Principles and Applications of Electrochemistry. Blackie Academic and Professional an imprint of Chapman and Hall

Cui X., Lee V. A., Raphael Y., Wiler J. A., Hetke J. F., Anderson D. J. and Martin D. C. Surface Modification of Neural Recording Electrodes with Conducting Polymer/Biomolecule Blends. *Journal of Biomedical Materials Research*. **56**, 261-272 (2001)

Curtis A. and Wilkinson C. Topographical Control of Cells. *Biomaterials*. **18**, 1573-1583 (1997)

Dall'olio A., Dascola G., Vacara V. and Bocchi V. Resonance Paramagnetique Electronique et Conductivité d'un noir d'oxypyrrol electrolytique. *Comptes Rendus de l'Academie des Sciences – Paris*. **267**, 433-435 (1968)

Della Santa A., Mazzoldi A., Tonci C. and De Rossi D. Passive Mechanical Properties of Polypyrrole Films. A Continuum Poroelastic Model. *Materials Science and Engineering C*. **5**, 101-109 (1997)

DePaola N., Phelps J. E., Florez L., Keese C. R., Minnear F. L., Giaever I. and Vincent P. Electrical Impedance of Cultured Endothelium Under Fluid Flow. *Annals of Biomedical Engineering*. **29**, 648-656 (2001)

Desai T. A. Micro- and Nanoscale Structures for Tissue Engineering Constructs. *Medical Engineering and Physics*. **22**, 595-606 (2000)

Deslouis C., El Moustafid T., Musiani M. M. and Tribollet B. Mixed Ionic-Electronic Conduction of a Conducting Polymer Film. AC Impedance Study of Polypyrrole. *Electrochimica Acta*. **41**, 1343-1349 (1996)

Diaz A. Electrochemical Preparation and Characterisation of Conducting Polymers. *Chemica Scripta*. **17**, 145-148 (1981)

Diaz A. F. and Kanazawa K. K. Electrochemical Polymerisation of Pyrrole. *Journal of the Chemical Society – Chemical Communications*. 635 (1979)

Diaz A. F., Castillo J. I., Logan J. A. and Lee W-Y. Electrochemistry of Conductive Polypyrrole Films. *Journal of Electroanalytical Chemistry*. **129**, 115-132 (1981)

Duchet J., Legras R. and Demoustier-Champagne S. Chemical Synthesis of Polypyrrole: Structure-Properties Relationship. *Synthetic Metals*. **98**, 113-122 (1998)

Eckes B., Zigrino P., Kessler D., Holtkötter O., Shephard P. Mauch C. and Krieg T. Fibroblast-Matrix Interactions in Wound Healing and Fibrosis. *Matrix Biology*. **19**, 325-332 (2000)

Eddy S., Warriner K., Christie I., Ashworth D., Purkiss C. and Vadgama P. The modification of enzyme electrode properties with non-conducting electropolymerised films. *Biosensors and Bioelectronics*. **10**, 831-839 (1995)

Ehrenbeck C., Juttner K., Ludwig S. and Paash G. The electrochemical Impedance of a Free Standing Polypyrrole Membrane. *Electrochemica Acta*. **43**, 2781-2789 (1998)

Ehret R., Bauman W., Brischwein M., Schwinde A., Stegbauer K. and Wolf B. Monitoring of Cellular Behaviour by Impedance Measurements on Interdigitated Electrode Structures. *Biosensors and Bioelectronics*. **12**, 29-41 (1997)

Farrington A. M. and Slater J. M. Prediction and Characterization of the Charge/Size Exclusion Properties of Over-Oxidised Poly(Pyrrole) Films. *Electroanalysis*. **9**, 843-847 (1997)

Ferloni P., Mastragostino M. and Meneghello L. Impedance Analysis of Electronically Conducting Polymers. *Electrochimica Acta*. **41**, 27-33 (1996)

Fine J-D. In: Leigh I. M., Lane E. B. and Watt F. M. Eds. (1994) The Keratinocyte Handbook. Cambridge University Press

Gamry Instruments (2004) Electrochemical Impedance Spectroscopy Primer http://www.gamry.com/App_Notes/EIS_Primer/EIS_Primer.pdf

Gandarillas A. Epidermal Differentiation, Apoptosis, and Senescence: Common Pathways? *Experimental Gerontology*. **35**, 53-62 (2000)

Gao Z. Q., Zi M. X. and Chen B. S. The Influence of Overoxidation Treatment on the Permeability of Polypyrrole Films. *Journal of Electroanalytical Chemistry*. **373**, 141-148 (1994)

Garner B., Georgevitch A., Hodgson A. J., Lin L. and Wallace G. G. Polypyrrole-Heparin Composites as Stimulus-Responsive Substrates for Endothelial Cell Growth. *Journal of Biomedical Materials Research*. **44**, 121-129 (1999b)

Garner B., Hodgson A. J., Wallace G. G. and Underwood P. A. Human Endothelial Cell Attachment to and Growth on Polypyrrole-Heparin is Vitronectin Dependent. *Journal of Materials Science: Materials in Medicine*. **10**, 19-27 (1999a)

Gawkrodger D. J. (2002) Dermatology – An Illustrated Colour Text. Churchill Livingstone

Gerwen P. V., Laureyn W., Laureys W., Huyberechts G., De Beek M. O., Baert K., Suls J. Samsen W., Jacobs P., Hermans L. and Mertens R. Nanoscaled Interdigitated Electrode Arrays for Biochemical Sensors. *Sensors and Actuators B*. **49**, 73-80 (1998)

Getsios S., Huen A. C. and Green K. J. Working out the strength and flexibility of desmosomes. *Nature Reviews*. **5**, 271-281 (2004)

Ghosh P. M., Keese C. R. and Giaever I. Morphological Response of Mammalian Cells to Pulsed AC Fields. *Bioelectrochemistry and Bioenenergetics*. **33**, 121-133 (1994)

Giaever I. and Keese C. R. Fractal Motion of Mammalian Cells. *Physica D*. **38**, 128-133 (1989)

Giaever I. and Keese C. R. Micromotion of Mammalian Cells Measured Electrically. *Proceedings of the National Academy of Sciences of the USA*. **88**, 7896-7900 (1991)

Giaever I. and Keese C. R. Monitoring Fibroblast Behavior in Tissue Culture with an Applied Electric Field. *Procceedings of the National Academy of Sciences of the USA*. **81**, 3761-3764 (1984)

Giaever I. and Keese C. R. Use of Electric Fields to Monitor the Dynamical Aspect of Cell Behaviour in Tissue Culture. *IEEE Transactions on Biomedical Engineering*. **33**, 242-247 (1986)

Gniadecki R. Regulation of keratinocyte proliferation. *General Pharmacology*. **30**, 619-622 (1998)

Goetinck P. F., Winterbottom N. In:Goldsmith L. A. ed. (1991) Physiology, Biochemistry, and Molecular Biology of the Skin Vol. 1. Oxford University Press

Green H., Kehinde O. and Thomas J. Growth of Cultured Human epidermal Cells into Multiple Epithelia Suitable for Grafting. *Proceedings of the National Academy of Science U.S.A.* **76**, 5665 (1979)

Griffith L. G. and Naughton G. Tissue Engineering – Current Challenges and Expanding Opportunities. *Science*. **295**, 1009 (2002)

Grimnes S. and Martinsen Ø. G. (2000) Bioimpedance and Bioelectricity Basics. Academic Press

Grinnell F. Fibroblast Biology in Three-Dimensional Collagen Matrices. *Trends in Cell Biology*. **13**, 264-269 (2003)

Guan J-G., Miao Y-Q. and Zhang Q-J. Impedimetric Biosensors. *Journal of Bioscience and Bioengineering*. **97**, 219-226 (2004)

Hauthal W. H. Advances with Supercritical Fluids [Review]. *Chemosphere*. **43**, 123-135 (2001)

Heinze J. Electronically Conducting Polymers. *Topics in Current Chemistry*. **152**, 1-19 (1989)

Hemler M. E. and Mihich E. eds. Cell Adhesion Molecules. Plenum Press

Hench L. L. and Polak J. M. Third-Generation Biomedical Materials. *Science*. **295**, 1014-1017 (2002)

Hodgson A. J., John M. J., Campbell T., Georgevich A., Woodhouse S., Aoki T., Ogata N. and Wallace G. G. Integration of Biocomponents with Synthetic Structures: Use of Conducting Polymer Polyelectrolyte Composites. *Proceedings of SPIE*. **2716**, 164-176 (1996)

Holbrook K. A. In: Leigh I. M., Lane E. B. and Watt F. M. Eds. (1994) The Keratinocyte Handbook. Cambridge University Press

Honda M. (1989) The Impedance Measurement Handbook – A Guide to Measurement Technology and Techniques. Yogawa-Hewlett-Packard Ltd.

Hynes R. O. Integrins: Versatility, Modulation and Signalling in Cell Adhesion. *Cell.* **69**, 11-25 (1992)

Inzelt G., Pineri M., Schultze J. W. and Vorotyntsev M. A. Electron and Proton Conducting Polymers: Recent Developments and Prospects. *Electrochimia Acta.* **45**, 2403-2421 (2000)

Janz G. J. In: Ives D. J. G. and Janz G. J. eds. (1961) Reference Electrodes, Theory and Practice. Academic Press

Kamalati T., Howard M. and Brooks R. F. IGF I Induces Differentiation in a Transformed Human Keratinocyte Line. *Development.* **106**, 283-293 (1989b)

Kamalati T., McIvor Z., Howard M., Green M. R. and Brooks R. F. Expression of Markers of Differentiation in a Transformed Human Keratinocyte Line Induced by Coculture with a Fibroblast Line. *Experimental Cell Research.* **185**, 453-463 (1989a)

Kanazawa K. K., Diaz A. F., Geiss R. H., Gill W. D., Kwak J. F. and Logan J. A. 'Organic Metals': Polypyrrole a Stable Synthetic 'Metallic' Polymer. *Journal of the Chemical Society - Chemical Communications*. 854 (1979)

Kane-Maguire L. A. P. and Wallace G. G. Communicating with the Building Blocks of Life using Organic Electronic Conductors. *Synthetic Metals*. **119**, 39-42 (2001)

Karyakin A. A., Vagin M. Y., Choba M. A. and Klyachko N. L. Self-Assembled Amphiphilic Bilayers of Surfactant Brij-52 on Gold Electrodes. *Electroanalysis*. **11**, 1094-1097 (1999)

Kasemo B., Biological Surface Science, *Current Opinion in Solid State Material Science*. **3**, 451-459 (1998)

Kazi M., Lundmark K., Religa P., Gouda I., Larm O., Ray A., Swedenborg J.and Hedin U. Inhibition of Rat Smooth Muscle Cell Adhesion and Proliferation by Non-Anticoagulant Heparins. *Journal of Cellular Physiology*. **193**, 365-372 (2002)

Keese C. R., Wegener J., Walker S. R. and Giaever I. Electrical Wound-Healing Assay for Cells *in vitro*. *Proceedings of the National Academy of Sciences of the USA*. **101**, 1554-1559 (2004)

Kim D-H., Abidian M. and Martin D. C. Conducting Polymers Grown in Hydrogel Scaffolds Coated on Neural Prosthetics Devices. *Journal of Biomedical Materials Research*. **71A**, 577-585 (2004)

Kloth L. C. and McCulloch. Promotion of Wound Healing with Electrical Stimulation. *Advance Wound Care*. **9**, 42-45 (1996)

Kohavi D., Pollack S. R. and Brighton C. Short-Term Effect of Guided Bone Regeneration and Electrical Stimulation on Bone Growth in a Surgically Modelled Resorbed Dog Mandibular Ridge. *Biomaterials Artificial Cells and Immobilization Biotechnology*. **20**, 131-138 (1992)

Komolov A., Schauemburg K., Molller P. J. and Monakhov V. Characterization of Conducting Molecular Films on Silicon: Auger Electron Spectroscopy, X-ray Photoelectron Spectroscopy, Atomic Force Microscopy and Surface Photovoltage. *Applied Surface Science*. **142**, 591-597 (1999)

Komura T., Goisihara S., Yamaguti T. and Takahasi K. Electron and Ion Transport in Polypyrrole/Polystyrenesulfonate Composite Films. *Journal of Electroanalytical Chemistry*. **456**, 121-129 (1998)

Kotwal A. and Schmidt C. E. Electrical Stimulation Alters Protein Adsorption and Nerve Cell Interactions with Electrically Conducting Biomaterials. *Biomaterials*. **22**, 1055-1064 (2001)

Kumar D. and Sharma R. C. Advances in Conductive Polymers. *European Polymer Journal* **34**, 1053-1060 (1998)

Labat-Robert J., Bihari-Varga M., Robert L. Extracellular Matrix. *FEBS Letters*. **268**, 386-393 (1990)

Lakard S., Herlem G., Valles-Villareal N., Michel G., Propper A., Gharbi T. and Fahys B. Culture of Neural Cells on Polymers Coated Surfaces for Biosensor Applications. *Biosensors and Bioelectronics*. **20**, 1946-1954 (2005)

Langer R. and Vacanti J. P. Tissue Engineering. *Science*. **260**, 920-926 (1993)

Lecuit T. Adhesion Remodeling Underlying Tissue Morphogenesis. *Trends in Cell Biology*. **15**, 34-42 (2005)

Lee C. E., Lee C. H., Yoon K. H. and Jin J. I. NMR Study of the PPV Conducting Polymers. *Synthetic Metals*. **69**, 427-428 (1995)

Lee D. A. and Knight M. N. In: Sabatini M., Pastoureau P. and De Ceunick F. Eds. (2004) Cartilage and Osteoarthritis – Vol 1: Cellular and Molecular Tools. Humana Press, Inc

Leigh I. M. and Watt F. M. In: Leigh I. M., Lane E. B. and Watt F. M. Eds. (1994) The Keratinocyte Handbook. Cambridge University Press

Levi M. D., Lopez C., Vieil E. and Vorotyntsey M. A. Influence of Ionic Size on the Mechanism of Electrochemical Doping of Polypyrrole Films Studied by Cyclic Voltammetry . *Electrochimica Acta*. **42**, 757-769 (1997)

Li C., Granger C., Schutte H. D. Jr., Biggers S. B. Jr., Kennedy J. M. and Latour R. A. Jr. Progressive Failure Analysis of Laminated Composite Femoral Prostheses for Total hip Arthroplasty. *Biomaterials*. **23**, 4249-4262 (2002)

Lillie G. C. (2001) Cyclic Voltammetric and Impedance Spectroscopic Studies of Bioaffinity Loaded Poly(Pyrrole) for Direct Reagentless Biosensors (Thesis). University of Manchester.

Lillie G., Payne P. and Vadgama P. Electrochemical Impedance Spectroscopy as a Platform for Reagentless Bioaffinity Sensing. *Sensors and Actuators B*. **78**, 249-259 (2001)

Lind R., Connolly P. Wilkinson C. D. W., Breckenridge L. J. and Dow J. A. T. Single Cell Mobility and Adhesion Monitoring Using Extracellular Electrodes. *Biosensors and Bioelectronics*, **6**, 359-367 (1991)

Lindsey R. W. Grobman J., Leggon R. E., Panjabi M. and Friedlaender G. E. Effects of Bone Grafts and Electrical Stimulation on the Strength of Healing Bony Defects in Dogs. *Clinical Orthopaedics and Related Research*. **222**, 275-280 (1987)

Li Y., Neoh K. G. and Kang E. T. Controlled Release of Heparin from Polypyrrole-Poly(Vinyl Alcohol) Assembly by Electrical Stimulation. *Journal of Biomedical Materials Research*. **73A**, 171-181 (2005)

Lo C-M., Keese C. R. and Giaever I. Monitoring Motion of Confluent Cells in Tissue Culture. *Experimental Cell Research*. **204**, 102-109 (1993)

Macdonald J. R. (1987) Impedance Spectroscopy: Emphasizing Solid Materials and Systems. John Wiley and Sons, Inc.

Malitesta C., Losito I., Sabbatini L. and Zambonin P. G. New Findings on Polypyrrole Chemical Structure by XPS Coupled to Chemical Derivatization Labelling. *Journal of Electron Spectroscopy and Related Phenomena*. **76**, 629-634 (1995)

Marler J. J., Upton J., Langer R. and Vacanti J. P. Transplantation of Cells in Matrices for Tissue Regeneration. *Advanced Drug Delivery Reviews*. **33**, 165-182 (1998)

Martindale D. The Body Electric. *New Scientist*. **182** (2447), 38-41 (2004)

Mattioli-Belmonte M., Giavaresi G., Biagini G., Virgili L., Giacomini M., Fini M., Giantomassi F., Natali D., Torricelli P., and Giardino R. Tailoring Biomaterial Compatibility: *In Vivo* Tissue Response Versus *In Vitro* cell behaviour. *International Journal of Artificial Organs*. **26**, 1077-1085 (2003)

Merrick P., Meyer A. A., Herzog S. and Woodley D. Scanning Electron Microscopy of Cultured Human Keratinocytes. *Scanning Electron Microscopy*. **11**, 228-236 (1990)

McLean W. H. I. and Epithelial Genetics Group. Genetic Disorders of Palm Skin and Nail. *Journal of Anatomy*. **202**, 133-142 (2003)

McKay I. A. and Leigh I. M. Epidermal Cytokines and their Role in Cutaneous Wound Healing. *British Journal of Dermatology*. **124**, 513-518 (1991)

Miller L. L., Zinger B. and Zhou Q-X. Electrically Controlled Release of Ferrocyanide from Polypyrrole. *Journal of the American Chemical Society*. **109**, 2267–2272 (1987)

Monkman A. P. (1989) The Characterisation of Conducting Polymer Polyaniline – PhD Thesis. Dept. Physics, QMUL

Mostany J. and Schariker B. R. Impedance Spectroscopy of Undoped, Doped and Overoxidised Polypyrrole Films. *Synthetic Metals*. **87**, 179-185 (1997)

Moy A. B., Engelenhoven J. V., Bodmer J. Kamath J., Keese C., Giaever I., Shasby S. and Shasby D. M. Histamine and Thrombin Modulate Endothelial Focal Adhesion Through Centripetal and Centrifugal Forces. *The Journal of Clinical Investigation*. **97**, 1020-1027 (1996)

Mutsaers S. E., Bishop J. E., McGrouther G. and Laurent G. J. Mechanisms of Tissue Repair: From Wound Healing to Fibrosis. *International Journal of Biochemistry and Cell Biology*. **29**, 5-17 (1997)

Natta G., Mazzanti G. and Corrandini P. *Atti della Accademia Nazionale dei Lincei Classe die Scienze Fisiche, Mater. Nat. Rend.* **8**, 25 (1958)

Naumowicz M., Petelska A. D. and Figaszewski Z. A. Impedance Analysis of Phosphatidylcholine-Cholesterol System in Bilayer Lipid Membranes. *Electrochimica Acta*. **50**, 2155-2161 (2005)

Navasaria H. (2000) Keratinocytes: A practical Course in Cultures and their Applications – Course Handbook. Centre for Cutaneous Research, QMUL

O'Brien J., Wilson I., Orton T. and Pognan F. Investigation of the Alamar Blue (Resazurin) Fluorescent Dye for the Assessment of Mammalian Cell Cytotoxicity. *European Journal of Biochemistry*. **267**, 5421-5426 (2000)

Oh E. J., Jang K. S., Park S. Y., Han S. S. and Suh J. S. Electrochemical Synthesis and Characterisation of Stretchable Polypyrrole Films. *Molecular Crystals and Liquid Crystals*. **371**, 243-246 (2001)

Ojeh N. O., Frame J. D. and Navsaria H. A. *In Vitro* Characterisation of an Artificial Dermal Scaffold. *Tissue Engineering*. **7**, 257-472 (2001)

Ojeh N. O. (2002) Measurement of Cell Proliferation using MTT versus Alamar Blue Assay – Unpublished Results. Centre for Cutaneous Research, QMUL

Oldham H. B. and Myland J. C. (1994) Fundamental of Electrochemistry Science. Academic Press, Inc.

Otero T. F. and Sansinena J. M. Artificial Muscles based on Conducting Polymers. *Bioeleetrochemistry and Bioenergetics*. **38,** 411-414 (1995)

Ouyang J. and Li Y. Great Improvement of Polypyrrole Films Prepared Electrochemically from Aqueous Solutions by Adding Nonaphenol Polyethyleneoxy (10) Ether. *Polymer* **38**(15), 3997-3999 (1997)

Owens D. W. and Lane E. B. The quest for the function of simple epithelial keratins. *BioEssays*. **25**, 748-758 (2003)

Parce J. W., Owicki J. C., Kercso K. M., Sigal G. B., Wada H. G., Muir V. C. Bousse L. J., Ross K. L., Branimir I. S. and McConnell H. M. Detection of Cell Affecting Agents with a Silicon Biosensor. *Science*. **246**, 243-247 (1989)

Pittelkow M. R., Coffrey R. J. Jr. and Moses H. L. In:Goldsmith L. A. ed. (1991) Physiology, Biochemistry, and Molecular Biology of the Skin Vol. 1. Oxford University Press

Pliquett F. and Pliquett U. Passive Electrical Properties of Human Stratum Corneum in Vitro Depending on Time after Separation. *Biophysical Chemistry*. **58**, 205-210 (1996)

Popkirov G. S. and Barsoukov E. *In Situ* Impedance Measurements During Oxidation and Reduction of Conducting Polymers: Significance of the Capacitive Currents. *Journal of Electroanalytical Chemistry*. **383**, 155-160 (1995)

Price R. D., Navsaria H. and Leigh I. M. Tissue Engineering: Skin Equivalents for Clinical Use. *Korean Journal of Investigative Dermatology*. **7**, 69-77 (2000)

Pu Y., Li Y., Han Y., Yuan C., and Wu L. Rat Keratinocyte Primary Cultures Based on Conductive Polypyrrole Primary Cell Culture Technique. *[Journal of Biomedical Engineering-China]*. **18**, 416-418 (2001) – Translated by Miss Bo Su

Pyo M., Maeder G., Kennedy R. T. and Reynolds J. R. Controlled Release of Biological Molecules from Conducting Polymer Modified Electrodes: The Potential Dependent Release of Adenosine 5-Triphosphate from Poly(Pyrrole Adenosine 5-Triphosphate) Films. *Journal of Electroanalytical Chemistry*. **368**, 329 –332 (1994)

Refaey S. A. M., Schwitzgebel G. and Schneider O. Electrochemical Impedance Studies on Oxidative Degradation, Overoxidative Degradation, Deactivation and Reactivation of Conducting Polymers. *Synthetic Metals*. **98**, 183-192 (1999)

Reger S. I. Hyodo A., Negami S. Kambic H. E. and Sahgal V. Experimental Wound Healing with Electrical Stimulation. *Artificial Organs*. **23**, 460-462 (1999)

Rheinwald J. G. and Green H. Serial Cultivation of Strains of Human Epidermal Keratinocytes: The Formation of Keratinizing Colonies from Single Cells. *Cell*. **6**, 331-344 (1975)

Rivers T. J., Hudson T. W. and Schmidt C. E. Synthesis of a Novel Biodegradable Electrically Conducting Polymer for Biomedical Applications. *Advanced Functional Materials*. **12**, 33-37 (2002)

Salmon M., Diaz A. F., Logan A. J. Krounbi M. and Bargon J. Chemical Modification of Conducting Polypyrrole Films. *Molecular Crystals and Liquid Crystals*. **83**, 265-276 (1982)

Saltzman W. M. and Olbricht W. Building Drug Delivery into Tissue Engineering. *Nature Reviews - Drug Discovery*. **1**, 177-183 (2002)

Saunders S., Jalkanen M., O'Farrell S. and Bernfield M. Molecular Cloning of Syndecan, an Integral Membrane Proteoglycan. *Journal of Cell Biology*. **108**, 1547-1556 (1989)

Seeger F. H., Blessing E., Gu L., Bornhold R., Denger S. and Kreuzer J. Fibrinogen Induces Chemotactic Activity in Endothelial Cells. *Acta Physiologica Scandinavia*. **176**, 109-115 (2002)

Schmidt C. E., Shastri V. R., Vacanti J. P. and Langer R. Stimulation of Neurite Outgrowth using an Electrically Conducting Polymer. *Proceedings of the National Academy of Sciences of the USA*. **94**, 8948-8953 (1997)

Seal B. L., Otero T. C. and Panitch A. Polymeric Biomaterials for Tissue and Organ Regeneration. *Materials Science and Engineering R*. **34**, 147-230 (2001)

Shakespeare P. Burn Wound Healing and Skin Substitutes. *Burns*. **27**, 517-522 (2001)

Shao Y., Jin Y., Wang J., Wang L., Zhao F. and Dong S. Conducting Polymer Polypyrrole Supported Bilayer Lipid Membranes. *Biosensors and Bioelectronics*. **20**, 1373-1379 (2005)

Shear J. B., Fishman H. A., Albritton N. L., Garigan D., Zare R. N. and Scheller R. H. Single Cells as Biosensors for Chemical Separations. *Science*. **267**, 74-77 (1995)

Sherley J. L. Asymmetric Cell Kinetics Genes: The Key to Expansion of Adult Stem Cells in Culture. *ScientificWorldJournal*. **2**, 1906-1921 (2002)

Shiigi H., Kishimoto M., Yakabe H., Deore B. and Nagaoka T. Highly Selective Molecularly Imprinted Overoxidised Polypyrrole Colloids: One Step Preparation Technique. *Analytical Sciences*. **18**, 41-44 (2002)

Shin H., Jo S. and Mikos A. G. Biomimetic Materials for Tissue Engineering. *Biomaterials*. **24**, 4353-4364 (2003)

Shinohara H., Kojima J. and Aizawa M. Electrically Controlled Ion Tranfer and pH Change Near a Conducting Polymer-Coated Electrode. *Journal of Electroanalytical Chemistry*. **266**, 297-308 (1989b)

Shinohara H., Kojima J., Yaoita M. and Aizawa M. Electrically Stimulated Rupture of Cell Membranes with a Conducting Polymer-Coated Electrode. *Bioelectrochemistry and Bioenergetics*. **22**, 23-25 (1989a)

Shirakawa H, Louis E. J., MacDiarmid A. G., Chiang C. K. and Heeger A. J. Synthesis of Electrically Conducting Organic Polymers: Halogen Derivatives of Polyacetylene, $(CH)_x$. *Journal of the Chemical Society – Chemical Communications*. 578 (1977)

Silk T., Hong Q., Tamm and Compton R. G. AFM Studies of Polypyrrole Film Surface Morphology – I. The Influence of Film Thickness and Dopant Nature. *Synthetic Metals*. **93**, 59-64 (1998)

Smith T. J., Wang H-S., Hogg M. G., Henrikson R. C., Keese C. R. and Giaever I. Prostaglandin E_2 Elicits a Morphological Change in Cultured Orbital Fibroblasts from Patients with Graves Ophthalmopathy. *Proceedings of the National Academy of Sciences of the USA*. **91**, 5094-5098 (1994)

Sorrell J. M. and Caplan A. I. Fibroblast Heterogeneity: More than Skin Deep. *Journal of Cell Science*. **117**, 667-675 (2004)

Steinberg M. L., Cassai N. and Defendi V. A Scanning Electron Microscope Study of Normal and SV40-Infected Human Keratinocytes. *Scanning Electron Microscopy*. **1**, 343-349 (1983)

Stenger-Smith J. D. Intrinsically Electrically Conducting Polymers. Synthesis, Characterisation and their Applictaions. *Progress in Polymer Science*. **23**, 57-79 (1998)

Street G. B. In: Skotheim J. A. Ed. (1986) Handbook of Conducting Polymers Vol I. Marcel Dekker, Inc.

Sugahara K., Mikami T., Uyama T., Mizuguchi S. Nomura K. and Kitagawa H. Recent Advances in the Structural Biology of Chondroitin Sulfate and Dermatan Sulfate. *Current Opinion in Structural Biology*. **13**, 612-620 (2003)

Sun Z. and Tachikawa H. In: Edelman P. G. and Wang J. Eds. (1992) Biosensors and Chemical Sensors – Optimising Performance through Polymeric Materials. American Chemical Society

Taylor-Papadimitriou J., Purkis P. Lane E. B. McKay I. A. and Chang S. E. Effects of SV40 Transformation on the Cytoskeleton and Behavioural Properties of Human Keratinocytes. *Cell Differentiation*. **11**, 169-180 (1982)

Tiefenauer L. and Ros R. Biointerface Analysis on a Molecular Level – New Tools for Biosensor Research. *Colloids and Surfaces B: Biointerfaces*. **23**, 95-114 (2002)

Tortora G. J. and Grabowski S. R. (1996) Principles of Anatomy and Physiology. Harper Collins Publishers Inc.

Trowbridge J. M. and Gallo R. L. Dermatan Sulfate: New Functions from an Old Glycosaminoglycan. *Glycobiology*. **12**, 117R-125R (2002)

Trowbridge J. M., Rudisill J. A., Ron D and Gallo R. L. Dermatan Sulfate Binds and Potentiates Activity of Keratinocyte Growth Factor (FGF-7). *The Journal of Biological Chemistry*. **277**, 42815-42820 (2002)

Turner A. P. F., Karube I. and Wilson G. S. (1987) Biosensors: Fundamentals and Applications. Oxford University Press, Oxford

Uitto J., Fazio M., Bashir M. and Rosenbloom J. In:Goldsmith L. A. ed. (1991) Physiology, Biochemistry, and Molecular Biology of the Skin Vol. 1. Oxford University Press

Valaski R., Ayoub S., Micaroni L. and Hümmelgen I. A. Influence of Film Thickness on Charge Transport of Electrodeposited Polypyrrole Thin Films. *Thin Solid Films*. **415**, 206-210 (2002)

Valenti R. F., Vargo T. G., Gardella J. A. and Aebischer P. Electrically Charged Polymeric Substrates Enhance Nerve Fibre Outgrowth In Vitro. *Biomaterials*. **13**, 183-190 (1992)

Velasco F. Neuromodulation: An Overview. *Archives of Medical Research*. **31**, 232-236 (2000)

Voet D. and Voet J. G. (1995) Biochemistry. John Wiley & Sons Inc.

Walker D. C. (2001) Modelling the Electrical Properties of Cervical Epithelium (Thesis). University of Sheffield.

Wallace G. G., Smyth M. and Zhao H. Conducting Electroactive Polymer-Based Biosensors. *Trends in Analytical Chemistry*. **18**, 245-251 (1999)

Wang X., Gu X., Yuan C., Chen S., Zhang P., Zhang T., Yao J., Chen F. and Chen G. Evaluation of Biocompatibility of Polypyrrole *in vitro* and *in vivo*. *Journal of Biomedical Materials Research*. **68A**, 411-422 (2004)

Wang E., Li J., Green M. and West P. E. *In Situ* AFM Study of the Surface Morphology of Polypyrrole Films. *Synthetic Metals*. **74**, 127-131 (1995)

Waterworth A. R. (2000) Data Analysis Techniques of Measured Biological Impedance (Thesis). University of Sheffield.

Wegener J., Keese C. R. and Giaever I. Electric Cell-Substrate Impedance Sensing (ECIS) as a non-invasive Means to Monitor the Kinetics of Cell Spreading to Artificial Surfaces. *Experimental Cell Research*. **259**, 158-166 (2000)

Wegener J., Sieber M. and Galla H-J. Impedance Analysis of Epithelial and Endothelial Cell Monolayers on Gold Surfaces. *Journal of Biochemical and Biophysical Methods*. **32**, 151-170 (1996)

Weigel P. H., Fuller G. M. and LeBouef R. D. A Model for the Role of Hyaluronic Acid and Fibrin in the Early Events During the Inflammatory Response and Wound Healing. *Journal of Theoretical Biology*. **119**, 219-234 (1986)

Wenstrup R. J., Murad S. and Pinnell A. R. In:Goldsmith L. A. ed. (1991) Physiology, Biochemistry, and Molecular Biology of the Skin Vol. 1. Oxford University Press

Wernet W. and Wegner G. Electrochemistry of Thin Polypyrrole Films. *Makromolekulare Chemie*. **188**, 1465-1475 (1987)

Williams R. L. and Doherty P. J. A preliminary Assessment of Polypyrrole in Nerve Guide Studies. *Journal of Materials Science: Materials in Medicine*. **5**, 429-433 (1994)

Wong J. Y., Leach J. B. and Brown X. Q. Balance of Chemistry, Topography, and Mechanics at the Cell-Biomaterial Interface: Issues and Challenges for Assessing the Role of Substrate Mechanics on Cell Response. *Surface Science*. **570**, 119-133 (2004)

Wong J. Y., Langer R. and Ingber E. Electrically Conducting Polymers can Noninvasively Control the Shape and Growth of Mammalian Cells. *Proceedings of the National Academy of Sciences of the USA*. **91**, 3201-3204 (1994)

Xing J. Z., Zhu L., Jackson J. A., Gabos S., Sun X-J., Wang X-B. and Xu X. Dynamic Monitoring of Cytotoxicity on Microelectronic Sensors. *Chemical Research and Toxicology*. **18**, 154-161 (2005)

Xiao C. and Luong J. H. T. On-Line Monitoring of Cell Growth and Cytotoxicity using Electric Cell-Substrate Impedance Sensing (ECIS). *Biotechnology Progress*. **19**, 1000-1005 (2003)

Xiao C., Lachance B., Sunahara G. and Luong J. H. T. Assessment of Cytotoxicity using Electric Cell-Substrate Impedance Sensing: Concentration and Time Response Function Approach. *Analytical Chemistry*. **74**, 5748-5753 (2002)

Yamato M. and Okano T. Cell Sheet Engineering. *Materials Today*. 7, 42-47 (2004)

Yin T. and Green K. J. Regulation of Desmosome Assembly and Adhesion. *Seminars in Cell and Developmental Biology*. **15**, 665-677 (2004)

Zhao P. and Nauer G. E. *In Situ* FTIR-ATR Spectroscopic Investigations on the Polymerization Process and the Redox Behaviour of Poly(thienylpyrrole) Thin Film Electrodes in Aqueous and Non-Aqueous Solutions. Part 1. Characterisation of the Polymerization Process in Acetonitrile Containing Different Supporting Salts. *Journal of Electroanalytical Chemistry*. **416**, 157-166 (1996)

Zelikin A. N., Lynn D. M., Farhadi J., Martin I., Shastri V and Langer R. Erodible Conducting Polymers for Potential Biomedical Applications. *Angewandte Chemie International Edition*. **41**, 141-144 (2002)

Zhou D., Too C. O. and Wallace G. G. Synthesis and Characterisation of Polypyrrole/Heparin Composites. *Reactive and Functional Polymers*. **39**, 19-26 (1999)

Zhou Q., Zhuang L. and Juntao L. *In Situ* ESR Studies Over Wide Temperature Range for Conducting Polymers. *Electrochemistry Communications*. **4**, 733-736 (2002)